Universidade de Brasília
Instituto de Geociências
Programa de Pós-graduação em Geologia

PROVENIÊNCIA SEDIMENTAR DAS FORMAÇÕES PONTA GROSSA E SÃO DOMINGOS (DEVONIANO) DO NW DA BACIA DO PARANÁ (BRASIL): IMPLICAÇÕES REGIONAIS PARA OS EVENTOS T-R DO SW DE GONDWANA

WILSON HUMBERTO LÓPEZ ABANTO

Dissertação de Mestrado N°496

Orientadora: Profa. Dra. Natalia Hauser

Brasília/DF

2022

Universidade de Brasília
Instituto de Geociências
Programa de Pós-graduação em Geologia

PROVENIÊNCIA SEDIMENTAR DAS FORMAÇÕES PONTA GROSSA E SÃO DOMINGOS (DEVONIANO) DO NW DA BACIA DO PARANÁ (BRASIL): IMPLICAÇÕES REGIONAIS PARA OS EVENTOS T-R DO SW DE GONDWANA

WILSON HUMBERTO LÓPEZ ABANTO

Dissertação apresentada ao Programa de Pós-Graduação em Geologia – Instituto de Geociências – IG da Universidade de Brasília – UnB como requisito parcial obrigatório para a obtenção do título de Mestre em Geologia.

Área de concentração: Geologia Regional.

Orientadora: Profa. Dra. Natalia Hauser

Comissão Examinadora:

Prof. Dr. Carlos José Souza de Alvarenga (IG/UnB);

Prof. Dr. Miguel Angelo Stipp Basei (USP);

Profa. Dra. Edi Mendes Guimarães (Suplente IG/UnB).

Ficha catalográfica elaborada automaticamente,
com os dados fornecidos pelo(a) autor(a)

López Abanto, Wilson Humberto
LL864p Proveniência sedimentar das formações Ponta Grossa e São Domingos (Devoniano) do NW da Bacia do Paraná (Brasil): implicações regionais para os eventos T-R do SW de Gondwana / Wilson Humberto López Abanto; orientador Natalia Hauser. -- Brasília, 2022.
122 p.

Dissertação(Mestrado em Geologia) -- Universidade de Brasília, 2022.

1. Formação Ponta Grossa. 2. Formação São Domingos. 3. geocronologia U-Pb. 4. Isótopos Sr-Nd. 5. Proveniência. I. Hauser, Natalia , orient. II. Título.

DEDICATÓRIA

"À minha querida mãe, Lucila Abanto, por todo o seu sacrifício e luta constante para que eu pudesse seguir em frente.
Ao meu pai, Humberto López Estrada, porque todos temos feridas na alma e, apesar disso, seguimos em frente."

AGRADECIMENTOS

Em primeiro lugar, quero agradecer a Deus por estar sempre no meu caminho e me dando forças para seguir em frente.

À minha família, em especial à minha mãe por sempre me apoiar nas decisões que tomei e, apesar de não ter recursos, ela me deu tudo.

À minha irmã Jazmín López Abanto por ser minha fonte de inspiração para continuar.

Ao Programa de Pós-Graduação em Geologia da Universidade de Brasília por todo o aprendizado proporcionado.

À minha orientadora Dra. Natalia Hauser pela confiança e apoio constante para continuar até alcançar meu objetivo e é minha fonte de motivação.

Aos meus colegas de pós-graduação Arnold García Zavaleta, Carolinna Souza, Gabriel Ribeiro Moizinho e Michele Andriolli pelo apoio no laboratório de geocronologia.

Às minhas amigas Alexandra Quispe, Leane Arias e Andrea Villaseca Robertson por todo o apoio que me deram.

À minha aluna Yessenia Puma Enriquez que me apoiou e me motivou a continuar pesquisando.

O presente trabalho foi realizado com apoio da Coordenação de Aperfeiçoamento de Pessoal de Nível Superior-Brasil (CAPES) – Código de Financiamento 001”

Gracias!

RESUMO

A Bacia do Paraná é uma típica bacia intracratônica localizada na plataforma brasileira. Três grandes variações do nível do mar de segunda ordem relacionadas à tectônica e eustasia ocorreram no sudoeste de Gondwana e também são reconhecidas na Bacia do Paraná. O primeiro desses eventos foi transgressivo e está relacionado à orogenia Precordillerana I. A Formação Furnas está relacionada à elevação do nível do mar, e os folhelhos da Formação Ponta Grossa representam a superfície máxima de inundação para esta primeira transgressão. A segunda variação do nível do mar foi regressiva e está relacionada à orogenia Precordillerana II. Os arenitos do Membro Tibagi da Formação São Domingos foram relacionados à queda do nível do mar durante este segundo evento. O terceiro evento foi novamente transgressivo e está relacionado a uma elevação global do nível do mar. Este evento tem sido relacionado com os Folhelhos da parte superior da Formação São Domingos. Como existe uma relação bem restrita entre a estratigrafia e as variações do nível do mar para a Bacia do Paraná durante o Devoniano, esta dissertação de mestrado foi desenvolvida para testar essas variações do nível do mar com estudos de datação U-Pb em zircão detrítico e isotopia Sr-Nd. Para nossa discussão, levamos em consideração que a configuração paleogeográfica atual da bacia é um substituto para a paleogeografia durante o Devoniano. Isso permite classificar as prováveis fontes em próximo, intermediária e distais: o Arco Magmático de Goiás (~630 Ma) representaria uma fonte próximo, a Serra da Mesa, o Grupo Paranoá e o Bloco Goiás (~1770 Ma e 2100 Ma para a Serra da Mesa, e apenas ~2100 Ma para o Grupo Paranoá, e ~2420 Ma para o Bloco Goiás) representariam fontes intermediárias; e o Grupo Trairas (~1520 e 2604 Ma), o Cinturão Sunsas (~900-1200 Ma) e o magmatismo Famatiniano (~435 Ma) poderiam representar fontes distais/muito distais, respectivamente. A principal diferença entre os padrões de proveniência das três unidades é um pico de idade de ~2604 Ma, que só é observado na parte superior da Formação São Domingos e provavelmente pode estar relacionado ao Grupo Trairas. Como a parte superior da Formação São Domingos registrou o segundo evento transgressivo, este pico está relacionado a uma fonte muito distais, como o Grupo Trairas, que representaria o embasamento da Faixa Brasília ao NE. O pico em ~435 Ma que foi observado na Formação Ponta Grossa (4% zircão), Tibagi (3% zircão) e Formação São Domingos (6% zircão), mas não na Formação Furnas subjacente, pode ser explicado como fonte direta do Arco Magmático Famatiniano ou zircões com essas idades derivadas do retrabalhamento da Bacia do Tarija. Também as relações $^{87}Sr/^{86}Sr(380)$ e os valores de TDM mostram uma diminuição quando há contribuições de fontes mais jovens, como é o caso da Formação Ponta Grossa e da parte superior da Formação São Domingos onde há maior presença de fontes muito jovens, fontes associadas ao Arco Magmático Famatiniano. Assim, fontes distais/muito distais são observadas para a primeira transgressão, representada pela Formação Ponta Grossa, e então registradas novamente para a segunda transgressão na parte superior da Formação São Domingos. Podemos concluir que a análise de proveniência U-Pb em zircão detrítico e isótopos Sr - Nd pode ser aplicada para reconhecer as variações do nível do mar em uma bacia.

ABSTRACT

The Paraná Basin is a typical intracratonic Basin located on the Brazilian platform. Three major second-order sea level variations related to tectonics and eustatic have occurred in southwestern Gondwana and are also recognized in the Paraná Basin. The first of these events was transgressive and it is related to the Precordillera orogeny I. In the Paraná Basin, the Furnas Formation is related to the sea level rise, and the shales of the Ponta Grossa Formation represent the maximum flood surface for this first transgression. The second sea level variation was regressive and is related to the Precordillera orogeny II. The sandstones of the Tibagi member of the São Domingos formation were related to the drop in sea level during this second event. The third event was again transgressive and it is related to a global rise in sea level. This event has been related to the shales of the upper part of the São Domingos Formation. As there is a very restricted relationship between stratigraphy and sea level variations for the Paraná Basin during the Devonian, this master's thesis was developed to test these sea level variations with U-Pb dating studies on detrital zircon and Sr-Nd isotope. For our discussion, we take into account that the current paleogeographic configuration of the basin is a substitute for paleogeography during the Devonian. This allows classifying the probable sources into near, intermediate, and distal: the Goiás magmatic arc (~630 Ma) would represent a near source, the Serra da Mesa, Paranoá Group, and Goiás block (~1770 Ma and 2100 Ma for the Serra da Mesa, and only ~2100 Ma for the Paranoá Group, and ~2420 Ma for the Goiás block) would represent intermediate sources; and the Trairas Group (~1520 and 2604 Ma), the Sunsas belt (~900-1200 Ma) and the Famatinian magmatism (~435 Ma) could represent distal/very distal sources, respectively. The main difference between the provenance patterns of the three units is an age peak of ~2604 Ma, which is only observed in the upper part of the São Domingos Formation and can probably be related to the Trairas Group. As the upper part of the São Domingos Formation recorded the second transgressive event, this peak is related to a very distal source, such as the Trairas Group. The peak at ~435 Ma that was observed in the Ponta Grossa Formation (4% zircon), Tibagi (3% zircon) and São Domingos Formation (6% zircon), but not in the underlying Furnas Formation, can be explained as direct source of the Famatinian magmatic arc or zircons with these ages derived from the reworking of the Tarija Basin. Also the 87sr/86Sr(380) ratios and the TDM values show a decrease when there are contributions from younger sources, as is the case of the Ponta Grossa Formation and the upper part of the São Domingos Formation where there is a greater presence of very young sources, sources associated with the Famatinian magmatic arc. Thus, distal/very distal sources are observed for the first transgression, represented by the Ponta Grossa Formation, and then recorded again for the second transgression in the upper part of the São Domingos Formation. We can conclude that u-Pb provenance analysis on detrital zircon and Sr - Nd isotopes can be applied to recognize sea level variations in a basin.

RESUMEN

La cuenca Paraná es una cuenca intracratónica típica ubicada en la plataforma brasileña. Tres importantes variaciones del nivel del mar de segundo orden relacionadas con la tectónica y la eustacia, ocurrieron en el suroeste de Gondwana y también se reconocen en la cuenca Paraná. El primero de estos eventos fue transgresivo y se ha relacionado con la orogenia Precordillerana I. La Formación Furnas está relacionada con un aumento del nivel del mar, y las lutitas de la Formación Ponta Grossa representan la superficie máxima de inundación para esta primera transgresión. La segunda variación del nivel del mar fue regresivo y se ha relacionado con la orogenia Precordillerana II. Las areniscas del Miembro Tibagi de la Formación São Domingos ha sido relacionada con la caída del nivel del mar durante este segundo evento. El tercer evento fue nuevamente transgresivo y está relacionado con una subida global del nivel del mar. Este evento se ha relacionado con las lutitas de la parte superior de la Formación São Domingos. Como existe una relación bien restringida entre la estratigrafía y las variaciones del nivel del mar para la cuenca del Paraná durante el Devónico, el presente trabajo de maestría fue diseñado para testar esas variaciones del nivel del mar con estudios de dataciones de U-Pb en circón detrítico e isotopía de Sr-Nd. Para nuestra discusión, tomamos en consideración que la actual configuración paleogeográfica de la cuenca es un sustituto de la paleogeografía durante el Devónico. Esto nos permite clasificar las fuentes probables en proximales, intermedias y distales: El Arco Magmático de Goiás (~630 Ma) representaría una fuente proximal, la Serra da Mesa, Grupo Paranoá y el Bloque Goiás (~1770 Ma y 2100 Ma para la Serra da Mesa, y solo ~2100 Ma para el Grupo Paranoá, y ~2420 Ma para el Bloque Goiás) representarían fuentes intermedias; y el Grupo Trairas (~1520 y 2604 Ma), el Cinturón Sunsas (~900-1200 Ma) y el magmatismo Famatiniano (~435 Ma) podrían representar fuentes distales/muy distales, respectivamente. La principal diferencia entre los patrones de procedencia de las tres unidades es un pico de edad de ~2604 Ma, que solo se observa en la parte superior de la Formación São Domingos y probablemente puede estar relacionado con el Grupo Trairas. Como la parte superior de la Formación São Domingos registró el segundo evento transgresivo, ese pico está relacionado con una fuente muy distal, como es el Grupo Trairas. El pico a ~435 Ma que se observó en las formaciones Ponta Grossa (4 % de zirconios), Tibagi (3 % de zirconios) y São Domingos (6 % de zirconios), pero no en la Formación Furnas subyacente, se puede explicarse como procedencia del Arco Magmático Famatiniano o a circones con estas edades derivados del retrabajo de los depósitos de la cuenca Tarija. También Las relaciones $^{87}Sr/^{86}Sr(380)$ y los valores de TDM muestran una disminución cuando hay aportes de fuentes más jóvenes, como es el caso de la Formación Ponta Grossa y la parte superior de la Formación São Domingos donde hay mayor presencia de fuentes muy jóvenes, fuentes asociadas al Arco Magmático Famatiniano. Así, las fuentes distales/muy distales se observan para la primera transgresión, representada por la Formación Ponta Grossa, y luego se registran nuevamente para la segunda transgresión en la parte superior de la Formación São Domingos. Podemos concluir que el análisis de procedencia U-Pb en circón detrítico e isotopos de Sr - Nd se pueden aplicar para reconocer variaciones del nivel del mar en una cuenca.

SUMÁRIO

LISTA DE FIGURAS

CAPÍTULO 1

CAPÍTULO 2

CAPÍTULO 3

LISTA DE TABELAS

CAPÍTULO 2

CAPÍTULO 1. INTRODUÇÃO

O intervalo de tempo Devoniano (ca. 420 até 360 Ma) foi muito importante na evolução das bacias da América do Sul. Esse período foi caracterizado por um nível médio do mar mais alto do que o observado hoje. Essa inundação foi do tipo tectônica/eustática, a qual favoreceu a deposição marinha rasa registrada em várias bacias do SW de Gondwana, como a Bacia do Paraná no Brasil.

A Bacia do Paraná localiza-se no centro-sul do Brasil, atingindo também parte do Uruguai, do Paraguai e da Argentina. Essa é uma bacia classificada do tipo intracratônica (Almeida, 1980; Milani et al., 2007; Henrique-Pinto et al., 2021) e sua estratigrafia é representada por rochas sedimentares e vulcânicas que atingem idades desde o Ordoviciano Médio até o Cretáceo Superior (Zalán et al., 1990; Milani et al., 2007). O registro estratigráfico da Bacia do Paraná foi dividido em seis Supersequências por Milani et al. (2007): Rio Ivaí (Ordoviciano-Siluriano), Paraná (Siluriano-Devoniano), Gondwana I (Carbonífero - Triássico Inferior), Gondwana II (Triássico), Gondwana III (Jurássico Superior-Cretáceo Inferior) e Bauru (Cretáceo).

A Supersequência Paraná (Siluriano-Devoniano) é constituída por três formações: Formação Furnas, composta principalmente por arenitos (Assine, 1996); Formação Ponta Grossa, formada por folhelhos (Lange e Petri, 1967; Grahn et al., 2013); e a Formação São Domingos, composta por folhelhos e siltitos (Assine, 1996; Bergamaschi, 1999; Sedorko et al., 2018a). Recentemente Vargas et al. (2020) reconheceram sequências transgressivo-regressivas de 2ª ordem que podem ser reconhecidas no registro estratigráfico das formações Ponta Grossa e São Domingos, respectivamente.

1.1 Justificativa

A motivação deste trabalho de mestrado é caracterizar esses grandes eventos T-R reconhecidos na Bacia de Paraná na parte Norte, relacionados primeiro com a tectônica e mais tarde com a eustática. Assim serão feitos estudos de proveniência sedimentar (U-Pb em zircão detrítico, DRX e Sr-Nd em rocha total) nas formações Ponta Grossa (ciclo T com a tectônica) e São Domingos (ciclos R-T relacionados com tectônica/eustática).

Este estudo foi incentivado pelo fato de que: 1) os ciclos transgressivos-regressivos (T-R) na sub-bacia do Alto Garças para o Devoniano foram bem definidos (Vargas et al., 2020) e 2) as áreas potenciais de origem dos sedimentos para a bacia do

Paraná, divididos em proximal, intermediário e distal/muito distal, possuem idades U-Pb contrastantes.

A comparação dos resultados obtidos com os mesmos intervalos em outras bacias (Tarija, Chaco-Paraná, Precordillera, Malvinas). Vários trabalhos paleontológicos (Clarke, 1913; Boucot et al., 2001; Horodyski et al., 2019), sedimentológicos (Assine, 1996; Assine et al., 1998; Bergamaschi e Pereira, 2001), paleoambientais (Melo, 1988; Grahn et al., 2013) e geoquímicos (Montibeller et al., 2017) foram realizados nas unidades do Devoniano, mas ainda não foram realizados estudos de proveniência sedimentar como os propostos neste trabalho.

1.2 Objetivos

O principal objetivo desse projeto é realizar um estudo de caso de proveniência sedimentar através do método U-Pb em zircão detrítico, para testar os ciclos transgressivos-regressivos (T-R) de segunda ordem das unidades Devonianas de Ponta Grossa e São Domingos na sub-bacia do Alto Garças parte Leste da bacia do Paraná.

Para atingir o objetivo principal, os seguintes objetivos específicos foram desenvolvidos nas formações Ponta Grossa e São Domingos:

• Petrografia de quatro arenitos da Formação Ponta Grossa e um arenito da Formação São Domingos mediante o método Gazzi-Dickinson para classificá-los.

• Análises isotópicos U-Pb em zircão das unidades para obter idade máxima de sedimentação e informação sobre as prováveis áreas fontes dos sedimentos.

• Isótopos de Sr-Nd nos níveis pelíticos ao longo das colunas sedimentares no limite estudado, para obter uma variação temporal das razões $^{87}Sr/^{86}Sr$ inicial, $\varepsilon Nd_{(t)}$ e T_{DM}. Além disso, esse estudo foi complementado com analises Sr-Nd da Formação Furnas e parte superior da Supersequência Rio Ivaí para realizar uma contextualização regional.

• DRX dos pelitos da Formações Ponta Grossa e São Domingos, para comparar com os resultados obtidos para o mesmo intervalo em outras bacias.

• Comparação das unidades do Devoniano das Bacias do Paraná, Tarija, Chaco-Paraná, Chaco-salteña, Precordillera, Malvinas e Cape para colocar os resultados obtidos dentro da evolução geodinâmica devoniana do SW de Gondwana.

1.3 Área de Estudo

A área de estudo está localizada à oeste da capital federal, Brasília, nos estados de Goiás (GO) e Mato Grosso (MT), na parte nordeste da Bacia do Paraná, entre os municípios de Barra do Garças, Iporá e Alto Garças (Fig. 1). A principal via de acesso à área de estudo, partindo do Distrito Federal, se dá pela BR-070, a qual estabelece um trajeto no sentido leste-oeste até chegar ao Município de Barra do Garças, como também seguindo pela GO-174 até o município de Iporá e pela MT-100 em direção ao Município de Araguainha.

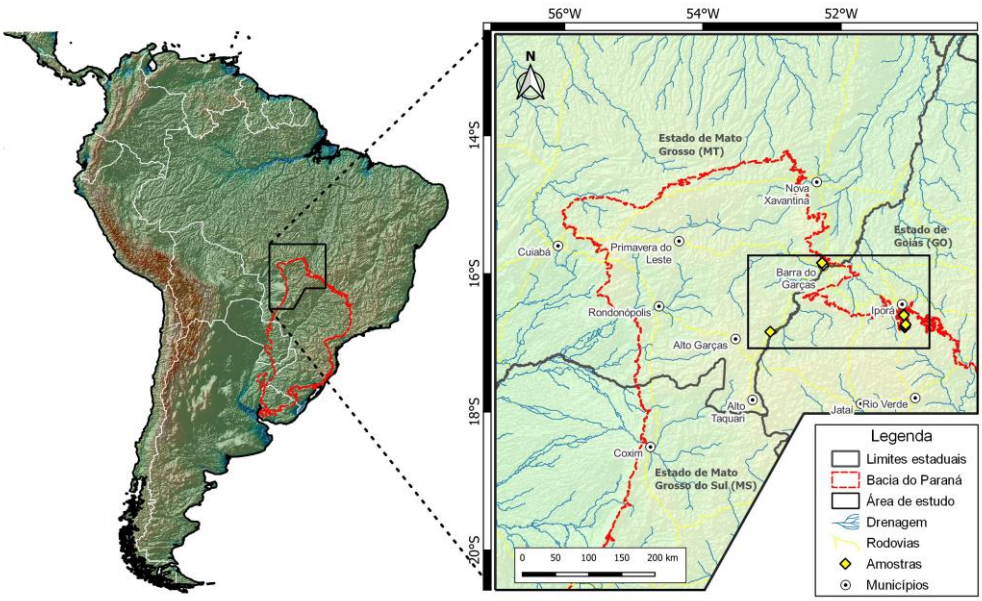

Figura 1. Mapa de localização da área de estudo. Os pontos amarelos indicam a localização das amostras.

CAPÍTULO 2. CONTEXTO GEOLÓGICO

2.1 Bacia do Paraná

A Bacia do Paraná é caracterizada por ser do tipo intracratônica em que se desenvolveu na plataforma Sul-Americana (Almeida, 1980; Henrique-Pinto et al., 2021). O preenchimento da bacia tem aproximadamente 7000 m de espessura e é constituída por rochas sedimentares e vulcânicas (Zalán et al., 1990; Milani et al., 2007). O registro estratigráfico da bacia foi dividido em seis Supersequências (Milani et al., 2007): Rio Ivaí (Ordoviciano-Siluriano), Paraná (Siluriano-Devoniano); Gondwana I (Carbonífero - Triássico Inferior); Gondwana II (Triássico) Gondwana III (Jurássico Superior-Cretáceo Inferior) e Bauru (Cretáceo). Além disso, a Bacia do Paraná está delimitada por faixas móveis: à norte e noroeste pela Faixa Paraguai, à noroeste pela Faixa Brasília, à leste pela Faixa Ribeira e ao sul pela Faixa Dom Feliciano (Zalán et al., 1990).

A Bacia do Paraná é dividida em duas sub-bacias (Melo, 1988; Grahn, 1992), a sub-bacia do Alto Garças ao norte e a sub-bacia de Apucarana ao centro-sul (Fig. 2.1). Este trabalho tem como objetivo estudar a Supersequência Paraná na porção nordeste da Bacia do Paraná (Fig. 2.1). Esta Supersequência é representada pela unidade litoestratigráfica do Grupo Paraná (Siluriano – Devoniano) que foi subdividida em unidades formacionais que, segundo o autor, recebem diferentes nomes (Tabela 1), entre eles Oliveira (1912), Oppenheim (1936), Almeida (1948, 1954), Andrade & Camarço (1978, 1980), Evans (1984), Melo (1985, 1988), Popp (1986), Assine (1996), Milani (2004), Grahn et al. (2013), Sedorko et al. (2018a) e Scheffler et al. (2020). Neste trabalho usaremos a divisão tripartida proposta por Grahn et al. (2013) do Grupo Paraná nas Formações Furnas, Ponta Grossa e São Domingos.

Tabela 1. Divisão estratigráfica da parte Norte da Bacia do Paraná (Subcuenca Alto Garças), modificado de Scheffler et al. (2020).

<table>
<tr><th>Oliveira (1912)</th><th colspan="2">Oppenheim (1936)</th><th>Almeida (1948, 1954)</th><th>Andrade & Camarço (1978, 1980)</th><th colspan="2">Evans (1984); Melo (1985, 1988)</th><th colspan="2">Popp (1986); Assine (1996); Milani (2004)</th><th>Sedorko et al. (2018)</th><th colspan="2">Grahn et al. (2013); Scheffler et al. (2020)</th></tr>
<tr><td rowspan="2">Arenito Tibaji</td><td rowspan="4">Série Paraná</td><td rowspan="3">Formação Ponta Grossa com Arenito Tibaji intercalado</td><td rowspan="3">Fácies Ponta Grossa</td><td>Membro superior</td><td colspan="2">Grupo Chapada IV</td><td rowspan="3">Formação Ponta Grossa</td><td>Membro São Domingos</td><td>Não resgitrada na borda leste</td><td rowspan="2">Formação São Domingos</td><td>Sub-unidades IV Givetiano- Frasniano</td></tr>
<tr><td rowspan="2">Folhelho Ponta Grossa</td><td>Membro medio</td><td colspan="2">Grupo Chapada III</td><td rowspan="2">Membro Tibaji</td><td>Sequência Devoniana II</td><td rowspan="2">Sub-unidades II e III; Emisiano médio- Eifeliano</td></tr>
<tr><td rowspan="2">Membro inferior</td><td rowspan="2">Grupo Chapada II</td><td>Superior</td><td>Sequência Devoniana I</td></tr>
<tr><td>Arenito Furnas</td><td>Arenito Furnas</td><td>Fácies Furnas</td><td>Formação Furnas</td><td colspan="2">Grupo Chapada I</td><td>Inferior</td><td>Membro Jaguariaiva</td><td>Sequência Siluro-devoniana</td><td>Formação Ponta Grossa</td><td>Praguiano-Emisiano Inicial</td></tr>
<tr><td></td><td></td><td></td><td></td><td></td><td colspan="2"></td><td colspan="2">Formação Furnas</td><td>Sequência Siluriana Inferior</td><td colspan="2">Formação Furnas</td></tr>
</table>

A Formação Furnas está constituída principalmente por arenitos de quartzo branco de granulação média a grossa e possui estratificações cruzadas de vários tipos (Assine, 1996; Milani, 1997; Milani et al., 2007). Esta formação foi dividida em três unidades ou intervalos: Unidade Inferior, Unidade Média e Unidade Superior (Assine, 1996, Sedorko et al., 2017). O ambiente sedimentar desta unidade ainda é debatido, para alguns autores é um ambiente marinho (Lange e Petri, 1967; Assine, 1996; Sedorko et al., 2017) e para outros é fluvial (Schneider et al., 1974; Zalan et al. al., 1987; Araújo, 2016). A espessura desta unidade é de aproximadamente 250 a 300 m (Milani et al., 2007) e sua deposição termina aproximadamente no Devoniano Inferior no Lochkovian – Pragian? (Serdorko et al., 2017).

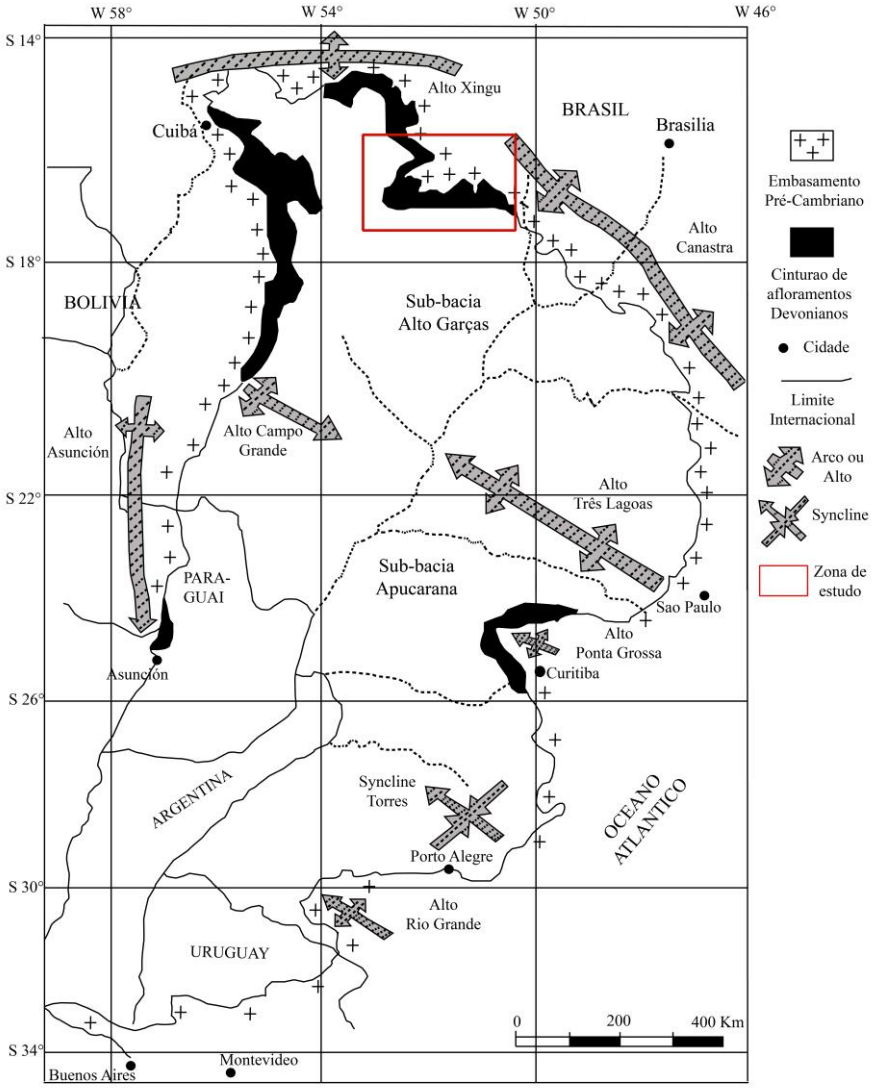

Figura 2.1 Mapa que mostra a separação das sub-bacias Alto Garças e Apucarana. Modificado de Grahn et al. (2010).

A Formação Ponta Grossa está composta principalmente por folhelhos intercalados com arenitos de grão fino (Lange e Petri, 1967). O ambiente sedimentar desta unidade é *offshore* (Grahn et al., 2013). A espessura da unidade é ~90 m (Sedorko et al., 2018a) e sua deposição termina com uma superfície de transgressão máxima durante o Emsiano (Grahn et al., 2013).

A Formação São Domingos é constituída principalmente por arenitos que representam o Membro Intraformacional Tibagi em sua parte inferior. A deposição do Membro Tibagi é consequência de uma regressão relacionada às reativações tectônicas, promovendo assim um aumento na quantidade de sedimentos disponíveis (Assine et al., 1994). O ambiente sedimentar desta unidade é deltaico em uma plataforma marinha rasa dominada por ondas (Assine et al., 1998; Grahn et al., 2010; Sedorko et al., 2018b). A espessura da unidade é ~100 m (Candido e Rostirolla, 2007) e sua deposição termina durante o Eifeliano (Grahn et al., 2013).

Já a parte superior da Formação São Domingos é composta principalmente por folhelhos negros, siltitos e arenitos de grão fino a médio. Os folhelhos representam um evento transgressivo de segunda ordem (Assine, 1996; Bergamaschi, 1999; Sedorko et al., 2018a) e se correlacionam com o *Kačák* (Horodyski et al., 2014), um evento transgressivo global (Bosetti et al. al., 2011). O ambiente sedimentar desta unidade é de *shoreface* a *offshore* (Grahn et al., 2013). Na parte noroeste da bacia há um intervalo regressivo acima do intervalo transgressivo, formado por arenitos e siltitos (Sedorko et al., 2021). O ambiente sedimentar desta unidade é estuarino (Sedorko et al., 2018a, 2021), sua espessura é de aproximadamente 150 m (Sedorko et al., 2018a) e sua deposição termina durante o Frasniano (Grahn et al., 2010, 2013).

A área de estudo corresponde à parte leste da sub-bacia do Alto Garças, a qual representa a parte norte da Bacia do Paraná (Fig. 2.1). Por outro lado, a sub-bacia de Apucarana, localizada ao sul, tinha um ambiente marinho mais raso e continha maiores proporções de arenitos e siltitos (Melo, 1988; Grahn et al., 2010). Como consequencia disso, essas unidades receberam nomes diferentes, denominadas unidades 1, 2, 3 e 4 do Grupo Chapada (Melo, 1988; Grahn et al., 2010).

As unidades do Grupo Chapada têm seus equivalentes com a parte sul da Bacia Paraná (Tabela 1; Fig. 2.2). A unidade 1 do Grupo Chapada correlaciona-se com a Formação Furnas (Melo, 1988; Grahn et al., 2013). A Unidade 2 do Grupo Chapada é dividida em duas partes, parte inferior correlaciona-se com a Formação Ponta Grossa e a parte superior com a Formação São Domingo inferior, Membro Tibagi (Grahn et al.,

2010, 2013). A Unidade 3 do Grupo Chapada correlaciona-se com a Formação São Domino, Membro Tibagi (Grahn et al., 2010, 2013). A unidade 4 do Grupo Chapada em sua parte inferior correlaciona-se com a parte superior do Grupo São Domingos aos folhelhos que representam um evento transgressivo de segunda ordem (Grahn et al., 2013) e sua parte superior está presente apenas na parte noroeste da Sub-bacia do Alto Garça, e são sequências regressivas formadas por arenitos e siltitos conhecidas como Formação São Domingo, chegando até o topo (Grahn et al., 2013; Sedorko et al., 2018; Scheffler et al. al., 2020).

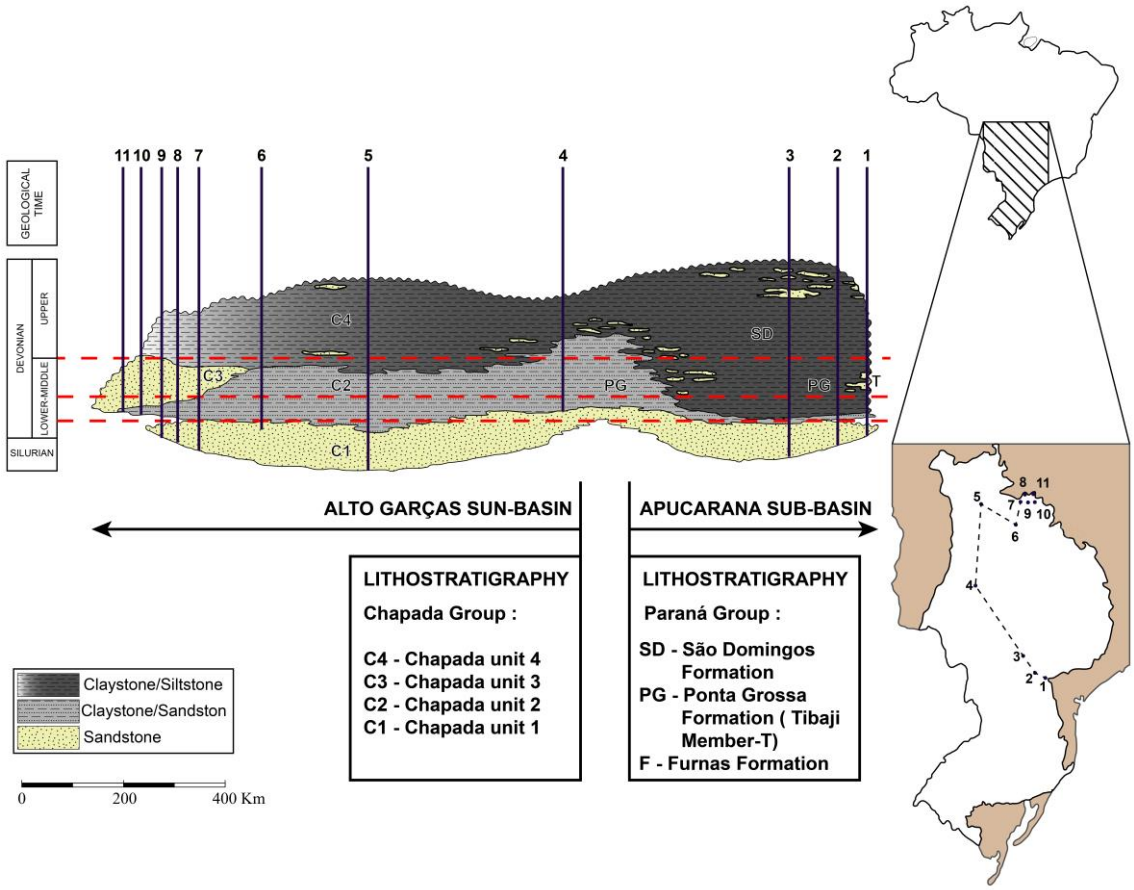

Figura 2.2 Perfil transversal de campo esquemático do Devônico da Bacia do Paraná mostrando a distribuição das unidades litoestratigráficas. (Dimensão vertical aproximadamente proporcional ao tempo geológico e sem relação com a espessura real dos sedimentos; a escala em km se refere a distâncias únicas e horizontais). Retirado de Melo (1988).

As paleocorrentes relatadas na parte norte da bacia do Paraná (Fig. 2.3; e.g., Bigarella & Oliveir, 1966; Assine, 1996; Santos et al., 2015; Vargas et al., 2020), em comparação coma Formação Furnas, apontam principalmente para oeste, sudoeste e noroeste, em menor grau na direção oposta, enquanto que a Formação São Domingos (Membro Tibagi) apontam principalmente para sudoeste. As orientações dessas paleocorrentes podem sugerir uma conexão lateral com as bacias Chaco-Salteña e Tarija.

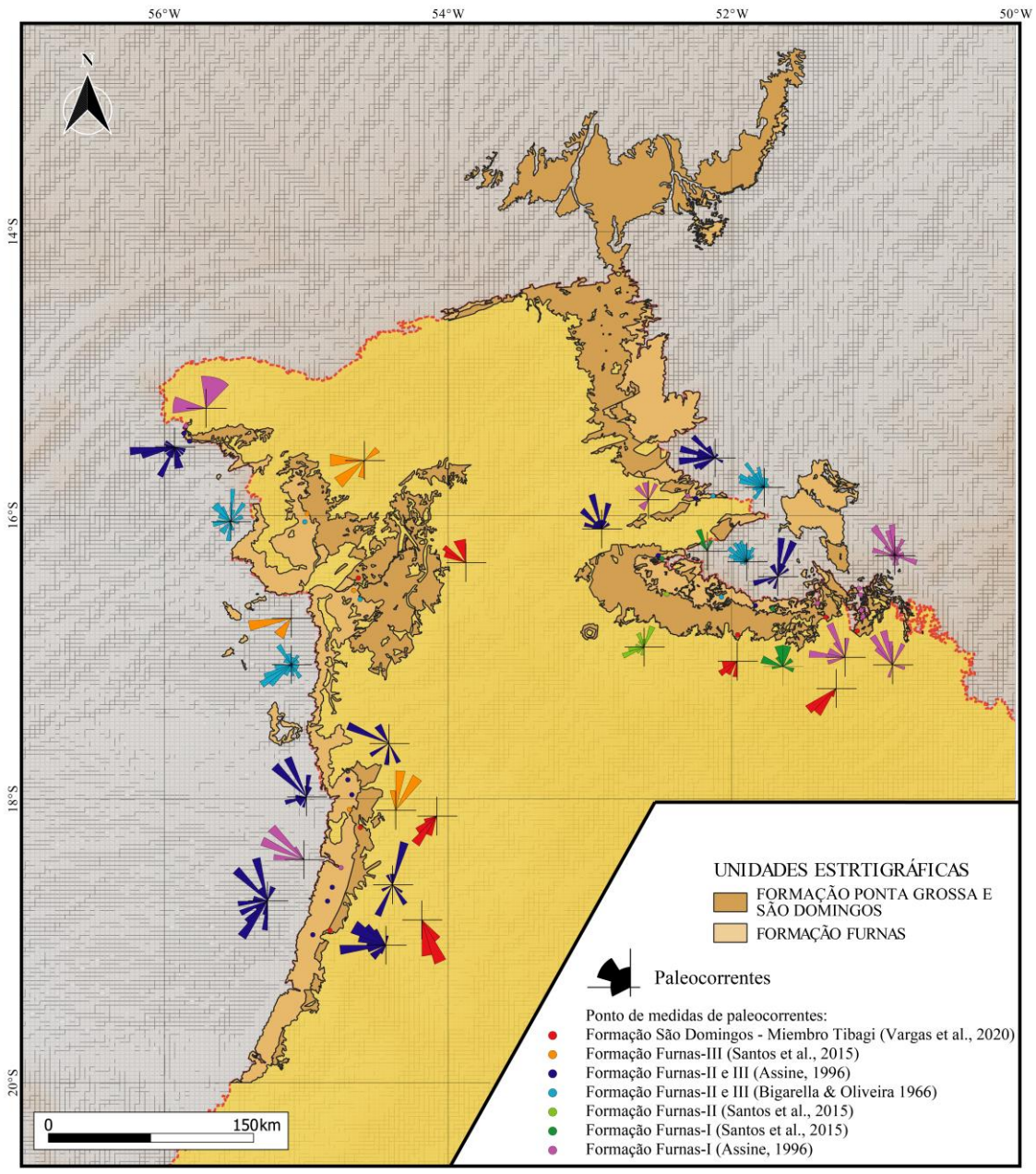

Figura 2.3. Paleocorrentes das formações Furnas, Ponta Grossa e São Domingos na parte norte da Bacia do Paraná.

2.2 Geologia Regional da Bacia do Paraná

A configuração geológica atual da Bacia do Paraná está composta por uma série de crátons (Amazonas, Rio Apa, Paranapanema e São Francisco) e cinturões orogênicos (Ribeira, Brasília e Paraguai) cobertos por sequências sedimentares do Paleozóico e Mesozóico (Fig. 2.4; Almeida et al., 1981). O seu registro sedimentar é composto por rochas sedimentares e vulcânicas com idades do Ordoviciano Médio ao Cretáceo Superior, consistindo em 6 sequências (Fig. 2.4; Zalán et al., 1990; Milani et al., 2007).

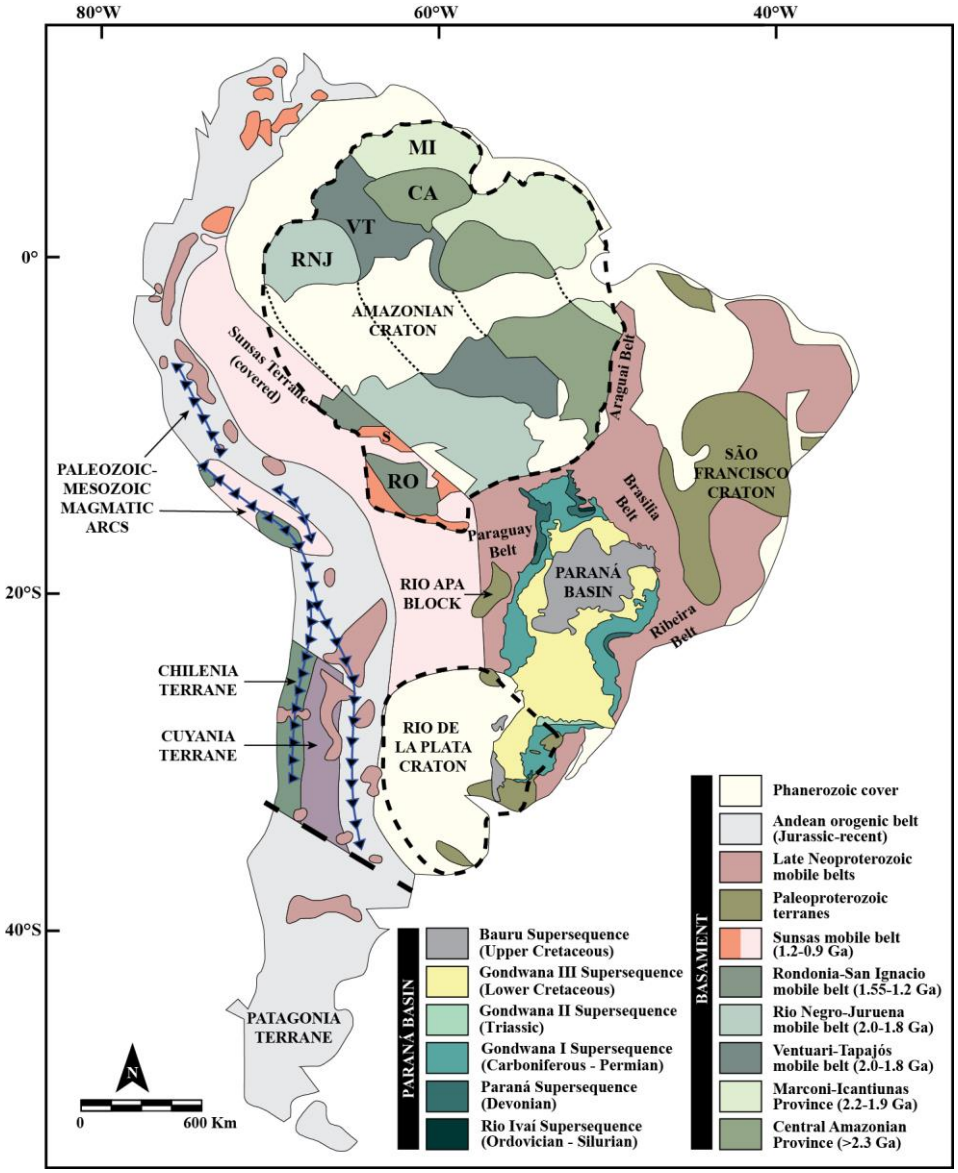

Figura 2.4. Mapa das províncias geotectônicas da América do Sul e supersequências da Bacia do Paraná (Cordani et al., 2000; Milani, 2004; Bahlburg et al., 2009).

2.2.1 Faixa Brasília

A Faixa Brasília tem orientação norte-sul e possui uma extensão de ~1100 km. Ela foi formada durante a colisão dos crátons Amazonas, São Francisco, Parapanema e blocos alóctones menores durante a Orogenia Brasileira no Neoproterozóico (Fuck et al., 1994; Pimentel, 2016).

A Faixa Brasília (Fig. 2.5) está localizada a NNE da área de estudo sendo composta por duas unidades tectônicas: zona interna e zona externa. A zona interna é subdividida em quatro unidades: Arco Magmático de Goiás, núcleo metamórfico,

Complexos Máfico-Ultramáficos e Maciço de Goiás (Pimentel e Fuck 1992; Fuck et al., 1994; Pimentel et al., 2000; Dardenne, 2000; Pimentel et al. al., 2004; Laux et al., 2005; Valeriano et al., 2008; Jost et al., 2010; Fuck et al., 2014; Cordeiro, 2014 e Pimental, 2016).

O arco magmático goiano é formado por duas porções, uma porção sul delimita com a parte norte da Bacia do Paraná denominada Arco Magmático de Arenópolis, com idades entre 916 e 630 Ma, e uma porção norte denominada Arco Magmático Mara Rosa com faixa etária entre 899 e 600 Ma (Pimentel & Fuck, 1992; Pimentel et al., 1999; Pimentel et al., 2003 e Matteini et al., 2010). O núcleo metamórfico é formado por dois complexos, o complexo Anapólis-Itauçu com faixa etária de 760 a 640 Ma (Piuzana et al. 2003b, Della Giustina et al., 2011; Pimentel, 2016) e o complexo Uruaçu com idade faixa de 690 a 651 Ma (Della Giustina et al., 2009). Os complexos Máfico-Utramáfico variam em idade de 1300 a 750 Ma (Ferreira Filho et al., 1994; Pimentel et al. 2004, 2006; Moraes et al. 2006).

O Maciço de Goiás é uma microplaca alóctone (Almeida, 1984; Jost et al., 2013) formada por metaplútons de 3100 e 2710 Ma (Pimentel et al. 2003), por greenstone belts de 2600 a 2100 Ma (Pimentel et al. 2003), por uma sequência vulcano-sedimentar, a sequência Campinorte, com idade máxima de deposição de ~2200 Ma (Giustina et al., 2009, Cordeiro et al., 2014) e por sequências sedimentares paleo-Mesoproterozóicas representadas pelos Grupos Araí, Traíras, Natividade e Serra da Mesa (Brito Neves, 2002; Toscani et al., 2021).

A zona externa da Faixa Brasília é um cinturão dobrado composto por sequências sedimentares de idade Meso-Neoproterozóica representada por seis grupos descritos abaixo com suas respectivas idades deposicional máxima obtidas em grãos de zircão detrítico: Grupo Bambuí, ~550 Ma (Kuchenbecker et al., 2020); Grupo Ibaí, ~640 Ma (Rodrigues et al., 2010; Dias et al., 2011); Grupo Araxá, ~650 Ma (Falci et al., 2018); Grupo Vazante, 935±14 Ma (Rodrigues et al. 2012); Grupo Canastra, ~1030 Ma (Rodrigues et al. 2010) e 1002±45 Ma (Bertoni et al. 2014) obtida pelo método Re-Os permitindo restringir a idade mínima de sedimentação; e o Grupo Paranoá, ~1540 Ma (Matteini et al. ., 2012) e 1042 Ma obtida no supercrescimento diagenético de xenotima em grãos de zircão restringindo a idade mínima de sedimentação (Matteini et al., 2012).

2.2.2 Faixa Paraguai

A Faixa Paraguai faz fronteira com a parte sudeste do Cráton Amazônico e com a parte ocidental do Bloco Rio Apa. Esta faixa é composta por sequências sedimentares ao longo de uma rampa continental que, posteriormente, foi dobrada e metamorfoseada durante a Orogenia brasileira (Almeida, 1984; Alvarenga et al., 2000).

A Faixa Paraguai (Fig. 2.5) está localizada a norte e oeste da área de estudo e constitui três domínios estruturais (Almeida, 1984; Alvarenga e Trompette, 1993): 1) uma plataforma de cobertura sedimentar, 2) uma dobrada e levemente metamorfoseada e 3) uma zona interna intensamente dobrada e metamorfoseada. A cobertura sedimentar da plataforma e da zona externa é composta por sequências sedimentares neoproterozóicas com idades entre 800 e 500 Ma (Pinho, 1990; Martinelli, 1998). A zona interna é composta pelas rochas metassedimentares do Grupo Cuiabá, com idade deposicional máxima de ~650 Ma com base em zircão detrítico (Babinski et al., 2018); e por duas suítes graníticas – ao sul, no estado de Mato Grosso do Sul, granitos sem colisão (Taboco 540±5 Ma, Rio Negro 547±5 Ma, Coxim 540±4 Ma e Sonora 548±6 Ma; Godoy et al., 2010), e ao norte pelos granitos pós-colisionais (São Vicente 518±4 Ma, Lajinha 505±4 e Araguaína 509±2 Ma; Godoy et al., 2010; McGee et al., 2012).

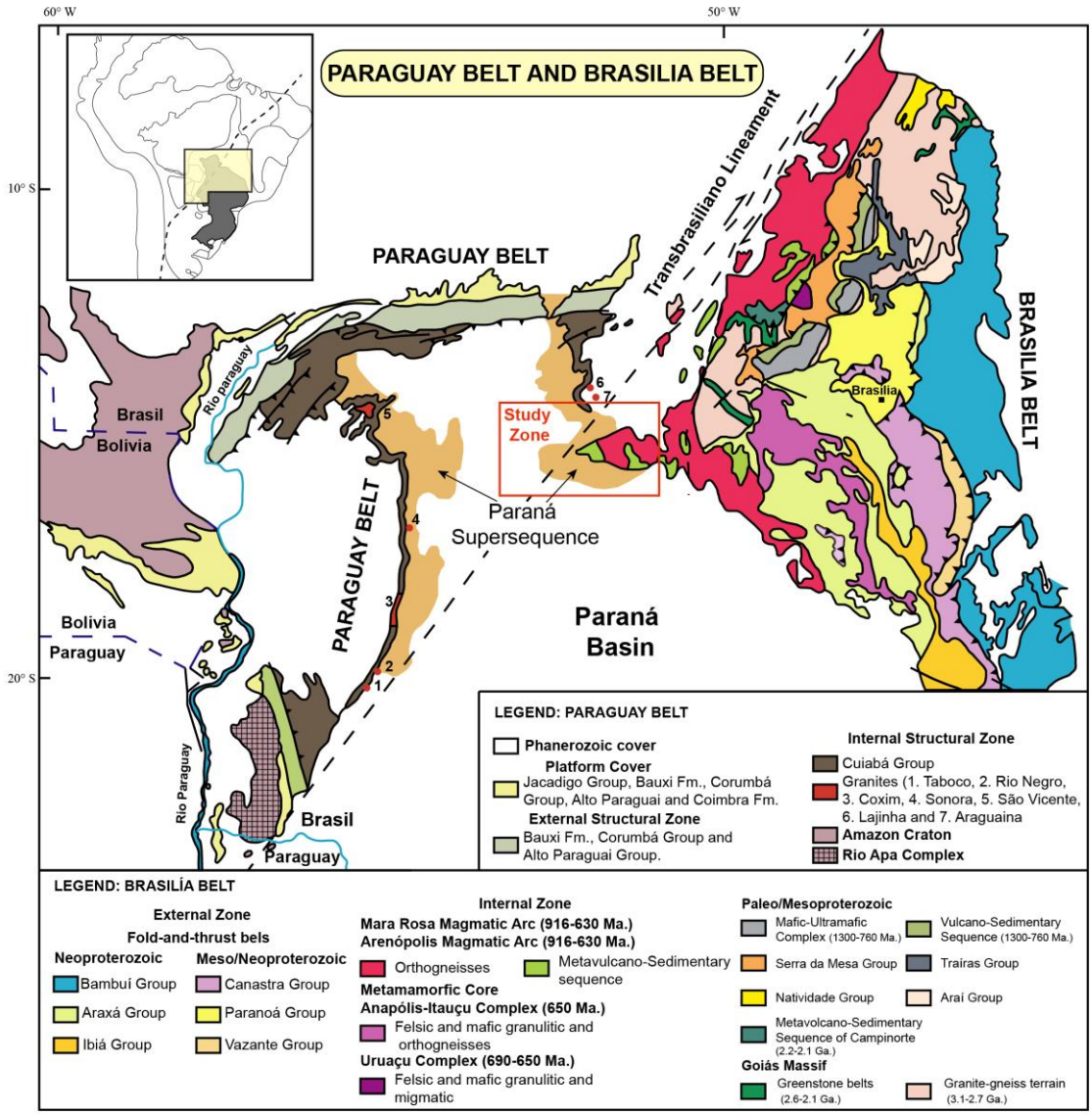

Figura 2.5. Mapa Geológico das Faixas Brasília e Paraguai (Modificado de Dardenne, 2000; Fuck et al., 2017).

2.3 Contexto geológico da América do Sul no Devoniano

Durante o Devoniano, no SW do Gondwana, houve um nível do mar mais alto do que o observado hoje (Albariño et al., 2000; Bergamaschi e Pereira, 2001; Uriz et al., 2016) e este evento tem sido reconhecido no registro de várias bacias ao redor mundo (Grabau, 1933; Haq e Schutter, 2008; Vargas et al., 2020). Nesse contexto, o Oceano Rheic inundou a margem SW do Gondwana gerando mares interiores, dominados por sistemas de depósitos siliciclásticos marinhos rasos (Melo, 1988; Torsvik e Cocks, 2013; Penn-Clarke et al., 2019; Vargas et al., 2020).

Durante o Devoniano Inferior ao Médio (Pragian/Emsian – Eifelian) existiu uma fauna endêmica nas diferentes Bacias do SW do Gondwana, denominada como Reino

Malvinokafrian (Fig. 2.6, Melo, 1988; Bosetti et al., 2012; Penn-Clarke, 2019, Sedorko et al., 2021). Essa fauna específica sofreu um declínio devido a um evento regressivo regional durante o Emsiano Médio causado pela atividade tectônica (Vargas et al., 2020). Na Bacia do Paraná essa diminuição do Reino Malvinokafrian foi registrada nos trabalhos de Bosetti et al. (2012) e Grahn et al. (2013). O Reino foi extinto por um evento transgressivo no Givetian que conectou essas bacias com mares mais frios e subtropicais temperados mais quentes no norte de Gondwana, gerando águas mais quentes no sul de Gondwana (e.g., Copper, 1977; Melo, 1988; Penn-Clarke, 2019; Vargas et al., 2020; Sedorko et al., 2021).

Nesse intervalo de tempo houve uma frente de colisão ativa ao oeste (e.g., Cawood, 2005; Nelson e Cottle, 2018) dividida por três setores de norte a sul: Setor Puneño, Setor Cuyano e Setor Patagônico (Heredia et al, 2016). No setor Puneño houve uma colisão entre a subplaca do Atacama com a placa Gondwana durante o Siluriano Médio – Devoniano, sendo parte da orogenia Oclóyica do Cambriano ao Carbonífero Inferior (Heredia et al, 2016). Uma subducção de mergulho de baixo ângulo neste setor durante o Devonian foi proposta por García et al. (2022).

No Setor Cuyano Inferior (Médio Devoniano) há início de subducção na margem leste da subplaca chilena, o qual gerou um orógeno tipo andino incipiente e um arco incipiente magmático que causou o fechamento do Oceano Chanico (Heredia et al., 2016, 2018). Este evento se correlaciona com a Orogenia Precordillera I (Milani e de Wit, 2008; Linol et al., 2015, Vargas et al., 2020). No Devoniano Médio a subducção da subplaca Cuyania sob a margem leste da subplaca Chilena gerou um complexo metamórfico de alta pressão levando à colisão entre as duas subplacas (Heredia et al., 2016, 2018). Esses eventos do desenvolvimento da subducção e o início da colisão estão correlacionados com a Orogenia Precordillera II (Milani e de Wit, 2008; Linol et al., 2015, Vargas et al., 2020), fazendo parte da Orogenia Chanica do Ediacarano ao Carbonífero Inferior, enquanto que os eventos orogênicos Precordillera I e II estão associados à Orogenia Precordillera (Milani e de Wit, 2008; Linol et al., 2015, Vargas et al., 2020). Dahlquist et al. (2021) propõe para o setor suroeste de Gondwana (27–32°LS) uma subducção normal até o início do Devoniano e do Devoniano Médio uma subducção de baixo ângulo até o início do Devoniano Superior.

No Setor Patagônico, após a colisão da Patagônia Ocidental com o Gondwana, iniciou-se uma subducção na margem oposta que gerou um arco magmático, cuja

atividade se iniciou no Devoniano e durou até o final do Carbonífero (Pankhurst et al., 2003, 2006; Heredia e outros, 2016).

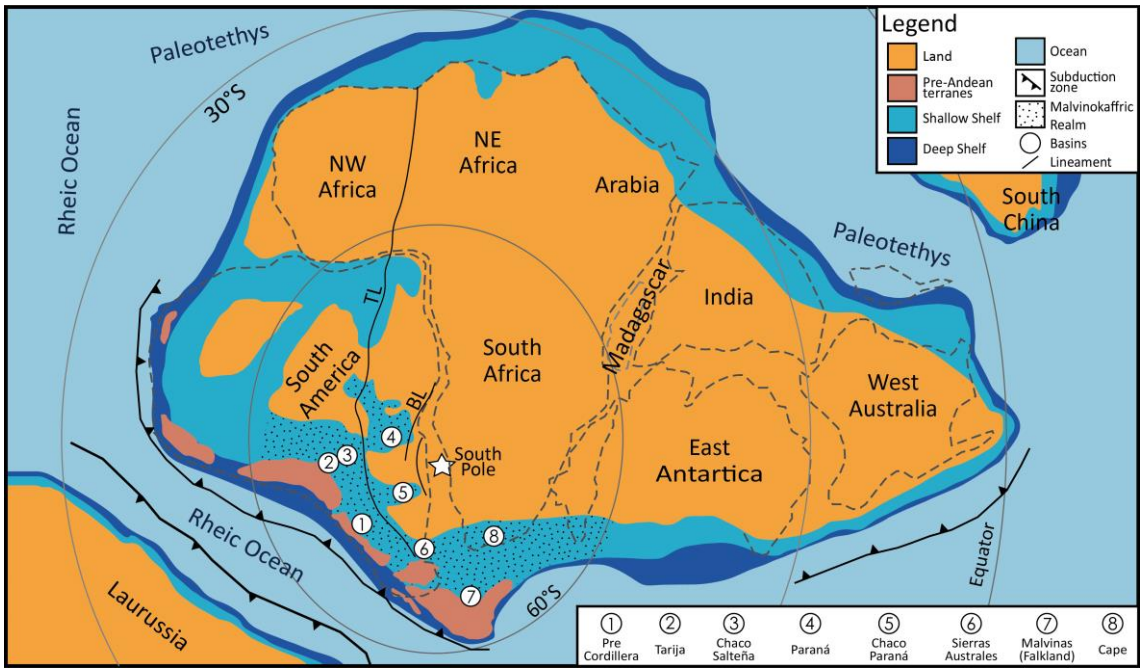

Figura 2.6. Paleogeografia do Devoniano Inferior de SW Gondwana. Terrenos pré-andinos, distribuição do Reino Malvinokafric e lineamentos regionais, como o Transbrasiliano (TL) e o Brasiliano (BL), conforme indicado na figura (Vargas et al., 2020; Sedorko et al., 2021).

CAPÍTULO 3 - AMOSTRAGEM E MÉTODOS

3.1 Amostragem

Os trabalhos de campo tiveram como objetivo principal coletar amostras das Formações Ponta Grossa e São Domingos, mas também foram coletadas amostras das sequências inferiores da Bacia do Paraná, Formação Furnas e Grupo Rio Ivaí (Formações Vila Maria e Alto Garças), no setor nordeste da bacia (Fig. 3.1; Zona A) entre os municípios de Barra do Garças, Iporá e Alto Garças.

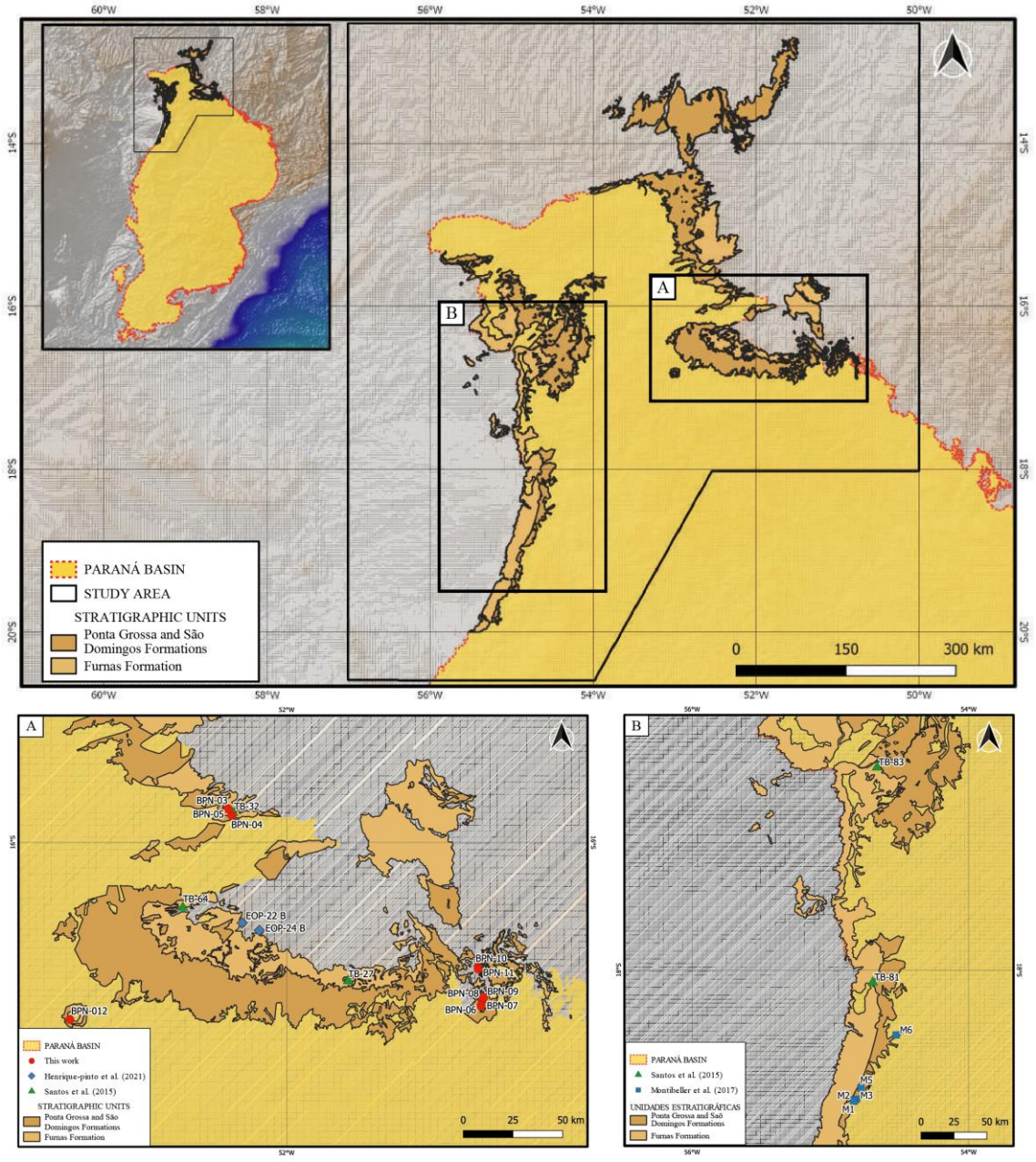

Figura 3. Mapa de afloramentos das unidades Devonianas da Bacia do Paraná e distribuição das amostras na área de estudo (Zona A e Zona B). Modificado de Montiebeller et al. (2017) e Vargas et al. (2020).

Um total de 19 amostras foram coletadas para análise laboratorial (Tabela 2): 7 amostras de arenito (aproximadamente 9 a 14 kg por amostra) foram selecionadas para serem analisados através do método de U-Pb em grãos de zircão detrítico; 11 amostras de folhelhos e siltitos, com aproximadamente 1 kg cada, foram coletadas para as análises de Sr-Nd; 6 amostras de arenitos selecionadas para as análises petrográficas; e 7 amostras entre folhelhos e siltitos foram coletadas para as análises de difratometria de raios-X.

Tabela 2. Amostras e técnicas aplicadas.

Leste	Norte	UNIDADE	TIPO DE ROCHA	AMOSTRA	METODOLOGIA
490111	8164660	Fm. São Domingos	Arenito	BPN-11A	Petrografia, U-Pb, morfologia de zircão
490111	8164660	Fm. São Domingos - Mb. Tibagi	Pelito	BPN-11B	XRD, Sr-Nd
363186	8248253		Pelito	BPN-3B	XRD, Sr-Nd
492063	8148155		Arenito	BPN-7A	Petrografia, U-Pb, morfologia de zircão
492063	8148155		Pelito	BPN-7B	XRD, Sr-Nd
492488	8149256		Arenito	BPN-8A	Petrografia, U-Pb, Zr morfologia
492488	8149256		Pelito	BPN-8B	XRD, Sr-Nd
489991	8165725	Fm. Ponta Grossa	Arenito	BPN-10A	Petrografia, U-Pb, morfologia de zircão
489991	8165725		Pelito	BPN-10B	XRD, Sr-Nd
492866	8149768		Pelito	BPN-9B	XRD, Sr-Nd
284111	8137088		Arenito	BPN-12A	Petrografia
491493	8145292		Arenito	BPN-6A	Petrografia, U-Pb, morfologia de zircão
491493	8145292		Pelito	BPN-6B	XRD, Sr-Nd
363218	8248054	Fm. Furnas	Pelito	BPN-5B	Sr-Nd
365150	8244761		Pelito	BPN-4B	Sr-Nd
363815	8245839		Arenito	BPN-1A	U-Pb, morfologia de zircão
363815	8245839		Pelito	BPN-1B	Sr-Nd
363851	8245792	Fm. Vila Maria	Pelito	BPN-2B	Sr-Nd
363840	8245861	Fm. Alto Garças	Conglomerado	CA-44	U-Pb

3.2 Petrologia de arenitos

Um total de 09 lâminas delgadas de arenito foram estudadas ao microscópio. Pelo menos 400 grãos foram contados pelo método do ponto de Gazzi-Dickinson proposto por Igersoll et al. (1984). A classificação petrográfica utilizada é a proposta por Garzanti (2019) e o esquema genético usado é o proposto por Dickinson (1985).

3.3 Difração de Raios-x (DRX)

A preparação das amostras foi realizada nas instalações do Laboratório de Estudos Geodinâmicos, Geocronológicos e Ambientais (LEGGA) da Universidade de Brasília. As análises de difração de raios X (DRX) foram realizadas em 7 amostras de folhelhos e siltitos na fração argila (<2 μm) das formações Ponta Grossa e São Domingos nos laboratórios do Instituto de Geocronologia e Geologia Isotópica (INGEIS) da Universidade de Buenos Aires e no Laboratório de Difração de Raios X (LARIX) do Instituto de Geociências.

No INGEIS foram preparadas 4 amostras (BPN 06B, BPN 07B, BPN 08B e BPN 10B) seguindo a metodologia proposta por Moore e Reynolds (1997) e no LARIX 3 amostras (BPN 03B, BPN 09B e BPN 11B) foram preparadas seguindo a metodologia proposta por Alves (1987).

As medições foram realizadas nas frações de argila orientada sob condições de secagem ao ar (AD), solvatação de etileno glicol (EG), solvatação de glicerol (GL) e aquecimento a 500°C (H). A identificação dos minerais constituintes das rochas pelíticas foi realizada por meio de difratogramas com auxílio do software Profex 4.3.3 (Döbelin e Kleeberg, 2015). A nomenclatura proposta por Fazio et al. (2019) para determinar a quantidade desses minerais como constituintes maiores (M), menores (m) ou traço (tr) foi estabelecido comparando as intensidades em difratogramas das reflexões com d em torno de 4,26 Å para o quartzo, 7 Å para caulinita, 10 Å para illita, 2,7 Å para hematita, 3,18 Å para plagioclásio, 3,25 Å para feldspato de potássio e potássio, 4,18 Å para goetita e 7 para clorita. A abreviatura do mineral foi retirada de Whitney e Evans (2010).

3.4 Estudos isotópicos Sm-Nd e Sr-Sr em rocha total

As análises isotópicas de Sm-Nd seguiram o método descrito por Gioia & Pimentel (2000). Neste procedimento cerca de 50 mg de amostra pulverizada é misturada a uma solução traçadora de ^{149}Sm e ^{150}Nd. A amostra é dissolvida em cápsulas de Savillex por meio de sucessivos ataques ácidos em HF, HNO3 e HCl. Os conteúdos de Sm e Nd são extraídos através de colunas de trocas catiônicas, confeccionadas em Teflon e preenchidas com resina LN-Spec. Os sais de Sm e Nd são depositados em filamentos de rênio com ácido nítrico e evaporados. As leituras das razões foram realizadas no espectrômetro de massas multicolector, modelo Finnigan MAT 262 em modo estático. As incertezas para as razoes de Sm/Nd e $^{143}Nd/^{144}Nd$ são inferiores a ±0.5% (2σ) e ±0.005% (2σ), respectivamente, baseados em repetidas análises nos padrões internacionais BHVO-1 e BCR-1. A razão $^{143}Nd/^{144}Nd$ foi normalizada em função da razão $^{146}Nd/^{144}Nd$ de 0,7219.

Para a determinação da razão $^{87}Sr/^{86}Sr$ foi seguido procedimento apresentado por Gioia et al. (1999), no qual cerca de 50 mg de rocha total pulverizada é pesada e adicionado 1 ml de ácido acético (0,5 N). Este material é centrifugado e o sobrenadante evaporado. O resíduo é dissolvido em 1 ml de HCl (6N) e a solução passa por coluna de troca catiônica para a extração do Sr. A coluna é preenchida pela resina Sr-spec (Dt Bu

CH18-C6 em 1-octanol). O sal de Sr é depositado em filamento e as leituras realizadas em processo idêntico ao método Sm-Nd, descrito acima.

3.5 Geocronologia U-Pb em Zircão

As amostras selecionadas foram desagregadas, peneiradas, e a fração menor que 250 µm foi selecionada. Posteriormente, o material foi bateado visando a pré-concentração dos minerais pesados. O concentrado obtido foi posto para secar sob lâmpada e em seguida passado no separador magnético Frantz. Depois disso, o concentrado de minerais pesados não magnéticos foi analisado via lupa binocular onde os grãos de zircão detrítico foram separados manualmente. 150 grãos de zircão foram dispostos aleatoriamente em um *mount* de resina epóxi e polidos, de forma a expor as partes internas dos grãos.

Os grãos de zircão foram separados manualmente em lupa binocular. Estudos prévios de catoluminescência (CL) e de elétrons retro-espalhados (BSE) foram realizados nos grãos de zircão com o objetivo de fornecer imagens de detalhes dos cristais estudados. Além disso, estes estudos possibilitaram a identificação de fraturas, inclusões e áreas com sobrecrescimento irregular dos zircões que devem ser descartados para análise. Essa fase foi realizada no Laboratório de Microanálises no DEGEO/UFOP.

As análises isotópicas U-Pb foram obtidas utilizando-se de um ICP-MS, modelo Thermo Scientific Element 2 sector field (SF), acoplado a um sistema de laser CETAC LSX-213 G2. O tamanho e a frequência do laser foram ajustados em 40 µm e 10 Hz, respectivamente. Os dados obtidos foram tratados e reduzidos com auxílio do software Glitter (Van Achterbergh et al. 2001) e os dados U-Pb foram plotados utilizando o programa Excel Isoplot 4 (Ludwig, 2003). Como padrão primário foi utilizado o zircão GJ-1 (608±1 Ma; Jackson et al. 2004) e para o controle da qualidade foi utilizado como padrão secundário o zircão Plesovice (337±1 Ma, Sláma et al., 2008). As idades dos grãos com discordância >10% foram rejeitadas neste estudo, baseados no trabalho de Gehrels (2011). As idades $^{206}Pb/^{238}U$ são usadas para os grãos com idades menores de 1300 Ma, enquanto as idades $^{207}Pb/^{206}Pb$ são usadas para os grãos com idade superior a 1000 Ma, seguindo as indicações de Dickinson & Gehrels (2003).

CAPÍTULO 4 – ARTIGO

RELATIVE SEA-LEVEL CHANGES: A CASE STUDY OF SEDIMENTARY PROVENANCE ANALYSIS FOR THE DEVONIAN PARANÁ GROUP IN NORTHERN PARANÁ BASIN, BRAZIL

Wilson López Abanto[1], Natalia Hauser[1], Arnold Garcia Zavaleta[1], Cristiano de Carvalho Lana[2], Pamela Aparicio González[3], Joyce de Souza Ribeiro[1], and Wolf Uwe Reimold[1]

[1]Laboratório de Geocronologia, Instituto de Geociências, Universidade de Brasília, Brasília, Brasil.
Instituto de Ecorregiones Andinas, INECOA-CONICET, Jujuy, Argentina. Jujuy, Argentina.
[2]Departamento de Geologia - Escola de Minas, Universidade Federal de Ouro Preto, Campus Morro do Cruzeiro, Minas Gerais, Brasil.
[3]UBA - INGEIS – CONICET, Universidad de Buenos Aires, Buenos Aires, Argentina.

Abstract

Three major second order sea level variations have been registered during the Devonian in the SW part of Gondwana. The last one, of global significance, was recognized in different basins of South America. In the Paraná Basin, the Devonian interval and sea level variation are well constrained in the Furnas, Ponta Grossa and São Domingos (plus Tibagi member) formations. In this sense, the Furnas Formation is related with a rising sea level and the shales of Ponta Grossa represent the maximum flood surface of this first transgression. The Tibagi Member of the São Domingos Formation sandstones are related with a fall of the sea level of the second event, whereas the third event is well represented by the shales of the upper part of the São Domingos Formation. Considering the present geographic configuration of South America as a proxy for the Devonian paleogeography of the Paraná Basin, and in order to track these variations, provenance analyses by U-Pb in detrital zircon and Sr-Nd and DRX analysis were applied to the Devonian sequence of the Northern Paraná Basin. The main findings are: 1) All units show provenance from proximal, intermediate and distal sources, represented by the Goiás Magmatic Arc (~630 Ma - proximal sources), Serra da Mesa and Paranoá groups (~1770 Ma and 2100 Ma for Serra da Mesa and only ~2100 Ma for Paranoá Group), and from the Goiás Block (~2420 Ma) – all representing intermediate sources, and from the Sunsas-Aguapeí Belt (~900-1200 Ma, – distal/very distal sources). Also, the values of εNd(380 Ma) are not very variable and range from -10.6 to -12.4, and in the diagram Age (Ga) versus εNd, a general increase of older crustal sources is observed. 2) the main differences between these units are a peak at ~2604 Ma only observed for the upper part of the São Domingos Formation and a peak at ~435 Ma observed for the Ponta Grossa and São Domingos formations, but not for the Tibagi Member,3) The upper part of the São Domingos Formation that represents the third transgressive event shows provenance from very distal sources, like the Trairas Group (with a ~2600 Ma diagnostic peak) that would be the basement of the Brasilia Belt to the east and the Famatinian Magmatic Arc (peak of ~435 Ma) from the west in the Andean region. 4) The $^{87}Sr/^{86}Sr_{(380)}$ ratios and the TDM values show a decrease when there are contributions from younger sources, as is the case of the Ponta

Grossa Formation and the upper part of the São Domingos Formation where there is the presence of younger sources associated with the Famatinian Magmatic Arc. The Famatinian ages could be related directly with provenance from the reworked section in the Tarija Basin, located to the west and probably connected to the Paraná Basin at that time. Thus, the distal/very distal sources are observed for the first transgression, represented by the Ponta Grossa Formation, and then register again for the second transgression, the upper part of the São Domingos Formation.

1. INTRODUCTION

Throughout geological history, the global sea level has experienced significant variations (e.g., Vail et al., 1977; Miller et al., 2005; Haq and Schutter, 2008) that gave rise to transgressive cycles (sea level rise) and regressive (lowering sea level), often well defined in the stratigraphic record (e.g., Haq et al., 1987; Hallam, 2001; Haq and Al-Qahtani, 2005; Ruban, 2011). For example, the study by Gale et al. (2008) in the Cenomanian in the US Western Interior Basin and by Ruban (2011) study in the Lochkovian along "Tethyan" Gondwana.

These sea level variations are known as “eustasy”, defined by Suess (1906) as any uniform global change in sea level that may reflect a change in the amount of water in the ocean, or a change in the shape and capacity of ocean basins. The main causes of these variations are climatic changes and tectonics (Rovere et al., 2016). For example, the buildup and subsequent melting of ice sheets is controlled by climate, and the rise and subsidence of continental blocks is controlled by regional tectonics, which can cause, intensify, or reverse these sea level variations (e.g., Moucha et al., 2008; Ruban, 2011; Ruban et al., 2012; Ruban and Conrad, 2013).

During the Paleozoic, approximately 172 eustatic events were recorded worldwide with variations in magnitude from tens to more than one hundred meters (Haq and Schutter, 2008). Specifically, during the Devonian (ca. 420 to 360 Ma) a high sea level was recorded in different parts of the world (Haq and Schutter, 2008). In southwestern Gondwana, this flood was of the Tectonic/Eustatic type and favored shallow siliciclastic marine deposition in various basins (Vargas et al., 2020), therefore, this time interval was very important in the evolution of the South American basins (Haf and Shutter, 2008; Vargas et al., 2020). At the same time, to the west there was an active collision front associated with the Precordilleran Orogeny (Milani and de Wit, 2008; Linol et al., 2015), which would have generated local variations in sea level. In addition, according to

Heredia et al. (2016) and Heredia et al. (2018), the Ocloyic and Precordilleran orogenies are related to the Puna and Cuyania sectors, respectively.

The Paraná basin, with 1.5 x 10^6 km^2 (Fig. 1), is one of the most important intracratonic basins developed on the South American platform during the Paleozoic of SW Gondwana (Almeida, 1980; Milani et al., 2007; Henrique-Pinto et al., 2021). It is located in the center-south of Brazil and in part of Uruguay, Paraguay and Argentina. The infill is approximately 7,000 m thick and is made up of sedimentary and volcanic rocks with ages ranging from the Middle Ordovician to the Late Cretaceous (Zalán et al., 1990; Milani et al., 2007). Two sub-basins were identified (Melo, 1988; Grahn, 1992), Alto Garças to the north and Apucarana to the center south. The sedimentary fill was divided by Milani et al. (2007) in six Supersequences (Fig. 1): Rio Ivaí (Ordovician-Silurian), Paraná (Silurian-Devonian); Gondwana I (Carboniferous-Lower Triassic); Gondwana II (Triassic) Gondwana III (Upper Jurassic-Lower Cretaceous) and Baurú (Cretaceous)

The Paraná Supersequence in the Alto Garças sub-basin has different types of studies such as paleontological (Carvalho et al., 1987; Marques, 2006; Carbonaro and Ghilardi, 2016; Carbonaro et al., 2018; Ribeiro et al., 2021), sedimentological (Alvarenga and Guimarães, 1994; Assine, 1996; Alvarenga et al., 1998; Asesine et al., 1998; Milanie et al., 2007), paleoenvironmental (Melo, 1988; Grahn et al., 2010; Sedorko et al., 2018c; Sedorko et al., 2021) and geochemists (Montibeller et al., 2017) works. Sedimentary provenance studies through methods such as U-Pb in detrital zircon can be summarized in the works of Santos et al. (2015) and Henrique-Pinto et al. (2021). There are currently no works on Sr-Nd isotopic geochemistry in the Devonian units. The studies by Enrique-Pinto et al. (2021, 2023) suggests that the Famatinian magmatic arc and the Eastern Pampean Cordillera have been exposed in the back thrust sector because of the Ocloyic and Precordilleran orogenies, and these contributed as secondary Cambrian-Ordovician sources to the Río Ivaí and Paraná groups.

Recently, Vargas et al. (2020) recognized second order transgressive-regressive (T-R) sequences in the Devonian units (Paraná Supersequence), which correspond to the lithostratigraphic units of the Ponta Grossa (transgressive sequence) and São Domingos (regressive sequence) Formations, respectively. According to Vargas et al. (2020), these surfaces of maximum transgression and regression corresponded to tectonic and eustatic events that could be regionally correlated with the Devonian units of other basins in SW

Gondwana, like Tarija, Chaco-Salteña, Chaco-Paraná, Precordillera, Sierras Australes, Malvinas and Cape. For that reason, the devonian units of Paraná basin becomes interesting because provide important information to understand the processes related with transgressive-regressive (T-R) cycles. In this study, the term is used the second-order (ca. 6^6 –12^6 yr) sequence of the hierarchical proposal of Mitchum and Van Wagoner (1991) with the associated time lapse according to Schlager (2010).

The U-Pb dating on method in detrital zircon, a powerful method for the reconstruction of the different sedimentary processes in the crust (Dickinson and Gehrels, 2008; Gehrels, 2014), was widely used to recognize orogenic events, understand the tectonic configuration, and reconstruct the paleogeography of a basin (e.g., Park et al., 2010; Cawood et al., 2012; Zhao et al., 2020; Sorcar et al., 2020 between several others). Associated with tectonics or not, a basin also registers changes in sea level, which would be indicated by the variation in the distribution of the U-Pb ages of the detrital zircons grains (Lee et al., 2021).

The aim of this work is to carry out a case study of sedimentary provenance through the U-Pb methods on detrital zircon, for the second order transgressive-regressive (T-R) cycles of Ponta Grossa and São Domingos Devonian units (Lange & Petri, 1967; Grahn, 1992) in the Alto Garças sub-basin of the Paraná basin. This study has been encouraged by the fact that: 1) the transgressive-regressive (T-R) cycles in the Alto Garças sub-basin for the Devonian were well defined (Vargas et al., 2020) and 2) the potential source areas of the sediments to the Paraná basin, divided by us in proximal, intermediate and distal/very distal, have contrasting U-Pb ages. A direct comparison with Sr-Nd isotopes and X-ray diffractometry (XRD) in the fine equivalents units (pelites), will be use to understand the potential of several techniques in drawing the rules that dominate the sedimentary processes associated with sea level variations.

Through the identification of the potential sedimentary provenance areas, here we intended to verify if there are variations in the provenance areas between the basal and upper units and if these could be associated with the variations in sea level recognized by Vargas et al. (2020). The integration of our data with previously published one (e.g., Gezatt 2011; Santos et al., 2016; Henrique-Pinto et al., 2021) will allow us to understanding the evolution of the northern part of the Paraná Basin in the Ordovician-Devonian interval. At the same time, it will be possible to correlate the data obtained with

the southern sector of the basin and other Devonian basins of SW Gondwana, such as Tarija, Chaco-Salteña, Precordillera, Chaco-Paraná, Sierras Australes, Malvinas and Cape. Overall, it will be possible to have a better understanding of the evolution of the basins to the SW of Gondwana in the Devonian interval in relation to the ages of detrital zircons grains reported in the stratigraphic units in these basins.

2. GEOLOGICAL SETTING

Archaean and Paleoproterozoic cratonic terranes are part of the Tocantins Province (Almeida et al., 1977, 1981), which is the most important geological province in the in Central Brazil. The Tocantins tectonic province, registered the convergence and collision of Amazonas, São-Francisco-Congo and Paranapanema paleo-continents (Pimentel et al., 2011). It is composed by three orogenic belts, Brasilia, Paraguay, and Araguaia, which represents part of the basement of the Paraná basin. The Transbrazilian Lineament (Schobbenhaus et al., 1975) is an important structure located northwest of the study area and corresponds to the last tectonic event related to the Braziliano/Panafrican Orogenic (Cordani et al., 2009). This structure represents a boundary between the Brasilia and Paraguay belts.

The northern part of the Paraná basin is mainly boundary by the Brasilia and Paraguay belts. The Brasilia Belt has a north-south orientation and an extension of ~1100 km, formed during the collision of these three paleocontinents, and minor allochthonous blocks, during the Neoproterozoic Brazilian Orogeny (Fuck et al., 1994; Pimentel, 2016). Whereas the Paraguay Belt borders the southeast of the Amazonian Craton and the western part of the Rio Apa Block, it is made up of sedimentary sequences along a continental ramp, which was later folded and metamorphosed during the Brazilian Orogeny (Almeida, 1984; Alvarenga et al., 2000).

2.1 The Tocantins Province: the Brasilia and Paraguay belts

The Brasília belt (Fig. 2) is located at the NNE of the study area and is composed by two tectonic units, denominated as internal zone and external zone. The internal zone is subdivided into four units: Goiás Magmatic Arc, metamorphic core, Mafic-Ultramafic Complexes and the Goiás Massif (Pimentel and Fuck 1992; Fuck et al., 1994; Pimentel et al., 2000; Dardenne, 2000; Pimentel et al., 2004; Laux et al., 2005; Valeriano et al., 2008; Jost et al., 2010; Fuck et al., 2014; Cordeiro, 2014 and Pimental, 2016). The Goiás magmatic arc is composed by two segments, a southern segment named the Arenópolis

Magmatic Arc, which delimits the northern part of the Paraná basin, with ages between 916 and 630 Ma, and a northern portion, named the Mara Rosa Magmatic Arc with arrange in ages between 899 and 600 Ma (Pimentel & Fuck, 1992; Pimentel et al., 1999; Pimentel et al., 2003 and Matteini et al., 2010).

The metamorphic core is composed by two complexes, the Anapólis-Itauçu complex with ages range from 760 to 640 Ma (Piuzana et al., 2003b; Giustina et al., 2011; Pimentel, 2016) and the Uruaçu complex with age between 690 and 651 Ma (Della Giustina et al., 2009). The mafic-ultramafic complexes range in age from 1300 to 750 Ma (Ferreira Filho et al., 1994; Pimentel et al., 2004, 2006; Moraes et al., 2006). The Goiás Massif was interpreted as an allochthonous microplate (Almeida, 1984; Jost et al., 2013) that is made up of metaplutons with ages of 3100 and 2710 Ma (Pimentel et al., 2003), sequences of greenstone belts with an age range from 2600 to 2100 Ga (Pimentel et al., 2003), the Campinorte metavolcanosedimentary sequence which have a maximum deposition ages of ~2200 Ma (Giustina et al., 2009; Cordeiro et al., 2014), and the Paleo-Mesoproterozoic sedimentary sequences represented by the Araí, Traíras, Natividade, and Serra da Mesa Groups (Brito Neves, 2002; Toscani et al., 2021).

The outer zone, which correspond to is a folded belt, is composed of sedimentary sequences of Meso-Neoproterozoic ages developed in different basins. The Paranoá Group, represens a passive margin sequence to the São Francisco paleo-continent that has a maximum depositional age of ~1540 Ma (Matteini et al., 2012). A youngest age obtained on the xenotime that overgrowth zircon during the diagenesis (Matteini et al., 2012) allows to constraint their minimum sedimentation age to 1042 Ma. A lateral equivalent to the Paranoá Group, the Canastra Group which has a maximum depositional age of ~1030 Ma (Rodrigues et al., 2010) have also a Re-Os isochron age (Bertoni et al., 2014) that constraint the sedimentation age to 1002 ± 45 Ma. The Vazante Group is also related with sequence of passive margin and has a maximum depositional age of 935 ± 14 Ma (Rodrigues et al., 2012), Youngest metavolcano-sedimentary sequences like the Ibiá Group with a maximum depositional age of ~640 Ma (Rodrigues et al., 2010; Dias et al., 2011) and Araxá Group with a maximum depositional age of ~650 Ma (Falci et al., 2018; Piauilino et al., 2021) registered the evolution in marginal basins. Additionally, the Bambuí Groups, which have a maximum deposition age of ~550 Ma (Kuchenbecker et al., 2020) was deposited into a foreland basin.

The Paraguay belt (Fig. 2) is located NNW of the study area and is made up of three structural domains (Almeida, 1984; Alvarenga and Trompette, 1993): 1) a platform sedimentary cover, 2) an external and slightly metamorphosed folded zone and 3) an internal zone intensely folded and metamorphosed. The sedimentary cover of the platform and the external zone is composed of Neoproterozoic sedimentary sequences with ages between 800 and 500 Ma (Pinho, 1990; Martinelli, 1998). The inner zone is composed of the metasedimentary rocks of the Cuiabá Group, which has a maximum depositional age of ~650 Ma (Babinski et al., 2018). Two granite suites were identified to the south and to the north. To the south in the State of Mato Grosso do Sul were recognized non-collision granites (Godoy et al., 2010), like Taboco (540 ± 5 Ma), Rio Negro (547 ± 5 Ma), Coxim (540 ± 4 Ma) and Sonora (548 ± 6 Ma). To the north part in the State of Mato Grosso were identified post-collision granites (Godoy et al., 2010; McGee et al., 2012) like São Vicente (518 ± 4 Ma), Lajinha (505 ± 4) and Araguaina (509 ± 2 Ma).

2.2 The main tectonic events of SW Gondwana during Devonian times

During the Devonian interval, there was an active collision front to the west (e.g., Cawood, 2005; Nelson and Cottle, 2018). Heredia et al. (2016) divided it in three sectors that from the North to the South were: Puneño, Cuyano and Patagonian sectors.

In the Puneño sector, the Ocloyic orogeny from the Cambrian to the Lower Carboniferous (Heredia et al., 2016), was result of the collision between the Atacama subplate agains Gondwana plate (Middle Silurian - Devonian).

In the Cuyano Sector, as a consequence of the subduction started on the eastern margin of the Chilenia subplate, an incipient magmatic arc of Andean-type was installed between the Lower to Middle Devonian. The subduction of Cuyania with Chilenia, as part of the Precordilleran Orogeny I event (Fig. 3; Milani and de Wit, 2008; Linol et al., 2015 and Vargas et al., 2020) caused the closure of the Chanic Ocean (Heredia et al., 2016, 2018). In the Middle Devonian the subduction of Cuyania under the eastern margin of Chilenia generated a high-pressure metamorphic complex, which finished with the collision between Chilena and Cuyania subplates (Heredia et al., 2016, 2018). This event is correlated with Precordilleran Orogeny II (Fig. 3; Milani and de Wit, 2008; Linol et al., 2015; Vargas et al., 2020), these events are part of the Chanic Orogeny from the Ediacaran to the Lower Carboniferous, the Precordilleran I and II orogenic events are associated with the Precordilleran Orogenic (Milani and de Wit, 2008; Linol et al., 2015; Vargas et

al., 2020). Dahlquist et al. (2021) proposed for this sector a normal subduction until the beginning of the Devonian and from the Middle Devonian, a low-angle subduction that lasted until the beginning of the Upper Devonian.

In the Patagonian Sector, after the collision of western Patagonia with Gondwana, subduction began on the opposite margin that generated a magmatic arc, whose activity began in the Devonian and lasted until the late Carboniferous (Pankhurst et al., 2003, 2006; Heredia et al., 2016).

2.3 The transgressive-regressive cycles of SW Gondwana

The Devonian time, was characterized by a sea level, much higher than the one observed today (e.g., Albariño et al., 2000; Bergamaschi and Pereira, 2001; Uriz et al., 2016). The Rheic Ocean flooded the SW margin of Gondwana, generating inland seas, dominated by shallow marine siliciclastic deposit systems (Melo, 1988; Torsvik and Cocks, 2013; Penn-Clarke et al., 2019; Vargas et al., 2020). For that reason, it was recognized in the record of several basins around the world (e.g., Grabau, 1933; Haq and Schutter, 2008; Vargas et al., 2020).

During the Lower to Middle Devonian (Pragian/ Emsian – Eifelian), there was registered an endemic fauna in different basins of SW Gondwana, the *Malvinokaffric Kingdom* (Melo, 1988; Bosetti et al., 2012; Penn -Clarke, 2019; Sedorko et al., 2021). This *Malvinokaffric Kingdom* suffers a decline due to a regional regressive event in the Middle Emsian caused by tectonic activity (Vargas et al., 2020). In the Paraná Basin this decrease of the *Malvinokaffric Kingdom* was recorded by Bosetti et al. (2012) and Grahn et al. (2013). A transgressive global event in the Givetian connected the SW Gondwana basins of cooler waters with subtropical seas of northern Gondwana increasing the temperature of SW Gondwana basins and the extinction of the *Malvinokaffric Kingdom* (Copper, 1977; Melo, 1988; Penn-Clarke, 2019; Vargas et al., 2020; Sedorko et al., 2021).

The first transgression (Lower Devonian)

The transgression at the Lower Devonian was responsible for the generation of facies of shallow to deep sedimentary environments that were generated under strong structural control (Sedorko et al., 2019; Vargas et al., 2020). A maximum transgression limit (i.e., maximum flood surface) of second order was estimated close to the Pragian-Emsian (e.g., Daemon et al., 1967; Grahn et al., 2013; Varga et al., 2020; Sedorko et al., 2021). This

interval corresponds to the Ponta Grossa Formation of the Paraná Basin and its upper limit corresponds to the maximum second-order flooding surface at the regional level (Fig. 3 and 4). A great diversity of the Malvinokaffric kingdom developed in the different basins to SW Gondwana (Carrera et al., 2019; Sedorko et al., 2021).

The first regression (Lower to Middle Devonian)

In the Lower to Middle Devonian there is a regressive interval composed mainly by sandstones (Assine et al., 1998), with a maximum regression limit (i.e., surface of maximum regression) of second order estimated in the Upper Emsian – Eifelian (e.g., Assine, 1996; Sedorko et al. 2018b; Vargas et al., 2020). In the Paraná basin this first regression is represented by the Tibagi Member of the São Domingos Formation. Its upper limit corresponds to the maximum second-order regression surface at the regional level (Fig. 3, 4). This event was probably produced by tectonic activity (Precordillera II), that influenced the decrease of *Malvinokaffric Kingdom* diversity in different basins to SW Gondwana (e.g., Bosetti et al., 2012; Grahn et al., 2013; Sedorko et al., 2021).

The second transgression (Middle-Upper Devonian)

The Middle to Upper Devonian, is represented by a transgressive interval, with an estimated maximum transgression limit (i.e., maximum flood surface) of the second order at the Givetian (e.g., Lange, 1967; Grahn et al., 2013, Milani et al., 2007; Sedorko et al., 2018b; Vargas et al., 2020). In the Paraná basin this second transgression is represented by the upper part of the São Domingos Formation and its upper limit corresponds to the maximum second-order flood surface at a global level (Fig. 4) correlated with the global eustatic maximum (Haq and Schutter, 2008), at the same time, this interval is correlated with the global anoxic event *Kačák* that caused the extinction of the *Mavinokaffric Kingdom* (House, 1996; Horodyski et al., 2014; Sedorko et al., 2021)

According to Vargas et al. (2020), the Precordillera I event (Lower Devonian) controlled the variation of sea level, associated with the deposition of the Ponta Grossa Formation. The Precordillera II event (Middle-Upper Devonian) controlled the sea level variations at the beginning of the deposition of the São Domingos Formation (Tibagi Member).

2.4 T-R cycles in the Paraná Supersequence: the Ponta Grossa and São Domingos formations

The Paraná Supersequence is represented by the lithostratigraphic unit of the Paraná Group (Silurian – Devonian), with ~ 400 m of thickness, which in turn is subdivided into formational units that, according to several authors (e.g., Oliveira, 1912; Oppenheim, 1936; Almeida, 1948; Almeida, 1954; Andrade and Camarço, 1978; Andrade and Camarco, 1980; Evans, 1984; Melo, 1985; Melo, 1988; Popp, 1986); Assine, 1996; Milani, 2004; Grahn et al., 2013; Sedorko et al., 2018a; and Scheffler et al., 2020), receive different names. In this research, was considered the tripartite division of the Paraná Group (Furnas, Ponta Grossa and São Domingos formations) proposed by Grahn et al. (2013). In the Alto Garças sub-basin, the Devonian receives different proposals regarding the stratigraphic division (Table 1). The main lithostratigraphic units are the Furnas Formation which is composed by coarse to medium-grained white sandstones (Milani et al., 2007), Ponta Grossa Formation mainly composed by pelites (Lange and Petri, 1967; Grahn et al., 2013) and the São Domingos Formation, composed by sandstones at the base (Tibagi intraformacional member) and shales and siltstones at the top (Grahn et al., 2013).

The Ponta Grossa Formation begins with a conglomerate followed by interbedded siltstones and shales (Grahn et al., 2010) with a late Lochkovian (?)-Emsian age (Grahn et al., 2013). Whereas the São Domingos Formation is divided into two parts, the lower part which is mainly composed by reddish sandstone and conglomerate levels, that correspond to the Tibagi member, representing a deltaic environment on a shallow marine platform dominated by waves (e.g., Assine et al., 1998; Grahn et al., 2010; Sedorko et al., 2018b) and the upper part, made up of black shales intercalated with siltstones and sandstones, which represents the transgressive interval associated with the *Kačák* regional event (Grahn et al., 2010; Grahn et al., 2016). At the northwestern part of the basin, there is a regressive interval over the transgressive interval, composed by sandstones and siltstones (Sedorko et al., 2021).

3. SAMPLING AND METHODOLOGY

3.1 Field characteristics and sample location

Our study focuses into the Alto Garças sub-basin, northern part of the Paraná basin (Zone A, Supplement fig. S1). The northern area was divided into A (east) and B (west) zones. Samples collected by Santos et al. (2015) and Montibeller et al. (2017) from Zone A, and samples collected by Santos et al. (2015) and Henrique-Pinto et al. (2021) from the Zone B, were taken into account. In addition, our samples were collected from Zone A (Fig.

S1), the figure 4 shows the stratigraphic position of the studied samples. Details of the sampled levels are detailed below:

Vila Maria Formation: Sample BPN-2B collected from the top of the unit, the outcrop consists of reddish shale with parallel lamination.

Furnas Formation: Sample BPN-01B obtained from the lower part of the Furnas Formation is composed by reddish siltstones, massive aspect and with presence of some granules. Samples BPN-04B and BPN-05B was collected from the upper part of the Furnas Formation. Sample BPN-04B was obtained from siltstone/claystone levels found as laminations within light grayish sandstones. Whereas, sample BPN-05B was collected from siltstones levels, which are intercalated with reddish very fine-grained sandstones.

Ponta Grossa Formation: the samples was collected from the denominated zone A (Supplementary fig. S1). The base of the unit is composed by a reddish sandstone that become conglomeratic and by the intercalations of sandstone and shale in the upper part (samples BPN-06, Supplementary fig. S2I). A medium-grained light gray to whitish, poorly selected with subangular to subrounded grains sandstone (BPN-06A) was obtained. The middle part of the units is represented by samples BPN-9 and BPN-12. The outcrop of sample BPN-09A is reddish, it is made up at the base by massive shales and by intercalations of shale and siltstone in the upper part (Supplementary fig. S2G). Sample BPN-12B, was taken from the outcrop made up of medium to very fine-grained sandstones that are light gray to whitish in color, well selected with subrounded to subangular grains, and have horizontal lamination (Supplementary fig. S2H). The outcrop of samples BPN-10A/B is mainly made up of sandstones with reddish color (Supplementary fig. S2F) and shales and siltstones at the top. Hand specimens indicated well-sorted whitish-grey medium to fine-grained sandstones with subangular to subrounded grains.

Tibagi Member: the samples were obtained in the eastern and northern parts of zone A (Supplementary fig. S1). The base of the member (Supplementary fig. S2E), is mainly made up of sandstones (BPN-08A) and in the upper part by reddish-yellowish shales (BPN-8B). A light gray to white moderately selected with subangular grains fine-grained sandstone (BPN-8A) was analyzed. Bioturbation was also observed. The middle part of the member is represented by samples BPN-07A and BPN-07B, made up of well selected medium to fine-grained white sandstones with subangular grains (Supplementary fig.

S2C) and reddish-colored siltstones in the upper part (Supplementary Fig. S2D). The upper part of the member is represented by sample BPN-3B, a reddish color shale with siltstone intercalations (Supplementary fig. S2B). Hummocky-type sedimentary structures, were identified in this part.

São Domingos Formation: the samples were obtained from the western part of zone A (Supplementary figure S1), samples BPN-11A and BPN-11B (Supplementary Fig. S2A). The outcrop is made up of fine to very fine-grained sandstones of gray color, well selected with sub-rounded grains. Bioturbation and laminations (horizontal and corrugated), and reddish shales with horizontal lamination to the top were identified.

3.2. Petrography and X-Ray diffraction

We studied a total of 9 thin sections of sandstone under the microscope (Fig. 4). At least 400 grains were counted using the Gazzi-Dickinson point method following Ingersoll et al. (1984). We followed the petrographic classification of Garzanti (2019), and the genetic scheme of Dickinson (1985). Raw data were parameterized for each sample and summed as total quartz [Q = monocrystalline quartz (Qm) + polycrystalline quartz (Qp)], feldspar [F = plagioclase feldspar (P) + potassium feldspar (Fk)] and lithic fragments [L = igneous (Li) + metamorphic (Lm)].

3.3. Ray diffraction

X-ray diffraction (XRD) was carried out on 7 very fine-grained sedimentary rock (siltstone and claystone) from the Ponta Grossa and São Domingos formations (Fig. 4). The analyses were made on the clay fraction (<2 μm), at the *X-Ray Diffraction of the Instituto de Geocronología y Geología Isotópica* (INGEIS) of the University of Buenos Aires, and at the *Laboratório de Difração de Raios-X* (LARIX) of the Geosciences Institute of the University of Brasilia. At INGEIS, 4 samples (BPN 06B, BPN 07B, BPN 08B, and BPN 10B) were prepared following the methodology proposed by Moore and Reynolds (1997), whereas at LARIX, 3 samples (BPN 03B, BPN 09B and BPN 11B) were prepared following the methodology proposed by Alves (1987).

Measurements were performed on the oriented clay fractions under air-drying (AD), ethylene glycol-solvated (EG), glycerol-solvated (GL), and heated to 500°C (H) conditions. The identification of the constituent minerals of the pelitic rocks was carried out using diffractograms with the help of the Profex 4.3.3 software (Döbelin and

Kleeberg, 2015). The nomenclature proposed by Fazio et al. (2019) to determine the amount constituents of minerals as major (M), minor (m), or trace (tr) was established by comparing the intensities, in diffractograms, of the reflections with d around 4.26 Å for quartz, 7 Å for kaolinite, 10 Å for illite, 2.7 Å for hematite, 3.18 Å for plagioclase, 3.25 Å for potassium feldspar, 4.18 Å for goethite and 7 Chlorite. The mineral abbreviation was taken from Whitney and Evans (2010; Table 2).

3.4 Sr and Sm-Nd isotopes

The preparation and isotopic analysis of Sr and Sm-Nd isotopes were carried out at the Laboratory of Geodynamic, Geochronological and Environmental Studies of the University of Brasília (Brazil). The analytical procedures have followed the procedure suggested by Gioia and Pimentel (2000). Between 50-100 mg of sample was mixed with ^{149}Sm-^{150}Nd spike solution, and then dissolved in Teflon Savillex beakers by a successive acid attack (HNO3, HF, and HCl). A separation of Nd, Sm, and Sr was performed using chromatographic columns. Rare earth elements and Sr (REE) were separated on a primary column packed with AG 50W-X8 cation exchange resin. In contrast, Sm and Nd elements were isolated following conventional cation exchange chromatography techniques, with Teflon columns filled with LN-Spec resin (HDEHP - di-2-ethylhexylphosphoric acid supported on Teflon powder). The Sr, Sm, and Nd fractions were deposited on Re double evaporation filaments, and isotopic measurements were performed with a multicollector TRITON Thermal Ionization Mass Spectrometer (TIMS). Analysis of the standard reference material NBS-987 yielded a mean value of ^{87}Sr ^{86}Sr = 0.71028 ± 0.000035 (2SE), in agreement with the recommended value (0.710240; Hodell et al., 2007). While repeated analysis of the standard reference material BHVO-2 yielded a value of $^{143}Nd/^{144}Nd$ = 0.512970 ± 0.000002 (2SE), which agrees with the recommended value (0.512986 ± 0.00001; Weis et al., 2005).

We expressed the measured $^{143}Nd/^{144}Nd$ ratios in Epsilon neodymium notation (ƐNd) as the fractional deviation in part per 10^4 (units) of the $^{143}Nd/^{144}Nd$ value of the chondritic uniform deposit (CHUR). In this work, the time correction (t = 300 Ma) was used for the $Ɛ_{Nd}$ and ^{87}Sr / ^{86}Sr ratios. Since the ^{87}Rb / ^{86}Sr ratios were not measured, average contents of Rb = 125 and Sr = 142 ppm were taken from the NASC reference values (Gromet et al., 1984), and average contents of Rb= 115 ppm and Sr= 92 ppm for the Ponta Grossa

Formation from the values obtained from the same formation in the northwest part of the basin (Montibeller et al., 2017) to recalculate the $^{87}Sr/^{86}Sr$ ratios at 380 Ma.

3.5 Zircon morphology

Cathodoluminescence (CL) imaging on zircon grains was performed on a JEOL 6510 Scanning Electron Microscope (SEM) at the Department of Geology (DEGEO) of the Federal University of Ouro Preto, Brazil. CL images were used to identify growth areas and zonation in zircon grains, and to perform morphological analysis of detrital zircon grains. The roundness and elongation classes follow the classification proposed by Augustsson et al. (2018). The roundness classification is based on the Powers (1953) scheme in a simplified way, which is divided into euhedral, subangular to subrounded, and rounded classes. The elongation classification uses length/width ratios to differentiate between elongated (less than 1.3), oval (between 1.3 and 1.8), and round (greater than 1.8) crystals follow the classification proposed by Augustsson et al (2018). At the same time CL images were used to identify zircon morphologies, nucleus, and zonation. The Th/U ratio of zircon is a commonly used to distinguish between the magmatic and metamorphic zircons (i.e., Th/U ratios < 0.1 are more likely to be metamorphic and zircon with Th/U ratios > 0, 1 can be igneous or metamorphic, Rubatto, 2017; Yakymchuk et al., 2018).

3.6 U-Pb methodology

The separation of zircon grains from six samples for U-Pb dating was carried out at Laboratory of Geodynamic, Geochronological and Environmental Studies of the University of Brasília (Brazil). Two samples (BPN-06A and BPN-10A) from the Ponta Grossa Formation and three samples (BPN-07A, BPN-08A and BPN-11BA from the São Domingos Formation were selected. Zircon concentrates were extracted from 5-8 kg of sandstone samples, then crushed and sieved to 250 and 160 µm grain sizes. From the 250 - 160 and <160 µm fractions, the heavy minerals were concentrated by hydraulic methods and magnetic separation using a Frantz isodynamic separator at 1.5 A°. Zircon grains were hand-picked and placed in an epoxy backing, polished, and cleaned with 3% nitric acid before analysis. Under cathodoluminescence (CL) in a JEOL 6510 scanning electron microscope housed at the Department of Geology (DEGEO), Federal University of Ouro Preto we obtained images of zircon grains to select suitable areas for U-Pb analysis.

U-Pb analyzes were performed using a Thermo-Finnigan Element 2 ICP-MS coupled with a CETAC 213 ultraviolet laser system (LA-SF-ICP-MS) at DEGEO, and the results are presented as supplementary data. The Laser ablation was performed in static mode with a spot size of 30 μm, a shot repetition rate of 10 Hz, and energy output between 6 and 8 J/cm^2. The ablated sample was carried out using He as carrier gas mixed with Ar before introduction into ICP-MS. Data were corrected for background signal, common Pb, laser-induced elemental fractionation, instrumental mass discrimination, and Pb/U time-dependent elemental fractionation using the MS Excel spreadsheet program (Gerdes and Zeh, 2006). The main reference material used was GJ-1 zircon (608 ± 1 Ma, Jackson, et al., 2004) and for quality control, we used Plešovice zircon (337 ± 1 Ma; Sláma et al., 2008) and the BB (562 ± 1 Ma; Santos et al., 2017) as a secondary standard. Signal data was reduced using Glitter software (van Achterbergh et al., 2001). Zircon ages that have > 10% discrepancy were rejected, these were obtained from the ratio of ages $^{206}Pb/^{238}U$ versus $^{207}Pb/^{235}U$ for grains with ages less than 1200 Ma, while the ratio of ages $^{206}Pb/^{238}U$ versus ^{207}Pb /^{206}Pb for grains older than 1200 Ma (Vermeesch, 2020). Kernel density estimates were calculated using detritalPy, a Python-based approach (Sharman et al., 2018). For this work, the age of maximum deposition (MDA) was determined by calculating the youngest peak from a density plot, ignoring single grain age peaks (Dickinson and Gehrels, 2009; Sharman and Malkowski, 2020).

4. RESULTS

4.1 Sandstone petrography

Petrographic analysis of sandstones is useful as a first approach for sedimentary provenance studies (Dickinson et al. 1983). However, matrix content must be considered (Cox and Lowe, 1996).

Three samples from the Ponta Grossa Formation, were analyzed (Figure 4; table 3). The sample BPN-06A, is a fine-grained, poorly selected sandstone with sub-angular to sub-rounded grains, and with ~25% of matrix (Supplementary fig. S2J). It is composed by monocrystalline quartz (Qm; 93%) with undulating and normal extinction and by metamorphic lithics (Lm; 7%). Muscovite is present as an accessory mineral that is elongated, tabular, and retains its original shape. The sample BPN-12A is a very fine-grained, and well-selected sandstone with sub-rounded grains, and with a matrix of 5% (Supplementary fig. S2K). This sample contains 94% quartz with undulating extinction

(See Table 4), of which 87% is monocrystalline quartz (Qm) and 7% polycrystalline quartz (Qp). The other component present is potassium (FK; orthoclase and microcline; 6%) with altered edges to sericite. Muscovite is present as an accessory mineral that is elongated, tabular, and retains its original shape, zircon was also found. The sample BPN-10A is a fine-grained, well-selected with subrounded grains, and with a matrix of 20% (Supplementary fig. S2L). It is composed entirely of monocrystalline quartz (Qm; 87%) with undulating and normal extinction. The other component present is potassium feldspar (FK; microcline; 13%) with edges altered to muscovite. In addition, it presents kaolinite and illite due to alteration of feldspars. Muscovite is an accessory mineral that is elongated, tabular, and retains its original shape.

From the lower part of the São Domingos Formation (Tibagi Member), 5 samples were analyzed (Figure 4; Table 3), 3 correspond to the TF-Universidad de Brasilia (2012), and 2 were collected during this study (supplementary fig. S2M and S2N). Sample are very fine to fine-grained sandstones, of good to moderate selection with sub-angular grains, and with a matrix between 2 and 25% in almost the entire sample, except in sample BPN-07A obtained at the base of this member, which has a 40% matrix. Composed almost exclusively of quartz between 98 to 100% with undulating extinction. Monocrystalline quartz predominates, varying between 98 to 99%, except in sample TF-IV-038, which has 93% monocrystalline quartz and 7% polycrystalline quartz. They contain between 1 to 2% feldspars (potassium feldspar and plagioclase) which present alteration of kaolinite and illite. Muscovite is an accessory mineral, which is elongated, tabular, and retains its original shape. In addition, zircon was found in sample TF-IV-38.

We analyzed a very fine-grained, well-selected sandstone with sub-rounded to sub-angular grains from the upper part of the São Domingos Formation, (Table 3, Supplementary fig. S2O), show until 15% of matrix throughout the sample. It is composed almost entirely of monocrystalline quartz (91%) with mainly undulating extinction and microcline (9%) with edges altered to sericite. Muscovite is an accessory mineral that is elongated, tabular, and retains its original shape. In addition, it presents kaolinite and illite due to alteration of feldspars.

In the QFL ternary diagram of sandstone classification (Garzanti, 2019), the sample from the Ponta Grossa Formation are classified as quartzose and feldspathic quartzose sandstones. Samples from the lower part of the São Domingos Formation (Tibagi

Member) are classified as pure quartzose sandstones (Fig. 5). The upper part of the São Domingos Formation is classified as quartzose sandstone. Furthermore, petrography of the upper part of the São Domingos Formation was complemented by data presented by Oliveira and Pereira (2011), in the northwest of the Paraná basin, these data also indicate that the samples are composed of pure quartzose sandstone and quartzose sandstone (Fig. 5).

In the QFL ternary provenance diagram (Dickinson et al., 1983) samples in all units are plotted in the inner craton field. Samples from the upper part of the São Domingos Formation and Ponta Grossa are also plotted in the recycled orogen field. In addition, taking into account the importance of the matrix in modal petrographic studies suggested by Cox and Lowe (1996), our data allow us to indicate that matrix not have a significant impact.

4.2 XRD mineral composition

The mineralogy of the clay fraction (<2 μm) of samples from the Ponta Grossa and São Domingos formations are composed by phyllosilicate minerals such as kaolinite, illite, and chlorite, (See Fig. S3 and Table 4). Kaolinite and illite appear as major and minor components in all samples; chlorite was identified as trace component, an exception can be observed in the sample BPN 08B, where chlorite is a minor component. The non-phyllosilicate minerals present in the samples are quartz, hematite, goethite, feldspars, and plagioclase, it should be noted that hematite is a major component in several samples (BPN-06B, BPN-07B, BPN-08B, and BPN-09B) and goethite is a minor element in the sample BPN-08B.

4.3 Sr-Nd isotopes:

Table 5 and Figure 6 presents the isotopic results of Sr and Sm-Nd isotopes obtained for 11 samples pelitic from the Vila María (1), Furnas (3), Ponta Grossa (3) and São Domingos (4) formations. In order to compare between isotopic data of units of different ages, all data were recalculated to 380 Ma. This age was chosen as the closest age to the youngest unit (São Domingos Formation).

The $^{147}Sm/^{144}Nd$ ratios of the samples studied are in the typical range for crustal rocks of 0.09-0.13 (Taylor and McLennan, 1985), a exception can be observed for sample BPN-09B ($^{147}Sm/^{144}Nd$ ratio >0.18). Since this high value of Sm/Nd generate a lot of

uncertainty, the BPN-09B sample will not be taken into account in the discussions. εNd (380) values ranging from -12.5 to -9.0, indicating strong crust reworking. The T_{DM} model of our samples range from Mesoproterozoic to Paleoproterozoic (1.48 - 2.07 Ga).

Samples BPN-09B, BPN-08B and BPN-06B present very low values $^{87}Sr/^{86}Sr_{(380)}$ ratios (nearly chondrites values). It could be due to the high content of hematite, which has been recognized XRD analysis. According to Wei et al. (2018), the presence of hematite generates a decrease the isotopic composition of Sr in samples. Since these very low values of $^{87}Sr/^{86}Sr$ generate a lot of uncertainty, samples BPN-09B, BPN-08B and BPN-06B will not be taken into account in the discussions. The highest $^{87}Sr/^{86}Sr_{(380)}$ ratios are present in the Furnas Formation and the Rio Ivaí Group (Vila Maria Formation) with values between 0.72301 and 0.72781, respectively, indicating more radiogenic sources. The lowest $^{87}Sr/^{86}Sr$ (380) ratios are present in the São Domingos (Tibagi Member) and Ponta Grossa formations with values between 0.69807 and 0.69945, respectively, indicating less radiogenic sources.

4.4 U-Pb provenance analyses

Detrital zircon ages of Ordovician (Rio Ivaí) and Devonian (Furnas and Ponta Grossa formations) units from the northern part of the Paraná Basin are reported in figure 7 and Supplementary Table S1. Only data with concordance between 90-110% and ≤ 5% of error (2 sigma) were considered for interpretation.

4.4.1 Furnas Formation

Sample BPN-01A (Unit I): from 99 analyses on zircon grains, 93 analyses presented a concordance between 90 -110% and ≤ 5% error (2 sigma). The data obtained shows a unimodal distribution, with the main populations between 520 - 1095 Ma (83%). The main peaks are at 683 and 928 Ma. The youngest peak age is at 570 Ma, which was obtained from 3 zircons grains.

4.4.2 Ponta Grossa Formation

Sample BPN-6A: from 104 analyses on zircon grains, 94 analyses presented a concordance between 90 - 110% and ≤ 5% error (2 sigma). The data obtained shows a bimodal distribution, with the main populations between 503 - 1195 Ma (57%) and a second population between 1852 - 2440 Ma (23%). The main peaks are at 638, 813 and 2108 Ma. The youngest peak age is at 450 Ma, which was obtained from 6 zircons grains.

Sample BPN-10A: from 101 analyses on zircon grains, 71 analyses presented a concordance between 90 - 110% and ≤ 5% error (2 sigma). The data obtained shows a polymodal distribution, with the main populations between 465 - 1072 Ma (54%), a second population between 2220 - 2500 Ma (17%) and a third population between 1742 - 2102 Ma (15%). The main peaks are at 606, 912, 1968 and 2413 Ma. The youngest peak age is at 536 Ma, which was obtained from 4 zircon grains.

4.4.3 São Domingos Formation

Sample BPN-08A (Tibagi Mb.): from 102 analyses on zircon grains, 99 analyses presented a concordance between 90 - 110% and ≤ 5% error (2 sigma). The data obtained shows a bimodal distribution, with the main populations between 580 – 1100 Ma (48%) and a second population between 1785 – 2374 Ma (30%). The main peaks are at 646 and 2120 Ma. The youngest peak age is at 485 Ma, which was obtained from 2 zircon grains.

Sample BPN-07A (Tibagi Mb.): from 118 analyses on zircon grains, 113 analyses presented a concordance between 90 - 110% and ≤5% error (2 sigma). The data obtained shows a polymodal distribution, with the main populations between 620 - 1220 Ma (34%), a second population between 1762 - 2500 Ma (33%) and a third population between 1220 - 1570 Ma (13%). The main peaks are at 704, 1306 and 2195 Ma. The youngest peak age is at 476 Ma, which was obtained from 4 zircon grains.

Sample BPN-11A: from 104 analyses on zircon grains, 93 analyses presented a concordance between 90 - 110% and ≤ 5% error (2 sigma). The obtained age shows a polymodal distribution, with the main populations between 497 - 991 Ma (38%), a second population between 1785 - 2500 Ma (30%) and a third population between 991 - 1380 Ma (14%). The main peaks are at 621, 1242 and 2151 Ma. The youngest peak age is at 429 Ma, which was obtained from 6 zircon grains.

4.5. Morphology of zircon

The zircon morphology analyses (Figs. 8 and 9) was made on unbroken grains and with concordance ages between 90 - 110% and ≤5% error (2 sigma). The Furnas Formation (BPN-01A) contain 59% subangular to subrounded, 39% rounded, and 2% euhedral grains. In terms of elongation, 71% are elongated grains, 21% are oval grains, and 8% are round grains. The Ponta Grossa Formation (BPN-06A and BPN-10A) contain 64 - 71% rounded, 28 - 33% subangular to subrounded, and 1 - 3% euhedral grains. In terms of

elongation, 58 -72% are elongated grains, 25 - 38% are oval grains, and 3 - 4% are round grains. The Tibagi member of the São Domingos Formation (BPN-8A and BPN-07A) contain 42 - 63% rounded, 32 - 56% subangular to subrounded, and 2 - 5% euhedral grains. In terms of elongation, 59 - 66% are elongated grains, 28 - 33% are oval grains, and 6 -9% are round grains. The São Domingos formation (BPN-11A) contain 78% rounded, 20% subangular to subrounded, and 2% euhedral grains. In terms of elongation, 63% are elongated grains, 32% are oval grains, and 5% are round grains.

Regarding the relationship of age with length, elongation and Th/U ratio, there are two populations. A population aged between 500 - 1200 Ma (55%) with a length interval between 80 - 220 μm, and another population between 1660-2500 Ma (28%) with a length interval between 90 - 200 μm. In the two populations with a predominance of elongated and oval grains (Fig. 8B) and with Th/U ratios between 0.1 - 0.9 (Fig. 8B).

Figure 8C shows the zircons with a Th/U ratio less than 0.1, this would indicate metamorphic zircons. However, when the cathodoluminescence images are reviewed, these zircons show typical zones of igneous (oscillatory) and metamorphic (irregular and homogeneous) zircon grains. The oscillatory zoning zircons grains are the number 098, 012 and 360, the irregular zoning are numbers 011, 125 and 190 and the homogeneous zoning is the number 185. This low Th/U ratio in these zircons is due to the fact that they have a high U content, except in zircon grains with numbers 012 and 185, which is due to the low content of Th.

5. DISCUSSIONS

5.1. Provenance constraints of the Silurian-Devonian interval of the northern part of the Paraná Basin

U-Pb provenance data and feature of the proximal, intermediate and distal sources

This study has the objective to understand the evolution of the Paraná basin, specifically during the Silurian-Devonian interval time. A total of 563 U-Pb data were obtained via LA-ICP-MS from the Furnas, Ponta Grossa and São Domingos formations (Devonian, Paraná Group). Figure 7 show the provenance data of samples analyzed in this work and Figure 10A show the compiled data by stratigraphic unit of the northern part of the Paraná Basin.

The provenance analyse from the Lower Furnas Fm. (sample BPN-01) presents a main population with a peak at 683 Ma (Fig. 7). This sample points to the Goiás Magmatic Arc as the main source, showing a correspondence with the work of Pimentel (2016). Comparing with data from the Alto Garças (Henrique - Pinto et al., 2021), Vila Maria (Gazatt, 2011) and Lower Furnas Formation (Santos et al., 2015; Henrique - Pinto et al., 2021), the main peaks are similar, with peak values of 627, 648 and 638 Ma (Fig. 10A). The Middle Furnas Fm. (Upper Silurian; Santos et al., 2015) shows two populations, with a peak at 666 Ma, clearly indicating the provenance from the Goiás Magmatic Arc and a secondary population, with a main peak at 2078 Ma. A minor population with a peak at 1741 Ma, probably related with an intermediate source, as the Serra da Mesa Group, a Paleoproterozoic basement, located to the northeast was also identified (Fig. 10B). The paleocurrents obtained by Bigarella and Oliveira (1966), Assine (1996) and Santos et al. (2015) are in agreement with our interpretation of the source area from the northeast.

The Ponta Grossa Formation (Figs. 7 and 10A), presents polymodal zircon age distribution. A main population with a peak at 631 Ma from the Goiás Magmatic Arc and several secondary populations from the Serra da Mesa Group (peaks at 1802 Ma and 2108 Ma; Fig. 10B), Paranoá Group (peak at 2108 Ma.; Fig. 10B) and from the Goiás block (2411 Ma) were also registered. Interesting, there are two populations that did not appear before, one with ages in the range of 900 and 1200 Ma and the another one, a smaller population with a peak at 445 Ma. The first one, is characteristic from the Sunsas belt (e.g., Nedel et al., 2020), that crops out probably at ~1700 km to the west (today). The Ordovician peak could be associated directly with the Famatinian magmatism, also well registered at the west, in the Andes region. If these areas are the direct source from these populations, they will be classified as distal sources and the presence of then in the sediments from the Paraná basin would indicate an important input from distal/very distal sources to the west.

The intraformational member of the São Domingos Formation, the Tibagi unit (Figs. 7 and 10A), shows a similar pattern population when compared with the lower Ponta Grossa Formation, except for the lack of the Famatinian peak (sample BPN-07A) and a peak at 1304 Ma, that did not appear before. The main population still is Neoproterozoic (peak at 667 Ma) and related with provenance from the Goiás Magmatic Arc. The new peak at 1304 Ma as part of a secondary population could be related either with mafic and ultramafic complexes from the Brasiliano belt (Pimentel, 2016) or still from very distal

sources, like the igneous rocks of the Pensamiento Suite (França et al., 2014) related with the San Ignacio Orogeny (Bettencourt et al., 2010) that crop out at the Paraguá Block in Bolivia, today at ~1700 km (Figs. 1 and 10B). The peak at 2121 Ma could be related with the Serra da Mesa and Paranoá groups (Fig. 10B) and the peak at 1802 Ma could be associated neither with the Serra da Mesa and/or Traíras groups (Fig. 10B). The Traíras Group is classified as a very distal source. As smaller populations have peaks at 2431 Ma and 2620 Ma that indicate provenance from the Goiás Block and Traíras Group sources, respectively. There is also a population of ages in the range of 900 to 1200 Ma which does indicate a contribution from the Sunsas belt (Nedel et al., 2020) to the west.

The São Domingo Formation, representing the upper Devonian unit (Fig. 8 and 10A) also show as the main provenance sources area, the Goiás Magmatic Arc (peak at 621 Ma). A population with a peak at 2151 Ma indicates additional sources areas like Serra da Mesa and Paranoá groups (Figs. 2 and 10B). Peaks at 429, 1242, 1297, 1520 and 2424 Ma indicates heterogeneous sources, probably related with the Famatinian Arc, Sunsas Arc, mafic and ultramafic complexes from the Goiás Magmatic Arc and Goiás block. There is an additional older peak at 2604 Ma that probably correspond with the Traíras Group (Fig. 10B), all of them categorized this work as distal-very distal sources. Paleocurrents reported from the Ponta Grossa and São Domingos formations (Vargas et al., 2020) are in agreement with the proposed areas of provenance.

It is also worth mentioning that mafic and ultramafic rocks could be probable sources of provenance. Similar ages the ~1300 Ma with ages from the mafic and ultramafic complexes (Ferreira Filho et al., 1994; Pimentel, 2016) were only registered by the São Domingos Formation plus the Tibagi Member. The geochemical data of the Ponta Grossa Formation (Montibeller et al., 2017) indicate that the sediments have as the main source, mafic and intermediate rocks.

The elongation of zircon grains could be related with areas of probably igneous origin (e.g., Gärtner et al., 2013; Yue et al., 2019) and the roundness of zircons with distal sources (e.g., Köster 1964, Dietz 1973), we can check these parameters in our samples (Figs. 8A and 9) and related (or not) with the cycles of transgression and regression recognized on these units.

In Figure 8A, it is possible to see that there are not many changes in the elongation and roundness between the units related with transgression and regression. Starting with the

Lower Furnas Formation (sample BPN-1A), before the first transgression, 71% of grains are elongated and 59% are subangular to rounded, while 39% are rounded (Fig. 8A). This data combined with the U-Pb ages indicate that proximal sources areas of probable igneous origin were the main areas of provenance, in this case, the Goiás Magmatic Arc. The rounded zircons can also indicate reworking from the lower units.

From the two samples of Ponta Grossa Formation related with the first transgression (BPN-06A and BPN-10A), only sample BPN-10A show a decrease in the percentage of elongated grains (up to 56%), with the increasing of oval grains (up to 36%). Considering the roundness, only samples BPN-06A and BPN-10A show an increase of rounded grains (before it was 39%) up to 71 and 64% respectively. Taking into account that Ponta Grossa Formation is the first unit that show provenance from distal/very distal sources (Paranoá Group, Serra da Mesa, Sunsas belt and Famatinian Arc), the increase of the rounded grains could be related to this. The rounded was used to deduce a provenance from distal areas. However, the rounded grains can also indicate reworking of the lower units. This possible reworking was suggested by Montibeller et al. (2017) using geochemistry data of pelites of the Ponta Grossa Formation.

Samples BPN-08A and BPN-07A was taken from the Tibagi Member, which represent the devonian regression cycle in the Paraná Basin. The elongation increases to 66% for the sample BPN-08A but immediately it decreases to 59% for sample BPN-07A. Whereas the roundness of zircon grains shows, a significant decrease in rounded grains from 64% (sample BPN-10A of the Ponta Grossa Formation) to 42% for sample BPN-08A. In contrast, in sample BPN-07A the rounded grains increase to 63%. In this sample was also observed the higher percentage of euhedral grains (5%) of the São Domingos Formation. The upper part of the São Domingos Formation related with the second transgression registered on the Devonian time, here is represented by the sample BPN-11A. The elongated grains increase to 63%, whereas the rounded grains increase significantly to 78%.

Relationship between Sr-Nd isotopes and U-Pb provenance data

Strontium and Neodymium concentrations and isotopic composition for 11 pelitic rocks from Ordovician and Devonian units are listed in Table 5. Figure 6 shows that samples can be split into five different groups based on isotopic characteristics

(1) The Ordovician Vila Maria Formation has $^{87}Sr/^{86}Sr_{(380)}$ ratios of 0.72781, $\varepsilon_{Nd(380)}$ value of -9.0, and T_{DM} of 1.58 Ga.

(2) The Furnas Formation is represented by 3 samples (1 at the base and 2 at the top). This unit has $^{87}Sr/^{86}Sr_{(380)}$ ratios ranging from 0.70569 to 0.72301, $\varepsilon_{Nd(380)}$ values between -12.5 and -10.0, and T_{DM} values from 1.48 to 1.76 Ga.

(3) The Ponta Grossa Formation has $^{87}Sr/^{86}Sr_{(380)}$ ratios of 0.70154, $\varepsilon_{Nd(380)}$ value of -11.4, and T_{DM} of 1.72 Ga. Some exception can be observed for samples BPN-06B and BPN-09B, in which the obtained value is no realistic, in the sense that it is not possible that a crustal rock has an achondrite value. As it was indicated before, the high concentrations of hematite, which were well contrasted by the XRD analyses, could generates an alarming decrease of the isotopic composition of Sr (Wei et al., 2018).

(4) The Tibagi Member. has $^{87}Sr/^{86}Sr_{(380)}$ ratios ranging from 0.70751to 0.71676, $\varepsilon_{Nd(380)}$ values between -10.6 and -12.4, and T_{DM} values from 2.05 to 2.07 Ga.

(5) The upper part of the São Domingo Formation has $^{87}Sr/^{86}Sr_{(380)}$ ratio of 0.70974, $\varepsilon_{Nd(380)}$ value of -12.4, and T_{DM} of 1.82 Ga

The increase of the negative values from -9.0 (Vila Maria Fm.) to -12.5 (top of the Furnas Fm.) that in terms of the average crustal residence ages of the sources areas (T_{DM}) is correlative with an increase in the T_{DM} from Vila Maria Formation to Furnas Fm. from 1.58 to 1.75 Ga. This increase, that normally would be assigned to an older reworked continental crust input was not accused for any significative changes in the provenance areas (Fig. 7, 13). The decrease in the ε_{Nd}(380 Ma) values from -10.9 (transition from Furnas to Ponta Grossa formations) to -11.6 (Ponta Grossa Fm.). On the T_{DM} diagram (Fig. 6), there is an increase of the T_{DM} from ~1.5 (BPN-05B) to 2.03 (BPN-06B) Ga and a decrease again to 1.72 Ga (BPN-10B). This could be directly related with the input of distal sources to the basin during the transgression, as the provenance data showed (Fig. 7), like Serra da Mesa and Paranoá Group or from the Goiás block. The internal variation from 2.03 (BPN-06B) to 1.72 Ga (BPN-10B) could be related with the first input of the youngest sources to the basin, like magmatic rocks from the Ordovician Famatinian magmatic Arc, only observed in the upper part of the Ponta Grossa Formation. The increase of the T_{DM} for Tibagi intraformational member to more than 2.0 Ga could be related with the input from the oldest (and more radiogenic) sources. The T_{DM} decrease again for the São Domingo Formation, to 1.82 Ga. As it was show in Figure 7, it is

probable related with the increase of provenance from the distal/very distal sources (Famatinian Arc) and the decrease from older sources, like the Archean ones.

In the Age (Ga) versus ε_{Nd} diagram (Fig. 11), it is observed a general increase of older crustal sources from Vila Maria Formation to Furnas Formation, nevertheless the input of old sources is only observed in the upper part of the unit (input from Serra da Mesa Group, Fig. 10B). The samples of the Ponta Grossa and São Domingo formations indicate the contribution of important sources of the Paleoproterozoic, which are associated with the Serra da Mesa, Paranoá, Traíras and Cinturón Sunsás Groups (Fig. populations (Fig. 10A).

The observed isotopic variations of the Devonian units from the Paraná basin are easily correlated with the observed provenance patterns (Fig. 7). Proximal sources, are represented by the Neoproterozoic Goiás Magmatic Arc. Two contrasting distal/very distal sources were also observed, one from the east, older and more radiogenic, related with the Traíras Group as part of the Paleoproterozoic basement of the Brasilia Belt and a second one, from the west, younger and less radiogenic, related with the Ordovician Famatinian Arc. These variations could be correlated with the variation of the sea level identified by Vargas et al. (2020) for this interval of time (?) as the first transgression (T1) was registered on the Ponta Grossa Formation, the small decrease (less negative) but variable $\varepsilon_{Nd(380)}$ values, and the increase/decrease of the T_{DM} values from the base to the top of the unit, could be related with the input of the distal/very distal sources, that are contrasting in terms of ages. The Traíras Group (a highly radiogenic Peleoproterozoic source), and the Famatinian magmatic rocks (a lees radiogeneic Ordovician source), probably were only available when the sea level increased, probably this situation was associated with the Precordilleran Orogeny I (Milani and de Wit, 2008; Linol et al., 2015, Vargas et al., 2020). The regression (R1) associated with the Tibagi intraformational member, associated with the Precordilleran Orogeny II (Milani and de Wit, 2008; Linol et al., 2015, Vargas et al., 2020), shows the reworking of the Ponta Grossa and lower units of the Paraná basin in addition to the input of proximal sources, like the Goiás Magmatic Arc. The new transgression (T2) of global incidence occurred still during the Precordilleran Orogeny II (Milani and de Wit, 2008; Linol et al., 2015, Vargas et al., 2020). This event is registered on the upper part of the São Domingo Formation, and could be responsible for the input of very distal sources from the west, from the Famatinian Arc.

5.2 Comparison with the southern part of the Paraná and Tarija Basin.

U-Pb zircon ages of the Iapó, Lower Furnas, Middle Furnas and Ponta Grossa formations, of the southern part of the Paraná Basin, is present by Henrique-Pinto et al. (2021). Detrital zircon ages from the Iapó Formation to Middle Furnas have one major population and two minor populations. The main population has peaks that vary from 604 to 589 Ma, which correspond to post and non-collisional intrusions (560 – 640 Ma; Meira et al., 2015); and the minor populations have peaks that vary from 780 to 760 Ma, which corresponds to Magmatic arc intrusions (640 – 800 Ma., Meira et al., 2019), and the other population has peaks that vary from 2139 Ma to 2182 Ma, which correspond to the Lajeado Group (Campanha et al., 2019). The ages of the detrital zircon grains of the Ponta Grossa Formation have a main population with a peak at 595 Ma, which correspond to post and non-collisional intrusions (560 – 640 Ma., Godoy et al., 2010; McGee et al., 2012), and a minor population with a peak at 776 Ma, which corresponds to Magmatic arc intrusions (640 – 800 Ma., Pimentel & Fuck, 1992; Pimentel et al., 1999; Pimentel et al., 2003 and Matteini et al., 2010). The source of the sediments of the southern part of the Paraná Basin correspond to the southern part of the Ribeira Belt.

Exist an important contrast between source areas for the northern and southern part of the Paraná Basin. According to some authors (Meira et al., 2015; Campanha et al., 2019; Henrique-Pinto et al., 2021; Henrique-Pinto et al., 2023) the source of the sediments for the southern part of Paraná Basin correspond to the Ribeiro Belt, on another hand, the sources for the northern part is the Brasilia Belt (This work; Gezatt, 2011; Santos et al., 2015; Henrique-Pinto, 2021; Henrique-Pinto et al., 2023). In addition, the palecurrents in the southern zone (Bigarella and Oliveira, 1966; Assine, 1996) indicate orientations to the west and southwest. The thickness of the Tibagi Member (São Domingos Formation) in the northern zone is thicker than the southern zone (Melo, 1988). In the Devonian interval of the southern zone, there are only one sample with U-Pb data at the base of the Ponta Grossa Formation (Henrique-Pinto et al., 2021), which make difficult establish comparisons with our samples.

The U-Pb data from the northern part of the Paraná Basin were plotted in the classic diagram proposed by Cawood et al. (2012) to discriminate the tectonic setting of the basin (Fig. 12). If more than 5% of the zircons show an age difference greater than 150 Ma between the crystallization (CA) and depositional (DA) ages, could be indicate

extensional setting (including intracratonic). On the other hand, convergent settings have CA-DA > 150 Ma at 5% and CA-DA < 100 Ma at 5% and 30% of the zircon population, respectively. Whereas collisional setting corresponds to CA-DA of < 150 Ma and CA-DA > 100 Ma at 5% and 30% of the zircon population, respectively. Taken into account this diagram, the Alto Garças, Lower Furnas, Ponta Grossa and São Domingos formations correspond to a collisional environment, whereas Vila Maria, Middle Furnas and Upper Furnas correspond to cratonic environment (see Fig. 12). It is worth mentioning that the basin is cataloged as a cratonic basin by several authors (e.g., Almeida, 1980; Milani et al., 2007; Henrique-Pinto et al., 2021). However, the tectonic discrimination graphs (Fig. 12) can give us another tectonic environment due to source areas with young ages almost equivalent to the sedimentation age or possibly to distal sources with younger zircons. The latter because the transgressions that are going to be able to reach those distal areas or connect with other basins.

In the southern part of the basin, the diagram proposed by Cawood et al. (2012) indicates a collisional environment, such as it was shown by Henrique-Pinto (2021, 2023). On the other hand, to the west, García Zavaleta et al. (2023) suggest convergent settings for the Tarija Basin during the Devonian based on isotopic and U-Pb data.

In this work, we suggest a connection between the Tarija Basin and the northern part of the Paraná Basin, taking into account features of the deposition of the Ponta Grossa Formation. This proposal is due to the fact that distal/very distal sources (magmatic rocks of the Famatinian and Sunsas belt) were recognized to the west of the Paraná Basin. In addition, the Kernel Density (KDE), multidimensional scaling (MDS) and ε_{Nd} evolution plots show this correlation (Figs. 10, 11 and 13).

5.3 EVOLUTION OF THE NORTHERN PART OF THE PARANÁ BASIN DURING THE DEVONIAN

The collision of the Cuyania with the western portion of the Pampean Terrain (e.g., Milani and Ramos 1998; Milani and De Wit, 2008; Linol et al., 2015, Heredia et al., 2018, Henrique Pinto et al., 2021) produced the Ocloyic Orogeny (460-430 Ma). This Orogeny caused a subsidence due to flexion in the cratonic terrane and the generation of the Paraná Basin.

From the upper Cambrian, the western margin of Gondwana suffered a continuous subduction that make possible the establishment of the Ordovician Famatinian Arc (~490 – 460 Ma; Ramos, 2018; Rapela et al., 2018). To the west of the northern part of the Paraná basin from the middle of the Lower Silurian occurred a progressive cessation of magmatism until the Carboniferous, that it was restarted again (e.g., Anderson et al., 2021; Bahlburg, 2021; García Zavaleta et al., 2023; Henrique-Pinto et al., 2021). Balhburg (2021) proposed a pause in magmatism (or lull) in the Devonian interval. In contraposition and in order to explain the lack of zircon grains with devonian ages in the devonian units of the Tarija basin, García Zavaleta et al. (2023) proposed a flat-slab subduction. In this study we are in favor of a flat-slab hypothesis, since various studies indicate a strong tectonic control, like the tectonic shortening (Anderson et al., 2021), subsidence and uplift in the western part (e.g., Anderson et al., 2021; Henrique-Pinto et al. al., 2021; Milani and De Wit, 2008, Fonseca et al., 2020). According to Vargas et al. (2020) tectonics has influenced the sedimentary processes in the Paraná basin. In the Paraná basin, there were recognized, for the Devonian, two transgression and one regression. Discussions are detailed in the following.

Lochovian-Pragian interval: the first transgression

In the northern part of the Paraná basin, at the beginning of the Devonian, a transgressive system begins with the deposition of the Upper Furnas Formation. Probably, the main provenance areas were the Goiás Magmatic Arc and the Serra da Mesa Group (proximal to mid sources). The transgression progressed until reaching a maximum transgression or second-order maximum transgression surface (Vargas et al., 2020) and coincides with the deposition of the Ponta Grossa Formation. The Pragian interval, related with the development of the transgression, is the time of the Malvinokaffric Kingdom (e.g., Melo, 1988; Bosetti et al., 2012; Penn-Clarke, 2019, Sedorko et al., 2021) and the great diversity (Sedorko et al., 2021).

The provenance sources areas of the Ponta Grossa Formation would be the same, but with an increase in the number of zircon grains with ages related with the Paranoá Group and the Goiás Massif (intermediate sources). In addition, “Famatinian and Sunsas zircon grains”, those zircon grains with Ordovician and Meso/Neoproterozoic ages, typical from the west (distal/very distal sources), and also registered in the Santa Rosa Formation (e.g., Calle, 2013), could indicate that at the end of the transgression there was a connection

with the Tarija basin. The provenance data from Ponta Grossa + Upper Furnas and Santa Rosa formations from the Tarija basin (Fig. 16) are in agreement with this interpretation.

The Age vs. ε_{Nd} diagram (Fig. 11) indicates that the Nd isotopic compositions of the sedimentary rocks of the Furnas Formation, are similar to the Goiás Magmatic Arc (Neoproterozoic) while sedimentary rocks of the Ponta Grossa Formation is similar to the Serra da Mesa and Paranoá Groups. Geochemical studies (e.g., Montibeller et al., 2017) in the Ponta Grossa Formation indicate a source of mafic rocks, that for the paleogeography (Fig. 2) indicates contributions from the Uruaçu complex (granulites and mafic migmatites) and mafic/ultramafic complexes. The mafic/ultramafic sources normally have scarce zircon grains and cannot give evidence of these source zones. The paleogeography also indicates that the source areas are more proximal to the Goiás Magmatic Arc and this is corroborated by the larger size of the detrital zircon grains, that indicate more proximal sources (Figure 10A and 10B).

According to García Zavaleta et al. (2023) the flat-slab subduction could have caused a shortening and uplift of the Tarija Basin. Taking into an account the tectonics and a possibly connection between Tarija and Paraná basins (this work; Henrique-Pinto et al., 2021), we believe that it could possibly have also affected the Paraná basin. Possibly this situation caused a transgression that was recorded in the Paraná Basin and was record by the Upper Furnas and Ponta Grossa formations. This transgression also is record in the Tarija basin and is represented by the Santa Rosa and Icla formations (Albariño et al., 2000). This transgression was clearly Tectonic in nature, since it has no correlation with the global eustatic curve (Haq and Schutter, 2008).

Late Emsian to Late Eifelian interval: the first regression

In the Late Emsian to Late Eifelian interval, there is a regressive system represent by the deposit of the Tibagi intraformational member of the São Domingos Formation. This member has similar provenance source areas as the previous units; however, in this case the regression shows a peak at 1306 Ma associated with the mafic and ultramafic complexes (Pimentel, 2016), which were also recognized by Montibeller et al., (2017) in the Ponta Grossa Formation.

During this time there is a decrease in population ages from the Famatinian Magmatism Arc. Furthermore, the Sunsas ages are also present, which could indicate that, despite having less distal deposits by the regression event (i.e., proximal and intermediate source

are more common), there was still a connection with the Tarija basin and this is evident also for the distribution of ages of detrital zircon grains that are found in the Tarija basin (e.g., García Zavaleta et al., 2023).

The Age versus ε_{Nd} diagram (Fig. 11) indicate an important source associated with the Serra da Mesa and Paranoá groups for the Tibagi member which is concordant with the ages obtained from the detrital zircon grains. In this period of time, there was decline of the diversity of the *Malvinokaffric Kingdom* caused by tectonic activity, which gave rise to a regressive system (e.g., Bosetti et al., 2012; Grahn et al., 2013, Vargas et al., 2020; Sedorko et al., 2020; Sedorko et al., 2021).

Taking into account tectonics inferred from sedimentary provenance by García Zavaleta et al. (2023) in the Tarija basin, the flat-slab subduction caused a survey that was for some authors (e.g., Fonseca et al., 2020; Anderson et al; 2021). The mentioned event resulted in a regression that was registered in the São Domingos Formation of the Paraná Basin (this work) and in the Huamampampa Formation of the Tarija Basin (Albariño et al., 2000). Apparently, the regional regression was partially controlled by eustasis; however, the main control was tectonic (e.g., Milani and De Wit, 2008; Vargas et al., 2020; this work).

Givetian to Frasnian interval – second transgression

In the Givetian to Frasnian interval, there is a transgressive system until reaching a maximum transgression or the surface of maximum transgression of the second order (Vargas et al., 2021) that coincides with the upper part of the São Domingos Formation. The sources are the same as the previous sequence, but with a new source represent by the Traíras Group, which indicates a far more distal source than the transgression originated in the early Devonian. In addition, many ages from the Famatinian magmatism and the Sunsas belt are present, which indicates that there could be a connection with the Tarija basin, which is also evidenced by the similar population of zircon ages between the São Domingos of the Paraná Basin (this work) and Iquiri Formation of the Paraná Basin (García Zavaleta et al., 2023). The evolution of ε_{Nd} (Fig. 11) shows a correlation between the Los Monos Formation with the isotopic data of the sequences of the Paraná Basin. Furthermore, Melo (1988), based on studies of marine marcofolisles, suggests a connection between the Tarija Basin and the northern part of the Paraná Basin. This fact reinforces our interpretations.

The ε_{nd} evolution diagram (Fig. 11) of the upper part of the São Domingos Formation indicates an important source associated with the Paranoá Group and Macizo de Goiás, which is concordant with the ages obtained from zircon grains, and it is possible to observe an increase in the zircon grain age populations that are associated with the Serra da Mesa, Paranoá and Traíras Groups. In this time interval, several authors (e.g., Copper, 1977; Melo, 1988; Penn-Clarke, 2019; Sedorko et al., 2021) suggest an extinction of the *Malvinokaffric Kingdom* caused by the transgression, due to the inflow of warmer waters into the cold sea.

Taking into account the tectonic events that affected the Tarija Basin (e.g., García Zavaleta et al., 2023), apparently, during the Givetian to Frasnian continued the flat-slap subduction in the southwestern margin of Gondwana, this situation despite a rise of the level sea during that time. On the other hand, a regional transgression is recorded in the São Domingos Formation (Paraná Basin, this work) and in the Los Monos Formation (Tarija Basin; Albariño et al., 2000). From our perspective, this transgression does not have a relationship with tectonics, although it could be related to eustasis (e.g., Haq and Schutter, 2008).

5.4 SEA LEVEL VARIATIONS DURING THE DEVONIAN AND ITS CORRELATION WITH OTHER BASINS

The western margin of Gondwana was a subduction zone (Ramos, 2018; Rapela et al., 2018) and an active front of collision in the Devonian associated with the Precordilleran Orogeny (Milani and de Wit, 2008; Linol et al., 2015; Henrique-Pinto et al., 2021), which generated local variations in sea level and controlled the sedimentation patterns of those basins. In this way, we compare the provenance data of the Devonian units fro the Paraná Basin with data for the same period from other SW Gondwanan basins, i.e., the Tarija, Chaco-Salteña, Precordillera, Sierras Australes, Malvinas and Cape basins (Figs. 14 and 15).

The record of detrital zircons in the Devonian stratigraphic units in the southwestern Gondwana basins (Fig. 16) is incomplete, to date. In the Tarija and Malvinas basins there is no clear a relation between T-R cycles and the distribution of the zircon grain age populations, whereas in the Precordillerana, Chaco-Paraná, Sierras Australes and Cape basins there are variations in the populations of detrital zircon ages, which may be associated with variations in sea level.

CONCLUSIONS

The sedimentary provenance of the Devonian units of the northeast sector of the Paraná basin has been evaluated through multidisciplinary studies (Petrography, XRD, Sr-Nd and U-Pb), which allowed us to recognize the different source zones.

It is proposed that the connection between the Paraná Basin and the Tarija Basin start fro the Pragian, in other words, during the deposition of the Ponta Grossa Formation.

Was possible to recognize the T-R cycle in the Devonian sedimentary record of the Paraná basin using geochronological (U-Pb on zircon grains) and isotopic data (Sr and Nd). The first transgressive event is represented by the Upper Furnas and Ponta Grossa formations, the first regressive event is represented by the São Domingos Formation (Tibagi Member), and the second transgressive event is represented by the upper part of the São Domingos.

The basins located in the SW of Gondwana no have a complete U-Pb data of the sedimentary record, which difficult to establish a relation between T-R cycles and zircon grain age populations. However, it is possible to see change in the zircon grain age populations in some basins, which could be related with transgressions and regressions (i.e., Precordillera, Chaco-Paraná, Sierras Australes and Cape basins). In basins such as Tarija and Malvinas, this relationship is no clear.

ACKNOWLEDGEMENTS

The authors are thankful to the *Laboratório de Estudos Geodinâmicos, Geocronológicos e Ambientais* (LEGGA) of the University of Brasília for the technical support. We also thank the *Coordenação de Aperfeiçoamento de Pessoal de Nível Superior – Brasil* (CAPES) for granting a Master scholarship to the first author. N. Hauser and W.U. Reimold are grateful for partial support of this study from the *Coordenação de Aperfeiçoamento de Pessoal de Nível Superior* (CAPES), under Finance Code 001. They were supported by Brazilian National Council for Scientific and Technological Development (CNPq) fellowships (No. 309878/2019-5).

FIGURE CAPTIONS:

Figure 1. Map of Geotectonic provinces of South America and Paraná basin supersequence (modified from Cordani et al., 2000; Bahlburg et al., 2009 and Milani, 2004). CA: Central Amazonian Province; MI: Marconi-Icantiunas Province; RNJ: Rio

Negro-Juruena mobile belt; RO: Rondoni-San Ignacio mobile belt; S: Sunsas mobile belt; VT: Ventuari-Tapajós mobile belt.

Figure 2. Geologic map of the Brasilia belt and Paraguay belt (Modified from Dardenne, 2000; Fuck et al., 2017).

Figure 3. Lower Paleozoic stratigraphic sequences of the Paraná Basin: A) Relationship with regional tectonic events (Milani and Ramos 1998; Milani and De Wit., 2008; Linol et al., 2015); B) Tectonic subsidence (Zalan et al. 1990; Milani and de Wit 2008; Linol et al., 2015). Taken from Linol et al. (2015).

Figure 4. Generalized stratigraphic column of the Silurian? - Devonian of the Paraná Basin, taken from Assine (1996) where the boundaries of the T and R sequences (Vargas et al, 2020) are represented (MRS: maximum regression surface and MTS: maximum transgression surface). The circles represent the samples obtained in this study, and the triangles and squares those used from the literature.

Figure 5. Ternary classification (Garzanti, 2019) and provenance (Dickinson, 1985) diagrams of sandstones from the São Domingos and Ponta Grossa formations. F: feldspars, Q: total quartz, L: lithic fragments.

Figure 6. Stratigraphic variation of Sr and Nd isotope compositions ($^{87}Sr/^{86}Sr$ and ε_{Nd}) and model age (T_{DM}) for the samples analyzed from Devonian units of the Paraná Basin. Ordv: Ordovician; Low: Lower; Silur: Silurian; Up: Upper.

Figure 7. Detrital zircon U-Pb dating and stratigraphic relationships. Kernel density estimator diagrams of detrital zircon grains from the São Domingos, Ponta Grossa, Furnas formations (Unit I, II and III) and the Rio Ivaí Group (Vila Maria and Alto Garças formations). Additional data from (a)Santos et al. (2015), (b)Henrique-Pinto (2021) and (c)Gezatt (2011). SA: Sedimentation age.

Figure 8. A) Elongation and percent roundness of unbroken zircon grains. B) Th/U ratio versus age. C) Th/U ratio less than 0.1.

Figure 9. Length of zircon grains versus age and elongation of zircon grains versus age.

Figure 10. A) Kernel density estimation plot of detrital zircon ages from the northern part of the Paraná Basin, including data from Gezatt (2011); Santos et al. (2015) and Henrique-Pinto et al. (2021). Proximal sources represented by field 2; intermediate sources

represented by fields 4, 6, 7 and 8; and distal/very distal sources represented by fields 1,3, 5 and 9. B) Kernel density estimation plot of detrital zircon ages from potential sources in the northern part of the Paraná Basin. S: Sunsas Belt; R-SI: Rondônia-San Ignacio Province; R-J: Rio Negro-Juruena Province; V-T: Ventuari-Tapajós Province; M-I: Maroni-Itacaiunas Province; CAP: Central Amazonian Province. Data obtained from Piuzana et al. (2003a), Marques (2009), Matteini et al. (2012), Rodrigues et al. (2012), McGee et al. (2015, 2018), Falci et al. (2018), Martins-Ferreira et al. (2018) and Silva et al. (2020).

Figure 11. Age (Ga) versus ε_{Nd} diagram for Devonian units of the northern part of the Paraná (this work) and Tarija (García Zavaleta et al., 2023) basins. Epsilon Nd (ε_{Nd}) were calculated to the time of deposition (380 Ma). Fields represent potential source areas. Data obtained from Pimente and Fuck (1992), Pimentel et al. (1996), Santos et al. (2000), Pimente et al. (2001), Junge et al. (2002), Laux et al. (2005), Marques (2009), Alasino et al. (2016, 2020).

Figure 12. Tectonic discrimination diagram for convergent, collisional, and extensional basins (Cawood et al., 2012) showing the possible tectonic setting of the northern part of the Paraná Basin based on differences between crystallization and depositional ages (CA–DA) of the zircon grains. Data from Gezatt (2011); Santos et al. (2015); and Henrique-Pinto et al. (2021). Notation N = (a, b/c) represents the number of zircon grains, where a = number of samples, b = number of zircon grains with concordant ages, and c = total number of zircon grains analyzed.

Figure 13. Multidirectional scaling plot (MDS) showing detrital zircon ratios of the northern part of the Paraná Basin, southern part of the Paraná Basin and Tarija Basin**.**

Figure 14. Paleogeography of the Lower Devonian of SW Gondwana. Pre-Andean terranes, distribution of the *Malvinokaffric Kingdom* and regional lineaments such as the Transbrasilian (TL) and Brasilian (BL) as indicated in the figure (Vargas et al., 2020; Sedorko et al., 2021).

Figure 15. Lithostratigraphic correlation of the different basins in SW Gondwana: (1) Precordillera according to García Muro et al. (2014); (2) Tarija according to Albariño et al. (2000); (3) Chaco-Salteña according to Noetinger (2010); (4) Paraná (this work); (5) Chaco-Paraná according to Uriz et al. (2016); (6) Sierras Australes according to Cingolani et al. (2002); (7) Malvinas-Falkland according to Marshall (2016) and Cabo according to

Penn-Clarke et al. (2019). T1: First Transgression, R1: First Regression, T2: Second Transgression, R2: Second regression, MRS: Maximum Regression Surface and MTS: Maximum Transgression Surface.

Figure 16. Kernel density estimation (KDE) plot of detrital zircon ages from different basins of SW Gondwana. Data obtained from Fourie et al. (2010); Uriz et al. (2011, 2016); Calle (2013); Ramos et al. (2014, 2017); Arnol et al. (2020, 2022); Henrique-Pinto et al., 2021) and García Zavaleta et al. (2023).

TABLE LIST:

Table 1. Stratigraphic division of the northern part of the Paraná Basin (Alto Garças sub-basin). Modified from Scheffler et al. (2020).

Table 2. Mineral abbreviations according to Whitney and Evans (2010).

Table 3. Summary of the modal composition of the sandstones of the Ponta Grossa and São Domingos Formations. F: feldspars; Q: quartz; Qm: single-crystalline quartz; Qp: polycrystalline quartz; L: lithic fragments; Lm: metamorphic lithic fragments; Li: igneous lithic fragments.

*Samples from the TF-University of Brasilia project (2012).

Table 4. Mineral composition, as defined by X-Ray Diffraction, of the pelitic samples collected from the Ponta Grossa and São Domingos formations.

*Samples from the TF-University of Brasilia project (2012).

Table 5. TDM ages calculated after the model of Goldstein et al. (1984). The $^{87}Sr/^{86}Sr_{(380)}$ ratios were calculated from the NASC references values for fine-grained rocks given by Gromet et al. (1984), where Rb: 125 ppm and Sr: 142 ppm and for the Ponta Grossa Formation from the values obtained from the same formation in the northwest part given by Montibeller et al. (2017), where Rb: 115 ppm and Sr: 92 ppm.

SUPPLEMENTARY DATA:

Supplementary Figure S1. Outcrop map of the Devonian units of the Paraná Basin and distribution of samples in the study area (Zone A and Zone B). Maps taken from Montiebeller et al. (2017) and Vargas et al. (2020).

Supplementary Figure S2. Field photographs where the samples for this study were obtained (A, B, C, D, E, F, G, H and I). Microphotographs of samples from the upper part of the São Domingos Formation (J), the lower part of the São Domingos Formation - Tibagi Member (K and L) and the Ponta Grossa Formation (M, N and O). Qz: quartz; Kfs: potassium feldspar; Pl: plagioclase; Ms: muscovite; Kln: kaolinite; Ilt: illite; Zrn: zircon; Hem: hematite, Goet: goethite; Mx: Matrix.

Supplementary Figure S3. Diffractograms of the São Domingos and Ponta Grossa formations.

Supplementary Table S1. U-Pb data of detrital zircon grains from sandstones samples of the Alto Garças, Furnas, Ponta Grossa and São Domingos formations.

Tables

<table>
<tr><th>Oliveira (1912)</th><th colspan="2">Oppenheim (1936)</th><th>Almeida (1948, 1954)</th><th>Andrade & Camarço (1978, 1980)</th><th colspan="2">Evans (1984); Melo (1985, 1988)</th><th colspan="2">Popp (1986); Assine (1996); Milani (2004)</th><th>Sedorko et al. (2018)</th><th colspan="2">Grahn et al. (2013); Scheffler et al. (2020)</th></tr>
<tr><td rowspan="2">Arenito Tibagi</td><td rowspan="4">Paraná Serie</td><td rowspan="3">Ponta Grossa com Arenito Tibagi intercalado Formation</td><td rowspan="3">Ponta Grossa Facies</td><td>Upper Member</td><td colspan="2">Chapada IV Group</td><td rowspan="4">Ponta Grossa Formation</td><td>São Domingos Member</td><td>Not registered on the eastern edge</td><td rowspan="2">São Domingos Formation</td><td>Subunits IV Givetiano- Frasniano</td></tr>
<tr><td rowspan="2">Folhelho Ponta Grossa</td><td>Middle Member</td><td colspan="2">Chapada III Group</td><td rowspan="2">Tibagi Member</td><td>Devonian II Sequence</td><td rowspan="2">Subunits II and III; Middle Emisian - Eifelian</td></tr>
<tr><td rowspan="2">Lower Member</td><td rowspan="2">Chapada II Group</td><td>Upper</td><td>Devonian I Sequence</td></tr>
<tr><td>Lower</td><td>Jaguariaíva Member</td><td>Silurian - Devonian Sequence</td><td>Ponta Grossa Formation</td><td>Praguian- Early Emisian</td></tr>
<tr><td>Arenito Furnas</td><td>Arenito Furnas</td><td>Furnas Facies</td><td>Furnas Formation</td><td colspan="2">Chapada I Group</td><td colspan="2">Furnas Formation</td><td>Lower Silurian sequence</td><td colspan="2">Furnas Formation</td></tr>
</table>

Table 1

kaolinite	Kln	Goethite	Goet
Illite	Ilt	Clorite	Chl
Quartz	Qz	Feldspar	Fld
Hematite	Hem	Plagioclase	Pl

Table 2

Units	Sample	Total	Q		F		L		Heavy Minerals	Accessory	Matrix (%)	% (Gazzi & Dickinson technique)						Petrographic classification (Sandstones)
			Qm	Qp	FK	P	Li	Lm	Zircon	Muscovite		Total quartz	(%)	Total feldspars	(%)	Total lithics	(%)	
São Domingos Fm.	BPN-11A	449	406	1	35	4	1			2	15	407	91	39	9	1	0	Quartzose
São Domingos Fm. - Tibagi Mb.	TF-II-200*	411	396	1		3				11	10	397	99	3	1			Quartzose - pure
São Domingos Fm. - Tibagi Mb.	TF-IV-038*	410	371	26	2	1			1	9	2	397	99	3	1			Quartzose - pure
São Domingos Fm. - Tibagi Mb.	TF-III-222*	418	394	2		8				14	25	396	98	8	2			Quartzose - pure
São Domingos Fm. - Tibagi Mb.	BPN-07A	439	427		8					4	40	427	98	8	2			Quartzose - pure
São Domingos Fm. - Tibagi Mb.	BPN-08A	441	433	5	2					1	25	438	100	2	0			Quartzose - pure
Ponta Grossa Fm.	BPN-10A	407	353	1	52						20	354	87	52	13			Feldspatho-quartzose
Ponta Grossa Fm.	BPN-12A	446	365	29	24	1			2	25	5	394	94	25	6			Quartzose
Ponta Grossa Fm.	BPN-06A	428	385	2	1			29		11	25	387	93	1	0	29	7	Quartzose

Table 3

Units	Sample	Lithology	Kln	Ilt	Qz	Hem	Goet	Chl	Fld	Pl
São Domingos Fm.	BPN-11B	Shale	M	m	m	tr	-	-	tr	-
São Domingos Fm. - Tibagi Mb.	TF-II-124*	Shale	m	m	M	-	-	-	M	M
São Domingos Fm. - Tibagi Mb.	TF-II-199*	Shale	m	m	M	-	tr	-	-	-
São Domingos Fm. - Tibagi Mb.	BPN-03B	Shale	M	m	tr	tr	-	tr	tr	-
São Domingos Fm. - Tibagi Mb.	BPN-07B	Siltstone	m	m	tr	M	-	-	-	-
São Domingos Fm. - Tibagi Mb.	BPN-08B	Shale	m	M	tr	M	m	m	-	tr
Ponta Grossa Fm.	BPN-10A	Shale	m	m	M	tr	-	-	tr	-
Ponta Grossa Fm.	BPN-09B	Shale	m	m	tr	M	-	-	-	-
Ponta Grossa Fm.	BPN-06B	Shale	m	m	tr	M	-	tr	-	tr

Table 4

Sample	Units	lithology	Estimated depositional age (Ma)	Sm (ppm)	Nd (ppm)	$^{147}Sm/^{144}Nd$	$^{143}Nd/^{144}Nd$	±2SE (10^{-5})	TDM (Ga)	εNd (0)	$\varepsilon Nd_{(380\ Ma)}$	87Sr/86Sr(0)	±2SE (10^{-5})	$87Sr/86Sr_{(380\ Ma)}$
BPN-11B	São Domingos Fm.	Shale	380	7.551	40.768	0.1120	0.51179	±6	1.82	-16.5	-12.4	0.72354	4	0.70974
BPN-03B	São Domingos Fm. - Tibagi Mb.	Shale	393	12.280	58.444	0.1270	0.51183	±4	2.05	-15.7	-12.4	0.73057	6	0.71676
BPN-07B	São Domingos Fm. - Tibagi Mb.	Siltstone	393	9.379	41.655	0.1361	0.51195	±4	2.07	-13.5	-10.6	0.72131	5	0.70751
BPN-08B	São Domingos Fm. - Tibagi Mb.	Shale	393	-	-	-	-	-	-	-	-	0.71186	5	0.69807
BPN-10B	Ponta Grossa Fm.	Shale	407	8.628	47.728	0.1093	0.51184	±5	1.72	-15.6	-11.4	0.72113	3	0.70154
BPN-09B	Ponta Grossa Fm.	Shale	407	14.845	49.574	0.1810	0.51195	±3	-	-13.3	-	0.71432	5	0.69474
BPN-06B	Ponta Grossa Fm.	Shale	407	14.737	68.754	0.1296	0.51188	±5	2.03	-14.8	-11.6	0.71324	6	0.69366
BPN-05B	Upper Furnas Fm.	Siltstone	419	9.001	62.026	0.0877	0.51181	±2	1.48	-16.1	-10.9	0.73683	6	0.72301
BPN-04B	Upper Furnas Fm.	Siltstone	419	6.517	37.588	0.1048	0.51177	±2	1.75	-17.0	-12.5	0.73030	4	0.71649
BPN-01B	Lower Furnas Fm.	Siltstone	427	6.546	35.445	0.1116	0.51191	±5	1.66	-14.2	-10.0	0.71949	4	0.70569
BPN-02B	Vila Maria Fm.	Shale	433	7.148	38.894	0.1111	0.51196	±6	1.58	-13.2	-9.0	0.74164	2	0.72781

Table 5

Figures

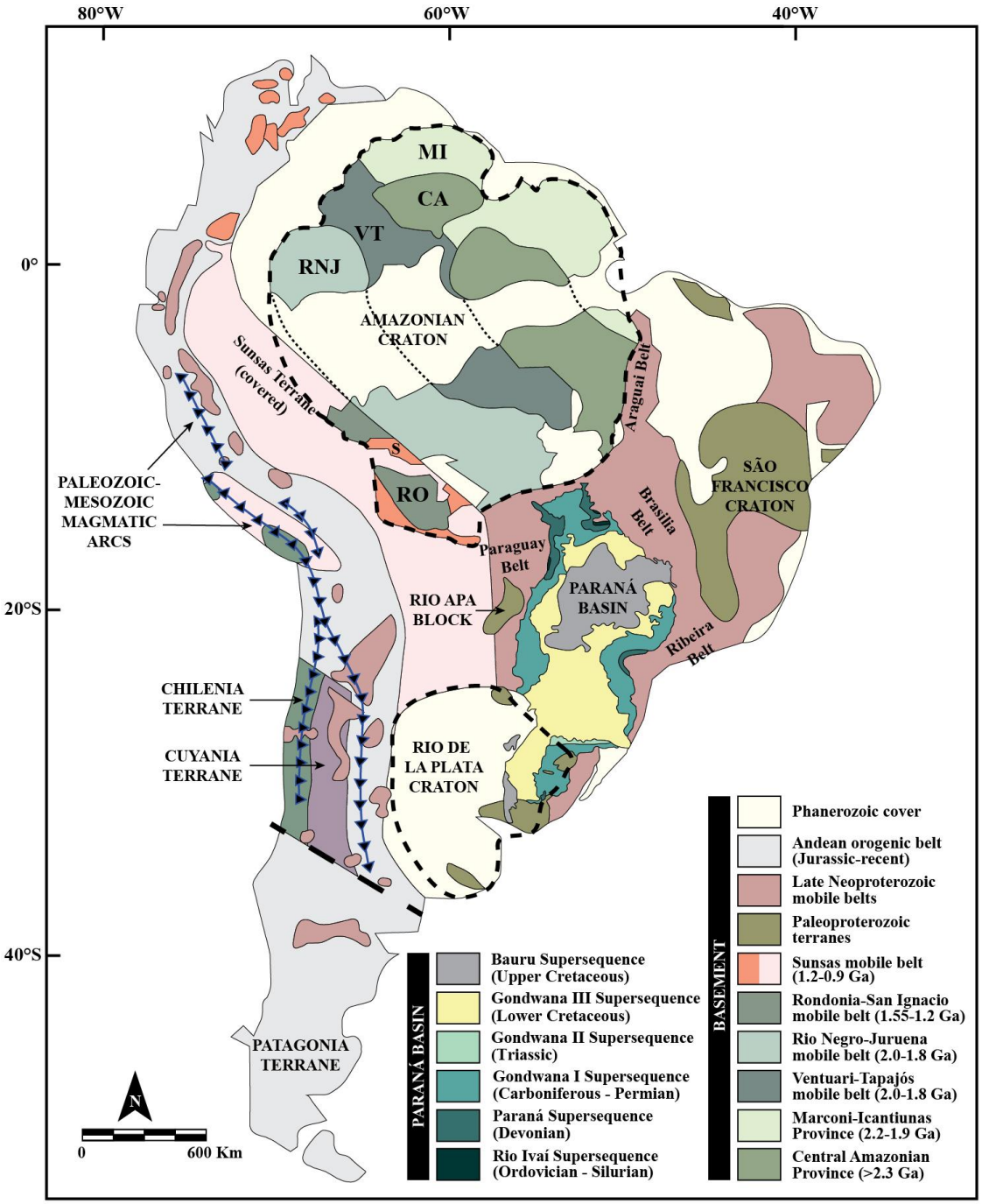

Figure 1

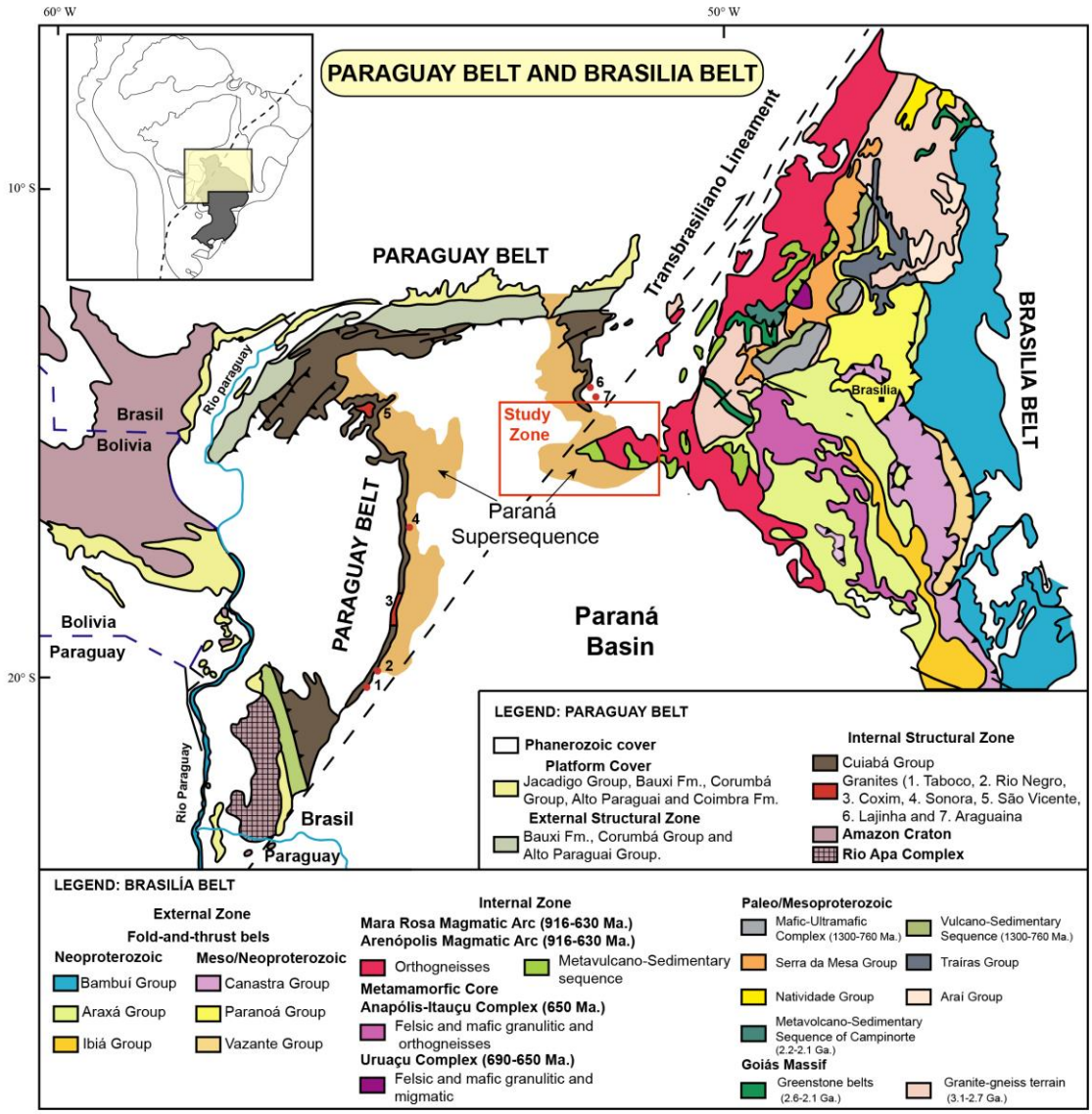
60° W
50° W
10° S
20° S
PARAGUAY BELT AND BRASILIA BELT
PARAGUAY BELT
Transbrasiliano Lineament
BRASILIA BELT
Brasilia
Brasil
Bolivia
Rio paraguay
Study Zone
Paraná Supersequence
PARAGUAY BELT
Paraná Basin
Bolivia
Paraguay
Rio Paraguay
Brasil
Paraguay
1
2
3
4
5
6
7
LEGEND: PARAGUAY BELT
Phanerozoic cover
Platform Cover
Jacadigo Group, Bauxi Fm., Corumbá Group, Alto Paraguai and Coimbra Fm.
External Structural Zone
Bauxi Fm., Corumbá Group and Alto Paraguai Group.
Internal Structural Zone
Cuiabá Group
Granites (1. Taboco, 2. Rio Negro, 3. Coxim, 4. Sonora, 5. São Vicente, 6. Lajinha and 7. Araguaina
Amazon Craton
Rio Apa Complex
LEGEND: BRASILIA BELT
External Zone
Fold-and-thrust bels
Neoproterozoic
Bambuí Group
Araxá Group
Ibiá Group
Meso/Neoproterozoic
Canastra Group
Paranoá Group
Vazante Group
Internal Zone
Mara Rosa Magmatic Arc (916-630 Ma.)
Arenópolis Magmatic Arc (916-630 Ma.)
Orthogneisses
Metavulcano-Sedimentary sequence
Metamamorfic Core
Anapólis-Itauçu Complex (650 Ma.)
Felsic and mafic granulitic and orthogneisses
Uruaçu Complex (690-650 Ma.)
Felsic and mafic granulitic and migmatic
Paleo/Mesoproterozoic
Mafic-Ultramafic Complex (1300-760 Ma.)
Vulcano-Sedimentary Sequence (1300-760 Ma.)
Serra da Mesa Group
Traíras Group
Natividade Group
Araí Group
Metavolcano-Sedimentary Sequence of Campinorte (2.2-2.1 Ga.)
Goiás Massif
Greenstone belts (2.6-2.1 Ga.)
Granite-gneiss terrain (3.1-2.7 Ga.)

Figure 2

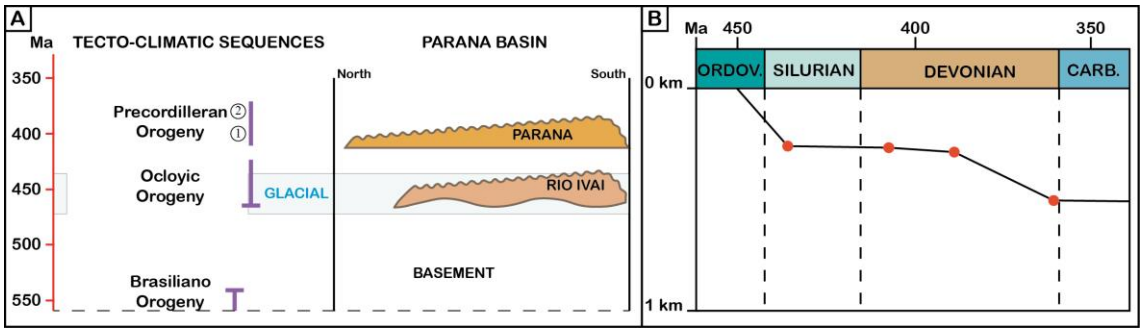

Figure 3

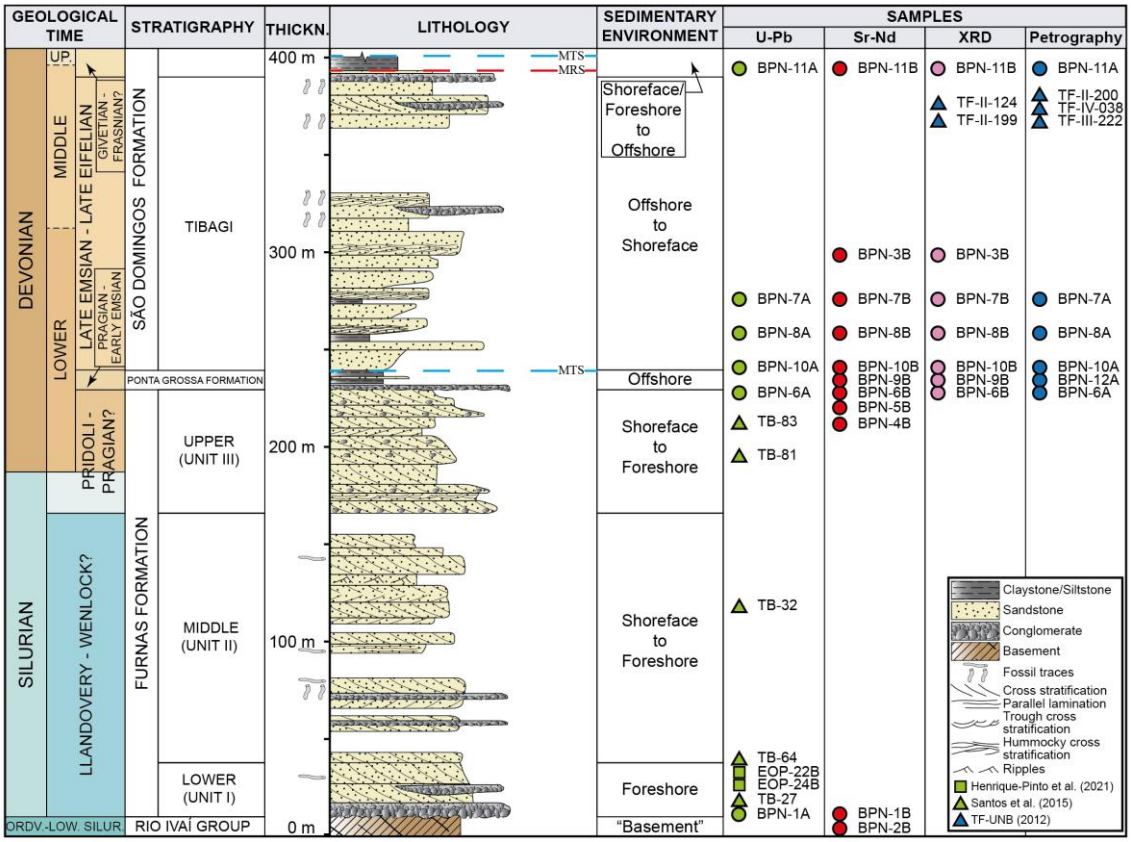

Figure 4

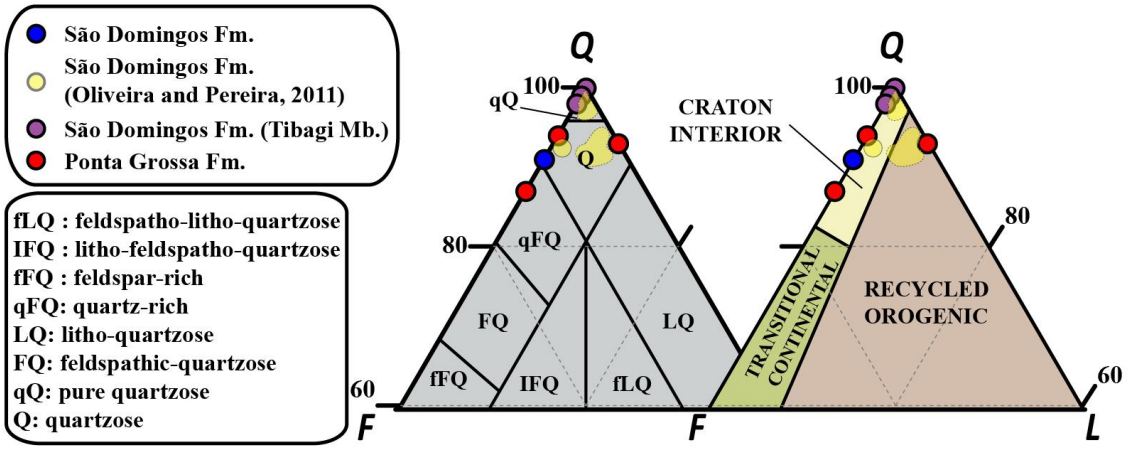

Figure 5

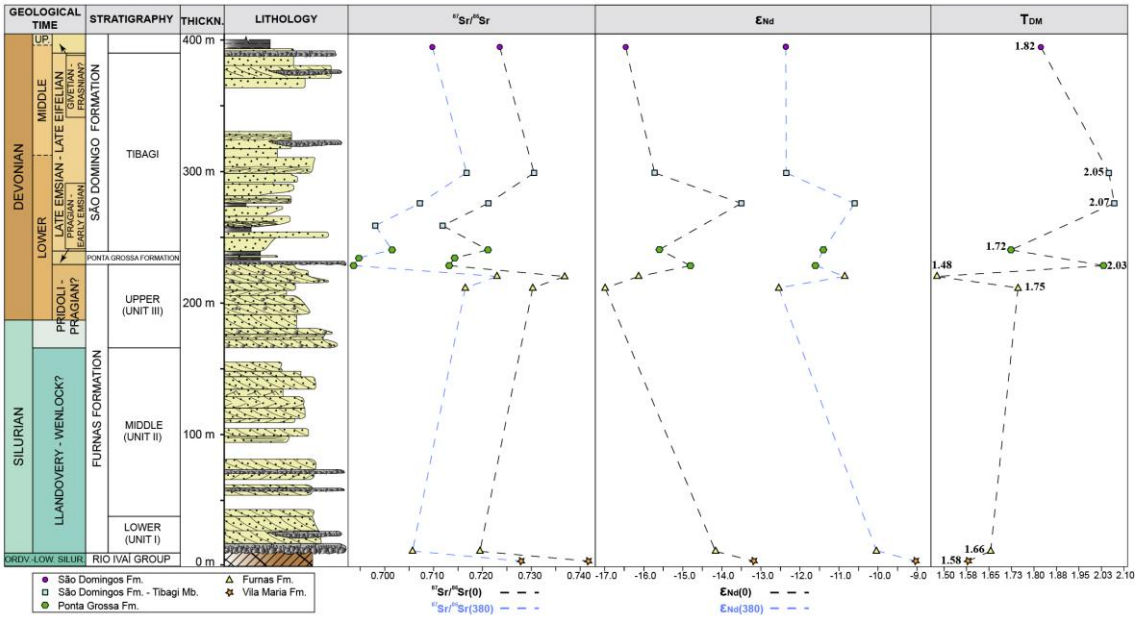

Figure 6

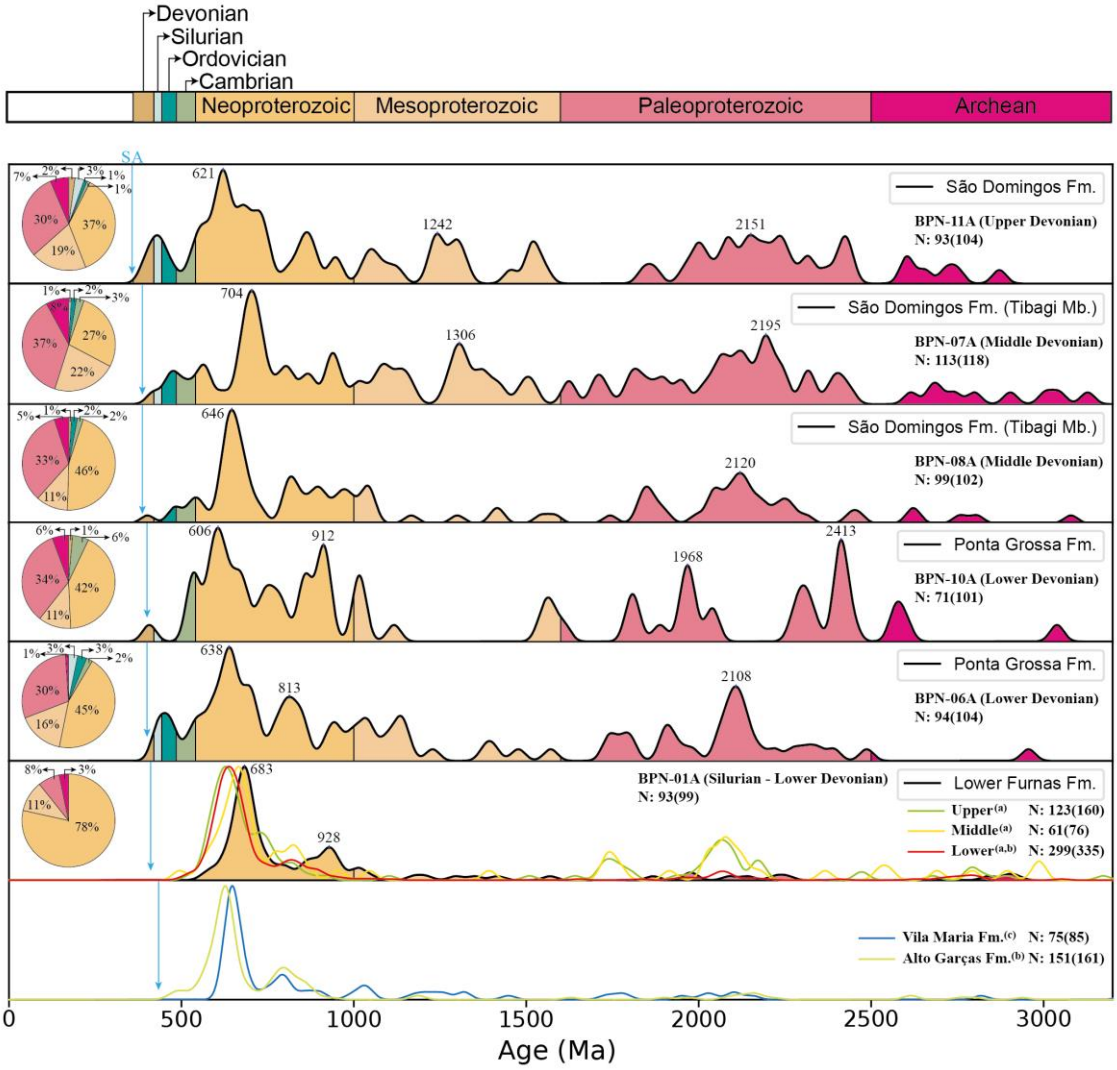
Devonian
Silurian
Ordovician
Cambrian
Neoproterozoic
Mesoproterozoic
Paleoproterozoic
Archean
SA
São Domingos Fm.
BPN-11A (Upper Devonian)
N: 93(104)
São Domingos Fm. (Tibagi Mb.)
BPN-07A (Middle Devonian)
N: 113(118)
São Domingos Fm. (Tibagi Mb.)
BPN-08A (Middle Devonian)
N: 99(102)
Ponta Grossa Fm.
BPN-10A (Lower Devonian)
N: 71(101)
Ponta Grossa Fm.
BPN-06A (Lower Devonian)
N: 94(104)
BPN-01A (Silurian - Lower Devonian)
N: 93(99)
Lower Furnas Fm.
Upper(a) N: 123(160)
Middle(a) N: 61(76)
Lower(a,b) N: 299(335)
Vila Maria Fm.(c) N: 75(85)
Alto Garças Fm.(b) N: 151(161)
Age (Ma)

Figure 7

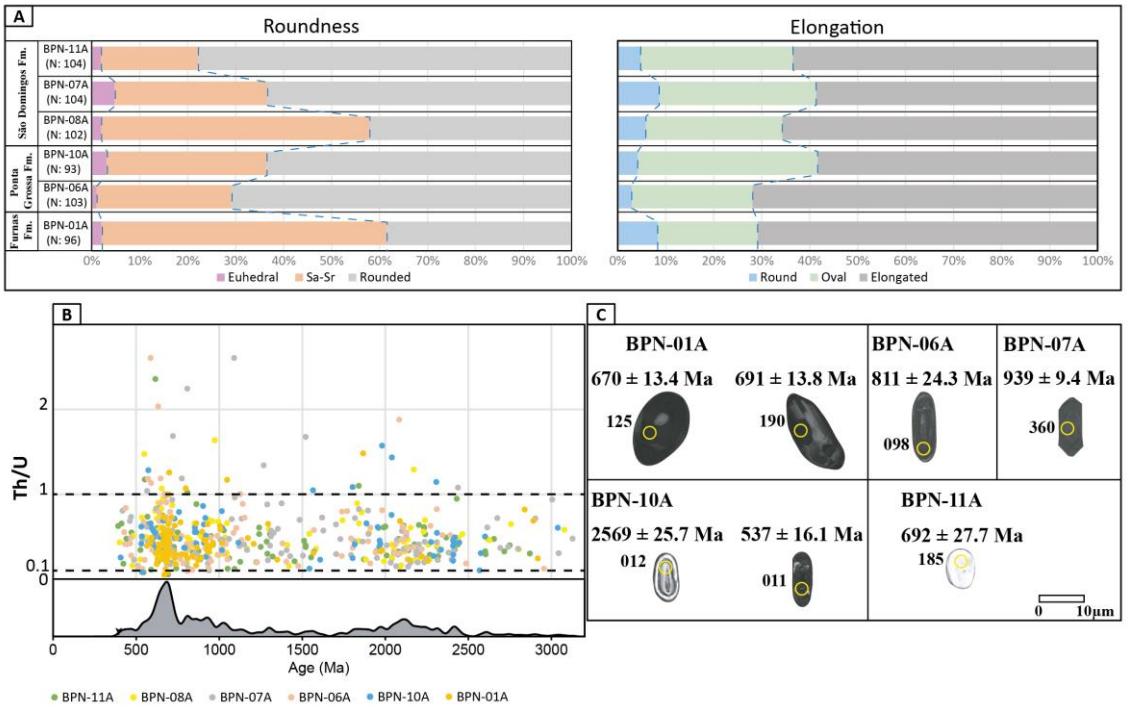
A
Roundness
Elongation
São Domingos Fm.
Ponta Grossa Fm.
Furnas Fm.
BPN-11A (N: 104)
BPN-07A (N: 104)
BPN-08A (N: 102)
BPN-10A (N: 93)
BPN-06A (N: 103)
BPN-01A (N: 96)
0% 10% 20% 30% 40% 50% 60% 70% 80% 90% 100%
Euhedral Sa-Sr Rounded
Round Oval Elongated
B
Th/U
2
1
0.1
0
0 500 1000 1500 2000 2500 3000
Age (Ma)
BPN-11A BPN-08A BPN-07A BPN-06A BPN-10A BPN-01A
C
BPN-01A
670 ± 13.4 Ma
691 ± 13.8 Ma
125
190
BPN-06A
811 ± 24.3 Ma
098
BPN-07A
939 ± 9.4 Ma
360
BPN-10A
2569 ± 25.7 Ma
537 ± 16.1 Ma
012
011
BPN-11A
692 ± 27.7 Ma
185
0 10µm

Figure 8

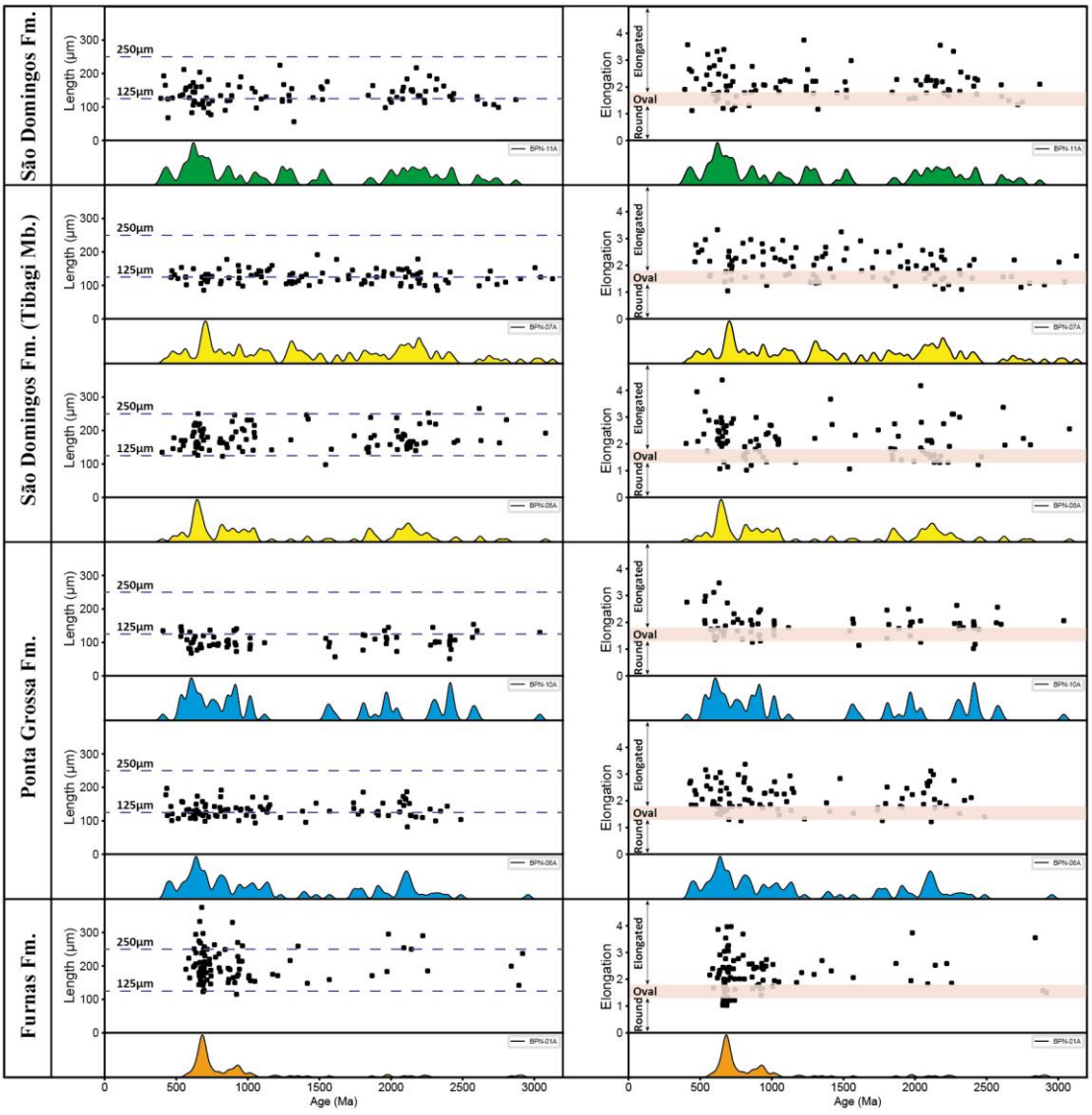
São Domingos Fm.
São Domingos Fm. (Tibagi Mb.)
Ponta Grossa Fm.
Furnas Fm.
Length (µm)
250µm
125µm
Elongation
Elongated
Oval
Round
BPN-11A
BPN-07A
BPN-08A
BPN-10A
BPN-06A
BPN-01A
Age (Ma)

Figure 9

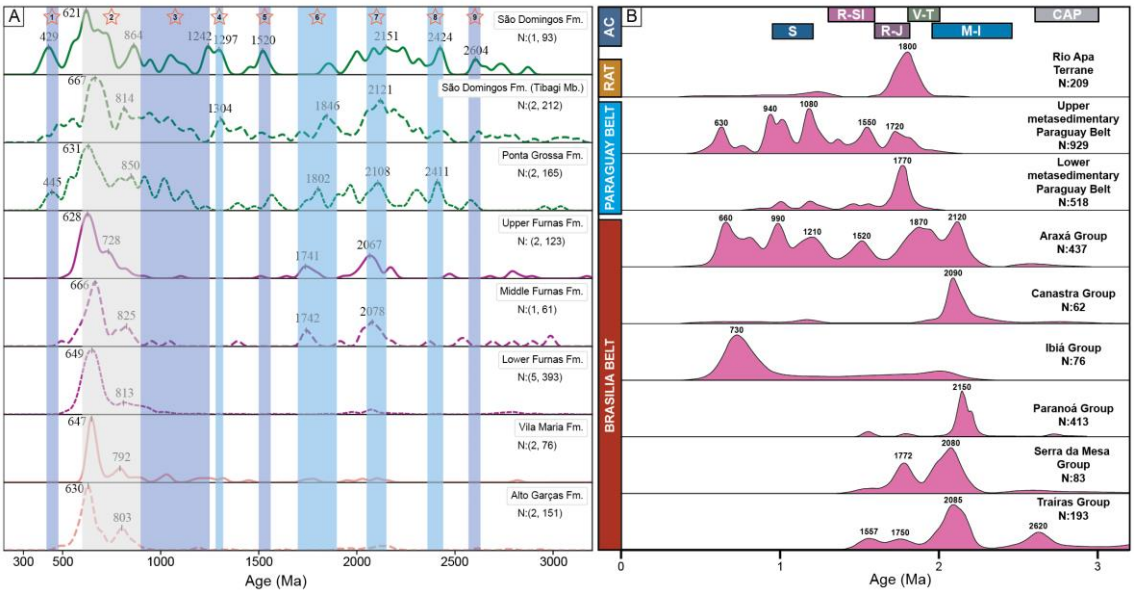

Figure 10

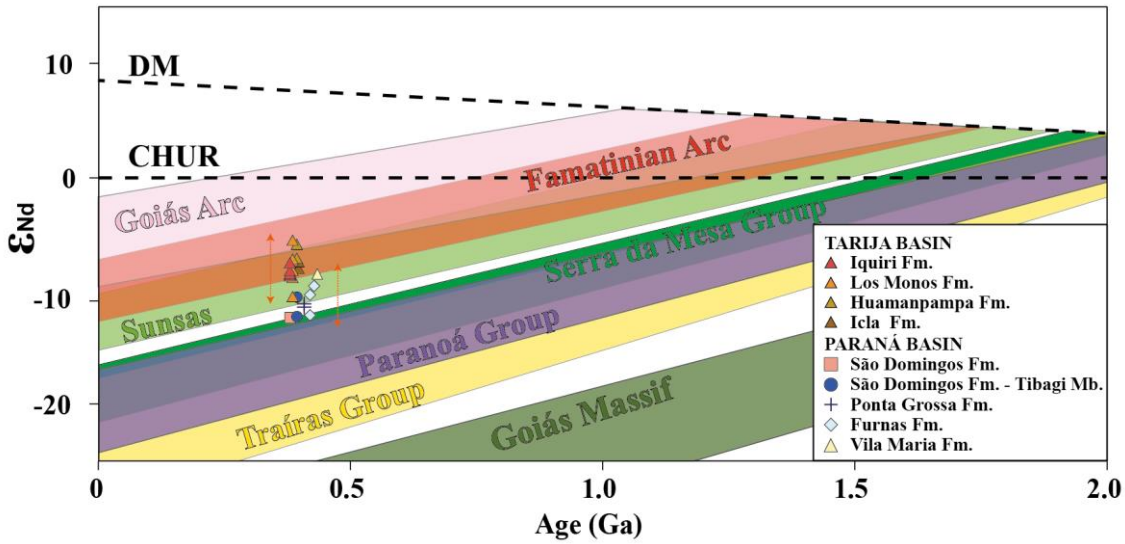

Figure 11

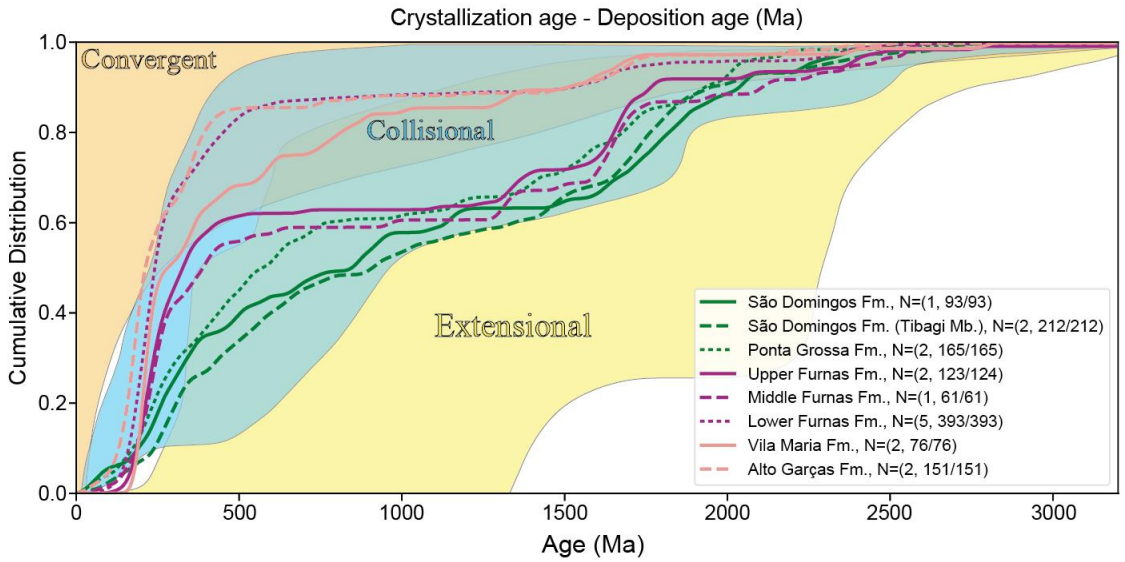

Figure 12

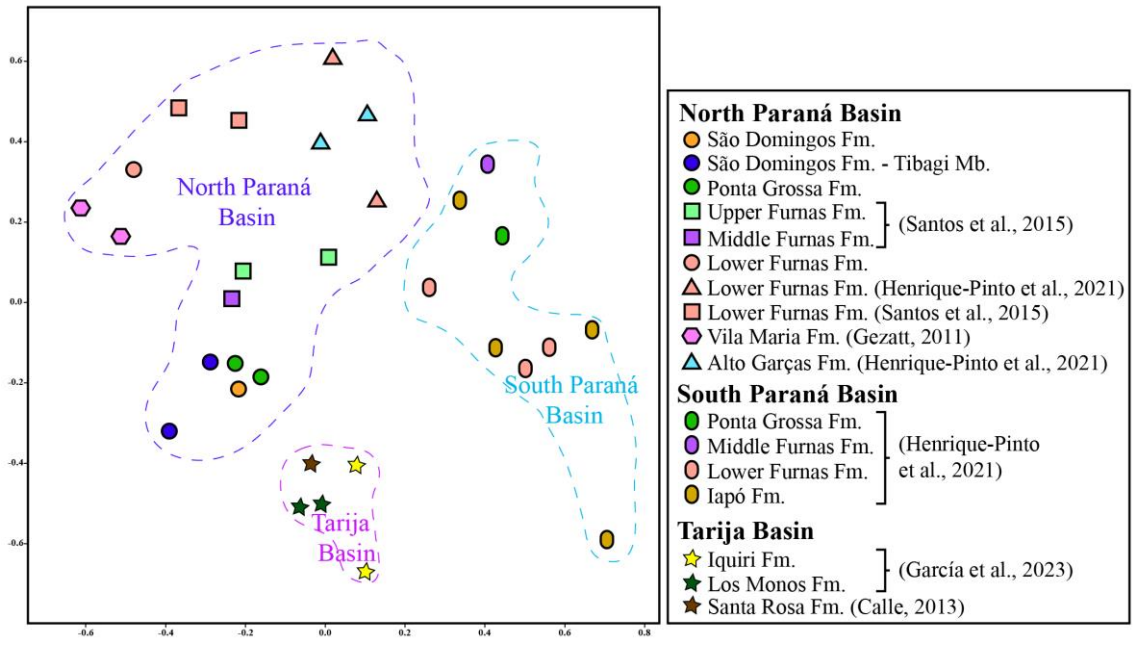

Figure 13

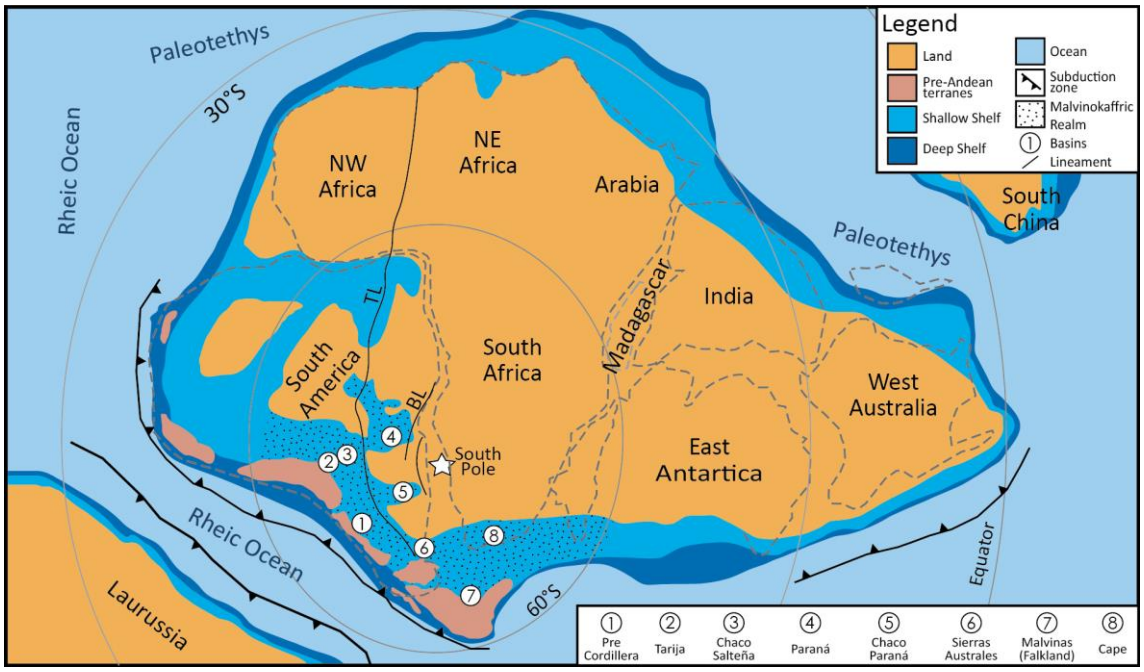

Figure 14

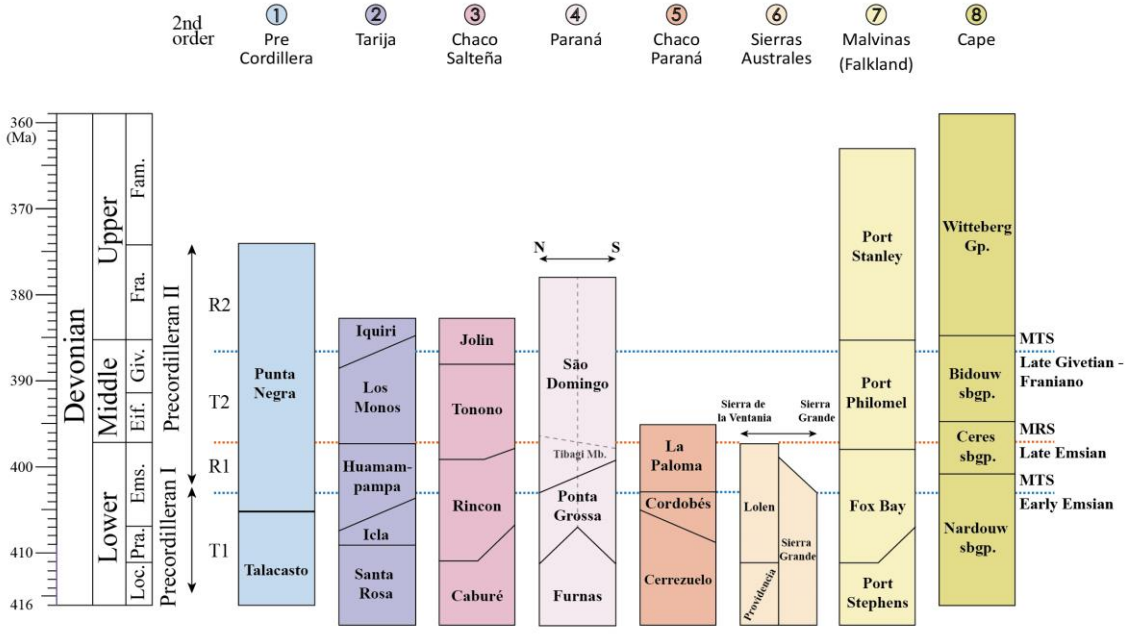

Figure 15

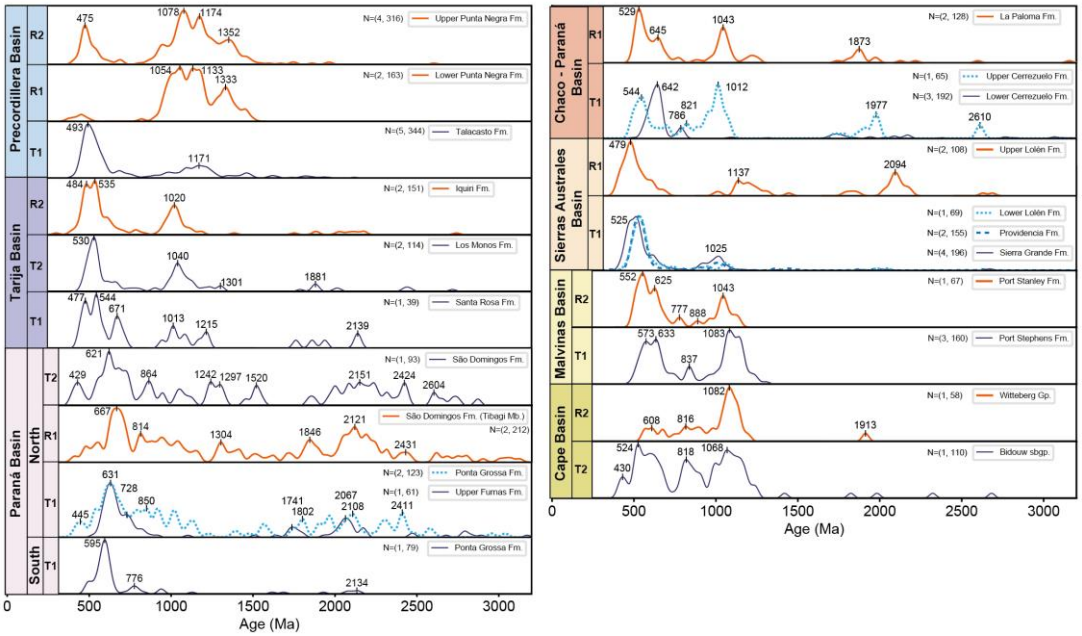
Precordillera Basin
R2
R1
T1
Tarija Basin
R2
T2
T1
Paraná Basin
North
T2
R1
T1
South
T1
Chaco - Paraná Basin
R1
T1
Sierras Australes Basin
R1
T1
Malvinas Basin
R2
T1
Cape Basin
R2
T2
N=(4, 316) Upper Punta Negra Fm.
N=(2, 163) Lower Punta Negra Fm.
N=(5, 344) Talacasto Fm.
N=(2, 151) Iquiri Fm.
N=(2, 114) Los Monos Fm.
N=(1, 39) Santa Rosa Fm.
N=(1, 93) São Domingos Fm.
São Domingos Fm. (Tibagi Mb.)
N=(2, 212)
N=(2, 123) Ponta Grossa Fm.
N=(1, 61) Upper Furnas Fm.
N=(1, 79) Ponta Grossa Fm.
N=(2, 128) La Paloma Fm.
N=(1, 65) Upper Cerrezuelo Fm.
N=(3, 192) Lower Cerrezuelo Fm.
N=(2, 108) Upper Lolén Fm.
N=(1, 69) Lower Lolén Fm.
N=(2, 155) Providencia Fm.
N=(4, 196) Sierra Grande Fm.
N=(1, 67) Port Stanley Fm.
N=(3, 160) Port Stephens Fm.
N=(1, 58) Witteberg Gp.
N=(1, 110) Bidouw sbgp.
0
500
1000
1500
2000
2500
3000
Age (Ma)

Figure 16

Supplementary data

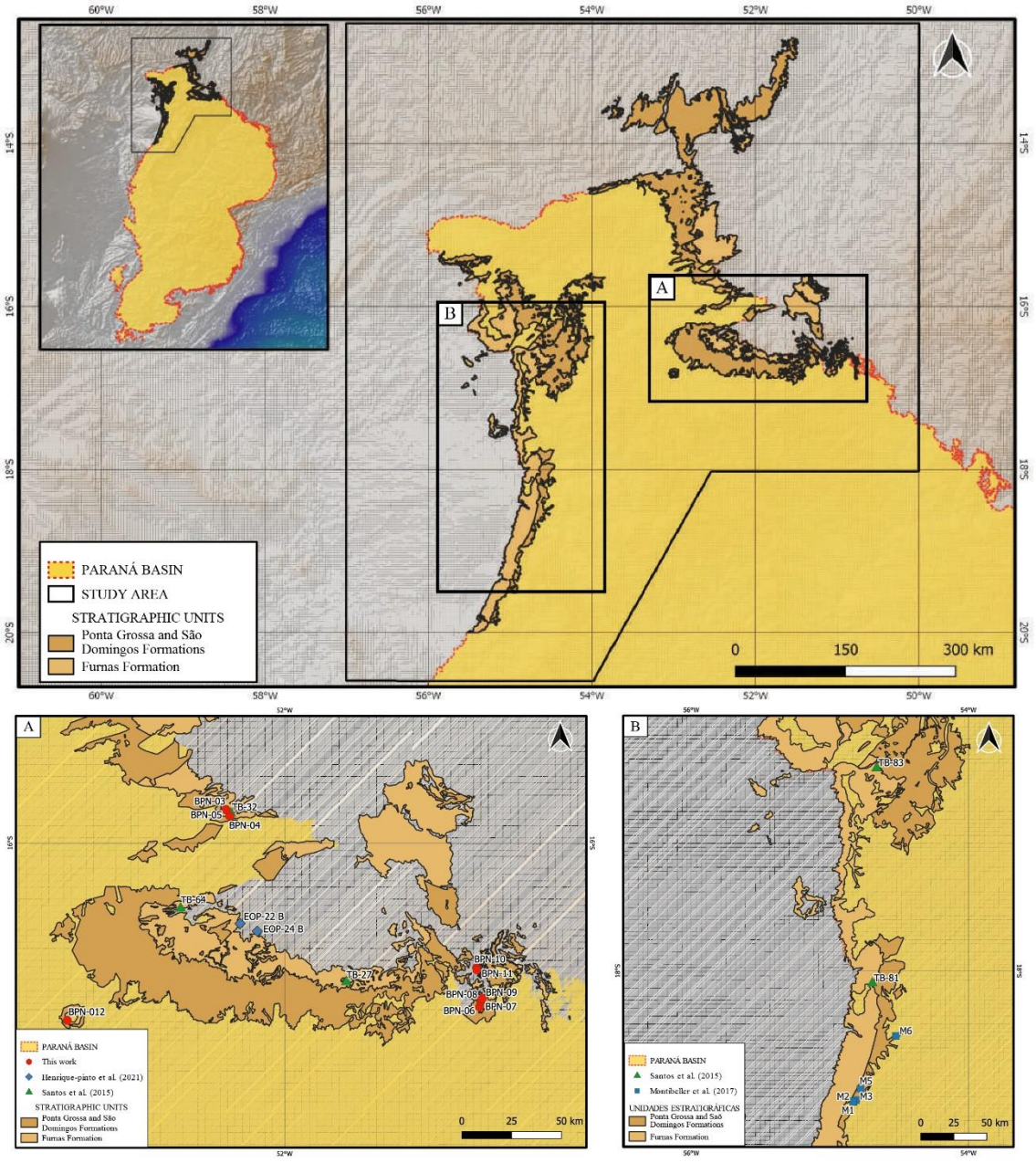

Figure 1

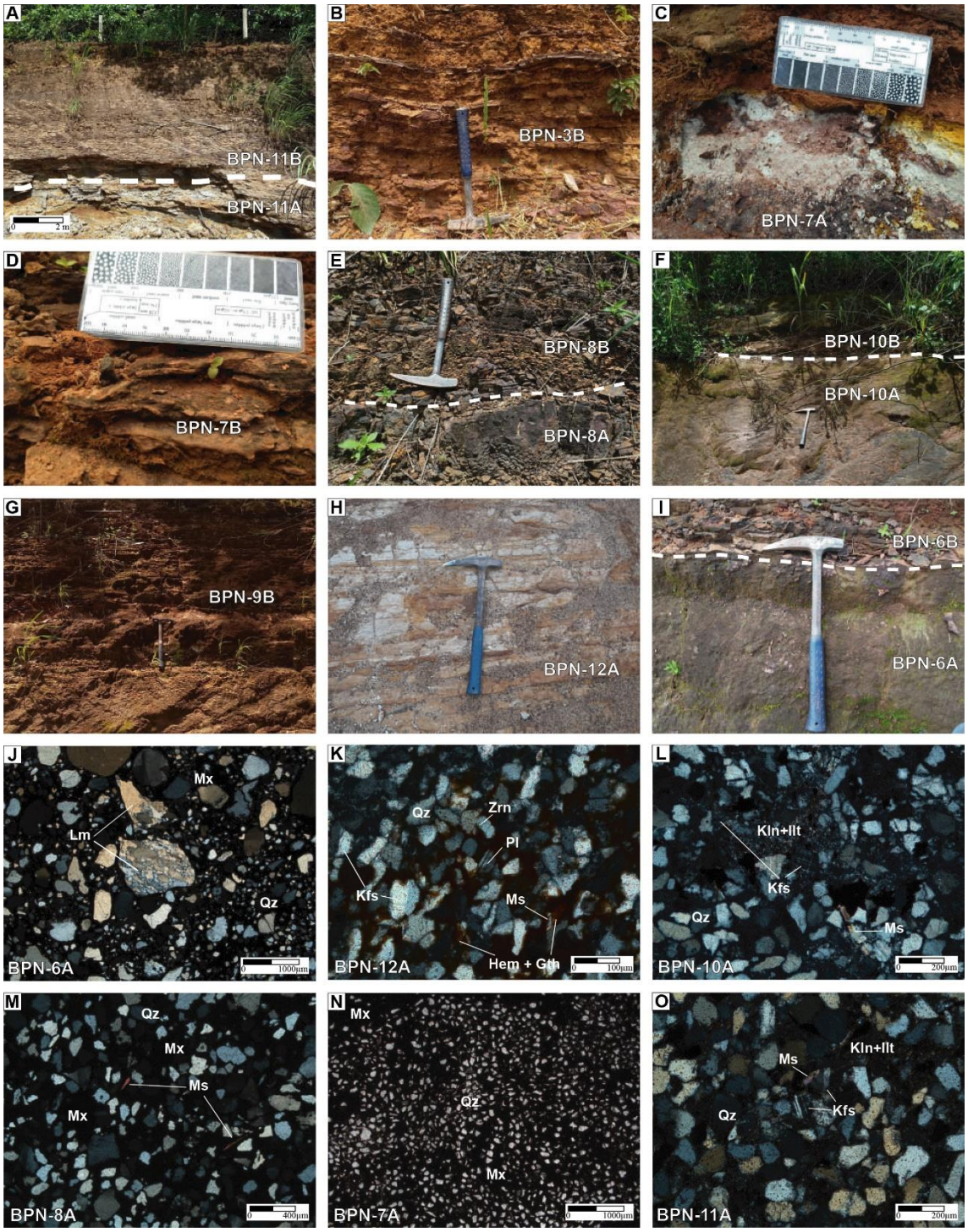
A
BPN-11B
BPN-11A
B
BPN-3B
C
BPN-7A
D
BPN-7B
E
BPN-8B
BPN-8A
F
BPN-10B
BPN-10A
G
BPN-9B
H
BPN-12A
I
BPN-6B
BPN-6A
J
Mx
Lm
Qz
BPN-6A
K
Qz
Zrn
Pl
Kfs
Ms
Hem + Gth
BPN-12A
L
Kln+Ilt
Kfs
Qz
Ms
BPN-10A
M
Qz
Mx
Ms
Mx
BPN-8A
N
Mx
Qz
Mx
BPN-7A
O
Ms
Kln+Ilt
Qz
Kfs
BPN-11A

Figure 2

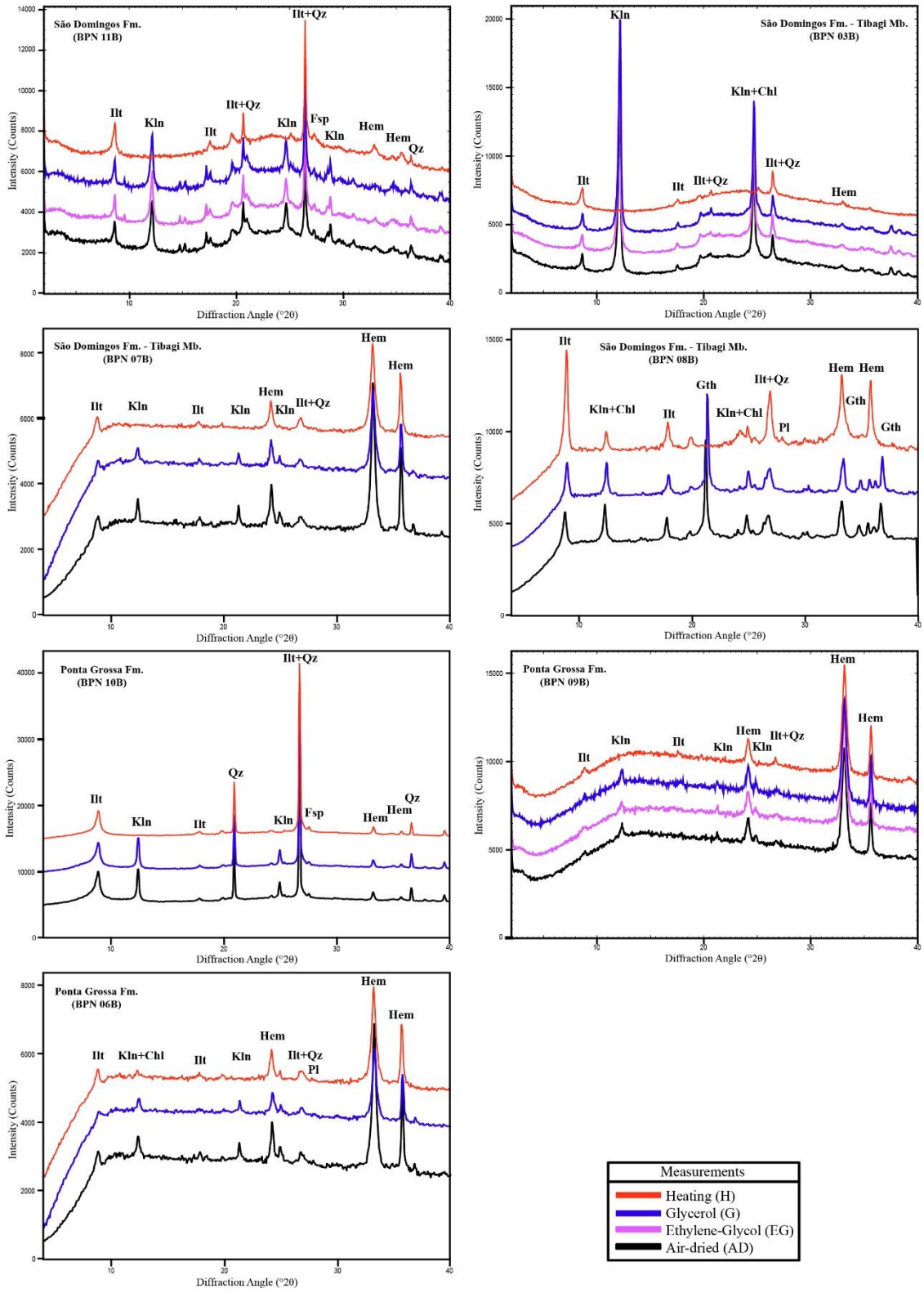
São Domingos Fm.
(BPN 11B)
Ilt
Kln
Ilt
Ilt+Qz
Kln
Fsp
Kln
Hem
Hem
Qz
São Domingos Fm. - Tibagi Mb.
(BPN 03B)
Kln
Kln+Chl
Ilt
Ilt
Ilt+Qz
Ilt+Qz
Hem
São Domingos Fm. - Tibagi Mb.
(BPN 07B)
Ilt
Kln
Ilt
Kln
Hem
Kln
Ilt+Qz
Hem
Hem
São Domingos Fm. - Tibagi Mb.
(BPN 08B)
Ilt
Kln+Chl
Ilt
Gth
Kln+Chl
Ilt+Qz
Pl
Hem
Hem
Gth
Gth
Ponta Grossa Fm.
(BPN 10B)
Ilt
Kln
Ilt
Qz
Kln
Fsp
Hem
Qz
Hem
Ilt+Qz
Ponta Grossa Fm.
(BPN 09B)
Ilt
Kln
Ilt
Kln
Hem
Kln
Ilt+Qz
Hem
Hem
Ponta Grossa Fm.
(BPN 06B)
Ilt
Kln+Chl
Ilt
Kln
Hem
Ilt+Qz
Pl
Hem
Hem
Intensity (Counts)
Diffraction Angle (°2θ)
Measurements
Heating (H)
Glycerol (G)
Ethylene-Glycol (EG)
Air-dried (AD)

Figure 3

CAPÍTULO 5 – CONCLUSÕES FINAIS

Os dados de U-Pb em zircão detrítico e isótopos Sr-Nd nas seqüências Devonianas da Bacia do Paraná foram úteis para reconhecer as variações do nível do mar. Foi possível reconhecer na distribuição das idades detríticas de zircão as diferentes zonas fontes e classificá-las como próxima, intermediária e distais. Nas unidades que registram elevações do nível do mar (eventos transgressivos), foram reconhecidas populações de fontes distais/muito distais, na Formação Ponta Grossa fontes muito distais a oeste associadas ao arco magmático Famatiniano e na última transgressão de natureza global novamente existem fontes muito distais associadas ao arco magmático e a leste o Grupo Trairas. Como nestas transgressões houve contribuição de fontes muito jovens associadas ao arco magmático Famatiniano, os valores da razão $^{87}Sr/^{86}Sr$ e TDM.

Foi possível reconhecer que a partir dos dados U-Pb em zircão detrítico que foi realizado neste estudo e com dados da literatura, que desde a deposição da Formação Alto Garças até a Formação São Domingo, preenchimento da bacia a partir do Ordoviciano até o Devoniano na parte norte da bacia, que desde a primeira transgressão no Devoniano com a deposição da Formação Ponta Grossa já havia uma conexão com a bacia do Tarija. Com os dados U-Pb em zircão detrítico da Bacia de Tarija (García et al., 2020 submetido) das unidades Devonianas usando o gráfico estatístico de escala multidirecional, pode-se ver uma correlação com as amostras das formações Ponta Grossa e São Domingos.

Uma revisão dos dados U-Pb em zircão detrítico foi realizada nas unidades estratigráficas das bacias localizadas na porção SW de Gondwana do intervalo Devoniano, e em quase todas as bacias não há registro completo, mas pode-se observar em algumas bacias variações das populações de zircão detríticos associadas a transgressões e regressões como nas bacias Precordillerana, Chaco-Paraná, Sierras Australes e Cape. Em bacias como Tarija e Malvinas, não há variação acentuada na distribuição das idades dos zircões detríticos. Vale ressaltar que um estudo mais detalhado dessas bacias é necessário para verificar a relação entre as idades U-Pb no zircão detrítico e as variações do nível do mar conhecidas ao SW de Gondwana.

CAPÍTULO 6 – RECOMENDAÇÕES

Realizar estudos Sr-Nd no setor noroeste da bacia, porque não tem esse tipo de estudos e complementar com mais análises na zona de estudo nas Formações Ponta Grossa e São Domingos. Também realizar este tipo de estudos na parte Sul da bacia e nas seqüências inferior (Formação Furnas e Grupo Rio Ivaí).

Realizar estudos de geoquímica das Formações Ponta Grossa e São Domingos na zona de estudo para melhorar o entendimento das zonas de procedências.

Realizar estudos de DRX na parte noroeste para complementar com os estúdios de geoquímica que se seguiram por parte de Montibeller et al. (2017) e melhorou o reconhecimento da parte norte da bacia.

Realizar estudos isotópicos Lu-Hf em zircões na zona de estudo para melhorar o entendimento das zonas de procedências.

Realizar estudos de geocronologia nas partes mais finas na zona de estudo para melhorar o entendimento das zonas de procedências.

Realizar estudos de Geocronologia U-Pb em zircões no setor noroeste da bacia nas Formações Ponta Grossa e São Domingos. Também realizar estudos de Geocronologia no setor Sul da bacia na Formação São Domingos para ver se pode reconhecer a transgressão global associada à parte alta desta unidade.

Realizar estudos multiproxy de geocronologia U-Pb tanto na parte norte e sul da bacia para ter uma melhor compressão das zonas fontes. Os minerais a estudar podem ser monazita, rutilo e apatita que foram reconhecidos, mas não foram estudados.

Para reconhecer a segunda regressão no Frasniano, se necessita estudar os afloramentos do Noroeste, donde foi reconhecido esta regressão na parte alta da Formação São Domingo, a diferença dos setores nordeste e Sul na bacia, donde solo se reconhecem hasta a segunda transgressão (Givetiano).

CAPÍTULO 7 – REFERÊNCIAS

Alasino, P., Casquet, C., Galindo, C., Pankhurst, R., Rapela, C., Dahlquist, J., Recio, C., Baldo, E., Larrovere, M., Ramacciotti, C., 2020. O–H–Sr–Nd isotope constraints on the origin of the Famatinian magmatic arc, NW Argentina. Geol. Mag. 157, 2067–2080.

Alasino, P.H., Casquet, C., Pankhurst, R.J., Rapela, C.W., Dahlquist, J.A., Galindo, C., Larrovere, M.A., Recio, C., Paterson, S.R., Colombo, F., Baldo, E.G., 2016. Mafic rocks of the Ordovician Famatinian magmatic arc (NW Argentina): new insights into the mantle contribution. Geological Society of American Bulletin 128, 1105–20, doi: 10.1130/B31417.1.

Albariño, L., Farjat, A.D., Alvarez, L., Hernandez, R., Leyton, M.P., 2000. Las secuencias sedimentarias del Devonico en el subandino sur y el Chaco: Bolivia y Argentina. 5to Congreso Exploración y Desarrollo de Hidrocarburos. Instituto Argentino del Petróleo y Gas (IAPG), Mar del Plata, pp. 1–24.

Almeida, F.F.M., 1948. Contribuição à geologia dos estados de Goiás e Mato Grosso. Notas Preliminares e Estudos, DGM, 46, 1-17.

Almeida, F.F.M., 1954. Geologia do centro-leste Mato-grossense. Boletim da Divisão de Geologia e Mineralogia, 150, 1-97.

Almeida, F.F.M., 1980. Tectônica da bacia do Paraná. Relatório Técnico IPT (Instituto de Pesquisas Tecnológicas), no. 14091. São Paulo, Paulipetro, 187 p.

Almeida, F.F.M., 1984. Província Tocantins — Setor Sudoeste. In: Almeida F.F.M., Hasui Y. O Pré-Cambriano do Brasil. Ed. Bluncher, São Paulo. p. 265-281.

Almeida, F.F.M., Hasui, Y., Brito Neves, B.B., Fuck, R.A., 1977. Províncias estruturais brasileiras, in: Atas do Simpósio de Geologia do Nordeste, 8, SBG, Campina Grande, 363-391.

Almeida, F.F.M., Melo, M.S., 1981. A Bacia do Paraná e o vulcanismo mesozoico, in: Mapa Geológico do Estado de São Paulo, escala 1:50.000. São Paulo, IPT, 1, pp. 46-81.

Alvarenga C.J.S., Moura C.A.V., Gorayeb P.S.S., Abreu F.A.M., 2000. Paraguay and Araguaia belts, in: Cordani U.G., Milani E.J., Thomaz Filho A. Campos D.A. (Eds). Tectonic evolution of South America. 31st. International Geological Congress, Rio de Janeiro, pp. 183-193.

Alvarenga, C.J.S., Guimarães, E.M, Assine, M.L., Perinotto, J.A., 1998. Sequência Orodovício-Siluriano e Devoniano no flanco norte da Bacia do Paraná. Anais da Academia Brasileira de Ciências, 70, 03, 587-606.

Alvarenga, C.J.S., Guimarães, E.M., 1994. Siluro-Devoniano no noroeste da Bacia do Paraná: Região entre Diorama e Amorinópolis, GO. In: Simp. Geol. Centro-Oeste, 4, Brasília, Anais., SBG-Núcleo Brasília e Centro Oeste, p. 53-56.

Alvarenga, C.J.S., Trompette, R. 1993. Evolução Tectônica da Faixa Paraguai: A Estruturação da Região de Cuiabá. Revista Brasileira de Geociências, 23(1):18-30.

Alves, D.B., 1987. Desenvolvimento da metodologia de preparação de amostras para análise difratométrica de argilominerais no Centro de Pesquisas da Petrobrás. Bol. Geociências da Petrobrás 1, 157–175.

Anderson, R.B., Long, S.P., Horton, B.K., Calle, A.Z., Soignard, E., 2021. Late Paleozoic Gondwanide deformation in the Central Andes: Insights from RSCM thermometry and thermal modeling, southern Bolivia. Gondwana Res. 94, 222–242. https://doi.org/10.1016/j.gr.2021.03.002.

Andrade, S.M., Camarço, P.E.N., 1978. Mapeamento Geológico a Leste das Cidades de Iporá-Amorinópolis. Relatório Final da Nuclebrás, Goiânia, 32 p.

Andrade, S.M., Camarço, P.E.N., 1980. Estratigrafia dos sedimentos devonianos do flanco nordeste da Bacia do Paraná. Congresso Brasileiro de Geologia, 31, 5, 2828-2834.

Araujo, T., 2016. Sistema fluvial ou dominado por maré? Estudos de processos de Sedimentação e arquitetura deposicional no canyon do Guartelá, Formação Furnas, Devoniano Inferior, Bacia do Paraná, Brasil. Dissertação de Mestrado, Instituto de Geociências, Universidade Estadual de Campinas, Campinas-Sp.

Arnol, J. A., Uriz, N. J., Cingolani, C. A., Abre, P., & Basei, M. A. S., 2022. Provenance evolution of the San Juan Precordillera Silurian-Devonian basin (Argentina): Linking with other depocentres in Cuyania terrane. Journal of South American Earth Sciences, 115, 103766. https://doi.org/10.1016/j.jsames.2022.103766.

Arnol, J.A., Uriz, N.J., Cingolani, C.A., Basei, M.A.S., Abre, P., 2020. Provenance analysis of Devonian peripheral foreland basins in SW Gondwana, case of the Gualilán group, Precordillera Argentina. Int. J. Earth Sci. 109 (7), 2467–2494. https://doi.org/ 10.1007/s00531-020-01914-9.

Assine, L., Soares, P., Milani, E., 1994. Sequências tectôno-sedimentares mesopaleozóicas da Bacia do Paraná, Sul do Brasil. Revista Brasileira de Geociências, 24 (2): 77-89.

Assine, M.L., 1996. Aspectos da Estratigrafia das Sequências Pré-Carboníferas da Bacia do Paraná no Brasil. (Ph.D. thesis). Universidade de São Paulo, São Paulo 207 pp.

Assine, M.L., Perinotto, J.A., Fulfaro, V.J., Petri, S., 1998. Progradação deltaica Tibagi no Devoniano médio da Bacia do Paraná. Revista Brasileira de Geociencias 28, 125–134.

Augustsson, C., Voigt, T., Bernhart, K., Kreißler, M., Gaupp, R., Gärtner, A., Hofmann, M., Linnemann, U., 2018. Zircon size-age sorting and source-area effect : The German Triassic Buntsandstein Group. Sediment. Geol. 375, 218–231. https://doi.org/10.1016/j.sedgeo.2017.11.004.

Babinski, M., McGee, B., Tokashiki, C. D. C., Tassinari, C. C., Saes, G. S., & Pinho, F. E. C., 2018. Comparing two arms of an orogenic belt during Gondwana amalgamation: Age and provenance of the Cuiabá Group, northern Paraguay Belt, Brazil. Journal of South American Earth Sciences, 85, 6–42. https://doi.org/10.1016/j.jsames.2018.04.009.

Bahlburg, H. (2021). A Silurian-Devonian active margin in the proto-Andes – new data on an old conundrum. International Geology Review, 1–22. https://doi.org/10.1080/00206814.2021.2012719.

Bahlburg, H., Vervoort, J.D., du Frane, S.A., Bock, B., Augustsson, C., Reimann, C., 2009. Timing of crust formation and recycling in accretionary orogens: Insights learned from the western margin of South America. Earth-Science Reviews 97 (1–4), 215–241. https://doi.org/10.1016/j.earscirev.2009.10.006.

Bergamaschi, S., 1999. Análise estratigráfica do Siluro-Devoniano (Formações Furnas e Ponta Grossa) da sub-Bacia do Apucarana, Bacia do Paraná, Brasil. Unpublished PhD Thesis. São Paulo University, São Paulo, p. 167.

Bertoni, M.E., Rooney, A.D., Selby, D., Alkmim, F.F., Le Heron, D.P., 2014. Neoproterozoic Re–Os systematics of organic-rich rocks in the São Francisco Basin, Brazil and implications for hydrocarbon exploration. Precambrian Research, 255:355-366. http://dx.doi.org/10.1016/j. precamres.2014.10.010.

Bettencourt, J. S., Leite, W. B., Ruiz, A. S., Matos, R., Payolla, B. L., & Tosdal, R. M., 2010. The Rondonian-San Ignacio Province in the SW Amazonian Craton: An

overview. Journal of South American Earth Sciences, 29(1), 28–46. https://doi.org/10.1016/j.jsames.2009.08.006.

Bigarella, J.J. & Comte, D., 1969. O Grupo Caacupé e sua importância na paleogeografia do Siluriano sul-americano. Bol. Soc. Bras. Geologia, 18(1): 31-37.

Bigarella, J.J. & Oliveira, M.A.M., 1966. Nota preliminar sobre as direções de transport dos arenitos Furnas e Botucatu na parte setetrional da Bacia do Paraná. Bol. Parana. Geografía. 18/20: 247-256.

Borghi, L., 1993. Caracterização e análise faciológicas da Formação Furnas (Pridoli-Eodevoniano) em afloramentos do flanco Sul do Arco Estrutural de Ponta Grossa, borda Leste da bacia do Paraná, Estado do Paraná. (Ph.D. thesis). Universidade Federal do Rio de Janeiro, Rio de Janeiro.

Bosetti, E.P., Grahn, Y., Horodyski, R.S., Mendlowicz-Mauller, P.M., 2012. The first recorded decline of the Malvinokaffric Devonian fauna in the Paraná Basin (southern Brazil) and its cause; taphonomic and fossil evidences. J. S. Am. Earth Sci. 37, 228–241. https://doi.org/10.1016/j.jsames.2012.02.006.

Brito Neves, B.B., 2002. Main stages of development of the sedimnetary Basins of South America and their relationship with the tectonics of Supercontinents. Gondwana Research, 5(1): 175-196. https://doi.org/10.1016/S1342-937X(05)70901-1.

Calle, A.Z., 2013. Neogene sedimentation and provenance record of the Subandean zone and Chaco foreland basin, southern Bolivia. The University of Texas at Austin.

Campanha, G., Basei, M., Faleiros, F., & Nutman, A., 2016. The Mesoproterozoic to early Neoproterozoic passive margin Lajeado Group and Apiaí Gabbro, Southeastern Brazil. Geoscience Frontiers, 7(4), 683–694. https://doi.org/10.1016/j.gsf.2015.08.004.

Candido, A.G., Rostirolla, S.P., 2007. Analise de fácies e revisão da estratigrafia de seqüencias da Formação Ponta Grossa, Bacia do Parana - ênfase nos arenitos do Membro Tibagi. Bol. Geociencias Petrobras 15, 45-62.

Carbonaro, F. A., Comniskey, J. C., Corral, H. S., & Ghilardi, R. P., 2018. Orbiculoidea baini e Orbiculoidea excentrica (Brachiopoda, Discinidae) do Devoniano Médio (Sub-bacia Alto Garças, Bacia do Paraná) de Caiapônia, Goiás (Brasil). Geologia USP. Série Científica, 18(4), 11-20.

Carbonaro, F.A., Ghilardi, R.P., 2016. Fósseis do Devoniano de Goiás, Brasil (Sub-bacia Alto Garças, Bacia do Paraná). Papéis Avulsos de Zoologia, 56(11), 135-149.

Carrera, M.G., Ernst, A., Rustán, J.J., 2019. Devonian bryozoans from Argentina: new cosmopolitan components of Southwestern Gondwanan basins. Journal of Paleontology 93, 232–243. https://doi.org/10.1017/jpa.2018.81.

Carvalho, M.G.P., Melo, J.H.G., Quadro, L.P., 1987. Trilobitas Devonianos do flanco noroeste da Bacia do Paraná. In: Congresso Brasileiro de Paleontologia, 10., Rio de Janeiro. Anais., p. 36. Rio de Janeiro: Sociedade Brasileira de Paleontologia.

Cawood, P.A., 2005. Terra Australis orogen: Rodinia breakup and development of the Pacific and Iapetus margins of Gondwana during the Neoproterozoic and Paleozoic. Earth Sci. Rev. 69, 249–279. https://doi.org/10.1016/j.earscirev.2004.09.001.

Cawood, P.A., Hawkesworth, C.J., Dhuime, B., 2012. Detrital zircon record and tectonic setting. Geology 40, 875–878. https://doi.org/10.1130/ G32945.1.

Cingolani, C.A., Berry, C.M., Morel, E., Tomezolli, R., 2002. Middle Devonian lycopsids from high southern palaeolatitudes of Gondwana (Argentina). Geological Magazine 139, 641–649.

Copper, P., 1977. Paleolatitudes in the Devonian of Brazil and the Fransnian-Famennian mass extinction. Palaeogeogr. Palaeoclimatol. Palaecol. 21, 165–207.

Cordani, U.G., Brito Neves, B.B., Thomaz Filho, A., 2009. Estudo preliminar de integração do pré-cambriano com os eventos tectônicos das bacias sedimentares brasileiras (Atualização). Boletim de Geociências da Petrobras, 17, 205-219.

Cordani, U.G., Sato, K., Teixeira, W., Tassinari, C.C.G., Basei, M.A.S., 2000. Crustal evolution of the South American platform. In: Cordani, U.G., Milani, E.J., Thomaz Filho, A., Campos, D.A. (Eds.), Tectonic Evolution of South America, pp. 19–40.

Cordeiro, P.O. F., 2014. Compartimentação geológica e geocronológica do embasamento norte da Faixa Brasília. PhD Thesis unpublished, 157 p. Universidade de Brasília.

Cox, R., Lowe, D., 1996. Quantification of the effects of secondary matrix on the analysis of sandstone composition, and a petrographic-chemical technique for retrieving original framework grain modes of altered sandstones. Journal of Sedimentary Research 66, 548–558. https://doi.org//10.1306/d42683a1-2b26-11d7-8648000102c1865d.

Daemon, R.F., Quadros, L.P., Silva, L.C., 1967. Devonian palynology and biostratigraphy of the Paranná basin. In: Bigarella, J.J. (Ed.), Problems in Brazilian Devonian Geology, 21/22. Boletim Paranaense de Geociências, pp. 99–132.

Dahlquist, J.A., Morales Cámera, M.M., Alasino, P.H., Pankhurst, R.J., Basei, M.A.S., Rapela, C.W., Moreno, J.A., Baldo, E.G., Galindo, C., 2021. A review of Devonian–

Carboniferous magmatism in the central region of Argentina, pre-Andean margin of SW Gondwana. Earth-Science Rev. 221, 34. https://doi.org/10.1016/j.earscirev.2021.103781.

Dardenne, M.A., 2000. The Brasília fold belt. In: Cordani U.G., Milani E.J., Thomaz Filho A., Campos D.A. (eds.). Tectonic Evolution of South America. 31st International Geological Congress, Rio de Janeiro, p. 231-236.

Dias, P.H.A., Noce, C.M., Pedrosa-Soares A.C., Seer H.J., Dussin, I.A., Valeriano, C.M., Kuchenbecker, M., 2011. O Grupo Ibiá (Faixa Brasília Meridional): evidências isotópicas Sm-Nd e U-Pb de bacia colisional tipo flysch. Geonomos, 19(2):90-99.

Dickinson, W.R., 1985. Interpreting Provenance Relations from Detrital Modes of Sandstones, in: Provenance of Arenites. Springer Netherlands, Dordrecht, pp. 333–361.

Dickinson, W.R., Beard, L.S., Brakenridge, G.R., Erjavec, J.L., Ferguson, R.C., Inman, K.F., Ryberg, P.T., 1983. Provenance of North American Phanerozoic sandstones in relation to tectonic setting. Geol Soc Am Bull 94(2):222–235.https://doi.org/10.1130/0016-7606(1983)94<222:PONAPS >2.0.CO;2.

Dickinson, W.R., Gehrels, G.E., 2008. U-Pb Ages of Detrital Zircons in Relation to Paleogeography: Triassic Paleodrainage Networks and Sediment Dispersal Across Southwest Laurentia. J. Sediment. Res. 78, 745–764. https://doi.org/10.2110/jsr.2008.088.

Dickinson, W.R., Gehrels, G.E., 2009. Use of U–Pb ages of detrital zircons to infer maximum depositional ages of strata: A test against a Colorado Plateau Mesozoic database. Earth Planet. Sci. Lett. 288, 115–125. https://doi.org/10.1016/j.epsl.2009.09.013.

Dietz, V., 1973. Experiments on the influence of transport on shape and roundness of heavy minerals. Contributions to Sedimentology, 1: 69 – 102, Stuttgart.

Döbelin, N., Kleeberg, R., 2015. Profex: a graphical user interface for the Rietveld refinement program BGMN. Journal of Applied Crystallography 48, 1573-1580. https://doi.org/10.1107/S1600576715014685.

Evans, J. W., 1984. The geology of Matto Grosso, particularly the region drained by the Upper Paraguay. Quarterly Journal of the Geological Society, v. 50, n. 2, p. 85-104. https://doi.org/10.1144/GSL.JGS.1894.050.01-04.10.

Falci, A., Caxito, F. de A., Seer, H.J., Valeriano, C. de M., Dias, P.H.A., Pedrosa-Soares, A.C., 2018. Provenance shift from a continental margin to a syn-orogenic basin in

the Neoproterozoic Araxá nappe system, southern Brasília belt, Brazil. Precambrian Research 306, 209–219. https://doi.org/10.1016/j.precamres.2018.01.004.

Faleiros, F.M., Pavan, M., Remédio, M.J., Rodrigues, J.B., Almeida, V.v., Caltabeloti, F.P., Pinto, L.G.R., Oliveira, A.A., Pinto de Azevedo, E.J., Costa, V.S., 2016. Zircon U-Pb ages of rocks from the Rio Apa Cratonic Terrane (Mato Grosso do Sul, Brazil): New insights for its connection with the Amazonian Craton in pre-Gondwana times. Gondwana Research 34, 187–204. https://doi.org/10.1016/j.gr.2015.02.018.

Fazio, G., Guimaraes, E.M., Walde, D.W.G., Carmo, D.A., Adorno, R.R., Vieira, L.C., Denezine, M., Silva, C.B., Godoy, H.V., Borges, P.C. and Pinho, D., 2019. Mineralogical and chemical composition of Ediacaran -Cambrian pelitic rocks of The Tamengo and Guaicurus formations, (Corumbá Group - MS, Brazil): Stratigraphic positioning and paleoenvironmental interpretations. J. S. Am. Earth Sci., 90, 487–503. https://doi.org/10.1016/j.jsames.2018.11.025.

Ferreira Filho, C.F., Kamo, S.L., Fuck, R.A., Krogh, T.E., Naldrett, A.J., 1994. Zircon and rutile U-Pb geochronology of the Niquelândia layered mafic and ultramafic intrusion, Brazil: constraints for the timing of magmatism and high grade metamorphism. Precambrian Research, 68:241-255. https://doi.org/10.1016/0301-9268(94)90032-9.

Fonseca, A. C., Piffer, G. V., Nachtergaele, S., van Ranst, G., de Grave, J., & Novo, T. A., 2020. Devonian to Permian post-orogenic denudation of the Brasília Belt of West Gondwana: insights from apatite fission track thermochronology. Journal of Geodynamics, 137, 101733. https://doi.org/10.1016/j.jog.2020.101733.

Fourie, P.H., Zimmermann, U., Beukes, N.J., Naidoo, T., Kobayashi, K., Kosler, J., Nakamura, E., Tait, J., Theron, J.N., 2011. Provenance and reconnaissance study of detrital zircons of the Palaeozoic Cape Supergroup in South Africa: revealing the interaction of the Kalahari and Río de la Plata cratons. Int. J. Earth Sci. 100, 527–541. https://doi.org/10.1007/s00531-010-0619-x.

França, O., Ruiz, S., Sousa, M. Z. A. D., Batata, M. E. F., & Lafon, J. M., 2014. Geology, petrology, U-Pb (shrimp) geochronology of the Morrinhos granite -Paraguá terrane, SW Amazonian craton: implications for the magmatic evolution of the San Ignácio orogeny. Brazilian Journal of Geology, 44(3), 415–432. https://doi.org/10.5327/z2317-4889201400030006.

Fuck, R. A., Dantas E. L., Pimentel, M. M., Botelho, N. F. Armstrong, R., Laux, J. H., Junges, S. L., Soares, J. E. P., Praxedes, I. F., 2014. Paleoproterozoic crust-formation

and reworking events in the Tocantins Province, Central Brazi: a contribution for Atlantica supercontinent reconstruction. Precambrian Research, 244, 53-74. https://doi.org/10.1016/j.precamres.2013.12.003.

Fuck, R.A., Pimentel, M.M., Alvarenga, C.J.S., Dantas, E.L., 2017. The northern Brasília belt. In: Heilbron, M., Cordani, U.G., Alkmim, F.F., Regional Geology Reviews (Eds.), São Francisco Craton, Eastern Brazil. Tectonic Genealogy of a Miniature Continent, 1ed. Springer, pp. 205–220. https://doi.org/10.1007/978-3-319-01715-0.

Fuck, R.A., Pimentel, M.M., Silva, L.J.H.D.R., 1994. Compartimentação tectônica na porção oriental da Província Tocantins, in: Boletim de Resumos Expandidos do Congresso Brasileiro de Geologia, 38, SBG, Balneário Camboriú, 215-216.

Gale, A. S., Voigt, S., Sageman, B. B., & Kennedy, W. J., 2008. Eustatic sea-level record for the Cenomanian (Late Cretaceous)—Extension to the Western Interior Basin, USA. Geology, 36(11), 859. https://doi.org/10.1130/g24838a.1.

García-Muro, V.J., Rubinstein, C.V., Steemans, P., 2014. Palynological record of the Silurian/ Devonian boundary in the argentine Precordillera, western Gondwana. Neues Jahrbuch für Geologie und Paläontologie Abhandlungen 274, 25–42.

Gärtner, A., Linnemann, U., Sagawe, A., Hofmann, M., Ullrich, B., Kleber, A., 2013. Morphology of zircon crystal grains in sediments–characteristics, classifications, definitions. Geol. Saxonica 2013, 59, 65–73.

Garzanti, E., 2019. Petrographic classification of sand and sandstone. Earth-Science Rev. 192, 545–563. https://doi.org/10.1016/j.earscirev.2018.12.014.

Gehrels, G., 2014. Detrital Zircon U-Pb Geochronology Applied to Tectonics. Annu. Rev. Earth Planet. Sci. 42, 127–149. https://doi.org/10.1146/annurev-earth-050212-124012.

Geraldes, M., Tassinari, C., Babinski, M., Martinelli, C., Iyer, S., Barboza, E., Pinho, F., Onoe, A., 2008. Isotopic evidence for the Late Brasiliano (500–550 Ma) ore-forming mineralization of the Araés Gold Deposit. Brazil: International Geology Review 50, 177– 190.

Gerdes, A., Zeh, A., 2006. Combined UePb and Hf isotope LA-(MC-)ICP-MS analyses of detrital zircons: comparison with SHRIMP and new constraints for the provenance and age of an Armoricanmetasediment in central Germany. Earth Planet Sci. Lett. 249, 47-61.

Gezatt, J. N., 2011. Proveniência de rochas sedimentares detríticas do Gráben de Piranhas e comparação com a Formação Vila Maria do Siluriano da Bacia do Paraná. Trabalho de conclusão de curso. Porto Alegre: Instituto de Geociências – UFRGS.

Gioia, S.M.C.., Pimentel, M., 2000. The Sm-Nd isotopic method in the geochronology laboratory of the University of Brasília. An. Acad. Bras. Cienc. 72, 219–245. https://doi.org/10.1590/S0001-37652000000200009.

Giustina, M.E.S.D., Oliveira, C.G., Pimentel, M.M., Buhn, B., 2009. Neoproterozoic magmatism and high-grade metamorphism in the Goiás Massif: new LAM-ICPMS U-Pb and Sm-Nd data and implications for the collisional history of the Brasília Belt. Precambrian Research, 172:67-79. https://doi.org/10.1016/j.precamres.2009.03.012.

Giustina, M.E.S.D., Oliveira, C.G.d., Pimentel, M.M., de Melo, L.V., Fuck, R.A., Dantas, E. L., Buhn, B., 2009. U–Pb and Sm–Nd constraints on the nature of the Campinorte sequence and related Palaeoproterozoic juvenile orthogneisses, Tocantins Province, central Brazil. 323 (1), 255–269. doi:10.1144/SP323.12.

Giustina, M.E.S.D., Pimentel, M.M., Ferreira Filho, C.F., Hollanda, M.H.B.M., 2011. Dating coeval mafic magmatism and ultrahigh temperature metamorphism in the Anápolis–Itauçu Complex, Central Brazil. Lithos, 124:82-102. https://doi.org/10.1016/j.lithos.2010.11.004.

Godoy, A.M.; Pinho, F. E. C.; Manzano, J. C.; Araújo, L.M. B.; Silva, J. A.; Figueiredo, M., 2010. Estudos isotópicos das rochas granitóides neoproterozoicas da Faixa de Dobramento Paraguai. Revista Brasileira de Geociências, v. 40, n. 3, p. 380-391.

Goldstein, S.L., O'Nions, R.K., Hamilton, P.J., 1984. A Sm-Nd isotopic study of atmospheric dusts and particulates from major river systems. Earth Planet. Sci. Lett. 70, 221–236. https://doi.org/https://doi.org/10.1016/0012-821X(84)90007-4.

González, P. A., Uriz, N., Arnol, J., Dopico, C. M., Cayo, L. E., Cingolani, C., Impiccini, A., & Stipp Basei, M. A., 2020. Sedimentary provenance analysis of the ordovician to devonian siliciclastic units of the Subandean Ranges and Santa Barbara System, northwestern Argentina. Journal of South American Earth Sciences, 101, 102629. https://doi.org/10.1016/j.jsames.2020.102629.

Grabau, A.W., 1933. Oscillation or pulsation. International Geological Congress Report on the 16th Session. Washington, DC, pp. 539–552.

Grahn, Y., 1992. Revision of Silurian and Devonian strata of Brazil. Palynology 16, 35–61.

Grahn, Y., Horodyski, R.S., Mendlowicz Mauller, P., Bosetti, E.P., Ghilardi, R.P., Carbonaro, F.A., 2016. A marine connection between Parnaíba and Paraná basins during the Eifelian/ Givetian transition: Review and new data. Revista Brasileira de Paleontologia 19, 357–366. https://doi.org/10.4072/rbp.2016.3.01.

Grahn, Y., Mauller, P.M., Bergamaschi, S., Bosetti, E.P., 2013. Palynology and sequence stratigraphy of three Devonian rock units in the Apucarana Sub-basin (Paraná Basin, South Brazil): additional data and correlation. Review of Palaeobotany and Palynology 198, 27–44. https://doi.org/10.1016/j.revpalbo.2011.10.006.

Grahn, Y., Mauller, P.M., Pereira, E., Loboziak, S., 2010. Palynostratigraphy of the Chapada Group and its significance in the Devonian stratigraphy of the Paraná Basin, South Brazil. Journal of South American Earth Sciences 29, 354–370. https://doi.org/10.1016/j.jsames.2009.09.001.

Gromet, L.P., Haskin, L.A., Korotev, R.L., Dymek, R.F., 1984. The "North American shale composite": Its compilation, major and trace element characteristics. Geochim. Cosmochim. Acta 48, 2469–2482. https://doi.org/10.1016/0016-7037(84)90298-9.

Hallam, A., 2001. A review of the broad pattern of Jurassic sea-level changes and their possible causes in the light of current knowledge. Palaeogeography, Palaeoclimatology, Palaeoecology 167, 23–37. https://doi.org/10.1016/S0031-0182(00)00229-7.

Haq, B.U., Al-Qahtani, A.M., 2005. Phanerozoic cycles of sea-level change on the Arabian Platform. GeoArabia 10, 127–160. https://doi.org/10.2113/geoarabia1002127.

Haq, B.U., Hardenbol, J., Vail, P.R., 1987. Chronology of fluctuating sea levels since the Triassic. Science 235, 1156–1167.

Haq, B.U., Schutter, S.R., 2008. A chronology of Paleozoic sea-level changes. Science 322, 64–68.

Henrique-Pinto, R., Basei, M.A.S., Santos, P.R., Saad, A.R., Milani, E.J., Cingolani, C.A., Frugis, G.L., 2021. Paleozoic Paraná Basin transition from collisional retro-foreland to pericratonic syneclise: Implications on the geodynamic model of Gondwana proto-Andean margin, Journal of South American Earth Sciences, 103511. https://doi.org/10.1016/j.jsames.2021.103511.

Heredia, N., García-Sansegundo, J., Gallastegui, G., Farias, P., Giacosa, R., Alonso, J., Busquets, P., Charrier, R., Clariana, P., Colombo, F., Cuesta, Gallastegui A.J., Giambiagi, L., González-Menéndez, L., Limarino, C.O., Martín-González, F.,

Méndez-Bedia, I., Pedreira, D., Quintana, L., Rodríguez-Fernández, L.R., Rubio-Ordoñez, A., Seggiaro, R., Serra-Varela, S., Spalletti, L., Card'o, R., Ramos, V., 2016. Evolución Geodinámica de los Andes argentino-chilenos y la Península Antártica durante el Neoproterozoico tardío y el Paleozoico. In: Trabajos de Geología, 36. Universidad de Oviedo, pp. 237–278.

Heredia, N., García-Sansegundo, J., Gallastegui, G., Farias, P., Giacosa, R.E., Giambiagi, L.B., Busquets, P., Colombo, F., Charrier, R., Cuesta, A., Rubio-Ordóñez, A., Ramos, V.A., 2018. Review of the geodynamic evolution of the SW margin of Gondwana preserved in the Central Andes of Argentina and Chile (28°–38° S latitude). Journal of South American Earth Sciences 87, 87–94. https://doi.org/10.1016/j.jsames.2017.11.019.

Hodell, D.A., Kamenov, G.D., Hathorne, E.C., Zachos, J.C., Röhl, U., Westerhold, T., 2007. Variations in the strontium isotope composition of seawater during the Paleocene and early Eocene from ODP Leg 208 (Walvis Ridge). Geochemistry, Geophys. Geosystems 8, 15. https://doi.org/10.1029/2007GC001607.

Horodyski, R.S., Holz, M., Grahn, Y., Bosetti, E.P., 2014. Remarks on sequence stratigraphy and taphonomy of the Malvinokaffric shelly fauna during the KAČÁK Event in the Apucarana Sub-basin (Paraná Basin), Brazil. International Journal of Earth Sciences 103, 367–380. https://doi.org/10.1007/s00531-013-0954-9.

House, M.R., 1996. The Middle Devonian Kačák Event. Proceedings of the Ussher Society 9, 79–84.

Ingersoll, R. V, Bullard, T.F., Ford, R.L., Grimm, J.P., Pickle, S.W., 1984. The Effect of Grain Size on Detrital Modes: A Test of the Gazzi-Dickinson Point-Counting Method. SEPM J. Sediment. Res. 54, 103–116. https://doi.org/10.1306/212F83B9-2B24-11D7-8648000102C1865D.

Jost, H., Chemale Jr. F., Dussin, I.A., Martins, R.A., 2010. U-Pb zircon Paleoproterozoic age for the metasedimentary host rocks and gold mineralization of the Crixás greenstone belt, Goiás, Central Brazil. Ore Geology Reviews, 37:127-139. https://doi.org/10.1016/j.oregeorev.2010.01.003.

Jost, H., Chemale, Jr. F., Fuck, R.A., Dussin, I.A., 2013. Uvá complex, the oldest orthogneisses of the Archean-Paleoproterozoic terrane of central Brazil. Journal of South American Earth Sciences, 47:201-212. https://doi.org/10.1016/j.jsames.2013.07.002.

Junges, S.L., Pimentel, M.M., Moraes, R., 2002. Nd isotopic study of the Neoproterozoic Mara Rosa arc, central Brazil: implications for the evolution of the Brasilia belt. Precambrian Research 117, 101-118. https://doi.org/10.1016/S0301-9268(02)00077-3.

Köster, E., 1964. Granulometrische und morphometrische Meßmethoden an Mineralkörnern, Steinen und sonstigen Stoffen. 1 – 336., Stuttgart (Enke).

Kuchenbecker, M., Pedrosa-Soares, A. C., Babinski, M., Reis, H. L. S., Atman, D., Costa, R. D. D., 2020. Towards an integrated tectonic model for the interaction between the Bambuí basin and the adjoining orogenic belts: Evidences from the detrital zircon record of syn-orogenic units. Journal of South American Earth Sciences, 104, 102831. https://doi.org/10.1016/j.jsames.2020.102831.

Lange, F.W., Petri, S., 1967. The Devonian of the Paraná Basin. Bol. Paran Geociênc. 21 (22), 5–55.

Laux, J.H., Pimentel, M.M., Dantas, E.L., Armstrong, R., Junges, S.L., 2005. Two Neoproterozoic custal accretion events in the Brasília Belt, central Brazil. Journal of South American Earth Sciences, 18:183-198. https://doi.org/10.1016/j.jsames.2004.09.003.

Lee, C.Y., Kwon, Y.K., Yeo, J.M., Kwon, Y.J., Han, H.C., 2021. U-Pb ages of detrital zircons in lower Palaeozoic quartzites of the Taebaeksan Basin, eastern Sino–Korean Block: sediment provenance response to relative sea-level changes, International Geology Review, 63:17, 2129-2145. https://doi.org/10.1080/00206814.2020.1827304.

Linol, B., de Wit, M.J., Milani, E.J., Guillocheau, F., Scherer, C., 2015. New regional correlations between the Congo, Paran a and Cape-Karoo basins of southwest Gondwana. In: de Wit, M.J., Guillocheau, F., de Wit, M.J.C. (Eds.), The Geology and Resource Potential of the Congo Basin. Springer-Verlag, pp. 245e268. https://doi.org/10.1007/978-3-642-29482-2_13.

Marques, G.C., 2009. Geologia dos grupos Araí e Serra da Mesa e seu embasamento no sul do Tocantins. Dissertação de Mestrado, Universidade de Brasília, p. 116p.

Marques, R.C., 2006. Taxonomia dos invertebrados da Formação Ponta Grossa (Eomesodevoniano) na borda norte da Bacia do Paraná e análise cladística de espiriferídeos basais. Dissertação (Mestrado). São Paulo: Instituto de Geociências - USP.

Marshall, J.E.A., 2016. Palynological calibration of Devonian events at near-polar palaeolatitudes in the Falkland Islands, South Atlantic. In: Becker, R.T., Königshof, P., Brett, C.E. (Eds.), Devonian Climate, Sea Level and Evolutionary Events. Special Publication vol. 423. Geological Society of London, London, pp. 25–44. https://doi.org/10.1144/SP423.13.

Martinelli, C.D., 1998. Petrografia, estrutural e fluidos da mineralização aurífera dos Araés - Nova Xavantina - MT. Curso de Pós-Graduação em Geociências, IGCE/UNESP, Tese de Doutorado em Geologia Regional, 183 p.

Martins-Ferreira, M.A.C., Chemale, F., Coelho Dias, A.N., Campos, J.E.G., 2018. Proterozoic intracontinental basin succession in the western margin of the São Francisco Craton: constraints from detrital zircon geochronology. J. S. Am. Earth Sci. 81, 165–176. https://doi.org/10.1016/j.jsames.2017.11.018.

Matteini, M., Dantas, E.L., Pimentel, M.M., Alvarenga, C.J.S., Dardenne, M.A., 2012. U-Pb and Hf isotope study on detrital zircons from the Paranoá Group, Brasília Belt Brazil: constraints on depositional age at Mesoproterozoic-Neoproterozoic transition and tectono-magmatic events in the São Francisco Craton. Precambrian Res. 206, 168–181. https://doi.org/10.1016/j.precamres.2012.03.007.

Matteini, M.; Junges, S.L.; Dantas, E.L.; Pimentel, M.M.; Bühn, B., 2010. In situ zircon U–Pb and Lu–Hf isotope systematic on magmatic rocks: insights on the crustal evolution of the Neoproterozoic Goiás Magmatic Arc, Brasília belt, Central Brazil. Gondwana Research. v. 17, p. 1–12. https://doi.org/10.1016/j.gr.2009.05.008.

McGee, B., Babinski, M., Trindade, R., Collins, A.S., 2018. Tracing final Gondwana assembly: Age and provenance of key stratigraphic units in the southern Paraguay Belt, Brazil. Precambrian Research 307, 1–33. https://doi.org/10.1016/j.precamres.2017.12.030.

McGee, B., Collins, A.S., Trindade, R.I.F., 2012. G'day Gondwana — the final accretion of a supercontinent: U-Pb ages from the post-orogenic São Vicente Granite, northern Paraguay Belt, Brazil. Gondwana Res. 21, 316–322. http://dx.doi.org/10.1016/j.gr. 2011.04.011.

McGee, B., Collins, A.S., Trindade, R.I.F., Payne, J., 2015. Age and provenance of the Cryogenian to cambrian passive margin to foreland basin sequence of the northern Paraguay Belt, Brazil. Bulletin Geological Society of America 127 (1–2), 76–86. https://doi.org/10.1130/B30842.1.

Meira, V. T., Garcia-Casco, A., Hyppolito, T., Juliani, C., & Schorscher, J. H. D., 2019. Tectono-Metamorphic Evolution of the Central Ribeira Belt, Brazil: A Case of Late Neoproterozoic Intracontinental Orogeny and Flow of Partially Molten Deep Crust During the Assembly of West Gondwana. Tectonics, 38(8), 3182–3209. https://doi.org/10.1029/2018tc004959.

Melo, J.H.G., 1985. A Província Malvinocáfrica no Devoniano do Brasil: estado atual dos conhecimentos. Dissertação de Mestrado, Departamento de Geologia, Instituto de Geociências, Universidade Federal do Rio de Janeiro, 890 p.

Melo, J.H.G., 1988. The Malvinokaffric Realm in the Devonian of Brazil. In: McMillan, N., Embry, A.F., Glass, D. (Eds.), Devonian of the World. Canadian Society of Petroleum Geologists Memoir vol. 14. Canadian Society of Petroleum Geologists, Calgary, pp. 669–976.

Milani, E. J., 1997. Evolução tectono-estratigráfica da Bacia do Paraná e seu relacionamento com a geodinâmica fanerozóica do Gondwana Sul-Ocidental. PhD Thesis, Intituto de Geociências, Universidade Federal do Rio Grande do Sul, 235 p.

Milani, E. J., 2004. Comentários sobre a origem e evolução tectônica da Bacia do Paraná, in Geologia do Continente Sul-Americano: Evolução da Obra de Fernando Flávio Marques de Almeida, edited by V. Mantesso-Neto et al., pp. 265–279, Beca, São Paulo, SP, Brazil.

Milani, E.J., De Wit, M.J., 2008. Correlations between the classic Paraná and Cape–Karoo sequences of South America and southern Africa and their basin infills flanking the Gondwanides: du Toit revisited. In: Pankhurst, R.J., Trouw, R.A.J., de Brito Neves, B. B., de Wit, M.J. (Eds.), West Gondwana: Pre-Cenozoic Correlations across the South Atlantic Region. Geological Society of London, London, pp. 319–342. https://doi.org/10.1144/SP294.17.

Milani, E.J., Melo, J.H.G., Souza, P.A., Fernandes, L.A., França, A.B., 2007. Bacia do Paraná. Boletim de Geociências da Petrobrás 15, 265–287.

Milani, E.J., Ramos, V.A., 1998. Orogenias Paleozóicas no Domínio Sul-Ocidental do Gondwana e os Ciclos de Subsidência da Bacia do Paraná. Revista Brasileira de Geociencias 28, 476–484.

Miller, K.G., Kominz, M.A., Browning, J.V., Wright, J.D., Mountain, G.S., Katz, M.E., Sugarman, P.J., Cramer, B.S., Christie-Blick, N., Pekar, S.F., 2005. The Phanerozoic record of global sea-level change. Science 310, 1293–1298.

Mitchum, R.M., Van Wagoner, J.C., 1991. High-frequency sequences and their stacking patterns: sequence-stratigraphic evidence of high-frequency eustatic cycles. Sedimentary Geology 70, 131–160. https://doi.org/10.1016/0037-0738(91)90139-5.

Montibeller, C. C., Zanardo, A., Navarro, G. R. B., 2017. Decifrando a proveniência dos folhelhos da formação Ponta Grossa na região de Rio Verde de Mato Grosso e Coxim (MS) através de métodos petrográficos e geoquímicos. Geologia USP. Série Científica, 17(1), 41-59. https://doi.org/10.11606/issn.2316-9095.v17-294.

Moore, D.M., Reynolds, R.C., 1997. X-ray Diffraction and the Identification and Analysis of Clay Minerals. Oxford University Press, New York.

Moraes, R., Fuck, R.A., Pimentel, M.M., Gioia, S.M.C.L., Hollanda, M.H.B.M., Armstrong, R., 2006. The bimodal rift-related Juscelândia volcano-sedimentary Sequence in Central Brazil: Mesoproterozoic extension and Neoproterozoic metamorphism. Journal of South American Earth Sciences, 20:287-301. https://doi.org/10.1016/j.jsames.2005.07.016.

Moucha, R., Forte, A.M., Mitrovica, J.X., Rowley, D.B., Quere, S., Simmons, N.A., Grand, S.P., 2008. Dynamic topography and long-term sea-level variations: there is no such thing as a stable continental platform. Earth and Planetary Science Letters 271, 101–108. https://doi.org/10.1016/j.epsl.2008.03.056.

Nedel, I. M., Fuck, R. A., Ruiz, A. S., Matos, R., & Ferreira, A. C. D., 2020. U–Pb geochronology and geochemistry of grenville-age plutons in the Sunsas Belt - Bolivia, SW Amazonian Craton: Tectonic and magmatic implications. Journal of South American Earth Sciences, 104, 102845. https://doi.org/10.1016/j.jsames.2020.102845.

Nelson, D.A., Cottle, J.M., 2018. The secular development of accretionary orogens: linking the Gondwana magmatic arc record of West Antarctica, Australia and South America. Gondwana Res. 63, 15–33. https://doi.org/10.1016/j.gr.2018.06.002.

Noetinger, S., 2010. Middle-Upper Devonian palynoflora from the Tonono x-1 borehole, Salta Province, Northwestern Argentina. Ameghiniana 47, 165–184.

Nogueira, A.C.R., Riccomini, C., Sial, A.N., Moura, C.A.V., Fairchild, T.R., 2003. Soft-sediment deformation at the base of the Neoproterozoic Puga cap carbonate (southwestern Amazon craton, Brazil): confirmation of rapid icehouse to green-house transition in snowball Earth. Geology 31, 613–616. https://doi.org/10.1130/0091-7613(2003)031<0613:SDATBO>2.0.CO;2.

Oliveira, E.P., 1912. Terreno Devoniano do Sul do Brasil. Anais da da Escola de Mina de Ouro Preto, 14: 31-41.

Oliveira, L.C., Pereira, E., 2011. Ocorrência de Ironstones no Devoniano da Bacia do Paraná. Revista Brasileira de Geociências 4, 447–462.

Oppenheim, V., 1936. Geology of Devonian areas of Paraná Basin. In Brazil, Uruguay and Paraguay. Am. Assoc. Petrol. Geologists Bull., 20(9):1208-1236.

Pankhurst, R. J., Rapela, C. W., Fanning, C. M. y Márquez, M., 2006. Gondwanide continental collision and the origin of Patagonia. Earth-Science Reviews, 7: 235-257. https://doi.org/10.1016/j.earscirev.2006.02.001.

Pankhurst, R. J., Rapela, C. W., Loske, W. P., Márquez, M. y Fanning, C. M., 2003. Chronological study of the pre-Permian basement rocks of southern Patagonia. Journal of South American Earth Sciences, 16: 27-44. https://doi.org/10.1016/S0895-9811(03)00017-8.

Parenti-Couto, J.G., Cordani, U.G., Kawashita, K., Iyer, S.S., Moraes, N.M.P., 1981. Considerações sobre a idade do Grupo Bambui, com base em análises isotópicas de Sr e Pb. Revista Brasileira de Geociências, 11(1):5-16. http://repositorio.ipen.br/handle/123456789/6900.

Park, H., Barbeau, D.L., Rickenbaker, A., Bachmann-Krug, D., Gehrels, G., 2010. Application of foreland basin detrital-zircon geochronology to the reconstruction of the southern and central Appalachian orogen. J Geol 118:23–44. https://doi.org/10.1086/648400.

Penn-Clarke, C.R., 2019. The Malvinokaffric Realm in the Early-Middle Devonian of South Africa. Journal of African Earth Sciences 158, 103549. https://doi.org/10.1016/j. jafrearsci.2019.103549.

Penn-Clarke, C.R., Rubidge, B.S., Jinnah, Z.A., 2018. High-paleolatitude environmental change during the Early to Middle Devonian: insights from Emsian–Eifelian (Lower–Middle Devonian) Siliciclastic depositional systems of the ceres subgroup (Bokkeveld Group) of South Africa. Journal of Sedimentary Research 88, 1040–1075. https://doi.org/10.2110/jsr.2018.53.

Penn-Clarke, C.R., Rubidge, B.S., Jinnah, Z.A., 2019. Eifelian–Givetian (Middle Devonian) high-paleolatitude storm- and wave-dominated shallow-marine depositional systems from the Bidouw Subgroup (Bokkeveld Group) of South Africa. Journal of Sedimentary Research 89, 1140–1170. https://doi.org/10.2110/jsr.2019.61.

Piauilino, P.F., Hauser, N., Dantas, E.L., 2019. From passive margin to continental collision: Geochemical and isotopic constraints for E-MORB and OIB-like magmatism during the neoproterozoic evolution of the southeast Brasília Belt. Precambrian Research, https://doi.org/10.1016/j.precamres.2019.105345.

Pimentel M.M., Ferreira Filho C.F., Armstrong R.A., 2004. SHRIMP U-Pb and Sm-Nd ages of the Niquelândia layered complex: Meso- (1.25 Ga) and Neoproterozoic(0.79 Ga) extensional events in central Brazil. Precambrian Research, 132:133-153. https://doi.org/10.1016/j.precamres.2004.02.009.

Pimentel, M.M. & Fuck, R.A., 1992. Neoproterozoic crustal accretion in central Brazil. Geology, 20:375-379. https://doi.org/10.1130/0091-7613(1992)020<0375:NCAICB>2.3.CO;2.

Pimentel, M.M., 2016. The tectonic evolution of the Neoproterozoic Brasília Belt, central Brazil: a geochronological and isotopic approach. Brazilian Journal of Geology, 46(Supl. 1):67-82. https://doi.org/10.1590/2317-4889201620150004.

Pimentel, M.M., Dardenne, M.A., Fuck, R.A., Viana, M.G., Junges, S.L., Fischel D.P., Seer H.J., Dantas E.L., 2001. Nd isotopes and the provenance of detrital sediments of the Neoproterozoic Brasília Belt, Central Brazil. Journal of South American Earth Sciences, 14(6):571-585. http://dx.doi. org/10.1016%2FS0895-9811(01)00041-4.

Pimentel, M.M., Ferreira, Filho, C.F., Armele, A., 2006. Neoproterozoic age of the Niquelândia Complex, central Brazil: Further ID-TIMS U-Pb and Sm-Nd isotopic evidence. Journal of South American Earth Sciences, 21:228-238. https://doi.org/10.1016/j.jsames.2006.05.001.

Pimentel, M.M., Fuck, R.A., Jost, H., Ferreira Filho, C.F., Araújo, S.M., 2000. The basement of the Brasília Fold Belt and the Goiás Magmatic Arc. In: Cordani U.G., Milani E.J., Thomaz Filho A., Campos D.A. (eds.). Tectonic Evolution of South America. 31st International Geological Congress, Rio de Janeiro, p. 195-229.

Pimentel, M.M., Fuck, R.A., Silva, L.J.H.D., 1996. Dados Rb–Sr e Sm–Nd da região de Jussara-Goiás-Mossâmedes (GO), e o limite entre terrenos antigos do Maciço de Goiás e o Arco Magmático de Goiás. Revista Brasileira de Geociências 26 (2), 61–70

Pimentel, M.M., Jost, H., Fuck, R.A., Armstrong, R.A., Dantas, E.L., Potrel, A., 2003. Neoproterozoic anatexis of 2.9 Ga old granitoids in the Goiás-Crixás block, Central Brazil: evidence from new SHRIMP U-Pb data and SmeNd isotopes. Geologia USP, Série Científica, 3:1-12. https://doi.org/10.5327/S1519-874X2003000100001.

Pimentel, M.M., Rodrigues, J.B., Della Giustina, M.E.S., Junges, S., Matteini, M., Armstrong R., 2011. The tectonic evolution of the Neoproterozoic Brasília Belt, central Brazil, based on SHRIMP and LA-ICPMS U-Pb sedimentary provenance data: A review. Journal of South American Earth Science, 31:345-357. https://doi.org/10.1016/j.jsames.2011.02.01.

Pimentel, M.M.; Fuck, R.A.; Botelho, N.F., 1999. Granites and the geodynamic history of the Brasília Belt, central Brazil: a review. Lithos. v. 46, p. 463-483. https://doi.org/10.1016/S0024-4937(98)00078-4

Pinho, F.E.C., 1990 Estudos das rochas encaixantes e veios mineralizados a ouro do Grupo Cuiabá, na região denominada Garimpo do Araés, Nova Xavantina, Estado de Mato Grosso. Dissertação de Mestrado, CPGEO-UFRGS, 114 p.

Piuzana, D., Pimentel, M.M., Fuck, R.A., Armstrong, R., 2003a. SHRIMP U-Pb and Sm-Nd data for the Araxá Group and associated magmatic rocks: Constraints for the age of sedimentation and geodynamic context of the southern Brasília Belt, Central Brazil. Precambrian Research 125 (1–2), 139–160. https://doi.org/10.1016/S0301-9268(03) 00107-4.

Piuzana, D., Pimentel, M.M., Fuck, R.A., Armstrong, R.A., 2003b. Neoproterozoic granulite facies metamorphism and coeval granitic magmatism in the Brasilia Belt, Central Brazil: regional implications of new SHRIMP U-Pb and Sm-Nd data. Precambrian Research, 125:245-273. https://doi.org/10.1016/S0301-9268(03)00108-6.

Poiré, D., Morel, E., 1996. Procesos sedimentarios vinculados a la depositación de niveles con plantas en secuencias Siluro-Devónicas de la Precordillera, Argentina. VI Reun. Argent. Sedimentol. 205–210. Actas.

Popp, J.H.; Barcellos-Popp, M., 1986. Análise estratigráfica da sequência devoniana da Bacia do Paraná (Brasil). Rev. Brás. Geociências, 16:187-194.

Powers, M.C., 1953. A New Roundness Scale for Sedimentary Particles. J. Sediment. Res. 23, 117–119. https://doi.org/10.1306/D4269567-2B26-11D7-8648000102C1865D.

Ramos, V. A., Cingolani, C., Junior, F. C., Naipauer, M., & Rapalini, A., 2017. The Malvinas (Falkland) Islands revisited: The tectonic evolution of southern Gondwana based on U-Pb and Lu-Hf detrital zircon isotopes in the Paleozoic cover. Journal of South American Earth Sciences, 76, 320–345. https://doi.org/10.1016/j.jsames.2016.12.013.

Ramos, V.A., 1988. Late Proterozoic-Early Paleozoic of South America - a collisional history. Episodes 11, 168–174.

Ramos, V.A., 2018. The famatinian orogen along the protomargin of western gondwana: evidence for a nearly continuous ordovician magmatic arc between Venezuela and Argentina, in Folguera, A. et al, eds., The evolution of the Chilean-Argentinean Andes: Berlin: Springer Earth System Sciences, p. 133–161

Ramos, V.A., Chemale, F., Naipauer, M., Pazos, P.J., 2014. A provenance study of the Paleozoic Ventania System (Argentina): Transient complex sources from Western and Eastern Gondwana. Gondwana Res. 26, 719–740. https://doi.org/10.1016/j.gr.2013.07.008.

Rapela, C.W., 2000. The Sierras Pampeanas of Argentina: Paleozoic building of the southern proto-Andes. 31° International Geological Congress. Secretariat Bureau, Rio de Janeiro, pp. 381–387.

Rapela, C.W., Pankhurst, R.J., Casquet, C., Juán, A., Dahlquist, J.A., Fanning, C.M., Baldo, E.G., Galindo, C., Alasino, P.H., Ramacciotti, C.R., Verdecchia, S.O., Murra, J. A., Basei, M.A.S., 2018. A review of the Famatinian Ordovician magmatism in southern South America: evidence of lithosphere reworking and continental subduction in the early proto-Andean margin of Gondwana. Earth Sci. Rev. 187, 259–285. https://doi.org/10.1016/j.earscirev.2018.10.006.

Ribeiro, V., Carbonaro, F. A., Caminha, S. A. F. da S., Piccoli, A. D., Sousa, F. N., & Ghilardi , R. P. . (2021). Trilobitas devonianos das bacias do Paraná e Parecis no estado de Mato Grosso, Brasil . Terr@ Plural, 15, 1–15.

Rodrigues, J.B., 2008. Proveniência de sedimentos dos grupos Canastra, Ibiá, Vazante e Bambuí - Um estudo de zircões detríticos e Idades Modelo Sm-Nd. Doctorate thesis, Universidade de Brasília, unpublished.

Rodrigues, J.B., Pimentel, M.M., Buhn, B., Matteini, M., Dardenne, M.A., Alvarenga, C.J.S., Armstrong, R.A., 2012. Provenance of the Vazante Group: New U-Pb, Sm-Nd, Lu-Hf isotopic data and implications for the tectonic evolution of the Neoproterozoic Brasília Belt. Gondwana Research 21 (2–3), 439–450. https://doi.org/10.1016/j.gr.2011.07.017.

Rodrigues, J.B., Pimentel, M.M., Dardenne, M.A., Armstrong, R.A., 2010. Age, provenance and tectonic setting of the Canastra and Ibiá Groups (Brasília Belt, Brazil): Implications for the age of a Neoproterozoic glacial event in central Brazil.

Journal of South American Earth Sciences, 29(2):512-521. https://doi.org/10.1016/j.jsames.2009.08.008.

Rovere, A., Stocchi, P., Vacchi, M., 2016. Eustatic and Relative Sea Level Changes, Current Climate Change Reports, 2, 221–231. https://doi.org/10.1007/s40641-016-0045-7.

Ruban, D.A., 2011. Lochkovian (earliest Devonian) transgressions and regressions along the ‘‘Tethyan’’ margin of Gondwana: a review of lithostratigraphical data. Gondwana Research 20, 739–744.

Ruban, D.A., Conrad C.P., 2013. Late Silurian-Middle Devonian long-term shoreline shifts on the northern Gondwanan margin: Eustatic versus tectonic controls.Proceedings of the Geologists' Association, 124, 883-892. doi:10.1016/j.pgeola.2012.12.004.

Ruban, D.A., Zorina, S.O., Conrad, C.P., Afanasieva, N.I., 2012. In quest of Paleocene global-scale transgressions and regressions: contraints from a synthesis of regional trends. Proceedings of the Geologists’ Associations 123, 7–18. https://doi.org/10.1016/j.pgeola.2011.08.003.

Rubatto, D., 2017. Zircon: the metamorphic mineral. Rev. Mineral. geochemistry 83, 261–295.

Saavedra, J.G., Poiré, D.G., Vergani, G.D., Salfity, J.A., Rubinstein, C.V., Pérez, M.A., 2021. Paleoenvironment and age of Los Monos Formation (Devonian), Tarija Basin, Argentina and Bolivia. Latin American journal of sedimentology and basin analysis, 28(1), 1-36.

Santos, J.O.S., Hartmann, L.A., Gaudette, H.E., Groves, D.I., Mcnaughton, N.J., Fletcher, I.R., 2000. A New Understanding of the Provinces of the Amazon Craton Based on Integration of Field Mapping and U-Pb and Sm-Nd Geochronology. Gondwana Res. 3, 453–488. https://doi.org/10.1016/S1342-937X(05)70755-3.

Santos, T.B., Mancini, F., Cury, L.F., Ferreira, F.J.F., 2015. Proveniência de zircões detríticos e implicações para a paleogeografia da Formação Furnas no noroeste da Bacia do Paraná. Geologia USP - Série Científica, 15:25-59. https://doi.org/10.11606/ issn.2316-9095.v15i2p25-59.

Scheffler, S.M., Silva, R.C., Sedorko, D., 2020. O Devoniano no estado do Mato Grosso do Sul, Brazil: nova área de distribuição e presença de típica fauna malvinocáfrica. Estudos Geológicos (UFPE) 2020.

Schlager, W., 2010. Ordered hierarchy versus scale invariance in sequence stratigraphy. International Journal of Earth Sciences 99, 139–151.

Schneider, R., Mülmann, H., Tommasi, E., Medeiros, A., Daemon, R., Nogueira, A., 1974. Revisão estratigráfica da Bacia do Paraná. In: Congr. Brás. Geol., 28. Porto Alegre, 1974. Anais... Porto Alegre, SBG. v. l, p. 41-65.

Schobbenhaus, C. et al., 1975. Texto Explicativo, Folha Goiás SD.22, in: Schobbenhaus, C (Ed.) Carta Geológica do Brasil ao Milionésimo, Brasília, DNPM, 99p.

Sedorko, D., Bosetti, E.P., Ghilardi, R.P., Myszynski-Júnior L.J., Silva R.C., Scheffler S.M., 2018c. Paleoenvironments of a regressive Devonian section from Paraná Basin (Mato Grosso do Sul state) by integration of ichnologic, taphonomic and sedimentologic analyses. Brazilian Journal of Geolology, 48(4), 805-820. https://doi.org/10.1590/2317- 4889201820180021.

Sedorko, D., Bosetti, E.P., Netto, R.G., 2018b. An integrative ichnological and taphonomic approach in a transgressive-regressive cycle: a case study from Devonian of Paraná Basin, Brazil. Lethaia 51, 15–34. https://doi.org/10.1111/let.12219.

Sedorko, D., Netto, R. G., Scheffler, S. M., Horodyski, R. S., Bosetti, E. P., Ghilardi, R. P., Mauller, P. M., de Vargas, M. R., Videira-Santos, R., da Silva, R. C., & Myzynski-Junior, L., 2021. Paleoecologic trends of Devonian Malvinokaffric fauna from the Paraná Basin as evidenced by trace fossils. Journal of South American Earth Sciences, 109. https://doi.org/10.1016/j.jsames.2021.103200.

Sedorko, D., Netto, R.G., Horodyski, R.S., 2019. Tracking Silurian-Devonian events and paleobathymetric curves by ichnologic and taphonomic analyzes in the southwestern Gondwana. Global Planet. Change 179, 43–56. https://doi.org/10.1016/j.gloplacha.2019.05.007.

Sedorko, D., Netto, R.G., Savrda, C.E., 2018a. Ichnology applied to sequence stratigraphic analysis of Siluro-Devonian mud-dominated shelf deposits, Paraná Basin, Brazil. J. S. Am. Earth Sci. 83, 81–95. https://doi.org/10.1016/j.jsames.2018.02.008.

Sharman, G.R., Malkowski, M.A., 2020. Needles in a haystack: Detrital zircon U Pb ages and the maximum depositional age of modern global sediment. Earth-Science Rev. 203, 103109. https://doi.org/10.1016/j.earscirev.2020.103109.

Sharman, G.R., Sharman, J.P., Sylvester, Z., 2018. detritalPy: A Python-based toolset for visualizing and analysing detrital geo-thermochronologic data. Depos. Rec. 4, 202–215. https://doi.org/10.1002/dep2.45.

Silva, A.J.C.A., Simões, L.S.A., DuFrane, S.A., Sá Alkmin, L.A., Cerri, R.I., 2020. U–Pb ages of detrital zircon grains for the Canastra Group and Passos Nappe units and U–Pb and Lu–Hf isotope analyses from orthogneisses: Provenance and tectonic implications, southern Brasília Belt, Brazil. Precambrian Research. vol. 346. Elsevier B.V, p. 105771. https://doi.org/10.1016/j.precamres.2020.105771.

Sláma, J., Košler, J., Condon, D.J., Crowley, J.L., Gerdes, A., Hanchar, J.M., Horstwood, M.S.A., Morris, G.A., Nasdala, L., Norberg, N., Schaltegger, U., Schoene, B., Tubrett, M.N., Whitehouse, M.J., 2008. Plešovice zircon e a new natural reference material for UePb and Hf isotopic microanalysis. Chem. Geol. 249, 1-35.

Soares, P.C., Barbosa Landim, P.M., Fulfaro, V.J., 1978. Tectonic cycles and sedimentary sequences in the Brazilian intracratonic basins. Geological Society of America Bulletin 89, 181–191.

Sorcar, N., Joshi, K.B., Oliveira, E.P., Tomson, J.K., Nandakumar, V., 2020. Characterization of partial melting events in garnet-cordierite gneiss from the Kerala Khondalite Belt. India Geosci Front 11. https://doi.org/10.1016/j. gsf.2019.05.013.

Spalletti, L.A.,1993. An iron-bearing wave-dominated siliciclastic shelf: facies analysis and paleogeographic implications (Silurian-Lower Devonian Sierra Grande Formation, Southern Argentina). Geol J 28:137–148.

Sprechmann, P., Montana, J. y, Gaucher, C., 1993. Dev ~ onico. En: Geología y Recursos Minerales del Departamento de Durazno. Intendencia Municipal de Durazno, pp. 25e55.

Suess, E., 1906. The face of the earth. Oxford: Clarendon Press.Thomaz Filho, A., Kawashita, K., Cordani, U.G., 1998. A origem do Grupo Bambuí no contexto da evolução geotectônica e de idades radiométricas. Anais da Academia Brasileira de Ciências, 70:527e548.

Taylor, S. R. & McLennan, S. M., 1985. The Continental Crust: Its Composition and Evolution. Oxford: Blackwell.

Tohver, E., Trindade, R.I.F., Solum, J.G., Hall, C.M., Riccomini, C., Nogueira, A.C., 2010. Closing the Clymene ocean and bending a Brasiliano belt: Evidence for the Cambrian formation of Gondwana, southeast Amazon craton. Geology, 38: 267-270.

Torsvik, T.H., Cocks, L.R.M., 2013. Gondwana from top to base in space and time. Gondwana Research 24, 999–1030. https://doi.org/10.1016/j.gr.2013.06.012.

Toscani, R., Campos, J.E.G., Matos, D.R., Martins-Ferreira, M.A.C., 2021. Complex depositional environments on a siliciclastic-carbonate platform with shallow-water

turbidites: The Natividade Group, central Brazil. Journal of South American Earth Sciences, 107:102939. https://doi.org/10.1016/j. jsames.2020.102939.

Uriz, N.J., Cingolani, C.A., Basei, M.A.S., Blanco, G., Abre, P., Portillo, N.S., Siccardi, A., 2016. Provenance and paleogeography of the Devonian Durazno Group, southern Paraná Basin in Uruguay. J. South Am. Earth Sci. 66, 248–267.

Uriz, N.J., Cingolani, C.A., Chemale, F., Macambira, M.B., Armstrong, R., 2011. Isotopic studies on detrital zircons of Silurian–Devonian siliciclastic sequences from Argentinean North Patagonia and Sierra de la Ventana regions: comparative provenance. Int. J. Earth Sci. 100, 571–589. https://doi.org/10.1007/s00531-010-0597-z.

Vail, P.R., Mitchum Jr., R.M., Thompson III, S., 1977. Seismic stratigraphy and global changes of sea level, part four: global cycles of relative changes of sea level. American Association of Petroleum Geologists Memoir 26, 83–98.

Valeriano, C.M., Pimentel, M.M., Heilbron, M., Almeida, J.C.H., Trouw, R.A., 2008. Tectonic evolution of the Brasília Belt, Central Brazil, and early assembly of Godwana. Geological Society, London, Special Publications, 294:197-210. https://doi.org/10.1144/SP294.11.

Van Achterbergh, E., Ryan, C.G., Jackson, S.E., Griffin, W., 2001. Appendix III. Data reduction software for LA-ICP-MS. In: Sylvester, P. (Ed.), Laser-ablation-ICP-MS in the Earth Sciences, Principles and Applications. Mineralogical Association of Canada. Short Course Series, vol. 29, pp. 239-243.

Vargas, M., Silveira, A., Bressane, A., D'Avila, R., Faccion, J. E., & Paim, P. S., 2020. The Devonian of the Paraná Basin, Brazil: sequence stratigraphy, paleogeography, and SW Gondwana interregional correlations. Sedimentary Geology. https://doi.org/10.1016/j.sedgeo.2020.105768

Vermeesch, P., 2020. On the treatment of discordant detrital zircon U–Pb data. Geochronology Discussions 1–19. https://doi.org/10.5194/gchron-2020-38.

Wei, X., Wang, S., Ji, H., & Shi, Z., 2018. Strontium isotopes reveal weathering processes in lateritic covers in southern China with implications for paleogeographic reconstructions. PLOS ONE, 13(1), e0191780. https://doi.org/10.1371/journal.pone.0191780.

Weis, D., Kieffer, B., Maerschalk, C., Pretorius, W., Barling, J., 2005. High-precision Pb-Sr-Nd-Hf isotopic characterization of USGS BHVO-1 and BHVO-2 reference materials. Geochemistry, Geophys. Geosystems 6, 10.

Whitney, D.L., Evans, B.W., 2010. Abbreviations for names of rock-forming minerals. Am. Mineral. 95, 185–187. https://doi.org/10.2138/am.2010.3371.

Yakymchuk, C., Kirkland, C.L., Clark, C., 2018. Th/U ratios in metamorphic zircon. J. Metamorph. Geol. 36, 715–737. https://doi.org/10.1111/jmg.12307.

Yue, W., Yue, X., Zhang, L., Liu, X., Song, J., 2019. Morphology of Detrital Zircon as a Fingerprint to Trace Sediment Provenance: Case Study of the Yangtze Delta. Minerals. 9(7):438. https://doi.org/10.3390/min9070438.

Zalán, P. V., Wolf, S., Astolfi, M. A. M., Vieira, I. S., Conceição, J. C. J., Appi, V. T., Neto, E. V. S, Cerqueira, J. R., Marques, A., 1990. The Paraná Basin, Brazil. Interior cratonic basins (681-707). American Association of Petroleum Geologists Bulletin, Memoir 51.

Zalan, P., Wolff, S., Conceição, J., Vieira, I., Astolfi, M., Appi, V., Zanotto, O., 1987. A divisão tripartite do Siluriano da Bacia do Paraná. Rev. Brás. Geoc., 17(3):242- 252.

Zhao, J., Zeng, X., Tian, J., Hu, C., Wang, D., Yan, Z., Wang, K., Zhao, X., 2020. Provenance and paleogeography of the Jurassic Northwestern Qaidam Basin (NW China): evidence from sedimentary records and detrital zircon geochronology. J Asian Earth Sci 190:104060.

ANEXO

Dados U-Pb e morfologia dos zircões detríticos dos arenitos da formação Alto Garças, Furnas, Ponta Grossa e São Domingos via LA-ICP-M

CA-44 (Fm. Alto Garças)

SPOT	Grain Length	Grain Width	Length / width	Shape*	Roundness**	Zoning***	# of growth phases	f206c	^{207}Pb	^{206}Pb	U (µg g^{-1}) [a]	Th/U	$^{206}Pb/^{204}Pb$	$^{207}Pb/^{206}Pb$	2s (%)
1.sSMPABC007.TXT	212	92	2,30	elongated	sa-sr	oscillatory	1	0,02	8955,19	125725,27	249,18	0,09	777,37	0,07	0,96
1.sSMPABC008.TXT	206	104	1,98	elongated	sa-sr	oscillatory	1	0,04	2092,65	32023,11	73,66	0,83	466,82	0,07	2,14
1.sSMPABC009.TXT					sa-sr	oscillatory	1	0,02	4581,16	75480,72	188,42	0,66	1007,29	0,06	1,04
1.sSMPABC010.TXT	241	103	2,34	elongated	sa-sr	oscillatory	1	0,02	4003,89	66037,48	152,23	1,06	1046,15	0,06	1,11
1.sSMPABC011.TXT	201	113	1,78	elongated	rounded	irregular	1	0,06	2476,12	42212,32	105,48	1,01	302,53	0,06	1,42
1.sSMPABC012.TXT	237	132	1,80	oval	sa-sr	irregular	1	0,00	5809,04	93638,69	233,98	0,40	-8691,37	0,06	2,26
1.sSMPABC013.TXT	207	100	2,07	elongated	rounded	irregular	2	0,02	3415,71	51690,35	102,22	0,22	857,63	0,07	2,16
1.sSMPABC015.TXT	194	90	2,16	elongated	rounded	oscillatory	1	0,07	1140,81	16708,17	41,77	0,30	246,96	0,07	4,25
1.sSMPABC016.TXT	172	85	2,02	elongated	rounded	oscillatory	2	0,01	3428,11	42866,30	52,49	0,35	1937,47	0,08	1,00
1.sSMPABC017.TXT	195	74	2,64	elongated	rounded	oscillatory	2	0,01	15731,59	124954,53	88,22	0,50	1366,32	0,13	0,55
1.sSMPABC018.TXT					sa-sr	oscillatory	1	0,04	5281,98	84228,93	195,51	0,29	442,04	0,06	1,26
1.sSMPABC019.TXT	148	86	1,72	oval	sa-sr	oscillatory	1	-0,01	1684,62	26878,70	67,16	0,39	-3417,17	0,06	4,11
1.sSMPABC020.TXT	184	106	1,74	oval	sa-sr	oscillatory	1	0,02	3272,62	52951,78	122,03	0,46	968,13	0,06	1,19
1.sSMPABC027.TXT	162	115	1,41	oval	sa-sr	oscillatory	2	0,05	1561,37	23741,08	46,80	0,67	358,10	0,07	2,05
1.sSMPABC029.TXT	164	112	1,46	oval	sa-sr	oscillatory	1	0,05	1555,18	25033,03	57,60	0,49	369,94	0,06	1,74
1.sSMPABC030.TXT	166	91	1,82	elongated	sa-sr	irregular	1	0,04	3261,17	52690,76	121,63	0,29	484,95	0,06	1,27
1.sSMPABC031.TXT	199	113	1,76	oval	sa-sr	irregular	1	0,01	6873,18	114154,03	284,63	0,43	1766,45	0,06	0,78
1.sSMPABC032.TXT	183	118	1,55	oval	rounded	irregular	2	0,02	5048,94	80036,74	184,32	0,19	788,92	0,06	1,02
1.sSMPABC033.TXT	148	144	1,03	round	rounded	oscillatory	1	0,01	9316,20	153659,15	382,86	0,33	1701,47	0,06	0,88
1.sSMPABC034.TXT	146	95	1,54	oval	rounded	oscillatory	1	0,00	27482,74	218176,87	147,84	0,46	3505,50	0,13	0,49
1.sSMPABC035.TXT	223	121	1,84	elongated	rounded	irregular	2	0,00	46133,87	378680,76	286,59	0,17	3449,50	0,12	0,61
1.sSMPABC036.TXT	209	114	1,83	elongated	rounded	irregular	1	0,04	1511,17	17772,30	21,86	0,69	455,97	0,08	2,27
1.sSMPABC037.TXT	175	87	2,01	elongated	rounded	oscillatory	1	0,00	32353,65	272934,49	196,05	0,47	4561,56	0,12	0,48
1.sSMPABC040.TXT	183	92	1,99	elongated	sa-sr	oscillatory	1	0,02	2399,98	39491,85	90,60	0,32	965,27	0,06	1,35
1.sSMPABC047.TXT	143	100	1,43	oval	rounded	irregular	1	0,05	1870,63	30177,76	69,14	0,85	383,03	0,06	2,03
1.sSMPABC048.TXT	176	116	1,52	oval	sa-sr	irregular	2	0,00	15771,25	116459,86	70,90	0,66	13433,08	0,13	0,57
1.sSMPABC049.TXT	199	95	2,09	elongated	sa-sr	oscillatory	2	0,01	21727,46	165696,04	113,77	0,31	1558,00	0,13	0,54
1.sSMPABC050.TXT	148	98	1,51	oval	sa-sr	oscillatory	1	0,03	549,43	8678,77	21,49	1,02	662,41	0,06	3,06
1.sSMPABC051.TXT	200	110	1,82	elongated	euhedral	oscillatory	1	0,03	1800,47	25812,26	45,44	0,69	573,67	0,07	2,30
1.sSMPABC052.TXT	191	84	2,27	elongated	sa-sr	oscillatory	2	0,01	23820,25	179291,66	125,57	0,54	3000,94	0,13	0,50
1.sSMPABC054.TXT					rounded	irregular	1	0,05	2056,53	34397,16	94,67	0,24	369,33	0,06	1,15
1.sSMPABC056.TXT	146	66	2,21	elongated	rounded	irregular	1	0,03	2170,78	24694,27	29,98	0,48	568,25	0,09	1,16
1.sSMPABC057.TXT	136	75	1,81	elongated	sa-sr	irregular	2	0,02	5549,18	82142,47	160,87	0,43	915,21	0,07	1,11
1.sSMPABC058.TXT	159	92	1,73	oval	rounded	irregular	1	0,02	3032,62	48312,22	110,29	0,56	760,87	0,06	1,01
1.sSMPABC059.TXT					sa-sr	homogeneous	1	-0,03	851,08	12309,08	28,09	0,00	-538,83	0,07	5,55
1.sSMPABC060.TXT	175	82	2,13	elongated	sa-sr	homogeneous	1	0,04	321,21	4325,63	8,46	0,00	422,64	0,07	12,95
1.sSMPABC069.TXT	165	92	1,79	oval	rounded	oscillatory	1	0,13	2671,80	31406,77	84,55	0,61	140,56	0,06	1,88
1.sSMPABC074.TXT	114	67	1,70	oval	rounded	homogeneous	1	0,64	963,15	5086,84	8,89	0,09	27,44	0,07	17,94
1.sSMPABC067.TXT					sa-sr	homogeneous	1	0,91	323,255	1404,656	2,3847927	0,13	19,325178	0,0699619	24,55
1.sSMPABC071.TXT	179	86	2,08	elongated	rounded	homogeneous	1	0,84	1141,55	2741,86	3,2591476	0,29	20,69905	0,0842739	52,44
1.sSMPABC072.TXT	128	84	1,52	oval	sa-sr	homogeneous	1	0,95	514,237	2409,11	4,1293487	0,07	18,538856	0,0701922	18,91
1.sSMPABC070.TXT	129	92	1,40	oval	sa-sr	homogeneous	1	0,06	1093,14	2681,047	3,7222499	0,12	298,10346	0,0771685	20,73
1.sSMPABC039.TXT					rounded	oscillatory	1	0,04	7701,26	107347,5	347,67418	0,58	452,53301	0,0712091	1,313
1.sSMPABC028.TXT	167	88	1,90	elongated	rounded	oscillatory, sector	2	0,02	6016,96	93301,68	184,35796	0,36	893,9	0,0643522	0,823
1.sSMPABC055.TXT	174	112	1,55	oval	rounded	oscillatory, sector	2	0,01	15786,1	121036,5	71,563704	0,44	2132,0209	0,1291758	0,591

Ratios [b]					Dates [c]						Ratios [c]							Dates [d]								
$^{207}Pb/^{235}U$	2s (%)	$^{206}Pb/^{238}U$	2s (%)	Rho	$^{207}Pb/^{206}Pb$	2s abs	$^{206}Pb/^{238}U$	2s abs	$^{207}Pb/^{235}U$	2s abs	$^{207}Pb/^{206}Pb$	2s (%)	$^{207}Pb/^{235}U$	2s (%)	$^{206}Pb/^{238}U$	2s (%)	Rho	$^{207}Pb/^{206}Pb$	2s abs	$^{206}Pb/^{238}U$	2s abs	$^{207}Pb/^{235}U$	2s abs	% conc [e]	% conc [f]	% Error
1,31	1,24	0,13	0,78	0,63	969	16,44	807	4,93	851	7,07	0,07	0,98	1,31	1,26	0,13	0,78	0,62	964	20,09	806	5,92	849	7,25	120	105	1
1,04	2,34	0,11	0,95	0,40	792	37,85	701	5,25	723	12,51	0,07	2,22	1,03	2,42	0,11	0,95	0,39	782	46,70	701	6,29	720	12,54	112	103	1
0,89	1,43	0,11	0,99	0,69	635	18,68	649	5,08	645	7,37	0,06	1,05	0,89	1,44	0,11	0,99	0,68	630	22,70	649	6,09	645	6,91	97	99	1
0,96	1,45	0,11	0,93	0,64	633	20,07	700	5,15	684	7,63	0,06	1,13	0,96	1,46	0,11	0,93	0,64	628	24,36	700	6,18	683	7,31	90	98	1
0,86	1,74	0,11	1,02	0,58	561	25,95	649	5,23	629	8,93	0,06	1,51	0,85	1,82	0,11	1,02	0,56	543	32,90	649	6,27	625	8,51	84	96	1
0,91	3,35	0,11	2,47	0,74	682	40,69	649	12,73	656	30,01	0,06	2,25	0,91	3,34	0,11	2,47	0,74	683	48,11	649	15,28	657	16,30	105	101	2
1,22	2,95	0,13	2,01	0,68	815	38,06	810	12,77	811	26,06	0,07	2,20	1,22	2,98	0,13	2,01	0,67	810	46,10	810	15,33	810	16,79	100	100	2
1,00	4,50	0,11	1,48	0,33	883	75,07	649	7,62	703	26,02	0,07	4,58	0,99	4,81	0,11	1,48	0,31	865	95,00	649	9,13	699	24,62	133	108	1
2,39	1,35	0,22	0,91	0,67	1201	16,54	1263	8,70	1239	10,13	0,08	1,01	2,39	1,36	0,22	0,91	0,67	1200	19,92	1263	10,44	1239	9,78	95	98	2
6,53	0,91	0,38	0,73	0,80	2046	8,06	2054	10,75	2048	7,31	0,13	0,55	6,52	0,92	0,38	0,73	0,80	2044	9,75	2054	12,90	2049	8,11	100	100	0
0,99	1,88	0,11	1,40	0,74	703	22,58	697	7,70	698	12,23	0,06	1,32	0,98	1,92	0,11	1,40	0,73	692	28,07	697	9,23	695	9,71	99	100	1
0,92	4,37	0,11	1,50	0,34	701	74,64	650	7,70	661	24,45	0,06	4,09	0,92	4,35	0,11	1,50	0,34	702	87,02	650	9,25	661	21,38	108	102	1
0,98	1,50	0,11	0,92	0,61	670	21,30	701	5,11	693	7,97	0,06	1,21	0,98	1,52	0,11	0,92	0,61	665	25,88	701	6,14	693	7,66	95	99	1
1,22	2,62	0,13	1,63	0,62	796	36,23	812	10,40	807	20,03	0,07	2,15	1,21	2,70	0,13	1,63	0,60	783	45,27	811	12,48	804	15,13	96	99	2
0,98	2,20	0,11	1,35	0,61	673	31,25	701	7,48	694	13,73	0,06	1,82	0,97	2,27	0,11	1,35	0,60	659	39,07	701	8,98	691	11,43	94	99	1
0,97	1,70	0,11	1,14	0,67	664	22,86	699	6,27	690	9,83	0,06	1,32	0,97	1,74	0,11	1,14	0,65	653	28,30	699	7,52	688	8,73	94	98	1
0,88	1,22	0,11	0,94	0,77	603	14,11	649	4,84	639	6,01	0,06	0,79	0,87	1,23	0,11	0,94	0,77	600	17,03	649	5,81	638	5,83	92	98	1
0,99	1,71	0,11	1,37	0,80	702	18,29	700	7,57	700	10,96	0,06	1,05	0,99	1,72	0,11	1,37	0,79	696	22,34	700	9,09	699	8,75	99	100	1
0,88	1,28	0,11	0,93	0,73	616	15,84	649	4,79	641	6,34	0,06	0,89	0,88	1,28	0,11	0,93	0,72	613	19,12	649	5,74	641	6,12	94	99	1
6,73	0,87	0,39	0,71	0,82	2033	7,28	2121	10,72	2075	6,75	0,13	0,49	6,73	0,87	0,39	0,71	0,82	2033	8,76	2121	12,87	2076	7,69	96	98	0
5,82	1,06	0,35	0,87	0,82	1973	9,14	1928	12,06	1948	8,99	0,12	0,62	5,82	1,06	0,35	0,87	0,82	1973	10,98	1928	14,48	1949	9,26	102	101	1
2,50	2,97	0,21	1,92	0,65	1304	37,11	1252	18,24	1270	32,76	0,08	2,35	2,49	3,04	0,21	1,92	0,63	1297	45,71	1252	21,89	1268	22,23	104	101	4
5,96	0,94	0,37	0,81	0,86	1923	7,11	2016	11,63	1968	7,38	0,12	0,48	5,96	0,94	0,37	0,81	0,86	1922	8,54	2016	13,96	1969	8,17	95	98	0
0,95	1,67	0,11	0,98	0,58	614	24,57	701	5,40	680	8,90	0,06	1,38	0,95	1,69	0,11	0,98	0,58	609	29,83	701	6,48	679	8,40	87	97	1
0,97	2,58	0,11	1,59	0,62	652	36,67	700	8,82	688	17,40	0,06	2,12	0,96	2,66	0,11	1,59	0,60	639	45,69	700	10,58	685	13,32	91	98	2
7,98	1,04	0,43	0,87	0,83	2152	8,33	2313	14,04	2226	9,02	0,13	0,57	7,97	1,04	0,43	0,87	0,83	2152	9,97	2313	16,85	2228	9,40	93	96	0
6,85	0,94	0,38	0,76	0,82	2095	7,93	2088	11,36	2090	7,60	0,13	0,55	6,84	0,94	0,38	0,76	0,81	2094	9,59	2088	13,63	2091	8,35	100	100	0
0,92	3,58	0,11	1,86	0,52	697	55,29	650	9,58	660	24,29	0,06	3,14	0,91	3,65	0,11	1,86	0,51	690	67,07	650	11,49	658	17,85	106	101	2
1,42	2,80	0,15	1,60	0,57	900	40,01	896	11,18	896	22,26	0,07	2,37	1,41	2,86	0,15	1,60	0,56	893	48,93	896	13,42	895	17,16	100	100	1
6,80	0,99	0,37	0,85	0,86	2118	7,39	2052	12,53	2083	8,24	0,13	0,51	6,79	0,99	0,37	0,85	0,86	2118	8,89	2052	15,03	2085	8,83	103	102	0
0,78	1,49	0,10	0,94	0,63	575	20,97	587	4,41	584	7,02	0,06	1,21	0,77	1,53	0,10	0,94	0,62	560	26,33	587	5,29	581	6,80	95	99	1
2,60	1,71	0,22	1,25	0,73	1362	18,82	1262	11,99	1298	15,23	0,09	1,20	2,59	1,74	0,22	1,25	0,72	1357	23,13	1261	14,39	1297	12,79	108	103	2
1,24	1,39	0,13	0,83	0,60	836	19,40	811	5,26	817	7,89	0,07	1,13	1,23	1,40	0,13	0,83	0,59	831	23,61	811	6,31	816	7,90	103	101	1
0,99	1,41	0,11	0,99	0,70	682	18,07	702	5,48	696	7,69	0,06	1,03	0,98	1,43	0,11	0,99	0,69	676	22,10	701	6,58	695	7,23	96	99	1
1,09	5,90	0,12	2,02	0,34	886	98,59	702	11,18	747	40,14	0,07	5,37	1,09	5,74	0,12	2,02	0,35	894	110,90	702	13,43	749	30,88	127	107	2
1,21	13,48	0,13	3,74	0,28	799	123,01	806	23,66	804	120,71	0,07	13,51	1,20	14,02	0,13	3,74	0,27	788	283,64	806	28,39	801	80,80	98	99	4
0,79	2,16	0,10	1,06	0,49	605	11,69	589	4,97	592	10,58	0,06	2,16	0,78	2,40	0,10	1,06	0,44	567	46,94	589	5,96	584	10,72	96	99	1
1,30	18,80	0,14	5,63	0,30	925	240,73	817	36,11	846	238,01	0,06	49,51	1,20	49,82	0,13	5,63	0,11	763	1043,50	812	43,12	799	321,47	94	98	5
1,279363	30,37	0,132627	17,884	0,59	927,23614	245,22	802,8325	113,5	835,8063	217,38	0,0624816	270,23	1,13177	270,82	0,131432	17,884	0,07	690,63475	5763,37	796	135,3	768,5971	#¡VALOR!	87	97	17
1,779446	53,193	0,153141	8,9271	0,17	1298,8822	1021,9	918,5448	64	1037,029	1019,9	0,0774173	324,68	1,620347	324,81	0,151867	8,9271	0,03	1131,9591	6464,62	911	76,32	978,1255	#¡VALOR!	124	107	8
1,298267	20,264	0,134145	7,2902	0,36	933,98057	361,2	811,4675	46,49	844,1849	358,2	0,062394	358,64	1,142689	358,71	0,132886	7,2902	0,02	687,641	7652,73	804	55,36	773,7844	#¡VALOR!	85	96	7
1,407025	21,402	0,132239	5,3216	0,25	1125,5472	249,05	800,6276	33,48	891,0896	246,79	0,0766919	22,017	1,396889	22,651	0,132162	5,3216	0,23	1113,1884	439,588	800	40,17	887,6192	143,75106	139	111	5
0,798776	1,5449	0,081356	0,8144	0,53	963,42332	22,505	504,2098	3,292	595,5937	7,0277	0,0708928	1,367	0,794556	1,5912	0,081324	0,8144	0,51	954	27,9564	504	3,95	593,7529	7,1788533	189	118	3
1,187804	1,184	0,133869	0,8516	0,72	621,41049	14,54	809,9	5,403	794,2158	6,5707	0,0641908	0,839	1,184062	1,1955	0,133843	0,8516	0,71	#¡NUM!	17,7279	810	6,483	793,2034	6,6021073	#¡NUM!	98	1
7,906032	1,0953	0,443891	0,9222	0,84	2086,7833	8,6887	2368,035	15,25	2218,34	9,801	0,1291143	0,5951	7,898181	1,0975	0,443861	0,9222	0,84	2086	10,4672	2368	18,3	2219,472	9,9399104	88	94	1

BPN-01A (Fm. Furnas)

SPOT	Grain Length	Grain Width	Length / width	Shape*	Roundness**	Zoning***	# of growth phases	f206c	^{207}Pb	^{206}Pb	U ($\mu g\ g^{-1}$) [a]	Th/U	$^{206}Pb/^{204}Pb$	$^{207}Pb/^{206}Pb$	2s (%)
1.sSMPABC105.TXT	294	126	2,33	elongated	rounded	oscillatory, sector	2	0,03	20442,47	304061,61	339,25	0,31	623,55	0,06	6,11
1.sSMPABC106.TXT	330	135	2,44	elongated	rounded	irregular	2	0,04	4927,97	73338,18	57,49	0,25	395,91	0,07	3,85
1.sSMPABC107.TXT	257	84	3,06	elongated	rounded	oscillatory	1	0,03	1809,95	24142,31	24,40	1,00	570,87	0,06	11,68
1.sSMPABC108.TXT	226	112	2,02	elongated	sa-sr	oscillatory, sector	1	0,07	5265,63	73825,82	67,08	0,29	235,98	0,07	5,57
1.sSMPABC109.TXT	270	111	2,43	elongated	sa-sr	oscillatory, sector	1	0,05	4606,15	67608,54	50,90	0,35	358,67	0,07	4,10
1.sSMPABC110.TXT	250	63	3,97	elongated	rounded	oscillatory, sector	1	0,05	11927,30	168031,03	166,10	0,72	351,30	0,06	3,89
1.sSMPABC111.TXT	259	96	2,70	elongated	sa-sr	oscillatory	1	0,02	23746,14	296359,18	156,45	0,23	1099,37	0,09	2,08
1.sSMPABC112.TXT	174	105	1,66	oval	sa-sr	oscillatory	1	0,02	5675,73	83193,50	62,54	0,32	709,42	0,07	3,44
1.sSMPABC113.TXT	148	64	2,31	elongated	sa-sr	oscillatory, sector	1	0,04	6786,76	84216,60	42,04	4,72	437,71	0,09	3,32
1.sSMPABC114.TXT	274	112	2,45	elongated	rounded	oscillatory	1	0,03	6231,75	104717,21	114,36	0,23	605,46	0,06	3,58
1.sSMPABC115.TXT	230	94	2,45	elongated	sa-sr	oscillatory	2	0,07	3727,28	55160,14	56,47	1,25	240,14	0,07	4,67
1.sSMPABC116.TXT	223	93	2,40	elongated	sa-sr	irregular	2	0,03	12089,27	190031,87	234,12	0,42	681,67	0,06	3,19
1.sSMPABC117.TXT	187	93	2,01	elongated	rounded	homogeneous	1	0,22	727,99	7600,06	7,13	0,29	80,03	0,07	18,83
1.sSMPABC118.TXT	142	113	1,26	round	sa-sr	oscillatory, sector	1	0,04	9825,53	156159,14	163,32	0,22	426,15	0,06	2,99
1.sSMPABC119.TXT	169	120	1,41	oval	sa-sr	irregular	2	0,08	2706,77	38617,04	29,46	0,40	215,90	0,07	5,39
1.sSMPABC125.TXT	188	124	1,52	oval	rounded	irregular	1	0,02	15160,61	250220,35	270,53	0,05	992,41	0,06	2,49
1.sSMPABC126.TXT	182	110	1,65	oval	sa-sr	irregular	2	0,03	14524,32	231819,71	251,08	0,39	670,42	0,06	2,82
1.sSMPABC127.TXT	150	113	1,33	oval	rounded	oscillatory	1	0,06	2339,87	35546,59	37,46	0,31	281,78	0,07	5,40
1.sSMPABC128.TXT	260	95	2,74	elongated	rounded	oscillatory	2	0,05	4180,33	59190,55	43,66	0,43	355,56	0,07	4,30
1.sSMPABC130.TXT	263	95	2,77	elongated	rounded	oscillatory	1	0,11	12571,65	107626,23	96,76	0,67	160,43	0,07	23,34
1.sSMPABC131.TXT	210	121	1,74	oval	sa-sr	homogeneous	2	0,10	2372,78	36051,98	39,49	0,73	170,11	0,07	6,50
1.sSMPABC132.TXT	171	66	2,59	elongated	sa-sr	oscillatory	1	0,02	31789,32	279044,54	99,04	1,48	805,13	0,11	1,96
1.sSMPABC133.TXT	154	81	1,90	elongated	sa-sr	oscillatory	2	0,03	13238,15	176800,24	119,48	1,17	503,97	0,08	2,88
1.sSMPABC134.TXT	164	98	1,67	oval	sa-sr	oscillatory	2	0,04	13152,68	174407,13	213,03	0,49	444,61	0,06	4,62
1.sSMPABC135.TXT	206	90	2,29	elongated	sa-sr	oscillatory	1	0,03	11636,69	181016,85	208,70	0,35	620,19	0,06	3,28
1.sSMPABC136.TXT	156	80	1,95	elongated	sa-sr	oscillatory	2	0,02	13043,90	156958,89	108,86	0,42	753,37	0,07	3,71
1.sSMPABC137.TXT	154	84	1,83	elongated	sa-sr	oscillatory	1	0,03	8022,25	131523,97	143,49	0,26	682,77	0,06	3,10
1.sSMPABC140.TXT	290	112	2,59	elongated	sa-sr	oscillatory	1	0,01	52479,60	420192,56	125,29	0,26	1415,95	0,14	1,58
1.sSMPABC145.TXT	238	86	2,77	elongated	sa-sr	oscillatory	1	0,03	8147,53	132339,05	144,17	0,12	523,81	0,06	3,22
1.sSMPABC146.TXT	251	65	3,86	elongated	rounded	oscillatory, sector	2	0,08	2247,67	34199,72	40,58	0,18	225,20	0,07	5,98
1.sSMPABC147.TXT	295	79	3,73	elongated	rounded	oscillatory	1	0,01	71486,93	588768,86	209,48	0,34	1494,68	0,12	1,76
1.sSMPABC148.TXT	375	106	3,54	elongated	sa-sr	irregular	1	0,01	5729,58	94459,98	103,04	0,39	1344,36	0,06	5,18
1.sSMPABC149.TXT	268	88	3,05	elongated	sa-sr	oscillatory	2	0,11	1049,64	17012,84	18,81	0,42	158,98	0,06	28,78
1.sSMPABC150.TXT	194	67	2,90	elongated	sa-sr	oscillatory	2	0,07	4298,47	63536,20	58,29	0,28	258,97	0,07	4,16
1.sSMPABC151.TXT	150	72	2,08	elongated	sa-sr	oscillatory, sector	1	0,06	5598,38	83058,18	70,38	0,65	293,33	0,07	5,78
1.sSMPABC152.TXT	201	92	2,18	elongated	sa-sr	oscillatory	1	0,04	4395,28	73618,80	87,12	0,23	446,27	0,06	3,64
1.sSMPABC153.TXT	214	109	1,96	elongated	sa-sr	oscillatory	1	0,03	8625,26	124233,98	96,36	0,36	505,52	0,07	3,12
1.sSMPABC154.TXT	207	85	2,44	elongated	sa-sr	homogeneous	1	0,03	2265,63	34212,10	36,15	0,54	530,90	0,07	5,67
1.sSMPABC155.TXT	190	88	2,16	elongated	rounded	oscillatory, sector	2	0,02	16386,02	274812,43	364,20	0,39	1065,93	0,06	2,51
1.sSMPABC156.TXT	249	97	2,57	elongated	rounded	oscillatory	1	0,02	12222,04	185517,36	162,29	0,27	985,27	0,07	2,52
1.sSMPABC158.TXT	197	96	2,05	elongated	rounded	oscillatory	1	0,02	21632,29	348450,41	421,36	0,30	863,10	0,06	2,48
1.sSMPABC159.TXT	165	94	1,76	oval	rounded	oscillatory, sector	1	0,02	13297,25	195648,23	160,13	0,56	999,26	0,07	2,98
1.sSMPABC160.TXT	127	106	1,20	round	rounded	oscillatory, sector	1	0,03	5127,49	83413,81	89,73	0,65	692,54	0,06	3,84
1.sSMPABC166.TXT	194	127	1,53	oval	sa-sr	irregular	1	0,06	1576,60	25900,89	29,01	0,40	292,41	0,06	6,87
1.sSMPABC167.TXT	170	129	1,32	oval	sa-sr	oscillatory, sector	2	0,04	11866,31	190985,59	208,11	0,23	490,16	0,06	7,44
1.sSMPABC168.TXT	181	80	2,26	elongated	rounded	oscillatory, sector	2	0,05	5671,06	79967,36	85,74	0,57	342,02	0,06	5,31
1.sSMPABC169.TXT	212	65	3,26	elongated	sa-sr	oscillatory	1	0,06	2238,55	36826,03	39,83	0,44	302,73	0,06	5,00
1.sSMPABC170.TXT	170	105	1,62	oval	rounded	irregular	1	0,04	4184,70	67675,07	68,55	0,48	440,37	0,06	3,93
1.sSMPABC174.TXT	236	64	3,69	elongated	sa-sr	oscillatory	1	0,02	19115,12	291040,45	273,64	1,07	730,77	0,07	2,06
1.sSMPABC175.TXT	144	140	1,03	round	sa-sr	oscillatory	2	0,02	13862,68	229724,26	265,28	0,52	827,59	0,06	2,68
1.sSMPABC176.TXT	185	100	1,85	elongated	rounded	oscillatory	1	0,01	41581,57	309541,96	90,58	0,21	2671,56	0,14	1,94
1.sSMPABC179.TXT	237	158	1,50	oval	sa-sr	oscillatory	1	0,01	80848,70	421494,05	90,18	0,24	1969,41	0,21	1,67
1.sSMPABC180.TXT	152	121	1,26	round	sa-sr	irregular	1	0,03	2877,62	46581,74	51,21	0,33	668,08	0,06	5,19
1.sSMPABC185.TXT	254	139	1,83	elongated	sa-sr	oscillatory	1	0,01	68712,28	554464,45	177,51	0,68	2257,04	0,13	1,77
1.sSMPABC186.TXT	333	166	2,01	elongated	rounded	oscillatory	1	0,03	10955,30	182014,51	210,06	0,45	632,02	0,06	2,63
1.sSMPABC187.TXT	183	91	2,01	elongated	sa-sr	homogeneous	1	0,02	7150,10	108368,61	101,77	0,24	1001,35	0,07	3,22
1.sSMPABC188.TXT	174	99	1,76	oval	sa-sr	oscillatory	2	0,03	7875,37	129614,15	147,90	0,72	673,89	0,06	3,07
1.sSMPABC189.TXT	190	80	2,38	elongated	sa-sr	oscillatory	1	0,04	7025,00	103487,65	82,96	0,32	436,89	0,07	3,19
1.sSMPABC190.TXT	210	91	2,31	elongated	rounded	irregular	1	0,03	9971,67	163021,45	181,22	0,08	520,42	0,06	2,77
1.sSMPABC191.TXT	239	82	2,91	elongated	sa-sr	oscillatory	1	0,04	20000,44	286827,58	344,83	0,41	504,17	0,06	9,92
1.sSMPABC192.TXT	160	133	1,20	round (broken)	sa-sr	irregular	1	0,01	7740,65	126882,58	146,50	0,54	2724,84	0,06	2,94
1.sSMPABC194.TXT	250	99	2,53	elongated	sa-sr	irregular	1	0,01	25959,61	204380,52	63,51	0,23	1341,21	0,13	2,09
1.sSMPABC196.TXT	160	97	1,65	oval	sa-sr	oscillatory	1	0,02	14296,36	213397,83	187,61	0,37	709,08	0,07	4,96
1.sSMPABC198.TXT	216	99	2,18	elongated	sa-sr	oscillatory, sector	1	0,03	8086,50	95932,20	54,32	0,65	482,11	0,08	3,11
1.sSMPABC199.TXT	193	75	2,57	elongated	sa-sr	oscillatory	2	0,02	16056,46	239011,09	211,87	0,16	831,48	0,07	3,24
1.sSMPABC200.TXT	220	92	2,39	elongated	sa-sr	irregular	1	0,03	6804,67	109055,33	115,30	0,25	524,66	0,06	3,27
1.sSMPABC205.TXT	115	70	1,64	oval	sa-sr	oscillatory	1	0,02	12412,29	175071,58	145,51	0,46	839,72	0,07	3,31
1.sSMPABC206.TXT	205	76	2,70	elongated	sa-sr	oscillatory	1	0,06	5264,99	76588,45	81,16	0,63	290,32	0,07	5,09
1.sSMPABC207.TXT	123	120	1,03	round (broken)	sa-sr	irregular	1	0,03	6319,97	101810,75	115,71	0,20	685,04	0,06	3,47
1.sSMPABC208.TXT	228	88	2,59	elongated	sa-sr	oscillatory, sector	1	0,02	4381,16	62976,56	51,89	0,64	689,97	0,07	4,19
1.sSMPABC209.TXT	198	100	1,98	elongated	rounded	oscillatory	2	0,02	6273,39	101094,30	113,46	0,29	907,35	0,06	3,47
1.sSMPABC210.TXT	214	86	2,49	elongated	rounded	oscillatory	1	0,03	4335,33	62402,52	49,84	0,40	570,07	0,07	4,07
1.sSMPABC211.TXT	164	95	1,73	oval	rounded	oscillatory, sector	2	0,02	12471,23	173241,89	131,56	0,62	690,53	0,07	2,89
1.sSMPABC213.TXT	189	79	2,39	elongated	sa-sr	oscillatory	2	0,02	11983,96	180564,16	159,69	0,22	1086,75	0,07	2,61
1.sSMPABC214.TXT	250	78	3,21	elongated	sa-sr	homogeneous	2	0,05	3978,76	65181,87	74,04	0,48	355,48	0,06	5,78
1.sSMPABC215.TXT	210	87	2,41	elongated	rounded	oscillatory	1	0,03	15019,72	228200,94	265,09	0,51	656,42	0,07	3,33
1.sSMPABC216.TXT	171	76	2,25	elongated	rounded	oscillatory	1	0,01	32725,02	422020,38	263,98	0,41	1259,27	0,08	2,11
1.sSMPABC217.TXT	159	77	2,06	elongated	rounded	oscillatory	1	0,01	39457,04	406307,88	206,07	0,31	1377,81	0,10	1,99
1.sSMPABC218.TXT	199	56	3,55	elongated	rounded	oscillatory	1	0,01	217898,74	1081057,70	279,71	0,82	1526,52	0,20	1,77
1.sSMPABC219.TXT	171	89	1,92	elongated	sa-sr	oscillatory	1	0,03	9824,12	160691,40	190,64	0,32	586,20	0,06	2,93
1.sSMPABC220.TXT	297	75	3,96	elongated	rounded	oscillatory	2	0,14	365,78	5510,49	6,33	0,39	123,10	0,07	23,37
1.sSMPABC225.TXT	158	130	1,22	round	rounded	oscillatory	2	0,05	5820,02	94149,37	104,37	0,53	348,92	0,06	3,59
1.sSMPABC226.TXT	240	150	1,60	oval	sa-sr	homogeneous	2	0,06	1292,60	21092,03	24,25	0,46	282,45	0,06	7,87
1.sSMPABC227.TXT	190	96	1,98	elongated	sa-sr	irregular	1	0,01	2509,22	41289,10	47,32	0,36	1571,01	0,06	5,31
1.sSMPABC228.TXT	180	87	2,07	elongated	rounded	homogeneous	2	0,02	7393,95	121320,64	135,81	0,32	1002,98	0,06	3,17
1.sSMPABC229.TXT	180	160	1,13	round	sa-sr	oscillatory	1	0,03	10749,08	179239,24	217,17	0,60	592,09	0,06	2,69
1.sSMPABC230.TXT	171	67	2,55	elongated	sa-sr	oscillatory	1	0,06	4242,62	55939,50	43,12	0,58	275,75	0,08	16,10
1.sSMPABC232.TXT	183	94	1,95	elongated	rounded	irregular	1	0,01	61162,34	504965,26	180,18	0,32	1558,85	0,12	1,89
1.sSMPABC234.TXT	150	83	1,81	elongated	euhedral	oscillatory	1	0,02	13820,26	198085,67	171,35	0,46	907,96	0,07	2,75
1.sSMPABC235.TXT	175	93	1,88	elongated (broken)	sa-sr	oscillatory	1	0,02	11914,58	169176,22	111,68	0,48	798,75	0,08	3,38
1.sSMPABC236.TXT	146	120	1,22	round	rounded	oscillatory	2	0,02	8322,08	126110,47	136,04	0,18	764,38	0,07	7,57
1.sSMPABC237.TXT	171	131	1,31	oval	sa-sr	oscillatory	2	0,02	13941,28	228013,86	277,36	0,26	991,98	0,06	2,40
1.sSMPABC238.TXT	142	90	1,58	oval	rounded	oscillatory	2	0,01	79089,00	425396,04	91,88	0,69	1075,25	0,21	2,09
1.sSMPABC165.TXT	197	138	1,43	oval	sa-sr	irregular	1	0,01	497,78	6434,07	4,18	1,01	2410,40	0,08	14,18
1.sSMPABC231.TXT	160	67	2,39	elongated	sa-sr	irregular	2	0,10	2289,47	24474,37	23,16	0,58	173,11	0,07	33,15
1.sSMPABC212.TXT	153	72	2,13	elongated	rounded	irregular	1	0,11	22371,25	167440,97	357,08	0,62	168,03	0,05	15,13
1.sSMPABC233.TXT	284	78	3,64	elongated	sa-sr	oscillatory	1	0,09	9181,22	84335,76	77,74	0,41	189,47	0,07	46,98
1.sSMPABC129.TXT	156	62	2,52	elongated	euhedral	oscillatory	1	0,10	7328,87	89863,83	101,11	0,82	176,56	0,06	8,06
1.sSMPABC120.TXT	195	160	1,22	round	rounded	oscillatory, sector	1	0,01	1689,59	27949,75	29,05	1,06	2878,23	0,06	6,04

Ratios [b]					Dates [c]						Ratios [c]							Dates [d]								
$^{207}Pb/^{235}U$	2s (%)	$^{206}Pb/^{238}U$	2s (%)	Rho	$^{207}Pb/^{206}Pb$	2s abs	$^{206}Pb/^{238}U$	2s abs	$^{207}Pb/^{235}U$	2s abs	$^{207}Pb/^{206}Pb$	2s (%)	$^{207}Pb/^{235}U$	2s (%)	$^{206}Pb/^{238}U$	2s (%)	Rho	$^{207}Pb/^{206}Pb$	2s abs	$^{206}Pb/^{238}U$	2s abs	$^{207}Pb/^{235}U$	2s abs	% conc[e]	% conc[f]	% Error
0,89	6,35	0,10	1,73	0,27	681	24,16	636	10,47	646	21,77	0,06	6,29	0,89	6,52	0,10	1,73	0,26	673	134,57	636	10,47	644	31,61	99	94	2
1,38	4,31	0,15	1,95	0,45	854	20,12	893	16,24	881	28,34	0,07	4,02	1,37	4,47	0,15	1,95	0,44	843	83,75	892	16,23	878	26,62	102	106	2
1,01	12,02	0,11	2,83	0,24	747	60,40	697	18,75	708	57,42	0,06	12,05	1,01	12,38	0,11	2,83	0,23	739	255,02	697	18,74	706	65,06	99	94	3
1,17	6,55	0,13	3,44	0,52	825	79,06	775	25,14	787	74,96	0,07	6,02	1,16	6,93	0,13	3,44	0,50	805	125,98	775	25,13	782	38,52	99	96	3
1,46	4,54	0,16	1,94	0,43	882	21,36	929	16,78	915	29,21	0,07	4,31	1,45	4,73	0,15	1,94	0,41	870	89,30	929	16,78	911	28,83	102	107	2
1,05	6,30	0,12	4,96	0,79	762	146,43	716	33,74	727	142,49	0,06	4,09	1,04	6,43	0,12	4,96	0,77	749	86,44	716	33,73	724	33,85	99	96	5
2,66	2,87	0,22	1,98	0,69	1353	40,51	1297	23,26	1317	33,17	0,09	2,11	2,66	2,89	0,22	1,98	0,68	1350	40,76	1297	23,25	1317	21,57	98	96	3
1,47	4,15	0,16	2,33	0,56	885	17,88	933	20,26	918	38,68	0,07	3,52	1,47	4,22	0,16	2,33	0,55	879	72,93	933	20,26	917	25,83	102	106	2
2,93	4,51	0,24	3,05	0,68	1422	88,35	1370	37,79	1389	79,87	0,09	3,45	2,92	4,61	0,24	3,05	0,66	1415	65,96	1369	37,77	1387	35,45	99	97	5
0,93	4,05	0,11	1,90	0,47	694	25,25	659	11,92	667	22,26	0,06	3,69	0,92	4,15	0,11	1,90	0,46	686	78,68	659	11,91	665	20,44	99	96	2
1,07	5,19	0,11	2,26	0,44	865	24,41	700	15,04	740	33,63	0,07	5,04	1,06	5,53	0,11	2,26	0,41	846	104,85	699	15,03	735	29,33	95	83	2
0,84	4,64	0,10	3,37	0,73	738	16,94	587	18,94	619	57,86	0,06	3,27	0,84	4,69	0,10	3,37	0,72	731	69,30	587	18,93	617	21,96	95	80	3
1,11	19,28	0,12	4,17	0,22	800	128,63	742	29,31	756	125,25	0,06	24,12	1,07	24,48	0,12	4,17	0,17	741	510,13	741	29,26	741	137,62	100	100	4
0,98	3,54	0,11	1,91	0,54	715	15,94	688	12,47	693	22,32	0,06	3,11	0,97	3,65	0,11	1,91	0,52	703	66,30	687	12,46	691	18,48	99	98	2
1,50	5,94	0,15	2,50	0,42	940	27,84	926	21,58	929	47,24	0,07	5,85	1,48	6,36	0,15	2,50	0,39	921	120,32	925	21,56	924	39,34	100	101	2
0,92	3,12	0,11	1,89	0,60	633	13,45	670	12,03	661	20,55	0,06	2,53	0,92	3,16	0,11	1,89	0,60	628	54,60	670	12,03	661	15,46	101	107	2
0,95	3,58	0,11	2,20	0,61	705	15,09	670	14,03	677	27,84	0,06	2,90	0,95	3,64	0,11	2,20	0,60	698	61,78	670	14,03	676	18,14	99	96	2
1,03	5,87	0,11	2,30	0,39	809	28,48	688	15,03	717	34,72	0,07	5,76	1,02	6,20	0,11	2,30	0,37	793	120,75	688	15,03	713	32,25	97	87	2
1,57	4,79	0,16	2,11	0,44	955	22,16	963	18,89	959	34,85	0,07	4,52	1,56	4,99	0,16	2,11	0,42	943	92,64	962	18,88	956	31,39	101	102	2
1,16	23,48	0,13	2,54	0,11	831	71,75	768	18,40	783	69,35	0,07	26,20	1,15	26,32	0,13	2,54	0,10	803	548,77	767	18,38	776	153,89	99	96	2
0,99	7,21	0,11	3,12	0,43	809	34,35	666	19,76	699	59,01	0,07	7,25	0,98	7,89	0,11	3,12	0,40	782	152,32	665	19,74	692	40,39	96	85	3
5,30	3,11	0,34	2,41	0,78	1870	8,87	1868	39,24	1867	55,34	0,11	2,00	5,29	3,13	0,34	2,41	0,77	1867	36,09	1867	39,23	1867	27,12	100	100	2
1,83	3,44	0,18	1,87	0,54	1073	14,54	1049	18,14	1056	28,10	0,07	2,98	1,82	3,52	0,18	1,87	0,53	1065	59,97	1048	18,14	1054	23,35	100	98	2
0,81	5,76	0,10	3,45	0,60	624	63,95	594	19,60	600	60,87	0,06	4,81	0,80	5,92	0,10	3,45	0,58	612	103,97	594	19,60	597	27,09	99	97	3
0,92	3,68	0,10	1,67	0,46	759	17,37	636	10,15	663	17,78	0,06	3,37	0,92	3,76	0,10	1,67	0,44	751	71,21	636	10,15	662	18,47	96	85	2
1,76	4,19	0,17	1,94	0,46	1055	35,96	1019	18,35	1029	30,93	0,07	3,80	1,75	4,27	0,17	1,94	0,46	1050	76,55	1019	18,35	1028	27,97	99	97	2
0,93	3,84	0,11	2,25	0,59	647	16,76	672	14,40	666	29,01	0,06	3,19	0,92	3,90	0,11	2,25	0,58	639	68,55	672	14,40	664	19,21	101	105	2
7,87	2,29	0,41	1,66	0,72	2223	42,44	2210	31,16	2215	28,81	0,14	1,60	7,87	2,31	0,41	1,66	0,72	2222	27,71	2210	31,16	2216	20,99	100	99	1
0,94	3,66	0,11	1,74	0,47	666	17,34	678	11,18	674	19,00	0,06	3,33	0,94	3,76	0,11	1,74	0,46	657	71,50	677	11,18	672	18,65	101	103	2
0,93	6,44	0,10	2,38	0,37	804	31,62	625	14,18	665	35,45	0,07	6,49	0,92	6,91	0,10	2,38	0,34	784	136,35	625	14,17	660	34,12	95	80	2
5,71	2,44	0,34	1,69	0,69	1983	7,83	1886	27,78	1931	29,00	0,12	1,77	5,70	2,45	0,34	1,69	0,69	1982	31,57	1886	27,78	1932	21,42	98	95	2
0,93	5,77	0,11	2,55	0,44	634	28,13	678	16,44	668	38,87	0,06	5,25	0,93	5,84	0,11	2,55	0,44	630	113,08	678	16,44	667	28,94	102	108	2
0,94	28,92	0,11	2,79	0,10	670	161,97	670	17,80	670	76,29	0,06	32,38	0,92	32,50	0,11	2,79	0,09	639	696,50	670	17,79	662	171,89	101	105	3
1,24	4,61	0,13	1,98	0,43	864	21,74	801	14,93	817	28,26	0,07	4,46	1,23	4,88	0,13	1,98	0,41	847	92,85	800	14,93	812	27,69	98	94	2
1,34	7,85	0,14	5,31	0,68	857	30,29	863	43,02	861	188,20	0,07	6,14	1,32	8,12	0,14	5,31	0,65	842	127,83	863	43,00	857	48,08	101	103	5
0,85	4,18	0,10	2,06	0,49	599	19,81	630	12,37	623	24,25	0,06	3,79	0,84	4,31	0,10	2,06	0,48	588	82,17	630	12,37	621	20,22	102	107	2
1,51	3,61	0,16	1,81	0,50	918	16,14	939	15,80	932	24,95	0,07	3,23	1,50	3,70	0,16	1,81	0,49	909	66,59	939	15,80	930	22,81	101	103	2
1,06	6,03	0,12	2,04	0,34	820	29,88	703	13,63	731	29,58	0,07	5,86	1,05	6,21	0,12	2,04	0,33	811	122,62	703	13,63	729	32,81	96	87	2
0,76	2,95	0,09	1,56	0,53	596	13,63	567	8,47	572	13,46	0,06	2,55	0,76	2,99	0,09	1,56	0,52	591	55,26	567	8,47	572	13,15	99	96	1
1,27	3,01	0,14	1,65	0,55	809	13,22	841	13,06	832	19,29	0,07	2,56	1,27	3,05	0,14	1,65	0,54	804	53,63	841	13,06	831	17,45	101	105	2
0,87	3,30	0,10	2,16	0,66	683	13,32	621	12,82	634	25,33	0,06	2,54	0,86	3,33	0,10	2,16	0,65	677	54,22	620	12,82	633	15,82	98	92	2
1,40	3,47	0,15	1,79	0,51	873	15,49	898	14,99	890	23,59	0,07	3,03	1,40	3,52	0,15	1,79	0,51	869	62,77	898	14,99	889	21,05	101	103	2
0,97	4,28	0,11	1,90	0,44	662	20,69	695	12,55	686	23,11	0,06	3,94	0,96	4,37	0,11	1,90	0,44	654	84,47	695	12,54	685	22,02	101	106	2
0,92	7,27	0,11	2,38	0,33	640	37,39	672	15,24	664	36,75	0,06	7,31	0,92	7,69	0,11	2,38	0,31	623	157,75	672	15,23	660	38,05	102	108	2
0,97	7,67	0,11	1,87	0,24	684	40,19	691	12,27	688	27,17	0,06	7,71	0,97	7,94	0,11	1,87	0,24	674	164,94	690	12,27	686	40,38	101	102	2
0,99	5,63	0,11	1,90	0,34	702	28,07	697	12,53	698	25,12	0,06	5,59	0,98	5,91	0,11	1,90	0,32	688	119,36	697	12,53	694	30,15	100	101	2
0,99	5,45	0,11	2,18	0,40	696	33,93	698	14,43	697	30,71	0,06	5,31	0,98	5,74	0,11	2,18	0,38	680	113,43	697	14,42	693	29,24	101	103	2
1,08	4,32	0,12	1,81	0,42	740	25,89	743	12,69	742	22,57	0,06	4,09	1,07	4,47	0,12	1,81	0,40	729	86,65	743	12,68	739	23,75	100	102	2
1,20	3,30	0,13	2,58	0,78	801	10,84	799	19,42	799	40,49	0,07	2,11	1,19	3,34	0,13	2,58	0,77	795	44,29	799	19,42	797	18,59	100	101	2
0,90	3,20	0,11	1,75	0,55	621	14,54	658	10,96	649	18,07	0,06	2,74	0,89	3,25	0,11	1,75	0,54	614	59,23	658	10,96	648	15,71	102	107	2
8,40	2,63	0,43	1,77	0,67	2256	47,77	2296	34,26	2273	33,29	0,14	1,95	8,39	2,63	0,43	1,77	0,67	2255	33,72	2296	34,26	2274	24,19	101	102	1
17,37	2,40	0,59	1,72	0,72	2919	53,09	3009	41,57	2953	33,02	0,21	1,68	17,36	2,40	0,59	1,72	0,72	2919	27,14	3009	41,57	2955	23,35	102	103	1
0,97	5,54	0,11	1,95	0,35	671	28,00	693	12,81	687	25,73	0,06	5,33	0,96	5,67	0,11	1,95	0,34	663	114,15	693	12,80	685	28,68	101	104	2
7,02	2,41	0,39	1,63	0,68	2090	40,67	2139	29,68	2112	27,81	0,13	1,78	7,01	2,41	0,39	1,63	0,67	2089	31,36	2139	29,67	2113	21,68	101	102	2
0,90	3,16	0,11	1,74	0,55	614	14,29	665	11,02	653	17,95	0,06	2,71	0,90	3,22	0,11	1,74	0,54	606	58,60	665	11,02	651	15,61	102	110	2
1,21	3,56	0,13	1,50	0,42	793	20,59	808	11,42	804	17,14	0,07	3,28	1,20	3,61	0,13	1,50	0,42	789	68,88	808	11,42	803	20,22	101	102	1
0,92	3,48	0,11	1,64	0,47	634	16,63	673	10,47	664	16,94	0,06	3,16	0,92	3,56	0,11	1,64	0,46	627	68,03	673	10,47	662	17,45	102	107	2
1,51	3,69	0,16	1,86	0,50	919	30,84	941	16,26	933	26,21	0,07	3,33	1,50	3,81	0,16	1,86	0,49	910	68,47	940	16,25	931	23,47	101	103	2
0,96	3,46	0,11	2,07	0,60	649	14,94	691	13,58	681	24,96	0,06	2,87	0,95	3,54	0,11	2,07	0,59	639	61,67	691	13,57	679	17,65	102	108	2
0,87	10,07	0,10	1,76	0,17	628	28,66	637	10,67	635	26,60	0,06	10,28	0,87	10,43	0,10	1,76	0,17	618	221,84	637	10,66	633	50,33	101	103	2
0,92	3,49	0,11	1,88	0,54	643	15,87	668	11,92	662	20,91	0,06	2,96	0,92	3,50	0,11	1,88	0,54	641	63,59	668	11,92	662	17,17	101	104	2
7,52	2,64	0,41	1,61	0,61	2143	41,33	2211	30,17	2174	28,24	0,13	2,12	7,51	2,66	0,41	1,61	0,61	2142	36,98	2210	30,17	2175	24,10	102	103	2
1,33	5,33	0,14	1,94	0,36	841	26,03	867	15,79	859	29,51	0,07	5,08	1,33	5,44	0,14	1,94	0,36	834	105,93	867	15,79	857	32,01	101	104	2
2,61	3,85	0,22	2,26	0,59	1302	15,20	1303	26,71	1301	44,10	0,08	3,22	2,60	3,94	0,22	2,26	0,57	1295	62,70	1302	26,70	1299	29,28	100	101	5
1,33	4,67	0,14	3,37	0,72	846	16,91	863	27,25	857	72,87	0,07	3,30	1,32	4,72	0,14	3,37	0,71	841	68,78	862	27,24	856	27,66	101	103	3
1,03	3,67	0,12	1,66	0,45	690	17,54	731	11,52	721	18,69	0,06	3,38	1,03	3,77	0,12	1,66	0,44	681	72,30	731	11,52	719	19,62	102	107	2
1,50	5,01	0,15	3,75	0,75	957	17,03	921	32,29	931	95,22	0,07	3,38	1,50	5,05	0,15	3,75	0,74	952	69,22	921	32,29	930	31,25	99	97	4
1,14	5,49	0,12	2,07	0,38	893	26,50	734	14,34	774	30,43	0,07	5,42	1,13	5,80	0,12	2,07	0,36	878	112,13	733	14,33	770	31,78	95	83	2
0,96	3,84	0,11	1,63	0,42	679	18,66	687	10,63	685	17,71	0,06	3,56	0,96	3,92	0,11	1,63	0,42	672	76,27	687	10,63	683	19,68	101	102	2
1,49	4,68	0,16	2,09	0,45	918	21,69	931	18,13	926	33,41	0,07	4,30	1,49	4,78	0,16	2,09	0,44	911	88,45	930	18,13	925	29,42	101	102	2
0,98	3,79	0,11	1,53	0,40	678	18,64	697	10,14	692	16,28	0,06	3,54	0,97	3,85	0,11	1,53	0,40	672	75,64	696	10,14	691	19,50	101	104	1
1,54	4,52	0,16	1,96	0,43	915	21,09	960	17,53	945	30,41	0,07	4,20	1,53	4,64	0,16	1,96	0,42	907	86,51	959	17,52	943	28,89	102	106	2
1,68	3,62	0,17	2,19	0,60	987	14,76	1006	20,43	1000	35,66	0,07	2,96	1,67	3,68	0,17	2,19	0,59	981	60,29	1006	20,42	998	23,67	101	103	2
1,33	3,23	0,15	1,90	0,59	820	13,68	875	15,55	859	24,97	0,07	2,65	1,33	3,26	0,15	1,90	0,58	816	55,39	875	15,55	858	19,06	102	107	2
0,95	6,13	0,11	2,05	0,33	642	31,35	692	13,44	680	28,29	0,06	6,08	0,95	6,41	0,11	2,05	0,32	628	130,97	691	13,43	676	32,17	102	110	2
1,01	3,70	0,11	1,62	0,44	802	17,51	678	10,43	707	17,73	0,07	3,42	1,00	3,78	0,11	1,62	0,43	795	71,65	678	10,42	705	19,41	96	85	2
2,22	2,75	0,21	1,76	0,64	1153	32,12	1209	19,39	1188	25,61	0,08	2,14	2,22	2,77	0,21	1,76	0,63	1150	42,46	1208	19,39	1187	19,56	102	105	2
3,41	3,15	0,25	2,44	0,77	1571	9,36	1461	31,92	1505	51,74	0,10	2,02	3,40	3,16	0,25	2,44	0,77	1569	37,78	1461	31,92	1505	25,12	97	93	2
13,88	4,60	0,50	4,25	0,92	2840	7,22	2610	91,84	2739	192,10	0,20	1,78	13,87	4,61	0,50	4,25	0,92	2839	29,07	2610	91,84	2741	44,61	95	92	1
0,92	3,43	0,11	1,78	0,52	645	15,84	667	11,29	661	19,16	0,06	3,03	0,91	3,51	0,11	1,78	0,51	637	65,11	666	11,29	659	17,17	101	105	2
1,03	23,88	0,11	4,88	0,20	819	127,05	688	31,93	719	165,52	0,07	27,28	1,01	27,71	0,11	4,88	0,18	782	573,22	687	31,88	710	152,39	97	88	5
1,00	4,11	0,12	2,01	0,49	669	19,30	715	13,58	703	25,26	0,06	3,78	0,99	4,28	0,12	2,01	0,47	654	81,01	714	13,58	700	21,85	102	109	2
0,96	8,22	0,11	2,37	0,29	650	42,81	691	15,56	681	38,38	0,06	8,39	0,95	8,72	0,11	2,37	0,27	632	180,74	691	15,55	677	44,02	102	109	2
0,96	5,69	0,11	2,06	0,36	655	31,25	694	13,58	684	28,14	0,06	5,37	0,96	5,75	0,11	2,06	0,36	651	115,20	694	13,58	684	29,02	101	107	2
0,99	3,66	0,12	1,84	0,50	669	24,62	710	12,37	700	21,28	0,06	3,23	0,99	3,71	0,12	1,84	0,49	664	69,09	710	12,36	699	18,93	102	107	2
0,90	3,18	0,11	1,70	0,53	621	20,23	659	10,65	650	17,20	0,06	2,77	0,89	3,25	0,11	1,70	0,52	612	59,91	659	10,64	648	15,70	102	108	2
1,77	16,74	0,17	4,58	0,27	1091	82,82	1009	42,87	1034	176,34	0,08	17,17	1,76	17,77	0,17	4,58	0,26	1078	344,55	1008	42,85	1030	122,02	98	94	4
6,12	2,39	0,37	1,45	0,61	1973	8,44	2013	25,21	1992	22,84	0,12	1,91	6,11	2,40	0,37	1,45	0,61	1972	34,02	2013	25,21	1992	21,16	101	102	2
1,46	4,27	0,15	3,26	0,76	922	14,21	909	27,73	912	70,57	0,07	2,81	1,45	4,30	0,15	3,26	0,76	917	57,71	909	27,72	911	26,22	100	99	3
2,09	5,14	0,20	3,87	0,75	1096	122,23	1174	41,66	1146	114,91	0,08	3,46	2,09	5,19	0,20	3,87	0,75	1092	69,22	1174	41,66	1145	36,26	103	108	4
1,11	7,73	0,12	1,60	0,21	806	40,10	740	11,17	756	23,93	0,07	7,74	1,10	7,91	0,12	1,60	0,20	800	162,24	740	11,17	755	43,01	98	93	2
0,91	3,21	0,11	2,12	0,66	644	12,97	661	13,34	657	24,94	0,06	2,45	0,91	3,24	0,11	2,12	0,65	639	52,66	661	13,34	656	15,77	101	103	2
17,94	3,24	0,62	2,47	0,76	2894	90,17	3126	61,56	2984	65,89	0,21	2,11	17,92	3,25	0,62	2,47	0,76	2893	34,29	3126	61,55	2985	31,78	105	108	1
2,03	20,16	0,19	14,33	0,71	1136	72,19	1118	148,82	1123	59,20	0,08	14,28	2,02	20,23	0,19	14,33	0,71	1134	284,14	1118	148,81	1123	147,69	100	99	13
1,21	34,69	0,13	10,22	0,29	784	665,38	814	78,60	805	660,73	0,06	36,86	1,19	38,25	0,13	10,22	0,27	757	777,59	813	78,53	798	237,04	102	107	10
0,42	16,59	0,06	6,80	0,41	362	162,98	352	23,33	353	161,30	0,05	16,96	0,41	18,28	0,06	6,80	0,37	325	385,19	351	23,31	348	55,30	101	108	7
1,24	47,44	0,14	6,60	0,14	804	374,67	825	51,34	819	371,13	0,07	51,73	1,23	52,15	0,14	6,60	0,13	779	1087,44	825	51,30	812	343,68	102	106	6
0,89	10,04	0,10	6,00	0,60	674	202,98	637	36,48	645	199,67	0,06	8,96	0,87	10,78	0,10	6,00	0,56	645	192,43	636	36,45	638	52,40	100	99	6
1,00	6,56	0,11	2,56	0,39	709	44,90	695	16,86	702	41,61	0,06	6,08	1,00	6,59	0,11	2,56	0,39	#¡NUM!	128,90	695	16,86	702	33,97	99	#¡NUM!	2

BPN-06A (Fm. Ponta Grossa)

SPOT	Grain Length	Grain Width	Length / width	Shape*	Roundness**	Zoning***	# of growth phases	f206c	^{207}Pb	^{206}Pb	U (µg g^{-1}) [a]	Th/U	$^{206}Pb/^{204}Pb$	$^{207}Pb/^{206}Pb$	2s (%)
1.sSMPABC005.TXT	150	49	3,06	elongated	sa-sr	irregular	1	0,08	4014,01	65212,87	116,27	0,50	219,18	0,06	3,13
1.sSMPABC006.TXT	135	49	2,76	elongated	rounded	irregular	2	0,02	20686,41	155998,00	69,16	0,63	669,79	0,14	1,55
1.sSMPABC007.TXT	120	74	1,62	oval	sa-sr	oscillatory	1	0,05	5112,97	76419,56	129,17	1,00	366,80	0,06	3,97
1.sSMPABC008.TXT	107	52	2,06	elongated	rounded	irregular	2	0,02	14982,82	232537,11	523,12	0,14	1002,20	0,06	1,90
1.sSMPABC009.TXT	170	58	2,93	elongated	rounded	oscillatory	1	0,04	8599,36	109711,61	107,35	1,00	462,59	0,08	3,37
1.sSMPABC010.TXT	134	68	1,97	elongated	sa-sr	oscillatory	1	0,05	8133,05	98426,47	98,59	0,60	331,18	0,08	2,93
1.sSMPABC011.TXT	152	51	2,98	elongated	rounded	irregular	1	0,01	43093,16	322951,86	156,32	0,55	1338,68	0,13	1,32
1.sSMPABC012.TXT	117	63	1,86	elongated	rounded	oscillatory	1	0,03	4245,72	54561,19	61,68	0,51	534,22	0,08	3,42
1.sSMPABC014.TXT	129	67	1,93	elongated	rounded	oscillatory	2	0,02	33015,50	284224,94	221,08	0,42	1077,79	0,09	2,21
1.sSMPABC015.TXT	129	64	2,02	elongated	sa-sr	oscillatory	1	0,02	14996,54	111272,58	47,50	0,52	890,53	0,15	1,83
1.sSMPABC016.TXT	101	58	1,74	oval	rounded	irregular	1	0,03	18359,11	204044,57	241,46	0,13	670,29	0,07	2,21
1.sSMPABC017.TXT	130	48	2,71	elongated	rounded	oscillatory	2	0,03	35662,76	277158,38	289,78	0,35	652,04	0,07	2,86
1.sSMPABC018.TXT	114	91	1,25	round	rounded	oscillatory	1	0,02	15825,86	226569,53	329,79	0,18	1064,07	0,07	1,81
1.sSMPABC019.TXT	149	78	1,91	elongated	rounded	oscillatory	1	0,04	8781,65	132255,78	215,93	0,79	425,80	0,07	3,11
1.sSMPABC020.TXT	132	58	2,28	elongated	rounded	oscillatory	1	0,03	11081,57	135431,91	161,37	0,49	534,74	0,08	2,66
1.sSMPABC025.TXT	110	61	1,80	oval	rounded	irregular	2	0,00	79412,68	568694,87	271,97	0,35	3360,49	0,14	1,26
1.sSMPABC026.TXT	125	69	1,81	elongated	rounded	irregular	1	0,03	8262,06	130312,65	244,09	0,35	552,54	0,06	2,42
1.sSMPABC027.TXT	156	68	2,29	elongated	rounded	homogeneous	2	0,01	22376,74	175710,47	87,98	0,41	1369,22	0,13	1,73
1.sSMPABC028.TXT	137	79	1,73	oval	rounded	homogeneous	1	0,01	13552,57	127273,43	70,53	0,79	1099,06	0,11	1,84
1.sSMPABC029.TXT	112	63	1,78	oval	rounded	homogeneous	2	0,03	8118,26	119557,87	190,22	0,48	694,81	0,07	2,40
1.sSMPABC030.TXT	126	77	1,64	oval	sa-sr	homogeneous	1	0,06	512,18	5976,99	5,89	0,46	302,77	0,09	10,88
1.sSMPABC031.TXT	129	63	2,05	elongated	rounded	oscillatory, sector	1	0,05	13221,20	158679,63	220,94	0,24	368,90	0,07	4,97
1.sSMPABC033.TXT	108	56	1,93	elongated	rounded	oscillatory	1	0,02	14472,49	213662,08	416,66	0,34	786,61	0,07	1,94
1.sSMPABC035.TXT	166	61	2,72	elongated	rounded	oscillatory	2	0,01	33592,86	260038,67	137,57	0,47	1650,15	0,13	1,35
1.sSMPABC037.TXT	96	60	1,60	oval	rounded	homogeneous	1	0,02	41556,52	317437,24	249,26	0,20	985,89	0,09	2,25
1.sSMPABC038.TXT	133	56	2,38	elongated	rounded	irregular	1	0,11	3062,28	47693,30	86,34	0,39	167,07	0,06	4,70
1.sSMPABC039.TXT	128	73	1,75	oval	rounded	irregular	1	0,01	37936,91	327984,37	174,05	0,18	1400,18	0,12	1,35
1.sSMPABC040.TXT	142	63	2,25	elongated	rounded	oscillatory, sector	1	0,06	2270,13	37992,33	62,70	0,51	293,26	0,06	4,74
1.sSMPABC045.TXT	173	65	2,66	elongated	sa-sr	irregular	1	0,01	37068,43	291762,72	139,76	1,88	1158,89	0,13	1,55
1.sSMPABC046.TXT	186	74	2,51	elongated	sa-sr	oscillatory	1	0,01	63549,93	379565,68	225,91	0,37	2054,70	0,11	2,29
1.sSMPABC047.TXT	126	80	1,58	oval	rounded	irregular	2	0,03	7286,77	96526,66	169,08	0,40	522,79	0,06	3,14
1.sSMPABC048.TXT	125	70	1,79	oval	sa-sr	homogeneous	2	0,07	1705,61	26585,50	43,41	0,29	254,42	0,07	8,29
1.sSMPABC049.TXT	120	95	1,26	round	sa-sr	oscillatory	1	0,03	3584,88	33631,47	19,06	0,80	509,68	0,11	3,61
1.sSMPABC050.TXT	192	57	3,37	elongated	rounded	oscillatory	1	0,01	48450,97	414976,77	558,90	0,35	1531,61	0,07	2,67
1.sSMPABC051.TXT	134	70	1,91	elongated	rounded	irregular	1	0,04	5853,05	84508,68	112,22	0,41	471,15	0,07	2,72
1.sSMPABC052.TXT	110	83	1,33	oval	rounded	irregular	1	0,02	13083,91	167915,93	151,64	0,20	929,12	0,08	2,09
1.sSMPABC053.TXT	104	74	1,41	oval	rounded	oscillatory, sector	1	0,11	3246,77	20210,59	8,27	0,18	133,69	0,16	3,97
1.sSMPABC054.TXT	129	84	1,54	oval	sa-sr	oscillatory, sector	1	0,01	12797,30	134280,74	84,03	0,58	1257,02	0,10	2,64
1.sSMPABC055.TXT	99	76	1,30	oval	rounded	irregular	1	0,06	1275,42	18690,08	30,82	0,67	297,99	0,07	5,97
1.sSMPABC056.TXT	144	68	2,12	elongated	sa-sr	oscillatory	1	0,03	11144,98	80358,54	34,33	0,51	517,66	0,15	2,13
1.sSMPABC057.TXT	113	67	1,69	oval	rounded	irregular	1	0,03	6109,87	86123,78	93,08	0,41	509,32	0,07	2,65
1.sSMPABC058.TXT	126	74	1,70	oval	rounded	oscillatory	2	0,02	4838,90	76814,97	137,49	1,18	731,26	0,06	3,24
1.sSMPABC059.TXT	132	54	2,44	elongated	euhedral	oscillatory	1	0,05	4177,99	63592,68	129,45	1,18	392,20	0,07	3,12
1.sSMPABC060.TXT	153	54	2,83	elongated	rounded	oscillatory	2	0,01	76968,99	614333,05	463,76	0,15	1598,03	0,09	1,85
1.sSMPABC065.TXT	174	65	2,68	elongated	sa-sr	oscillatory	1	0,05	2983,29	52943,89	94,73	0,90	340,67	0,06	4,28
1.sSMPABC066.TXT	134	72	1,86	elongated	rounded	oscillatory, sector	1	0,09	2638,86	40507,45	80,18	2,60	191,48	0,07	5,19
1.sSMPABC067.TXT	153	62	2,47	elongated	rounded	homogeneous	2	0,00	51633,41	322964,33	176,89	0,31	3811,64	0,12	2,37
1.sSMPABC069.TXT	139	75	1,85	elongated	sa-sr	oscillatory	1	0,03	8618,07	127626,25	157,67	0,36	547,13	0,07	2,25
1.sSMPABC070.TXT	158	50	3,16	elongated	rounded	irregular	1	0,04	8660,10	127793,79	274,56	0,12	434,79	0,06	2,61
1.sSMPABC072.TXT	128	65	1,97	elongated	sa-sr	oscillatory	1	0,04	4655,27	75416,06	148,29	1,13	444,75	0,06	3,09
1.sSMPABC073.TXT	117	57	2,05	elongated	rounded	oscillatory	2	0,00	62906,34	481040,29	246,37	0,23	3184,83	0,13	1,31
1.sSMPABC074.TXT	137	58	2,36	elongated	sa-sr	irregular	1	0,02	6166,64	84109,58	94,87	0,28	686,58	0,07	2,62
1.sSMPABC075.TXT	158	64	2,47	elongated	rounded	oscillatory	2	0,04	5896,15	94967,18	160,18	0,90	441,12	0,06	2,85
1.sSMPABC076.TXT	124	69	1,80	oval	rounded	oscillatory, sector	2	0,02	21266,60	185320,48	111,13	0,45	886,67	0,12	1,71
1.sSMPABC077.TXT	142	63	2,25	elongated	rounded	irregular	2	0,06	4948,82	65286,01	66,97	0,54	268,36	0,08	12,13
1.sSMPABC078.TXT	146	57	2,56	elongated	rounded	irregular	2	0,02	17253,07	134808,34	62,63	0,30	767,45	0,13	1,77
1.sSMPABC079.TXT	140	52	2,69	elongated	rounded	oscillatory, sector	1	0,03	8848,61	133443,25	188,94	0,41	595,68	0,07	2,16
1.sSMPABC080.TXT	127	68	1,87	elongated	rounded	oscillatory	1	0,01	40403,77	320536,58	175,87	0,30	1287,35	0,13	1,61
1.sSMPABC085.TXT	116	63	1,84	elongated	sa-sr	oscillatory	1	0,05	7790,10	121980,59	326,69	0,84	340,69	0,06	2,37
1.sSMPABC086.TXT	171	76	2,25	elongated	rounded	irregular	2	0,01	47391,19	382866,26	396,20	0,30	1796,60	0,08	2,73
1.sSMPABC087.TXT	116	52	2,23	elongated	rounded	irregular	2	0,01	44367,37	365756,29	189,69	0,81	1950,00	0,12	1,39
1.sSMPABC088.TXT	140	57	2,46	elongated	rounded	oscillatory, sector	1	0,02	2109,87	29434,02	28,59	0,88	1021,99	0,07	5,16
1.sSMPABC089.TXT	143	60	2,38	elongated	rounded	irregular	2	0,04	10578,14	155985,74	390,50	0,42	439,23	0,06	2,43
1.sSMPABC090.TXT	187	60	3,12	elongated	rounded	oscillatory	1	0,02	8924,13	68168,81	31,42	0,61	740,75	0,13	2,62
1.sSMPABC091.TXT	143	48	2,98	elongated	sa-sr	oscillatory	1	0,02	32299,65	266353,74	377,40	0,24	841,31	0,07	2,92
1.sSMPABC093.TXT	117	56	2,09	elongated	rounded	oscillatory	2	0,01	28348,84	241805,78	126,18	0,61	1451,81	0,12	1,83
1.sSMPABC094.TXT	113	56	2,02	elongated	rounded	oscillatory	2	0,02	15468,37	153370,18	201,41	0,11	977,40	0,07	3,26
1.sSMPABC096.TXT	129	68	1,90	elongated	sa-sr	oscillatory	1	0,01	20797,58	188735,62	107,44	0,48	1282,77	0,11	1,74
1.sSMPABC097.TXT	116	70	1,66	oval	rounded	oscillatory	1	0,02	4183,91	71715,23	120,30	0,73	1023,71	0,06	3,31
1.sSMPABC098.TXT	172	60	2,87	elongated	rounded	oscillatory	3	0,01	29430,59	326963,32	449,94	0,09	2157,39	0,07	2,91
1.sSMPABC099.TXT	148	64	2,31	elongated	sa-sr	irregular	1	0,08	3096,14	27773,64	25,89	0,72	203,37	0,08	8,30
1.sSMPABC100.TXT	121	54	2,24	elongated	sa-sr	irregular	1	0,02	15315,71	234680,31	583,29	0,28	1016,02	0,06	2,92
1.sSMPABC106.TXT	107	61	1,75	oval	sa-sr	oscillatory	1	0,02	2837,16	47725,82	87,12	2,03	781,82	0,06	4,43
1.sSMPABC107.TXT	117	65	1,80	oval	sa-sr	oscillatory	1	0,03	6299,52	79480,95	115,90	0,51	527,22	0,06	3,78
1.sSMPABC108.TXT	116	67	1,73	oval	rounded	irregular	2	0,01	18842,91	140756,33	67,01	0,36	2592,79	0,13	1,88
1.sSMPABC109.TXT	135	59	2,29	elongated	rounded	oscillatory	1	0,01	48950,16	401243,90	454,35	0,21	1358,48	0,07	2,48
1.sSMPABC110.TXT								0,00	266787,93	1226551,71	432,40	0,12	5595,52	0,22	1,34
1.sSMPABC111.TXT	123	83	1,48	oval	rounded	oscillatory	1	0,03	6465,10	105876,12	191,69	0,68	552,99	0,06	2,75
1.sSMPABC112.TXT	122	59	2,07	elongated	sa-sr	irregular	1	0,04	5023,73	78915,69	142,95	0,78	499,10	0,06	3,11
1.sSMPABC113.TXT	133	54	2,46	elongated	rounded	homogeneous	2	0,04	5598,87	79440,97	107,49	0,42	461,27	0,07	2,97
1.sSMPABC114.TXT	100	66	1,52	oval	rounded	homogeneous	1	0,05	6695,70	50095,61	21,88	0,82	272,58	0,15	2,62
1.sSMPABC115.TXT	164	60	2,73	elongated	sa-sr	irregular	1	0,02	16653,73	127813,13	61,71	0,62	957,80	0,13	1,84
1.sSMPABC116.TXT	119	41	2,90	elongated	rounded	oscillatory	1	0,08	76888,27	458947,62	878,59	0,23	211,53	0,06	4,01
1.sSMPABC117.TXT	129	45	2,87	elongated	sa-sr	irregular	1	0,02	12487,09	181955,73	347,25	0,42	1051,46	0,07	2,06
1.sSMPABC119.TXT	94	64	1,47	oval	sa-sr	homogeneous	1	0,01	53572,40	473212,94	488,71	0,23	1506,65	0,08	2,02
1.sSMPABC120.TXT	114	75	1,52	oval	sa-sr	irregular	1	0,02	21465,37	299885,34	557,42	0,56	1123,60	0,06	1,98
1.sSMPABC125.TXT	197	72	2,74	elongated	rounded	irregular	1	0,06	4233,43	59803,13	161,16	0,41	322,66	0,06	9,81
1.sSMPABC126.TXT	156	61	2,56	elongated	rounded	irregular	1	0,01	3927,67	66938,56	144,29	0,67	1255,41	0,06	3,90
1.sSMPABC127.TXT	178	67	2,66	elongated	rounded	oscillatory	1	0,04	4029,82	65021,93	179,36	0,55	450,61	0,06	3,87
1.sSMPABC128.TXT	82	67	1,22	round	rounded	oscillatory	1	0,01	14326,01	106222,53	63,88	0,47	1384,19	0,13	2,05
1.sSMPABC129.TXT	154	93	1,66	oval	rounded	oscillatory	1	0,03	20986,26	152507,70	111,47	0,27	528,20	0,11	2,88
1.sSMPABC130.TXT	112	58	1,93	elongated	rounded	irregular	1	0,02	17582,08	130933,07	74,57	0,38	932,04	0,14	1,82
1.sSMPABC131.TXT	101	55	1,84	elongated	rounded	oscillatory	2	0,03	11701,45	167410,89	525,28	0,48	516,19	0,05	2,59
1.sSMPABC132.TXT	133	55	2,42	elongated	rounded	oscillatory	1	0,02	24086,39	190926,69	307,91	0,25	783,66	0,07	5,15
1.sSMPABC105.TXT	166	52	3,19	elongated	rounded	sector	1	0,02	47928,98	410520,26	1022,97	0,14	783,71	0,06	4,75
1.sSMPABC034.TXT	203	63	3,22	elongated	rounded	oscillatory	1	0,02	38938,38	303439,88	382,90	0,36	1073,13	0,07	2,87
1.sSMPABC032.TXT	158	56	2,82	elongated	sa-sr	oscillatory	1	0,02	15043,82	237888,98	795,04	0,25	1188,45	0,05	2,12
1.sSMPABC118.TXT	131	60	2,18	elongated	rounded	irregular	1	0,03	30896,37	307764,60	1537,24	0,07	577,22	0,05	3,29
1.sSMPABC071.TXT	135	61	2,21	elongated	rounded	oscillatory	2	0,02	12924,00	170602,79	249,54	0,20	724,35	0,08	2,12
1.sSMPABC095.TXT	116	52	2,23	elongated	rounded	oscillatory	1	0,03	13451,70	202059,62	686,73	0,24	602,95	0,05	2,42
1.sSMPABC092.TXT	123	66	1,86	elongated	sa-sr	irregular	2	0,03	8829,74	106463,78	131,45	0,30	622,86	0,08	2,61
1.sSMPABC036.TXT	159	57	2,79	elongated	rounded	oscillatory	2	0,01	45778,85	350615,62	205,82	0,41	1495,69	0,13	1,25
1.sSMPABC068.TXT	126	64	1,97	elongated	rounded	oscillatory	1	0,01	79550,70	432013,43	195,28	0,29	2448,67	0,19	1,17
1.sSMPABC013.TXT	134	50	2,68	elongated	rounded	irregular	2	0,02	28144,83	217120,93	99,22	0,29	730,79	0,14	1,43

Ratios [b]						Dates [c]						Ratios [c]							Dates [d]								
$^{207}Pb/^{235}U$	2s (%)	$^{206}Pb/^{238}U$	2s (%)	Rho	$^{207}Pb/^{206}Pb$	2s abs	$^{206}Pb/^{238}U$	2s abs	$^{207}Pb/^{235}U$	2s abs	$^{207}Pb/^{206}Pb$	2s (%)	$^{207}Pb/^{235}U$	2s (%)	$^{206}Pb/^{238}U$	2s (%)	Rho	$^{207}Pb/^{206}Pb$	2s abs	$^{206}Pb/^{238}U$	2s abs	$^{207}Pb/^{235}U$	2s abs	% conc [e]	% conc [f]	% Error
0,88	3,39	0,10	1,30	0,38	637	14,65	640	6,60	638	13,07	0,06	3,41	0,87	3,65	0,10	1,30	0,36	613	73,68	639	7,92	633	17,34	101	104	1
8,45	2,49	0,43	1,95	0,78	2275	44,49	2286	31,38	2278	31,54	0,14	1,59	8,43	2,52	0,43	1,95	0,78	2273	27,37	2285	37,67	2278	23,10	100	101	1
0,94	4,14	0,11	1,17	0,28	667	15,76	672	6,22	670	14,48	0,06	4,17	0,93	4,33	0,11	1,17	0,27	654	89,42	672	7,46	667	21,40	101	103	1
0,73	3,52	0,08	2,96	0,84	740	20,23	514	12,22	557	30,69	0,06	1,94	0,73	3,54	0,08	2,96	0,84	735	40,97	514	14,66	557	15,28	92	70	3
2,05	3,68	0,19	1,50	0,41	1141	33,85	1128	12,90	1131	22,31	0,08	3,49	2,04	3,80	0,19	1,50	0,39	1133	69,57	1127	15,48	1129	26,23	100	99	1
2,11	3,21	0,19	1,32	0,41	1244	28,99	1105	11,16	1152	18,57	0,08	3,09	2,10	3,36	0,19	1,32	0,39	1234	60,62	1104	13,39	1149	23,37	96	89	1
7,06	1,72	0,39	1,10	0,64	2129	11,62	2110	16,49	2118	13,41	0,13	1,34	7,06	1,73	0,39	1,10	0,63	2128	23,41	2110	19,80	2118	15,51	100	99	1
1,77	3,83	0,17	1,72	0,45	1125	34,49	990	13,17	1032	24,69	0,08	3,54	1,76	3,93	0,17	1,72	0,44	1119	70,53	990	15,80	1030	25,77	96	88	2
2,86	2,81	0,24	1,74	0,62	1385	30,24	1363	17,85	1370	24,41	0,09	2,24	2,85	2,84	0,24	1,74	0,61	1382	43,07	1363	21,42	1370	21,57	99	99	3
9,28	2,38	0,45	1,52	0,64	2347	34,47	2388	25,34	2364	23,37	0,15	1,86	9,26	2,40	0,45	1,52	0,63	2345	31,86	2388	30,42	2364	22,28	101	102	1
1,52	3,32	0,16	2,48	0,75	939	37,94	937	18,03	936	33,38	0,07	2,26	1,51	3,36	0,16	2,48	0,74	932	46,45	936	21,64	935	20,72	100	100	2
1,76	3,41	0,17	1,87	0,55	1056	29,24	1020	14,72	1030	25,27	0,07	2,93	1,75	3,48	0,17	1,87	0,54	1050	59,13	1020	17,66	1029	22,76	99	97	2
1,24	2,44	0,13	1,63	0,67	910	18,73	785	10,07	818	15,60	0,07	1,84	1,24	2,46	0,13	1,63	0,66	906	37,88	785	12,09	817	13,90	96	87	2
1,05	5,40	0,12	4,41	0,82	806	32,86	705	24,62	729	81,67	0,07	3,24	1,05	5,48	0,12	4,41	0,81	796	67,95	705	29,54	727	28,83	97	89	4
1,78	3,12	0,16	1,64	0,52	1231	26,33	948	12,04	1037	20,94	0,08	2,75	1,77	3,20	0,16	1,64	0,51	1224	53,99	948	14,45	1035	20,98	92	77	2
7,61	1,71	0,40	1,15	0,67	2220	10,99	2150	17,47	2184	13,92	0,14	1,27	7,60	1,71	0,40	1,15	0,67	2220	21,99	2150	20,97	2185	15,46	98	97	1
0,88	2,88	0,10	1,56	0,54	720	25,87	621	7,70	642	13,89	0,06	2,50	0,88	2,95	0,10	1,56	0,53	712	53,11	621	9,24	640	14,09	97	87	1
6,65	2,20	0,38	1,37	0,62	2063	27,86	2069	20,17	2064	19,22	0,13	1,75	6,64	2,22	0,38	1,37	0,62	2061	30,82	2069	24,21	2064	19,76	100	100	1
5,03	2,19	0,34	1,20	0,55	1742	16,91	1896	16,49	1822	16,40	0,11	1,86	5,02	2,22	0,34	1,20	0,54	1740	34,11	1896	19,80	1822	18,94	104	109	2
1,12	3,16	0,12	2,06	0,65	870	25,08	726	11,79	761	22,46	0,07	2,46	1,11	3,21	0,12	2,06	0,64	864	51,11	726	14,15	760	17,33	95	84	2
2,28	11,43	0,19	3,50	0,31	1337	108,96	1135	30,41	1206	103,39	0,09	11,52	2,27	12,04	0,19	3,50	0,29	1327	223,02	1134	36,49	1202	88,58	94	85	3
1,23	5,43	0,13	2,19	0,40	828	36,02	812	13,96	815	33,20	0,07	5,22	1,23	5,66	0,13	2,19	0,39	816	109,03	811	16,75	812	32,15	100	99	2
0,91	2,32	0,10	1,28	0,55	873	20,19	599	6,10	659	10,25	0,07	1,98	0,91	2,36	0,10	1,28	0,54	867	41,08	598	7,31	658	11,48	91	69	1
6,44	1,65	0,36	0,96	0,58	2101	11,88	1976	13,58	2036	11,56	0,13	1,36	6,43	1,66	0,36	0,96	0,58	2100	23,88	1976	16,30	2037	14,72	97	94	1
2,85	4,66	0,23	4,08	0,88	1407	108,43	1345	41,44	1368	100,20	0,09	2,29	2,85	4,68	0,23	4,08	0,87	1404	43,81	1345	49,76	1368	35,79	98	96	3
0,94	5,03	0,10	1,81	0,36	771	50,21	643	9,22	671	22,93	0,06	5,25	0,92	5,55	0,10	1,81	0,33	743	111,06	642	11,06	665	27,46	97	86	2
5,77	1,86	0,36	1,28	0,69	1911	12,18	1971	18,08	1940	15,73	0,12	1,37	5,76	1,87	0,36	1,28	0,68	1910	24,53	1971	21,70	1941	16,30	102	103	1
0,96	5,07	0,12	1,78	0,35	622	52,01	702	9,88	682	22,99	0,06	5,05	0,95	5,35	0,11	1,78	0,33	604	109,20	702	11,85	679	26,84	103	116	2
7,05	2,19	0,40	1,55	0,71	2086	13,68	2152	23,62	2116	21,87	0,13	1,57	7,04	2,20	0,40	1,55	0,70	2085	27,59	2151	28,35	2117	19,78	102	103	1
4,57	3,09	0,30	2,08	0,67	1807	43,51	1694	25,81	1743	35,03	0,11	2,31	4,57	3,10	0,30	2,08	0,67	1805	41,99	1693	30,98	1744	26,20	97	94	2
0,92	4,89	0,11	3,75	0,77	697	60,05	655	19,50	664	56,79	0,06	3,25	0,92	4,96	0,11	3,75	0,76	688	69,41	655	23,40	662	24,44	99	95	4
1,05	8,50	0,12	1,89	0,22	785	89,58	709	10,59	727	35,01	0,06	8,91	1,04	9,11	0,12	1,89	0,21	767	187,63	708	12,71	722	48,18	98	92	2
5,01	4,05	0,33	1,84	0,45	1776	33,29	1861	24,88	1820	35,84	0,11	3,72	5,00	4,15	0,33	1,84	0,44	1772	67,93	1861	29,87	1819	35,75	102	105	4
1,27	3,53	0,13	2,30	0,65	885	32,43	814	14,69	832	28,91	0,07	2,70	1,27	3,55	0,13	2,30	0,65	882	55,84	814	17,63	832	20,36	98	92	2
1,39	3,15	0,14	1,59	0,50	947	28,10	860	10,66	884	18,50	0,07	2,82	1,38	3,24	0,14	1,59	0,49	938	57,90	860	12,79	882	19,27	98	92	1
2,30	2,53	0,21	1,42	0,56	1184	20,79	1228	13,24	1211	17,42	0,08	2,13	2,29	2,56	0,21	1,42	0,55	1181	42,07	1228	15,88	1211	18,25	101	104	1
10,47	4,65	0,46	2,42	0,52	2497	33,85	2454	41,23	2475	57,54	0,16	4,45	10,40	5,06	0,46	2,42	0,48	2487	74,93	2452	49,48	2471	47,99	99	99	3
4,06	3,33	0,30	2,02	0,61	1573	24,93	1705	25,32	1645	34,47	0,10	2,67	4,06	3,35	0,30	2,02	0,60	1570	50,08	1705	30,39	1645	27,69	104	109	3
1,10	6,33	0,11	2,11	0,33	919	62,60	701	11,68	755	32,82	0,07	6,34	1,10	6,68	0,11	2,11	0,32	904	130,70	701	14,01	751	36,10	93	77	2
9,56	2,64	0,45	1,56	0,59	2395	36,52	2392	26,03	2391	25,62	0,15	2,19	9,54	2,69	0,45	1,56	0,58	2392	37,29	2391	31,24	2391	25,02	100	100	2
1,75	3,02	0,18	1,45	0,48	999	27,18	1041	11,61	1026	18,12	0,07	2,74	1,74	3,10	0,18	1,45	0,47	991	55,81	1041	13,93	1024	20,22	102	105	1
0,94	5,62	0,11	4,58	0,82	753	34,61	648	23,60	671	82,93	0,06	3,32	0,93	5,66	0,11	4,58	0,81	746	70,23	648	28,33	670	28,16	97	87	4
0,86	3,41	0,09	1,39	0,41	841	32,77	573	6,37	630	13,72	0,07	3,26	0,85	3,55	0,09	1,39	0,39	829	68,07	573	7,64	627	16,74	91	69	1
3,09	2,29	0,24	1,34	0,59	1479	21,95	1400	14,09	1430	16,84	0,09	1,87	3,09	2,30	0,24	1,34	0,58	1477	35,53	1399	16,90	1430	17,83	98	95	2
0,84	4,57	0,11	1,60	0,35	510	47,71	647	8,24	617	18,32	0,06	4,51	0,83	4,79	0,11	1,60	0,34	494	99,44	647	9,89	614	22,30	105	131	2
0,87	5,44	0,10	1,64	0,30	820	55,14	588	7,67	637	21,32	0,07	5,72	0,86	5,95	0,10	1,64	0,28	796	119,92	587	9,20	632	28,39	93	74	2
5,42	4,67	0,33	4,02	0,86	1943	124,69	1840	53,88	1887	112,44	0,12	2,38	5,42	4,67	0,33	4,02	0,86	1943	42,54	1839	64,71	1888	40,88	97	95	2
1,45	2,69	0,15	1,47	0,55	892	23,42	917	10,47	909	15,87	0,07	2,32	1,44	2,75	0,15	1,47	0,53	884	48,06	917	12,56	907	16,63	101	104	1
0,71	3,12	0,09	1,72	0,55	581	16,13	539	7,43	546	14,32	0,06	2,72	0,71	3,22	0,09	1,72	0,54	569	59,15	539	8,91	544	13,65	99	95	2
0,83	3,44	0,10	1,50	0,44	700	33,24	591	7,08	613	14,44	0,06	3,22	0,83	3,55	0,10	1,50	0,42	689	68,65	591	8,49	611	16,44	97	86	1
6,75	1,75	0,37	1,16	0,66	2136	11,52	2022	16,82	2077	14,17	0,13	1,32	6,74	1,76	0,37	1,16	0,66	2136	23,06	2022	20,18	2078	15,65	97	95	1
1,72	3,04	0,17	1,55	0,51	1053	26,60	997	11,91	1014	19,20	0,07	2,68	1,71	3,10	0,17	1,55	0,50	1048	54,13	997	14,29	1012	20,05	98	95	1
0,97	3,98	0,11	2,77	0,70	708	30,64	683	15,01	688	34,43	0,06	2,97	0,97	4,07	0,11	2,77	0,68	697	63,33	683	18,01	686	20,48	100	98	3
5,04	2,08	0,31	1,18	0,57	1901	15,46	1763	15,16	1825	15,52	0,12	1,74	5,03	2,10	0,31	1,18	0,56	1898	31,31	1762	18,19	1825	17,97	97	93	2
1,95	12,25	0,18	1,73	0,14	1115	126,01	1088	14,43	1096	56,04	0,08	12,94	1,93	13,06	0,18	1,73	0,13	1102	258,83	1087	17,31	1092	91,32	100	99	2
7,25	2,19	0,41	1,29	0,59	2092	15,62	2196	20,02	2140	18,34	0,13	1,80	7,23	2,22	0,41	1,29	0,58	2089	31,70	2195	24,03	2140	19,97	103	105	2
1,23	2,44	0,13	1,14	0,46	839	22,69	806	7,17	814	11,13	0,07	2,23	1,23	2,50	0,13	1,14	0,45	832	46,47	805	8,61	812	14,08	99	97	1
6,03	2,58	0,34	2,02	0,78	2062	14,23	1903	27,77	1978	32,09	0,13	1,62	6,02	2,59	0,34	2,02	0,78	2060	28,66	1903	33,34	1979	22,81	96	92	1
0,62	2,80	0,07	1,50	0,53	749	25,23	438	5,29	491	10,73	0,06	2,50	0,62	2,92	0,07	1,50	0,51	735	52,98	438	6,34	489	11,37	90	60	1
1,82	3,36	0,17	1,96	0,58	1090	31,02	1034	15,64	1051	26,79	0,08	2,76	1,81	3,38	0,17	1,96	0,58	1088	55,27	1034	18,77	1051	22,40	98	95	2
6,10	2,00	0,36	1,44	0,72	1982	12,42	1997	20,65	1988	18,79	0,12	1,40	6,09	2,01	0,36	1,44	0,72	1981	24,93	1997	24,79	1989	17,68	100	101	1
1,92	5,52	0,19	1,95	0,35	983	53,45	1142	17,07	1088	35,52	0,07	5,25	1,92	5,60	0,19	1,95	0,35	979	106,91	1142	20,48	1087	38,07	105	117	2
0,58	3,87	0,07	3,02	0,78	473	30,59	463	11,24	464	28,46	0,06	2,53	0,58	3,94	0,07	3,02	0,77	460	56,12	463	13,48	462	14,73	100	101	3
7,38	3,18	0,41	1,81	0,57	2112	23,16	2208	28,19	2157	32,44	0,13	2,67	7,37	3,23	0,41	1,81	0,56	2110	46,89	2208	33,84	2157	29,26	102	105	2
1,15	3,34	0,13	1,63	0,49	807	20,59	767	9,83	776	18,09	0,07	2,98	1,15	3,40	0,13	1,63	0,48	802	62,48	767	11,79	775	18,60	99	96	2
5,82	2,36	0,36	1,48	0,63	1912	16,55	1986	21,16	1948	21,39	0,12	1,85	5,82	2,37	0,36	1,48	0,62	1911	33,26	1986	25,40	1949	20,78	102	104	2
1,30	3,81	0,14	1,98	0,52	862	28,40	840	13,00	845	25,25	0,07	3,32	1,30	3,86	0,14	1,98	0,51	857	68,85	840	15,60	844	22,38	99	98	2
5,01	2,18	0,33	1,31	0,60	1797	15,89	1842	17,52	1819	17,57	0,11	1,76	5,00	2,19	0,33	1,31	0,60	1795	32,01	1842	21,02	1820	18,72	101	103	2
0,90	3,60	0,11	1,40	0,39	534	36,65	686	7,61	651	14,63	0,06	3,37	0,90	3,65	0,11	1,40	0,38	529	73,81	686	9,14	650	17,67	105	130	1
1,23	3,98	0,13	2,72	0,68	819	41,35	811	17,30	812	37,56	0,07	2,93	1,23	4,00	0,13	2,72	0,68	817	61,26	811	20,76	812	22,61	100	99	3
2,14	8,55	0,20	2,07	0,24	1179	53,62	1154	18,21	1162	50,43	0,08	9,05	2,12	9,28	0,20	2,07	0,22	1162	179,36	1154	21,85	1156	66,16	100	99	2
0,68	4,32	0,08	3,19	0,74	772	31,04	471	12,08	525	35,56	0,06	2,97	0,68	4,36	0,08	3,19	0,73	767	62,63	471	14,50	525	18,02	90	61	3
0,84	4,70	0,10	1,56	0,33	571	48,90	634	7,88	620	18,31	0,06	4,53	0,84	4,79	0,10	1,56	0,33	564	98,67	634	9,45	618	22,44	102	112	1
1,14	4,07	0,13	1,52	0,37	773	21,22	775	9,26	774	19,09	0,06	3,91	1,14	4,19	0,13	1,52	0,36	764	82,30	775	11,11	772	22,91	100	101	1
7,28	2,33	0,40	1,37	0,59	2140	16,55	2152	20,92	2144	20,22	0,13	1,89	7,27	2,34	0,40	1,37	0,59	2140	33,11	2152	25,12	2145	21,08	100	101	2
1,58	3,39	0,16	2,31	0,68	985	35,55	952	17,06	961	31,19	0,07	2,51	1,58	3,41	0,16	2,31	0,68	982	51,16	952	20,47	961	21,42	99	97	2
16,00	2,07	0,54	1,58	0,76	2956	10,88	2765	29,59	2874	23,14	0,22	1,35	15,99	2,07	0,54	1,58	0,76	2956	21,73	2765	35,53	2876	20,01	96	94	1
0,88	3,06	0,10	1,34	0,44	635	29,87	640	6,82	638	12,53	0,06	2,84	0,87	3,14	0,10	1,34	0,43	626	61,24	639	8,19	636	14,97	101	102	1
0,91	3,54	0,10	1,68	0,48	726	33,37	640	8,53	658	17,19	0,06	3,23	0,91	3,64	0,10	1,68	0,46	716	68,56	639	10,24	656	17,75	97	89	2
1,36	3,26	0,14	1,34	0,41	940	30,74	843	8,85	869	16,11	0,07	3,09	1,35	3,37	0,14	1,34	0,40	931	63,34	843	10,62	867	19,82	97	90	1
8,93	3,07	0,44	1,61	0,52	2316	39,02	2347	26,41	2328	28,72	0,15	2,76	8,89	3,20	0,44	1,61	0,50	2311	47,44	2346	31,70	2327	29,61	101	102	2
7,05	2,43	0,39	1,59	0,66	2105	16,19	2131	24,15	2116	24,11	0,13	1,86	7,04	2,45	0,39	1,59	0,65	2104	32,73	2131	28,98	2116	22,04	101	101	2
0,74	4,81	0,09	2,65	0,55	614	32,45	553	11,72	564	30,26	0,06	4,38	0,73	5,12	0,09	2,65	0,52	589	94,96	552	14,05	559	22,26	99	94	3
0,94	2,82	0,10	1,93	0,68	899	21,38	610	9,37	674	17,98	0,07	2,09	0,94	2,85	0,10	1,93	0,68	895	43,21	610	11,24	674	14,12	90	68	2
1,86	2,87	0,18	2,04	0,71	1102	30,78	1051	16,49	1067	26,00	0,08	2,04	1,86	2,88	0,18	2,04	0,71	1100	40,80	1051	19,79	1067	19,21	99	96	2
0,85	3,22	0,10	2,54	0,79	650	28,81	620	12,55	626	25,94	0,06	2,01	0,85	3,24	0,10	2,54	0,78	646	43,15	620	15,06	626	15,25	99	96	2
0,55	10,11	0,07	2,47	0,24	501	34,49	434	8,63	444	33,39	0,06	10,39	0,54	10,67	0,07	2,47	0,23	484	229,35	434	10,36	442	38,96	98	90	2
0,74	4,46	0,09	2,16	0,48	628	42,64	545	9,44	561	22,67	0,06	3,96	0,74	4,51	0,09	2,16	0,48	623	85,42	545	11,32	560	19,63	97	87	2
0,54	4,33	0,07	1,94	0,45	511	17,72	428	6,70	441	16,41	0,06	4,03	0,54	4,47	0,07	1,94	0,43	498	88,76	428	8,04	439	16,06	97	86	2
7,23	2,42	0,40	1,29	0,53	2115	18,11	2166	19,78	2138	19,61	0,13	2,08	7,22	2,44	0,40	1,29	0,53	2114	36,40	2166	23,75	2139	22,03	101	102	2
4,70	4,22	0,32	3,08	0,73	1743	80,32	1787	40,20	1765	69,53	0,11	2,96	4,68	4,28	0,32	3,08	0,72	1738	54,33	1786	48,26	1764	36,42	101	103	3
7,93	2,45	0,42	1,64	0,67	2175	36,50	2276	26,27	2221	25,34	0,14	1,85	7,92	2,47	0,42	1,64	0,66	2173	32,19	2276	31,54	2222	22,52	102	105	1
0,57	3,60	0,08	2,50	0,69	407	23,00	469	9,43	459	20,97	0,05	2,68	0,57	3,66	0,08	2,50	0,68	396	60,08	469	11,31	457	13,57	103	119	2
1,29	7,60	0,14	5,59	0,74	822	153,79	850	37,19	841	149,23	0,07	5,27	1,29	7,68	0,14	5,59	0,73	817	110,15	850	44,64	840	44,88	101	104	5
0,55	11,43	0,07	10,40	0,91	458	330,22	446	37,47	448	328,08	0,06	4,86	0,55	11,48	0,07	10,40	0,91	450	107,99	446	44,98	447	42,35	100	99	10
1,36	7,33	0,14	6,74	0,92	913	219,19	858	45,31	873	214,45	0,07	2,92	1,36	7,35	0,14	6,74	0,92	909	60,10	858	54,40	872	43,94	98	94	6
0,42	4,10	0,06	3,51	0,86	366	30,91	353	10,07	354	29,23	0,05	2,15	0,42	4,12	0,06	3,51	0,85	360	48,47	353	12,08	354	12,38	100	98	3
0,26	4,67	0,04	3,32	0,71	257	20,48	230	6,26	232	19,50	0,05	3,40	0,26	4,75	0,04	3,32	0,70	245	78,26	230	7,51	231	9,87	99	94	3
1,37	3,36	0,13	2,60	0,78	1123	21,27	782	15,99	876	34,35	0,08	2,17	1,37	3,39	0,13	2,60	0,77	1118	43,33	782	19,19	875	20,07	89	70	2
0,40	3,17	0,05	2,05	0,65	343	13,42	344	5,73	343	12,13	0,05	2,49	0,40	3,23	0,05	2,05	0,64	332	56,56	344	6,88	342	9,43	100	103	2
1,74	2,95	0,15	1,38	0,47	1267	25,71	915	9,80	1024	17,05	0,08	2,69	1,74	3,02	0,15	1,38	0,46	1262	52,48	915	11,76	1022	19,64	89	72	1
5,87	1,70	0,32	1,14	0,67	2121	11,03	1806	14,99	1956	13,35	0,13	1,27	5,87	1,70	0,32	1,14	0,67	2120	22,21	1806	17,99	1956	14,90	92	85	1
10,81	1,76	0,42	1,32	0,75	2721	9,65	2251	20,92	2505	16,78	0,19	1,17	10,80	1,77	0,42	1,32	0,75	2721	19,35	2251	25,12	2506	16,55	90	83	1
7,96	1,96	0,42	1,34	0,68	743	27,62	2240	21,12	2224	17,81	0,14	1,46	7,94	1,98	0,42	1,34	0,67	#¡NUM!	25,38	2239	25,34	2225	18,04	101	#¡NUM!	#¡NUM!

BPN-07A (Mb. Tibagi)

SPOT	Grain Length	Grain Width	Length / width	Shape*	Roundness**	Zoning***	# of growth phases	f206c	^{207}Pb	^{206}Pb	U (µg g^{-1}) [a]	Th/U	$^{206}Pb/^{204}Pb$	$^{207}Pb/^{206}Pb$	2s (%)
1.sSMPABC245.TXT	135	68	1,99	elongated	rounded	irregular	2	0,03	63512,22	420531,83	133,91	0,40	467,19	0,12	0,45
1.sSMPABC246.TXT	130	57	2,28	elongated	rounded	oscillatory, sector	1	0,01	24235,18	328856,50	208,39	0,46	1152,85	0,07	0,45
1.sSMPABC247.TXT	153	72	2,13	elongated	rounded	oscillatory, sector	1	0,01	31402,72	243071,22	47,62	0,94	1325,36	0,22	0,23
1.sSMPABC248.TXT	127	56	2,27	elongated	rounded	oscillatory	2	0,04	46462,57	516819,86	450,78	0,28	415,13	0,07	1,52
1.sSMPABC249.TXT	111	67	1,66	oval	rounded	oscillatory	1	0,01	23905,82	285605,76	131,69	0,88	1142,25	0,08	0,43
1.sSMPABC250.TXT	127	52	2,44	elongated	rounded	oscillatory	1	0,01	39484,96	451585,89	205,21	0,30	1828,38	0,09	0,45
1.sSMPABC251.TXT	117	65	1,80	oval	sa-sr	oscillatory	2	0,01	44869,39	327307,46	132,59	0,57	1161,44	0,10	0,61
1.sSMPABC252.TXT	128	60	2,13	elongated	rounded	oscillatory	1	0,01	98566,25	826988,74	270,38	0,33	1593,25	0,12	0,33
1.sSMPABC253.TXT	146	58	2,52	elongated	rounded	irregular	1	0,01	37785,74	357497,10	124,91	0,47	2643,05	0,11	0,43
1.sSMPABC254.TXT	154	52	2,96	elongated	rounded	oscillatory	1	0,05	38996,01	467963,03	591,12	0,47	368,05	0,06	0,73
1.sSMPABC255.TXT	141	75	1,88	elongated	rounded	irregular	2	0,01	54151,64	453410,92	146,98	0,25	2178,66	0,12	0,40
1.sSMPABC256.TXT	111	76	1,46	oval	rounded	irregular	1	0,02	12639,65	207185,78	198,49	0,93	1118,87	0,06	0,52
1.sSMPABC257.TXT	178	61	2,92	elongated	sa-sr	oscillatory	2	0,01	81957,96	822718,29	361,52	0,72	1713,64	0,10	0,38
1.sSMPABC258.TXT	99	55	1,80	oval	rounded	irregular	1	0,01	37071,14	290922,79	92,31	0,15	1233,86	0,13	0,44
1.sSMPABC259.TXT	121	47	2,57	elongated	rounded	oscillatory	1	0,07	50340,43	472936,50	623,69	0,15	273,85	0,06	2,11
1.sSMPABC265.TXT	113	73	1,55	oval	rounded	oscillatory	2	0,02	16254,26	248671,04	213,10	0,12	1075,58	0,07	0,44
1.sSMPABC266.TXT	130	71	1,83	elongated	rounded	irregular	2	0,02	75310,19	562895,54	164,33	0,19	856,52	0,13	0,39
1.sSMPABC267.TXT	106	76	1,39	oval	rounded	oscillatory	1	0,02	39262,62	540653,05	564,03	0,23	854,65	0,06	0,80
1.sSMPABC269.TXT	99	63	1,57	oval	sa-sr	irregular	1	0,02	26603,47	193919,06	45,09	0,61	669,23	0,18	0,32
1.sSMPABC271.TXT	143	65	2,20	elongated	rounded	irregular	2	0,00	161913,50	968767,39	217,48	0,37	2840,49	0,18	0,32
1.sSMPABC272.TXT	120	77	1,56	oval	sa-sr	oscillatory	1	0,01	34709,35	333456,69	127,66	0,29	1764,37	0,10	0,38
1.sSMPABC273.TXT	126	77	1,64	oval	sa-sr	irregular	1	0,04	115606,16	800718,60	475,43	0,96	381,67	0,08	0,62
1.sSMPABC274.TXT	106	70	1,51	oval	sa-sr	irregular	2	0,01	36140,43	283589,02	83,61	0,46	2283,94	0,13	0,39
1.sSMPABC275.TXT	130	68	1,91	elongated	sa-sr	homogeneous	1	0,03	6996,94	71540,51	27,53	0,64	525,40	0,10	0,62
1.sSMPABC276.TXT	109	80	1,36	oval	rounded	irregular	2	0,01	39067,22	458013,52	223,66	0,54	1188,74	0,09	0,41
1.sSMPABC277.TXT	120	78	1,54	oval	sa-sr	oscillatory, sector	2	0,01	59035,35	467608,59	133,81	0,41	2233,77	0,14	0,36
1.sSMPABC278.TXT	132	73	1,81	elongated	rounded	sector	2	0,00	22889,16	167727,14	45,37	0,43	4050,31	0,15	0,42
1.sSMPABC279.TXT	100	64	1,56	oval	rounded	irregular	1	-0,01	3687,73	41182,14	19,29	0,27	-1706,92	0,09	0,85
1.sSMPABC280.TXT	133	71	1,87	elongated	rounded	homogeneous	1	0,02	10038,19	113030,98	51,60	0,34	745,28	0,09	0,56
1.sSMPABC285.TXT	124	58	2,14	elongated	sa-sr	oscillatory	1	0,10	24716,61	201241,47	301,92	0,68	178,27	0,06	5,42
1.sSMPABC286.TXT	144	63	2,29	elongated	rounded	irregular	3	0,02	23227,29	255367,45	157,47	0,71	896,42	0,09	0,42
1.sSMPABC287.TXT	105	85	1,24	round	rounded	oscillatory, sector	1	0,01	36811,29	340561,85	118,65	0,44	2056,48	0,11	0,36
1.sSMPABC288.TXT	120	94	1,28	round	rounded	irregular	1	0,01	68673,86	440720,13	90,26	0,71	1131,72	0,21	0,27
1.sSMPABC289.TXT	120	76	1,58	oval	sa-sr	irregular	2	0,01	41049,75	243327,80	55,15	0,72	2357,94	0,18	0,39
1.sSMPABC290.TXT	133	60	2,22	elongated	rounded	oscillatory	2	0,04	174987,19	1235641,17	774,02	0,47	467,64	0,08	1,03
1.sSMPABC291.TXT	149	58	2,57	elongated	sa-sr	oscillatory	1	0,01	103956,88	824807,86	257,41	0,30	2319,03	0,13	0,34
1.sSMPABC292.TXT	129	51	2,53	elongated	rounded	homogeneous	1	0,02	14588,68	228897,31	237,25	0,42	739,99	0,06	0,45
1.sSMPABC293.TXT	120	51	2,35	elongated	sa-sr	homogeneous	2	0,00	708105,84	3173558,89	592,10	0,48	3209,67	0,24	1,67
1.sSMPABC294.TXT	130	76	1,71	oval	rounded	irregular	1	0,01	15804,87	141127,84	47,69	0,82	2330,07	0,11	0,45
1.sSMPABC295.TXT	121	82	1,48	oval	rounded	oscillatory	1	0,03	21966,77	161329,17	47,07	0,32	527,49	0,14	0,45
1.sSMPABC296.TXT	106	79	1,34	oval	rounded	homogeneous	1	0,07	121786,17	702521,22	362,26	0,39	240,74	0,09	1,13
1.sSMPABC297.TXT	107	95	1,13	round	sa-sr	irregular	1	0,01	33640,93	261401,67	75,12	0,19	1488,81	0,14	0,36
1.sSMPABC298.TXT	98	78	1,26	round	sa-sr	homogeneous	1	0,03	3030,31	43147,69	31,93	0,41	525,29	0,07	0,89
1.sSMPABC299.TXT	150	62	2,42	elongated	sa-sr	oscillatory	2	0,01	40901,66	313711,91	92,71	0,35	1021,39	0,13	0,39
1.sSMPABC300.TXT	125	78	1,60	oval	euhedral	oscillatory	1	0,06	21926,21	222143,84	279,41	0,61	315,82	0,06	1,51
1.sSMPABC305.TXT	114	49	2,33	elongated	euhedral	irregular	1	0,04	61747,92	425246,45	211,46	0,59	462,37	0,09	0,55
1.sSMPABC306.TXT	192	59	3,25	elongated	rounded	oscillatory, sector	1	0,04	81195,45	489173,40	219,28	0,70	430,55	0,09	0,63
1.sSMPABC307.TXT	139	63	2,21	elongated	rounded	oscillatory		0,01	82415,40	638564,59	182,21	0,31	2246,31	0,14	0,32
1.sSMPABC308.TXT	123	53	2,32	elongated	rounded	irregular	2	0,02	9111,37	137293,58	113,91	0,28	783,27	0,07	0,56
1.sSMPABC309.TXT	111	72	1,54	oval	rounded	oscillatory	1	0,02	16539,41	203101,71	104,72	0,50	957,96	0,08	0,43
1.sSMPABC310.TXT	126	47	2,68	elongated	rounded	homogeneous	2	0,02	31690,61	245503,40	119,97	0,89	840,46	0,09	0,63
1.sSMPABC311.TXT	105	49	2,14	elongated	rounded	oscillatory	1	0,06	10764,69	135485,32	119,73	2,24	306,70	0,07	0,62
1.sSMPABC312.TXT	125	90	1,39	oval	rounded	homogeneous	2	0,00	175041,84	766372,98	146,78	0,30	2531,48	0,23	0,35
1.sSMPABC313.TXT	179	70	2,56	elongated	sa-sr	irregular	1	0,01	35676,47	277017,70	79,74	0,28	1594,75	0,14	0,35
1.sSMPABC314.TXT	147	78	1,88	elongated	sa-sr	oscillatory	2	0,01	69376,58	540933,34	162,99	0,29	2465,99	0,13	0,32
1.sSMPABC315.TXT	178	60	2,97	elongated	rounded	oscillatory	2	0,03	18258,57	215407,67	179,02	0,30	520,77	0,07	0,96
1.sSMPABC316.TXT	134	58	2,31	elongated	sa-sr	oscillatory	2	0,01	59045,84	458190,77	131,92	0,35	1485,43	0,14	0,40
1.sSMPABC317.TXT	86	82	1,05	round	sa-sr	oscillatory	1	0,03	7852,95	126365,06	133,11	0,34	513,20	0,06	0,68
1.sSMPABC318.TXT	133	66	2,02	elongated	rounded	irregular	2	0,04	17116,63	228543,74	232,89	0,17	428,67	0,06	0,87
1.sSMPABC319.TXT	144	52	2,77	elongated	rounded	irregular	1	0,06	18310,02	211564,75	325,45	0,73	293,42	0,06	0,73
1.sSMPABC320.TXT	104	69	1,51	oval	rounded	irregular	1	0,03	74880,56	510804,40	184,40	0,28	488,24	0,11	0,55
1.sSMPABC325.TXT	120	67	1,79	oval	rounded	irregular	2	0,07	16669,64	203173,93	202,23	0,57	259,34	0,06	2,81
1.sSMPABC326.TXT	150	45	3,33	elongated	rounded	oscillatory	1	0,01	6610,53	107907,91	127,61	0,83	1346,78	0,06	0,77
1.sSMPABC327.TXT	125	58	2,16	elongated	rounded	irregular	1	0,07	10808,18	135314,12	172,54	1,04	261,79	0,06	1,94
1.sSMPABC328.TXT	160	60	2,67	elongated	euhedral	oscillatory	2	0,02	47119,06	541535,28	325,28	0,34	960,11	0,09	0,42
1.sSMPABC329.TXT	133	61	2,18	elongated	rounded	oscillatory	2	0,02	3751,70	58593,54	59,02	1,68	938,48	0,06	0,82
1.sSMPABC330.TXT	106	67	1,58	oval	sa-sr	oscillatory	2	0,02	53043,54	417166,68	303,51	0,18	701,07	0,07	1,09
1.sSMPABC331.TXT	125	71	1,76	oval	rounded	sector	2	0,03	11694,70	163196,72	175,08	0,98	523,98	0,07	1,07
1.sSMPABC332.TXT	115	80	1,44	oval	rounded	irregular	1	0,00	44656,14	428038,70	153,14	0,45	4645,46	0,11	0,38
1.sSMPABC333.TXT	97	75	1,29	round	rounded	oscillatory	1	0,01	35515,35	267008,62	78,24	0,14	1086,69	0,13	0,45
1.sSMPABC334.TXT	102	62	1,65	oval	sa-sr	homogeneous	2	0,05	20102,73	227098,61	285,59	0,44	381,55	0,06	1,07
1.sSMPABC335.TXT	116	50	2,32	elongated	sa-sr	oscillatory	2	0,04	44615,85	472598,42	480,01	0,44	480,37	0,06	0,66
1.sSMPABC336.TXT	131	65	2,02	elongated	rounded	oscillatory	2	0,03	88135,30	640768,01	334,58	0,22	578,07	0,08	0,67
1.sSMPABC337.TXT	100	78	1,28	round	sa-sr	irregular	1	0,01	14776,25	110894,80	31,13	0,20	1051,62	0,14	0,48
1.sSMPABC338.TXT								0,02	2491,21	39390,89	41,98	0,18	749,47	0,06	0,98
1.sSMPABC339.TXT	154	59	2,61	elongated	rounded	oscillatory	1	0,02	18161,17	257448,30	182,05	0,47	1027,86	0,07	0,47
1.sSMPABC340.TXT	122	60	2,03	elongated	rounded	oscillatory	2	0,02	34442,35	386366,27	289,45	0,24	1105,51	0,07	0,64
1.sSMPABC344.TXT								0,01	27014,59	205604,74	54,84	0,35	2743,46	0,13	0,42
1.sSMPABC345.TXT	149	76	1,96	elongated	rounded	oscillatory	1	0,02	27237,78	292831,15	163,98	0,41	1117,49	0,08	0,56
1.sSMPABC346.TXT	140	70	2,00	elongated	rounded	irregular	1	0,01	27587,90	209222,49	61,70	0,51	1140,98	0,13	0,47
1.sSMPABC347.TXT	140	63	2,22	elongated	rounded	irregular	1	0,00	116680,42	866044,55	219,99	0,33	3021,82	0,16	0,29
1.sSMPABC348.TXT	108	71	1,52	oval	rounded	oscillatory	2	0,02	33039,70	213583,20	51,46	0,23	701,65	0,15	0,44
1.sSMPABC349.TXT	151	55	2,75	elongated	sa-sr	oscillatory	1	0,02	36957,36	350307,13	117,93	0,81	1003,55	0,12	0,37
1.sSMPABC351.TXT	144	49	2,94	elongated	sa-sr	irregular	1	0,02	6490,88	84865,94	52,46	0,70	736,66	0,08	0,92
1.sSMPABC352.TXT	110	44	2,50	elongated	rounded	oscillatory	1	0,07	77168,99	436814,36	153,56	0,72	223,81	0,11	0,78
1.sSMPABC353.TXT	150	53	2,83	elongated	rounded	oscillatory	1	0,03	18763,73	247322,15	210,11	0,18	642,29	0,07	0,78
1.sSMPABC354.TXT	98	59	1,66	oval	sa-sr	oscillatory	3	0,02	117440,24	638201,07	169,82	0,22	952,83	0,15	0,43
1.sSMPABC355.TXT	142	66	2,15	elongated	sa-sr	irregular	2	0,01	10100,50	131625,65	81,09	2,60	1685,84	0,08	1,96
1.sSMPABC356.TXT	116	58	2,00	elongated	rounded	oscillatory	1	0,01	91581,18	667350,49	171,73	0,31	2215,54	0,15	0,34
1.sSMPABC359.TXT	132	53	2,49	elongated	euhedral	oscillatory	1	0,07	44732,50	403523,99	561,37	0,23	258,95	0,06	1,59
1.sSMPABC360.TXT	143	57	2,51	elongated	euhedral	oscillatory	1	0,01	31046,04	414570,38	303,01	0,10	1269,61	0,07	0,50
1.sSMPABC361.TXT								0,04	7070,97	104088,35	109,05	0,59	485,91	0,06	1,03
1.sSMPABC362.TXT								0,09	92960,22	643472,38	572,49	0,29	193,43	0,07	0,66
1.sSMPABC363.TXT								0,00	58942,66	456877,12	126,44	0,44	3013,94	0,14	0,32
1.sSMPABC364.TXT								0,01	11589,18	171424,96	136,18	0,23	1168,26	0,07	0,69
1.sSMPABC365.TXT	125	74	1,69	oval	rounded	irregular	2	0,00	83932,41	694088,79	206,74	0,57	3535,66	0,13	0,32
1.sSMPABC366.TXT	110	82	1,34	oval	rounded	homogeneous	2	0,02	58012,88	370801,30	78,26	0,36	718,56	0,20	0,25
1.sSMPABC367.TXT	103	87	1,18	round	rounded	irregular	2	0,00	59149,99	450174,23	97,56	0,38	2709,08	0,19	0,23
1.sSMPABC368.TXT	120	61	1,97	elongated	sa-sr	oscillatory	1	0,01	3885,18	59280,20	58,65	0,34	1591,91	0,06	0,96
1.sSMPABC369.TXT	125	64	1,95	elongated (broken)	sa-sr	oscillatory	2	0,04	87236,18	562244,90	187,48	0,53	376,65	0,12	0,48
1.sSMPABC370.TXT	86	78	1,10	round	rounded	irregular	1	0,01	72721,39	517987,15	136,73	0,34	2719,38	0,15	0,35
1.sSMPABC371.TXT	136	60	2,27	elongated	rounded	oscillatory	1	0,01	36276,35	363122,44	183,32	0,57	1217,62	0,09	0,49
1.sSMPABC372.TXT	108	64	1,69	oval	rounded	irregular	1	0,03	141846,84	1011206,14	595,59	0,39	518,09	0,08	0,65
1.sSMPABC373.TXT	137	52	2,63	elongated	sa-sr	homogeneous	1	0,10	88823,75	441861,36	187,60	1,67	168,27	0,10	0,90
1.sSMPABC374.TXT	112	51	2,20	elongated	sa-sr	oscillatory	2	0,04	90943,86	648769,40	280,46	0,27	429,12	0,09	0,73
1.sSMPABC375.TXT	160	57	2,81	elongated	sa-sr	oscillatory	2	0,04	32754,70	322671,56	241,00	0,49	397,21	0,07	1,13
1.sSMPABC376.TXT	105	76	1,38	oval	sa-sr	oscillatory	1	0,03	69016,18	553643,03	288,86	1,34	620,72	0,08	0,78
1.sSMPABC377.TXT								0,07	19437,64	179152,69	306,48	0,80	254,20	0,05	2,16
1.sSMPABC378.TXT								0,03	7004,97	105929,28	111,53	0,37	517,26	0,07	0,64
1.sSMPABC379.TXT								0,00	182708,20	1279724,78	352,29	0,24	3291,95	0,14	0,34
1.sSMPABC384.TXT								0,05	90879,86	472295,00	144,95	0,19	288,33	0,13	0,45
1.sSMPABC385.TXT								0,04	5982,24	62591,02	58,61	1,18	416,52	0,06	1,44
1.sSMPABC386.TXT								0,01	74717,69	527924,88	131,18	1,08	1357,25	0,16	0,50
1.sSMPABC387.TXT								0,10	10422,71	56417,23	51,04	1,06	167,94	0,06	3,36
1.sSMPABC260.TXT	118	81	1,46	oval	rounded	irregular	1	0,02	4475,39	70901,68	68,27	0,56	1007,93	0,06	0,83
1.sSMPABC350.TXT	126	67	1,88	elongated	sa-sr	oscillatory	1	0,03	35192,40	386363,08	203,18	0,53	526,04	0,09	0,40
1.sSMPABC270.TXT	123	70	1,76	oval	rounded	oscillatory, sector	1	0,02	48329,66	432622,46	175,37	1,45	930,97	0,11	0,38
1.sSMPABC268.TXT	129	62	2,08	elongated	rounded	oscillatory	1	0,01	133187,94	1109481,38	449,39	0,25	1873,38	0,12	0,35

Ratios [b]					Dates [c]						Ratios [c]							Dates [d]						% conc[e]	% conc[f]	% Error
$^{207}Pb/^{235}U$	2s (%)	$^{206}Pb/^{238}U$	2s (%)	Rho	$^{207}Pb/^{206}Pb$	2s abs	$^{206}Pb/^{238}U$	2s abs	$^{207}Pb/^{235}U$	2s abs	$^{207}Pb/^{206}Pb$	2s (%)	$^{207}Pb/^{235}U$	2s (%)	$^{206}Pb/^{238}U$	2s (%)	Rho	$^{207}Pb/^{206}Pb$	2s abs	$^{206}Pb/^{238}U$	2s abs	$^{207}Pb/^{235}U$	2s abs			
5,66	2,80	0,33	2,76	0,99	2013	61,69	1845	37,01	1924	49,36	0,12	0,47	5,64	2,80	0,33	2,76	0,99	2009	8,29	1845	44,42	1923	24,43	96	92	0,4
1,76	1,60	0,17	1,53	0,96	1043	6,04	1023	12,08	1028	12,53	0,07	0,45	1,75	1,60	0,17	1,53	0,96	1039	9,18	1023	14,50	1028	10,38	100	98	1,4
18,99	2,32	0,62	2,31	1,00	3006	60,59	3095	47,40	3039	37,73	0,22	0,23	18,98	2,32	0,62	2,31	1,00	3005	3,68	3095	56,92	3041	22,60	102	103	0,1
1,13	1,92	0,12	1,18	0,61	813	12,71	749	6,93	765	10,65	0,07	1,59	1,12	1,97	0,12	1,18	0,60	802	33,21	749	8,32	762	10,64	98	93	1,1
2,77	1,16	0,24	1,07	0,93	1292	5,60	1382	11,12	1346	8,12	0,08	0,44	2,76	1,16	0,24	1,07	0,93	1290	8,52	1382	13,35	1346	8,67	103	107	0,7
2,94	1,52	0,24	1,45	0,96	1376	5,77	1404	15,26	1392	13,40	0,09	0,45	2,94	1,52	0,24	1,45	0,95	1375	8,72	1404	18,31	1392	11,57	101	102	0,6
3,65	3,50	0,26	3,44	0,98	1630	81,05	1511	38,75	1560	71,19	0,10	0,62	3,65	3,50	0,26	3,44	0,98	1627	11,53	1511	46,52	1560	28,25	97	93	0,7
5,61	2,80	0,34	2,78	0,99	1949	3,98	1890	38,05	1916	49,30	0,12	0,34	5,61	2,80	0,34	2,78	0,99	1948	6,02	1890	45,69	1917	24,42	99	97	0,3
4,67	1,37	0,32	1,31	0,95	1731	5,23	1789	17,03	1761	12,36	0,11	0,43	4,67	1,38	0,32	1,31	0,95	1730	7,87	1789	20,44	1762	11,57	102	103	0,5
0,71	1,94	0,09	1,80	0,93	572	13,89	537	7,72	543	11,55	0,06	0,77	0,70	1,95	0,09	1,80	0,92	557	16,81	537	9,26	540	8,23	99	96	1,7
5,73	1,59	0,35	1,54	0,97	1952	4,72	1920	21,29	1933	16,57	0,12	0,40	5,72	1,59	0,35	1,54	0,97	1951	7,12	1919	25,56	1934	13,81	99	98	0,4
0,99	1,10	0,12	0,97	0,88	645	7,50	717	5,50	699	5,08	0,06	0,53	0,99	1,11	0,12	0,97	0,88	640	11,41	717	6,59	699	5,60	103	112	0,9
3,54	1,34	0,26	1,28	0,96	1621	4,78	1476	14,14	1536	11,15	0,10	0,39	3,54	1,34	0,26	1,28	0,96	1620	7,23	1476	16,97	1536	10,68	96	91	0,4
6,30	1,67	0,36	1,61	0,96	2067	5,19	1970	22,80	2016	18,48	0,13	0,45	6,29	1,67	0,36	1,61	0,96	2065	7,86	1970	27,37	2017	14,73	98	95	0,4
0,67	2,74	0,08	1,75	0,64	549	16,15	512	7,19	518	14,46	0,06	2,26	0,66	2,86	0,08	1,75	0,61	529	49,46	511	8,62	514	11,60	99	97	1,7
1,22	1,19	0,13	1,11	0,93	793	6,17	814	7,06	808	6,40	0,07	0,45	1,21	1,19	0,13	1,11	0,93	788	9,40	814	8,48	807	6,67	101	103	1,0
7,33	1,34	0,40	1,28	0,96	2154	4,55	2151	19,53	2151	12,55	0,13	0,40	7,32	1,34	0,40	1,28	0,95	2152	6,94	2151	23,44	2151	12,04	100	100	0,3
0,95	1,92	0,11	1,74	0,91	687	16,06	673	9,28	676	13,11	0,06	0,82	0,94	1,92	0,11	1,74	0,91	682	17,44	673	11,14	675	9,53	100	99	1,7
12,64	2,07	0,52	2,05	0,99	2617	48,05	2702	37,73	2651	29,76	0,18	0,33	12,62	2,07	0,52	2,05	0,99	2615	5,48	2702	45,30	2652	19,68	102	103	0,2
13,46	1,19	0,53	1,15	0,96	2693	23,99	2738	21,44	2710	10,76	0,18	0,32	13,45	1,20	0,53	1,15	0,96	2693	5,31	2738	25,74	2712	11,36	101	102	0,2
4,40	2,19	0,31	2,15	0,98	1706	4,65	1718	27,13	1711	29,13	0,10	0,38	4,40	2,19	0,31	2,15	0,98	1705	7,03	1718	32,56	1712	18,26	100	101	0,4
2,01	3,65	0,19	3,60	0,99	1160	72,49	1095	30,30	1116	65,85	0,08	0,65	1,99	3,66	0,19	3,60	0,98	1151	12,89	1095	36,37	1113	25,05	98	95	3,3
7,02	1,28	0,40	1,22	0,95	2071	4,63	2159	18,65	2112	11,55	0,13	0,40	7,02	1,28	0,40	1,22	0,95	2070	6,99	2159	22,39	2114	11,45	102	104	0,3
4,43	1,40	0,31	1,25	0,90	1708	20,18	1726	15,84	1717	12,50	0,10	0,63	4,42	1,40	0,31	1,25	0,89	1704	11,69	1726	19,00	1716	11,70	101	101	0,7
2,85	1,13	0,24	1,05	0,93	1332	5,33	1391	10,94	1367	7,82	0,09	0,42	2,84	1,13	0,24	1,05	0,93	1329	8,10	1391	13,13	1367	8,51	102	105	0,6
7,93	0,98	0,42	0,91	0,93	2204	16,23	2244	14,44	2221	7,40	0,14	0,36	7,92	0,98	0,42	0,91	0,93	2203	6,27	2243	17,33	2222	8,89	101	102	0,3
8,92	1,19	0,44	1,11	0,94	2311	21,05	2352	18,28	2328	10,43	0,15	0,42	8,92	1,19	0,44	1,11	0,94	2310	7,21	2352	21,95	2329	10,91	101	102	0,3
3,13	1,62	0,25	1,37	0,85	1426	10,92	1449	14,88	1438	14,57	0,09	0,85	3,13	1,61	0,25	1,37	0,85	1428	16,16	1449	17,86	1440	12,50	101	101	1,1
3,19	1,26	0,26	1,13	0,90	1411	7,12	1484	12,54	1453	9,82	0,09	0,57	3,18	1,27	0,26	1,13	0,89	1407	10,90	1484	15,05	1452	9,85	102	105	0,8
0,59	5,90	0,07	2,33	0,39	494	29,41	464	8,70	468	28,10	0,06	6,03	0,58	6,47	0,07	2,33	0,36	462	133,72	463	10,43	463	24,33	100	100	2,3
2,43	1,33	0,19	1,26	0,95	1457	5,33	1136	10,98	1251	10,04	0,09	0,43	2,43	1,33	0,19	1,26	0,95	1454	8,14	1136	13,18	1250	9,64	91	78	1,2
5,39	1,12	0,34	1,06	0,95	1865	17,07	1901	14,61	1882	8,83	0,11	0,37	5,39	1,12	0,34	1,06	0,95	1864	6,61	1901	17,54	1883	9,68	101	102	0,4
17,78	1,69	0,61	1,67	0,99	2904	39,93	3089	34,23	2975	20,55	0,21	0,28	17,77	1,69	0,61	1,67	0,99	2904	4,47	3088	41,10	2977	16,40	104	106	0,2
13,40	1,28	0,53	1,22	0,95	2676	25,93	2752	22,83	2706	12,28	0,18	0,39	13,39	1,28	0,53	1,22	0,95	2676	6,42	2752	27,41	2708	12,18	102	103	0,2
1,89	5,71	0,18	5,62	0,98	1108	168,73	1060	45,96	1075	162,35	0,08	1,07	1,88	5,72	0,18	5,62	0,98	1100	21,34	1060	55,17	1073	38,63	99	96	5,2
6,68	1,39	0,38	1,35	0,97	2054	4,03	2085	20,01	2068	13,19	0,13	0,34	6,67	1,39	0,38	1,35	0,97	2054	6,07	2085	24,02	2069	12,34	101	102	0,3
1,02	1,09	0,12	0,99	0,91	746	6,42	702	5,50	712	5,06	0,06	0,47	1,01	1,10	0,12	0,99	0,91	739	9,86	702	6,60	711	5,62	99	95	0,9
21,66	2,47	0,65	1,83	0,74	3128	51,45	3233	38,80	3166	33,79	0,24	1,67	21,65	2,48	0,65	1,83	0,74	3128	26,64	3233	46,59	3168	24,34	102	103	0,9
5,49	1,08	0,35	0,98	0,91	1843	5,50	1950	13,70	1897	8,31	0,11	0,46	5,48	1,08	0,35	0,98	0,91	1842	8,28	1950	16,44	1898	9,30	103	106	0,4
7,73	1,13	0,41	1,03	0,92	2189	5,27	2211	16,11	2198	9,40	0,14	0,47	7,71	1,13	0,41	1,03	0,91	2186	8,12	2211	19,34	2197	10,23	101	101	0,4
2,49	2,64	0,21	2,39	0,90	1320	41,31	1242	22,49	1269	34,66	0,08	1,21	2,47	2,68	0,21	2,39	0,89	1307	23,53	1241	26,98	1265	19,54	98	95	1,8
7,95	1,01	0,42	0,94	0,93	2197	16,81	2256	14,93	2223	7,72	0,14	0,36	7,94	1,01	0,42	0,94	0,93	2196	6,30	2256	17,92	2224	9,13	101	103	0,3
1,57	1,53	0,16	1,24	0,81	946	12,22	965	9,26	958	10,34	0,07	0,92	1,56	1,54	0,16	1,24	0,80	939	18,89	964	11,11	956	9,61	101	103	1,2
7,31	1,07	0,40	1,00	0,93	2113	4,62	2189	15,48	2148	8,57	0,13	0,40	7,30	1,08	0,40	1,00	0,93	2111	7,03	2189	18,58	2148	9,66	102	104	0,3
0,75	2,06	0,09	1,40	0,68	580	12,17	566	6,34	568	10,39	0,06	1,60	0,74	2,13	0,09	1,40	0,66	563	34,83	565	7,61	565	9,26	100	100	1,3
2,73	2,13	0,23	2,06	0,97	1361	32,33	1320	20,56	1334	24,96	0,09	0,57	2,71	2,14	0,23	2,06	0,96	1354	10,95	1320	24,67	1332	16,01	99	97	0,8
3,19	3,27	0,25	3,21	0,98	1492	69,28	1429	34,35	1453	60,16	0,09	0,65	3,18	3,27	0,25	3,21	0,98	1485	12,36	1429	41,23	1451	25,60	98	96	0,8
8,07	0,93	0,42	0,87	0,94	2207	15,48	2273	13,95	2236	6,71	0,14	0,32	8,06	0,93	0,42	0,87	0,94	2206	5,55	2273	16,74	2238	8,43	102	103	0,3
1,32	1,19	0,14	1,05	0,88	825	7,81	868	7,10	855	6,60	0,07	0,57	1,32	1,20	0,14	1,05	0,88	820	11,97	868	8,52	854	6,93	102	106	1,0
2,73	1,15	0,23	1,07	0,93	1315	13,45	1348	10,82	1334	8,00	0,08	0,43	2,72	1,15	0,23	1,07	0,93	1312	8,39	1348	12,98	1334	8,58	101	103	0,6
2,85	4,53	0,24	4,48	0,99	1380	123,00	1361	46,00	1367	114,07	0,09	0,64	2,84	4,53	0,24	4,48	0,99	1376	12,30	1361	55,23	1367	34,59	100	99	0,9
1,21	1,71	0,13	1,59	0,93	802	15,82	808	10,10	806	12,18	0,07	0,65	1,20	1,72	0,13	1,59	0,93	787	13,73	808	12,12	802	9,60	101	103	1,5
19,71	1,35	0,62	1,30	0,97	3045	3,74	3126	26,90	3074	13,68	0,23	0,35	19,70	1,35	0,62	1,30	0,97	3045	5,63	3126	32,29	3077	13,10	102	103	0,2
7,90	0,98	0,42	0,92	0,93	2188	16,35	2254	14,58	2218	7,40	0,14	0,35	7,89	0,98	0,42	0,92	0,93	2187	6,14	2254	17,49	2219	8,91	102	103	0,3
7,03	1,01	0,40	0,96	0,95	2078	3,74	2154	14,71	2113	7,63	0,13	0,32	7,02	1,01	0,40	0,96	0,95	2077	5,64	2154	17,65	2114	9,06	102	104	0,3
1,31	1,61	0,14	1,30	0,80	847	13,56	853	8,64	851	10,45	0,07	0,99	1,31	1,63	0,14	1,30	0,79	838	20,68	853	10,36	849	9,43	101	102	1,2
7,89	1,07	0,42	0,99	0,93	2186	17,92	2253	15,74	2216	8,56	0,14	0,40	7,88	1,07	0,42	0,99	0,93	2185	6,94	2253	18,89	2217	9,68	102	103	0,3
0,97	1,33	0,11	1,15	0,86	682	9,77	693	6,27	690	6,86	0,06	0,71	0,97	1,35	0,11	1,15	0,85	673	15,16	692	7,52	688	6,75	101	103	1,1
1,00	1,86	0,12	1,64	0,88	698	15,49	707	9,15	705	12,50	0,06	0,91	1,00	1,87	0,12	1,64	0,87	687	19,40	707	10,98	702	9,54	101	103	1,6
0,59	1,24	0,08	1,00	0,81	471	5,83	470	3,77	470	4,44	0,06	0,78	0,58	1,27	0,08	1,00	0,79	452	17,29	470	4,52	467	4,74	101	104	1,0
4,84	1,25	0,32	1,12	0,90	1799	17,97	1785	14,58	1790	10,50	0,11	0,57	4,82	1,26	0,32	1,12	0,89	1794	10,41	1784	17,50	1788	10,64	100	99	0,6
1,03	3,11	0,12	1,31	0,42	712	17,58	719	7,45	717	15,92	0,06	3,02	1,02	3,29	0,12	1,31	0,40	693	64,34	718	8,94	712	16,99	101	104	1,2
0,85	1,35	0,10	1,11	0,82	649	11,12	620	5,47	626	6,42	0,06	0,78	0,85	1,36	0,10	1,11	0,82	646	16,86	620	6,56	625	6,36	99	96	1,1
0,75	2,83	0,09	2,06	0,73	563	20,78	567	9,33	566	18,57	0,06	2,08	0,74	2,93	0,09	2,06	0,70	542	45,44	567	11,19	561	12,71	101	105	2,0
2,39	1,52	0,20	1,46	0,96	1362	5,44	1169	13,00	1237	12,65	0,09	0,43	2,38	1,52	0,20	1,46	0,96	1359	8,30	1169	15,60	1237	10,93	94	86	1,3
1,05	1,61	0,12	1,38	0,86	744	11,59	722	7,89	727	9,79	0,06	0,83	1,04	1,62	0,12	1,38	0,86	739	17,66	722	9,46	726	8,42	99	98	1,3
1,52	1,85	0,16	1,50	0,81	956	17,82	933	10,87	939	14,12	0,07	1,12	1,52	1,87	0,16	1,50	0,80	950	22,87	933	13,05	938	11,52	99	98	1,4
1,10	1,84	0,11	1,49	0,81	978	14,66	680	8,02	753	12,07	0,07	1,11	1,10	1,86	0,11	1,49	0,80	971	22,68	680	9,62	751	9,91	91	70	1,4
5,13	1,04	0,34	0,97	0,93	1813	15,15	1867	13,06	1840	7,67	0,11	0,38	5,13	1,04	0,34	0,97	0,93	1813	6,90	1867	15,68	1841	8,86	101	103	0,4
7,49	1,59	0,41	1,52	0,96	2141	5,26	2204	23,75	2169	17,26	0,13	0,46	7,48	1,59	0,41	1,52	0,96	2139	7,98	2204	28,50	2170	14,35	102	103	0,4
0,75	1,64	0,09	1,25	0,76	573	9,71	571	5,69	571	7,87	0,06	1,12	0,75	1,68	0,09	1,25	0,74	559	24,40	570	6,82	568	7,32	100	102	1,2
0,99	2,08	0,11	1,97	0,95	702	19,35	698	10,89	698	15,99	0,06	0,68	0,98	2,09	0,11	1,97	0,94	692	14,58	698	13,06	696	10,58	100	101	1,9
2,53	1,50	0,22	1,34	0,90	1299	17,87	1268	12,89	1279	12,39	0,08	0,69	2,52	1,51	0,22	1,34	0,89	1294	13,32	1268	15,46	1277	11,01	99	98	1,0
8,32	1,26	0,43	1,17	0,93	2236	22,17	2301	18,91	2265	11,57	0,14	0,48	8,31	1,27	0,43	1,17	0,92	2235	8,37	2301	22,70	2266	11,55	102	103	0,4
0,98	1,66	0,11	1,34	0,81	725	13,85	685	7,27	694	9,59	0,06	1,00	0,98	1,67	0,11	1,34	0,80	718	21,21	685	8,72	693	8,43	99	95	1,3
1,65	1,04	0,17	0,93	0,89	953	6,39	1007	7,25	990	5,81	0,07	0,48	1,65	1,05	0,17	0,93	0,89	949	9,73	1007	8,70	989	6,64	102	106	0,9
1,52	1,40	0,16	1,24	0,89	939	12,91	940	9,05	939	9,21	0,07	0,65	1,52	1,40	0,16	1,24	0,89	936	13,37	940	10,86	938	8,62	100	100	1,2
7,52	1,39	0,41	1,33	0,95	2122	4,88	2233	20,90	2174	13,53	0,13	0,42	7,52	1,39	0,41	1,33	0,95	2121	7,35	2233	25,09	2175	12,55	103	105	0,3
2,17	2,58	0,20	2,52	0,98	1210	40,26	1150	22,12	1170	33,64	0,08	0,57	2,16	2,58	0,20	2,52	0,98	1207	11,15	1150	26,55	1170	18,07	98	95	2,3
6,86	2,42	0,38	2,37	0,98	2127	5,45	2059	34,91	2091	37,99	0,13	0,47	6,85	2,42	0,38	2,37	0,98	2126	8,26	2059	41,91	2092	21,64	98	97	0,4
9,63	1,17	0,45	1,14	0,97	2413	21,45	2384	18,93	2397	10,09	0,16	0,29	9,62	1,17	0,45	1,14	0,97	2412	4,95	2384	22,72	2399	10,86	99	99	0,2
9,89	2,33	0,46	2,29	0,98	2402	4,96	2452	39,01	2423	36,85	0,15	0,45	9,88	2,33	0,46	2,29	0,98	2400	7,59	2452	46,84	2423	21,73	101	102	0,3
5,38	3,57	0,34	3,55	0,99	1899	93,49	1866	48,14	1880	80,15	0,12	0,37	5,37	3,57	0,34	3,55	0,99	1897	6,69	1865	57,80	1880	31,04	99	98	0,4
1,92	1,57	0,18	1,28	0,81	1110	12,27	1077	10,58	1087	11,72	0,08	0,94	1,91	1,59	0,18	1,28	0,81	1105	18,78	1077	12,69	1086	10,64	99	97	1,2
4,62	5,37	0,30	5,31	0,99	1827	194,83	1691	66,18	1751	183,25	0,11	0,84	4,59	5,38	0,30	5,31	0,99	1817	15,21	1690	79,45	1748	45,84	97	93	0,8
1,21	1,82	0,13	1,64	0,90	820	16,86	799	10,29	804	13,36	0,07	0,80	1,20	1,83	0,13	1,64	0,90	813	16,75	798	12,34	802	10,18	100	98	1,5
8,33	2,29	0,41	2,25	0,98	2318	49,68	2213	35,21	2266	35,05	0,15	0,44	8,32	2,29	0,41	2,25	0,98	2316	7,55	2213	42,28	2267	20,99	98	96	0,3
1,95	3,32	0,18	2,68	0,81	1115	26,29	1091	22,44	1098	43,07	0,08	1,98	1,95	3,33	0,18	2,68	0,80	1112	39,51	1091	26,93	1098	22,59	99	98	2,5
9,51	1,28	0,45	1,24	0,96	2383	23,87	2395	20,67	2386	11,93	0,15	0,34	9,50	1,28	0,45	1,24	0,96	2382	5,84	2395	24,81	2387	11,87	100	101	0,2
0,62	2,66	0,08	2,13	0,80	510	18,53	488	8,35	492	16,54	0,06	1,70	0,62	2,73	0,08	2,13	0,78	489	37,59	488	10,02	488	10,62	100	100	2,1
1,52	1,46	0,16	1,37	0,94	940	14,13	939	9,96	939	10,03	0,07	0,51	1,52	1,46	0,16	1,37	0,94	937	10,42	939	11,95	938	8,96	100	100	1,3
0,93	1,66	0,11	1,30	0,79	669	11,48	670	6,92	669	9,17	0,06	1,06	0,93	1,68	0,11	1,30	0,77	658	22,81	670	8,30	667	8,26	100	102	1,2
1,09	4,51	0,12	4,47	0,99	780	82,63	736	25,92	746	78,45	0,06	0,73	1,07	4,53	0,12	4,47	0,99	756	15,38	735	31,10	740	24,06	99	97	4,2
8,24	1,19	0,42	1,14	0,96	2238	20,99	2281	18,34	2256	10,22	0,14	0,32	8,24	1,19	0,42	1,14	0,96	2238	5,60	2280	22,01	2257	10,82	101	102	0,3
1,37	4,94	0,15	4,89	0,99	867	110,76	881	33,66	877	105,52	0,07	0,70	1,37	4,94	0,15	4,89	0,99	864	14,55	881	40,41	876	29,42	101	102	4,6
7,10	1,21	0,40	1,16	0,96	2101	20,50	2148	17,72	2122	10,31	0,13	0,32	7,10	1,21	0,40	1,16	0,96	2101	5,68	2148	21,27	2124	10,80	101	102	0,3
15,72	1,08	0,58	1,05	0,97	2801	22,66	2944	20,79	2857	9,01	0,20	0,26	15,69	1,09	0,58	1,05	0,97	2799	4,23	2944	24,95	2858	10,41	103	105	0,2
15,07	2,26	0,58	2,25	0,99	2741	56,86	2931	44,36	2817	35,57	0,19	0,23	15,06	2,26	0,58	2,25	0,99	2740	3,75	2931	53,27	2819	21,79	104	107	0,1
1,03	3,28	0,12	3,14	0,96	702	43,01	722	17,88	717	39,12	0,06	0,97	1,02	3,28	0,12	3,14	0,96	699	20,70	722	21,46	716	17,01	101	103	3,0
5,47	4,29	0,34	4,26	0,99	1905	131,05	1888	58,35	1894	117,34	0,12	0,50	5,45	4,29	0,34	4,26	0,99	1899	8,92	1887	70,07	1892	37,48	100	99	0,5
9,24	1,22	0,45	1,17	0,96	2326	22,48	2403	19,65	2360	10,92	0,15	0,35	9,23	1,22	0,45	1,17	0,96	2325	5,96	2403	23,59	2361	11,27	102	103	0,3
2,71	1,90	0,23	1,83	0,97	1316	27,16	1343	18,52	1331	19,87	0,08	0,50	2,71	1,90	0,23	1,83	0,96	1313	9,69	1343	22,22	1331	14,17	101	102	0,7
2,04	1,74	0,19	1,61	0,93	1142	20,66	1123	13,84	1128	15,33	0,08	0,67	2,03	1,74	0,19	1,61	0,92	1135	13,37	1123	16,61	1126	11,94	100	99	1,5
3,32	2,66	0,25	2,51	0,94	1537	47,94	1451	27,21	1485	39,47	0,09	1,00	3,29	2,70	0,25	2,51	0,93	1521	18,77	1450	32,64	1479	21,23	98	95	1,2
3,44	3,39	0,26	3,31	0,98	1512	75,47	1513	37,29	1511	65,62	0,09	0,75	3,42	3,39	0,26	3,31	0,98	1506	14,24	1512	44,76	1509	27,02	100	100	0,9
1,49	1,67	0,16	1,23	0,74	913	14,15	934	8,90	927	11,00	0,07	1,18	1,48	1,70	0,16	1,23	0,72	902	24,35	934	10,68	924	10,39	101	103	1,1
2,54	3,78	0,22	3,70	0,98	1274	83,74	1290	36,10	1283	75,55	0,08	0,80	2,53	3,78	0,22	3,70	0,98	1269	15,59	1290	43,34	1282	27,90	101	102	1,2
0,51	3,49	0,07	2,74	0,79	407	24,87	419	9,29	417	23,07	0,05	2,32	0,50	3,60	0,07	2,74	0,76	383	52,23	419	11,15	413	12,29	101	109	2,7
1,04	1,32	0,11	1,15	0,88	798	8,94	700	6,38	723	7,00	0,07	0,66	1,04	1,33	0,11	1,15	0,87	789	13,87	700	7,66	721	6,89	97	89	1,1
8,61	1,35	0,44	1,31	0,97	2250	3,93	2352	21,51	2296	12,94	0,14	0,34	8,60	1,35	0,44	1,31	0,97	2250	5,92	2352	25,82	2297	12,37	102	105	0,3
6,48	1,84	0,37	1,79	0,97	2039	34,46	2048	26,19	2042	22,40	0,13	0,48	6,45	1,85	0,37	1,79	0,97	2033	8,47	2047	31,43	2040	16,40	100	101	0,4
1,12	2,05	0,13	1,45	0,71	730	15,83	776	8,87	764	13,12	0,06	1,50	1,12	2,09	0,13	1,45	0,70	719	31,93	776	10,64	761	11,26	102	108	1,4
11,08	3,09	0,51	3,05	0,99	2440	85,78	2644	55,45	2528	65,44	0,16	0,50	11,07	3,10	0,51	3,05	0,99	2439	8,49	2644	66,59	2529	29,25	105	108	0,3
1,09	7,99	0,12	7,25	0,91	754	232,73	744	42,64	746	228,79	0,06	3,76	1,07	8,17	0,12	7,25	0,89	726	79,63	744	51,15	739	43,81	101	102	6,9
1,03	1,48	0,12	1,22	0,83	1113	11,80	722	6,94	720	8,21	0,06	0,85	1,03	1,48	0,12	1,22	0,82	#¡NUM!	17,97	721	8,33	719	7,68	100	#¡NUM!	1,2
2,68	1,75	0,21	1,71	0,97	1451	5,09	1246	16,13	1322	17,05	0,09	0,41	2,67	1,76	0,21	1,71	0,97	1446	7,87	1245	19,35	1321	13,05	94	86	0,5
4,45	1,56	0,29	1,51	0,97	1835	4,63	1629	18,17	1719	15,39	0,11	0,39	4,44	1,56	0,29	1,51	0,97	1832	7,06	1629	21,81	1719	13,03	95	89	0,4
4,76	1,18	0,29	1,13	0,96	1963	4,16	1625	13,56	1777	9,46	0,12	0,35	4,76	1,19	0,29	1,13	0,95	1962	6,28	1625	16,28	1777	10,00	91	83	0,3

BPN-08A (Mb. Tibagi)

SPOT	Grain Length	Grain Width	Length / width	Shape*	Roundness**	Zoning***	# of growth phases	f206c	^{207}Pb	^{206}Pb	U (µg g^{-1}) [a]	Th/U	$^{206}Pb/^{204}Pb$	$^{207}Pb/^{206}Pb$	2s (%)
1.sSMPABC267.TXT	150	106	1,42	oval	sa-sr	irregular	1	0,02	11403,55	106816,40	74,99	0,65	698,63	0,11	1,55
1.sSMPABC268.TXT	232	118	1,97	elongated	sa-sr	irregular	2	0,01	33258,89	185572,83	79,34	0,35	1617,26	0,20	1,34
1.sSMPABC269.TXT	142	60	2,37	elongated	sa-sr	oscillatory	2	0,04	11128,41	133058,99	358,10	0,23	469,33	0,06	6,42
1.sSMPABC270.TXT	220	80	2,75	elongated	rounded	irregular	1	0,01	25126,64	197691,91	113,14	0,23	1192,13	0,14	1,19
1.sSMPABC271.TXT	215	49	4,39	elongated	rounded	irregular	1	0,05	3947,89	63362,80	138,83	0,59	350,05	0,06	2,62
1.sSMPABC272.TXT	167	107	1,56	oval	rounded	oscillatory	1	0,04	6527,58	48897,49	27,45	0,38	415,00	0,13	1,96
1.sSMPABC273.TXT	146	60	2,43	elongated	sa-sr	irregular	1	0,05	5261,83	71132,98	148,12	0,39	341,87	0,06	3,60
1.sSMPABC274.TXT	195	78	2,50	elongated	sa-sr	oscillatory	1	0,06	3835,71	59758,11	136,94	0,71	288,18	0,06	2,55
1.sSMPABC275.TXT	200	151	1,32	oval	rounded	homogeneous	1	0,05	3077,68	50565,93	108,40	0,71	365,39	0,06	2,54
1.sSMPABC276.TXT	222	91	2,44	elongated	rounded	irregular	2	0,04	4285,14	69767,09	157,63	0,90	402,23	0,06	2,23
1.sSMPABC277.TXT	178	99	1,80	oval	sa-sr	oscillatory	2	0,02	16389,26	143132,07	93,39	0,79	813,84	0,11	1,64
1.sSMPABC278.TXT	189	89	2,12	elongated	sa-sr	irregular	1	0,01	31207,82	240096,68	147,24	0,14	1289,78	0,13	1,30
1.sSMPABC279.TXT	159	103	1,54	oval	rounded	oscillatory	2	0,06	5775,88	42024,46	23,48	0,22	256,95	0,14	2,24
1.sSMPABC280.TXT	190	71	2,68	elongated	rounded	oscillatory	1	0,11	651,17	9691,70	20,20	0,68	164,43	0,07	5,43
1.sSMPABC285.TXT	135	67	2,01	elongated	rounded	oscillatory	2	0,05	9799,98	149289,87	535,56	0,43	372,46	0,05	2,83
1.sSMPABC286.TXT	252	81	3,11	elongated	sa-sr	oscillatory, sector	1	0,02	18334,95	137436,31	76,12	0,40	754,26	0,14	1,33
1.sSMPABC287.TXT	144	62	2,32	elongated	rounded	irregular	1	0,01	64283,43	500865,05	417,30	0,36	1832,28	0,10	1,47
1.sSMPABC289.TXT	151	141	1,07	round	sa-sr	irregular	1	0,07	1493,60	24170,38	54,02	0,39	263,08	0,06	3,76
1.sSMPABC290.TXT	182	90	2,02	elongated	sa-sr	irregular	1	0,05	1551,33	24467,42	51,27	0,39	385,01	0,06	3,59
1.sSMPABC291.TXT	215	99	2,17	elongated	rounded	irregular	2	0,04	1635,56	22003,59	28,99	0,29	380,44	0,07	3,51
1.sSMPABC292.TXT	150	100	1,50	oval	sa-sr	oscillatory	1	0,09	3174,70	45711,24	67,58	0,69	201,25	0,07	2,57
1.sSMPABC293.TXT	163	74	2,20	elongated	rounded	oscillatory	2	0,01	25696,56	147085,11	64,18	0,65	1109,65	0,19	1,23
1.sSMPABC294.TXT	175	109	1,61	oval	sa-sr	oscillatory	2	0,02	6866,19	105460,25	183,06	0,18	757,26	0,06	1,90
1.sSMPABC295.TXT	250	89	2,81	elongated	sa-sr	homogeneous	1	0,15	559,50	7275,96	15,60	0,83	121,71	0,06	8,27
1.sSMPABC296.TXT	164	86	1,91	elongated	rounded	oscillatory	1	0,02	10449,63	79275,73	44,35	0,69	848,21	0,14	1,74
1.sSMPABC297.TXT	185	115	1,61	oval	rounded	oscillatory	1	0,02	13494,76	103148,70	58,72	0,16	951,61	0,13	1,76
1.sSMPABC298.TXT	192	75	2,56	elongated	sa-sr	oscillatory, sector	2	0,00	144292,19	612736,46	226,25	0,58	4337,56	0,23	1,61
1.sSMPABC299.TXT	219	73	3,00	elongated	sa-sr	irregular	1	0,03	5658,58	41464,00	22,34	0,39	452,26	0,15	2,20
1.sSMPABC300.TXT	164	134	1,22	round	rounded	irregular	1	0,10	2490,21	19081,78	9,61	0,49	144,27	0,16	3,57
1.sSMPABC306.TXT	205	87	2,36	elongated	sa-sr	irregular	1	0,05	2032,89	28175,66	40,49	0,68	315,19	0,07	3,25
1.sSMPABC307.TXT	234	86	2,72	elongated	rounded	irregular	2	0,01	13651,39	150787,12	133,04	0,16	1177,43	0,09	1,49
1.sSMPABC308.TXT	175	97	1,80	oval	sa-sr	oscillatory	1	0,03	3016,06	43647,64	68,48	0,52	519,32	0,07	2,62
1.sSMPABC309.TXT	167	122	1,37	oval	sa-sr	irregular	1	0,01	8847,80	65441,68	37,05	0,60	1241,79	0,13	1,87
1.sSMPABC310.TXT	246	67	3,67	elongated	rounded	oscillatory	2	0,01	24193,12	190219,96	179,98	0,40	1653,76	0,09	2,04
1.sSMPABC311.TXT	266	79	3,37	elongated	rounded	irregular	2	0,01	74680,94	421102,15	187,16	0,47	2649,71	0,18	1,21
1.sSMPABC312.TXT	145	68	2,13	elongated	rounded	oscillatory	1	0,01	11933,73	90444,17	50,79	0,44	2766,80	0,13	1,78
1.sSMPABC313.TXT	155	104	1,49	oval	rounded	sector	2	0,01	23787,51	180364,63	101,31	0,61	1086,82	0,13	1,43
1.sSMPABC314.TXT	246	127	1,94	elongated	sa-sr	irregular	1	0,04	1930,90	26451,02	40,33	0,52	451,51	0,07	29,02
1.sSMPABC316.TXT	135	85	1,59	oval	sa-sr	oscillatory	1	0,02	3006,10	26465,39	18,72	0,45	727,54	0,11	2,93
1.sSMPABC317.TXT	133	61	2,18	elongated	sa-sr	oscillatory	2	0,12	2050,41	30936,61	69,57	0,37	152,80	0,07	4,09
1.sSMPABC318.TXT	165	109	1,51	oval	rounded	irregular	1	0,02	5159,13	77700,64	134,89	0,35	820,59	0,07	2,20
1.sSMPABC319.TXT	172	78	2,21	elongated	sa-sr	irregular	1	0,06	2914,63	34115,56	34,82	0,58	276,94	0,08	2,99
1.sSMPABC320.TXT	170	112	1,52	oval	sa-sr	irregular	1	0,02	12754,12	78624,65	37,11	0,53	560,38	0,16	1,62
1.sSMPABC325.TXT	220	85	2,59	elongated	sa-sr	homogeneous	1	0,03	3665,61	59173,47	125,56	0,95	684,52	0,06	2,53
1.sSMPABC326.TXT	171	150	1,14	round	sa-sr	oscillatory	1	0,04	3306,36	53097,23	107,75	0,17	446,24	0,06	2,74
1.sSMPABC327.TXT	159	70	2,27	elongated	euhedral	oscillatory	1	0,08	2033,20	32073,56	68,93	1,07	224,84	0,06	2,92
1.sSMPABC328.TXT	126	66	1,91	elongated	sa-sr	oscillatory	1	0,06	2560,67	40389,99	87,35	0,70	282,81	0,06	2,73
1.sSMPABC329.TXT	193	90	2,14	elongated	rounded	irregular	1	0,10	1329,62	21414,22	48,66	0,32	181,53	0,06	3,91
1.sSMPABC330.TXT	153	55	2,78	elongated	rounded	oscillatory	1	0,04	5023,04	82532,94	178,83	0,61	485,32	0,06	2,73
1.sSMPABC331.TXT	165	116	1,42	oval	rounded	irregular	1	0,01	1561,95	23308,89	39,55	0,42	2445,65	0,07	3,81
1.sSMPABC332.TXT	239	87	2,75	elongated	rounded	oscillatory	1	0,02	10056,81	94363,83	65,50	0,78	693,51	0,11	1,49
1.sSMPABC333.TXT	163	86	1,90	elongated	sa-sr	oscillatory	1	0,02	6240,18	94775,83	162,35	0,49	1035,62	0,07	2,20
1.sSMPABC334.TXT	180	83	2,17	elongated	sa-sr	oscillatory	1	0,06	2724,59	39544,13	61,14	0,50	282,27	0,07	2,81
1.sSMPABC335.TXT	156	112	1,39	oval	sa-sr	oscillatory	2	0,01	23025,42	195972,49	126,08	0,55	1987,93	0,12	1,50
1.sSMPABC336.TXT	166	82	2,02	elongated	rounded	oscillatory	1	0,02	5124,14	81728,67	178,09	0,51	1064,74	0,06	2,60
1.sSMPABC337.TXT	173	64	2,70	elongated	rounded	oscillatory	1	0,02	28406,32	227228,60	299,91	0,29	1104,42	0,07	2,06
1.sSMPABC338.TXT	215	98	2,19	elongated	sa-sr	oscillatory	1	0,02	4633,90	75273,49	169,68	0,57	709,47	0,06	2,12
1.sSMPABC339.TXT	157	99	1,59	oval	sa-sr	irregular	2	0,01	9033,64	67538,91	37,23	0,46	2137,10	0,13	1,85
1.sSMPABC345.TXT	123	121	1,02	round	sa-sr	irregular	1	0,06	2085,75	31202,48	52,50	0,47	312,40	0,07	2,99
1.sSMPABC346.TXT	141	48	2,94	elongated	rounded	oscillatory	2	0,04	7592,74	114982,10	219,55	0,26	483,94	0,07	5,04
1.sSMPABC348.TXT	146	80	1,83	elongated	rounded	oscillatory	2	0,01	29159,27	258444,63	179,99	0,89	1156,86	0,11	1,38
1.sSMPABC349.TXT	137	103	1,33	oval	sa-sr	irregular	2	-0,01	2049,87	28047,10	39,92	0,39	-3248,86	0,07	3,20
1.sSMPABC350.TXT	141	65	2,17	elongated	rounded	oscillatory	2	0,00	5478,34	73294,53	96,39	0,49	11336,26	0,07	2,26
1.sSMPABC351.TXT	170	87	1,95	elongated	sa-sr	irregular	1	0,03	7981,49	44633,44	20,20	0,46	408,05	0,18	2,10
1.sSMPABC352.TXT	143	51	2,80	elongated	rounded	homogeneous	1	0,01	18335,46	144255,32	89,53	0,40	1071,17	0,13	1,43
1.sSMPABC354.TXT	164	97	1,69	oval	sa-sr	oscillatory	1	0,02	12664,19	187553,01	314,39	0,38	809,44	0,07	1,54
1.sSMPABC355.TXT	199	108	1,84	elongated	sa-sr	oscillatory	2	0,01	23479,32	185256,95	109,16	0,25	1510,62	0,13	1,30
1.sSMPABC356.TXT	231	86	2,69	elongated	sa-sr	irregular	1	0,06	2740,28	35421,00	48,66	0,68	288,79	0,08	3,04
1.sSMPABC357.TXT	194	98	1,98	elongated	sa-sr	irregular	1	0,06	2633,06	35939,33	46,88	0,31	301,23	0,07	3,07
1.sSMPABC358.TXT	231	102	2,26	elongated	sa-sr	irregular	1	0,04	3790,85	51933,68	69,22	0,29	438,19	0,07	2,42
1.sSMPABC359.TXT	155	90	1,72	oval	sa-sr	oscillatory	2	0,18	1101,44	17052,45	43,91	1,47	98,44	0,06	7,32
1.sSMPABC360.TXT	142	108	1,31	oval	sa-sr	homogeneous	1	0,03	2666,39	33609,94	38,93	0,36	498,93	0,08	2,79
1.sSMPABC365.TXT	174	106	1,64	oval	sa-sr	irregular	1	0,02	6302,40	48716,34	28,03	0,44	681,39	0,13	2,28
1.sSMPABC366.TXT	149	50	2,98	elongated	rounded	oscillatory	2	0,02	6065,30	88270,78	192,77	0,28	790,59	0,07	2,27
1.sSMPABC367.TXT	170	59	2,88	elongated	sa-sr	oscillatory	1	0,05	3976,45	60561,86	153,36	0,50	332,38	0,07	5,16
1.sSMPABC368.TXT	196	115	1,70	oval	sa-sr	irregular	1	0,09	1876,55	26567,97	40,04	0,50	193,34	0,07	3,19
1.sSMPABC369.TXT	181	104	1,74	oval	sa-sr	sector	2	0,02	4640,82	36359,29	22,58	0,34	693,51	0,13	2,52
1.sSMPABC370.TXT	162	123	1,32	oval	rounded	irregular	1	0,03	9067,01	69883,03	39,27	0,56	435,16	0,14	1,67
1.sSMPABC371.TXT	184	73	2,52	elongated	rounded	oscillatory	1	0,01	9361,37	87192,00	61,06	0,69	1738,00	0,11	1,86
1.sSMPABC372.TXT	170	53	3,21	elongated	sa-sr	irregular	1	0,02	6415,75	105055,30	280,17	0,73	819,34	0,06	2,25
1.sSMPABC373.TXT	183	65	2,82	elongated	sa-sr	oscillatory	1	0,00	3434,47	55271,15	127,74	0,80	-5439,13	0,06	2,79
1.sSMPABC374.TXT	150	114	1,32	oval	sa-sr	homogeneous	2	0,05	3840,37	28681,48	16,10	0,47	302,56	0,13	2,85
1.sSMPABC376.TXT	204	97	2,10	elongated	rounded	oscillatory, sector	2	0,03	3931,21	62102,99	126,99	0,67	671,62	0,06	2,35
1.sSMPABC377.TXT	185	81	2,28	elongated	rounded	oscillatory	2	0,01	34889,52	300952,06	203,12	0,23	2409,45	0,12	1,75
1.sSMPABC378.TXT	149	124	1,20	round	sa-sr	irregular	1	0,01	4623,20	68664,93	111,87	0,39	2259,78	0,07	2,48
1.sSMPABC379.TXT	158	116	1,36	oval	rounded	homogeneous	1	0,01	71893,15	583426,81	372,40	0,21	2488,08	0,12	1,63
1.sSMPABC380.TXT	159	76	2,09	elongated	sa-sr	irregular	1	0,08	1498,21	21998,31	36,09	0,65	216,67	0,07	3,87
1.sSMPABC385.TXT	98	92	1,07	round	sa-sr	oscillatory	1	0,01	11399,55	118343,10	102,47	0,53	1392,05	0,10	1,85
1.sSMPABC388.TXT	162	81	2,00	elongated	rounded	oscillatory	2	0,06	2333,01	36543,75	82,05	0,72	279,07	0,06	3,72
1.sSMPABC389.TXT	146	37	3,95	elongated	sa-sr	oscillatory	2	0,05	6485,39	97153,38	292,38	0,16	345,47	0,06	17,19
1.sSMPABC390.TXT	162	79	2,05	elongated	rounded	oscillatory	1	0,00	17925,73	135617,21	80,90	0,32	3148,91	0,13	1,57
1.sSMPABC391.TXT	178	85	2,09	elongated	rounded	oscillatory	1	0,04	6369,53	98524,58	295,62	0,51	497,16	0,06	2,01
1.sSMPABC392.TXT	180	88	2,05	elongated	sa-sr	oscillatory	1	0,03	788,90	9651,99	12,80	0,66	664,91	0,08	5,09
1.sSMPABC393.TXT	238	57	4,18	elongated	sa-sr	oscillatory	1	0,03	7886,02	62283,23	37,72	0,41	443,73	0,13	2,14
1.sSMPABC394.TXT	200	83	2,41	elongated	rounded	irregular	1	0,22	765,82	10689,10	15,34	1,64	77,91	0,07	4,83
1.sSMPABC395.TXT	224	72	3,11	elongated	sa-sr	oscillatory	1	0,01	9052,21	68220,52	37,70	0,23	2247,02	0,14	1,71
1.sSMPABC396.TXT	227	76	2,99	elongated	sa-sr	oscillatory	2	0,03	7294,07	98065,78	155,63	0,54	596,76	0,07	2,00
1.sSMPABC397.TXT	180	65	2,77	elongated	euhedral	oscillatory	1	0,06	2628,92	38814,39	77,47	0,87	311,47	0,07	7,39
1.sSMPABC398.TXT	140	107	1,31	oval	sa-sr	irregular	1	0,01	21376,73	167366,75	97,35	1,29	1236,16	0,14	2,60
1.sSMPABC375.TXT	140	54	2,59	elongated	rounded	oscillatory	1	0,04	18944,34	231336,41	1056,58	0,27	492,14	0,05	2,53
1.sSMPABC315.TXT	188	85	2,21	elongated	rounded	oscillatory	2	0,04	9099,39	125124,91	543,05	0,24	469,05	0,05	2,51
1.sSMPABC305.TXT	166	107	1,55	oval	rounded	irregular	2	0,01	22418,86	166977,36	123,02	0,27	1391,28	0,13	1,48

Ratios [b]					Dates [c]						Ratios [c]						Dates [d]								
$^{207}Pb/^{235}U$	2s (%)	$^{206}Pb/^{238}U$	2s (%)	Rho	$^{207}Pb/^{206}Pb$	2s abs	$^{206}Pb/^{238}U$	2s abs	$^{207}Pb/^{235}U$	2s abs	$^{207}Pb/^{206}Pb$	2s (%)	$^{207}Pb/^{235}U$	2s (%)	$^{206}Pb/^{238}U$	2s (%)	Rho	$^{207}Pb/^{206}Pb$	2s abs	$^{206}Pb/^{238}U$	2s abs	$^{207}Pb/^{235}U$	2s abs	% conc[e]	% conc[f]	% Error
5,22	2,27	0,34	1,66	0,73	1846	33,94	1865	22,45	1854	25,45	0,11	1,59	5,21	2,30	0,34	1,66	0,72	1842	28,77	1865	26,95	1854	19,77	101	101	2
15,22	2,14	0,56	1,67	0,78	2806	42,27	2862	32,26	2827	27,31	0,20	1,35	15,21	2,15	0,56	1,67	0,78	2806	22,03	2861	38,73	2829	20,66	101	102	1
0,68	6,94	0,08	2,63	0,38	526	39,47	526	11,06	525	37,89	0,06	6,68	0,67	7,18	0,08	2,63	0,37	514	146,72	526	13,26	523	29,77	100	102	3
7,86	1,95	0,41	1,55	0,79	2201	33,07	2230	24,37	2213	22,36	0,14	1,20	7,85	1,96	0,41	1,55	0,79	2200	20,93	2230	29,25	2214	17,82	101	101	1
0,91	5,51	0,11	4,85	0,88	673	37,81	653	25,17	657	91,54	0,06	2,76	0,90	5,58	0,11	4,85	0,87	658	59,17	653	30,21	654	27,28	100	99	5
7,62	2,69	0,42	1,85	0,69	2135	23,04	2243	29,20	2185	33,48	0,13	2,03	7,59	2,74	0,42	1,85	0,67	2131	35,56	2243	35,05	2184	24,93	103	105	2
0,95	4,21	0,11	2,18	0,52	675	30,88	679	11,71	677	28,57	0,06	3,80	0,94	4,38	0,11	2,18	0,50	660	81,44	678	14,05	674	21,81	101	103	2
0,90	3,21	0,10	1,96	0,61	736	36,35	626	9,73	649	21,12	0,06	2,71	0,89	3,35	0,10	1,96	0,59	719	57,59	625	11,67	646	16,11	97	87	2
0,91	3,14	0,11	1,85	0,59	622	36,98	666	9,75	656	19,81	0,06	2,67	0,90	3,25	0,11	1,85	0,57	608	57,75	666	11,69	653	15,75	102	110	2
0,87	2,90	0,10	1,85	0,64	642	32,31	634	9,32	635	18,42	0,06	2,33	0,86	2,98	0,10	1,85	0,62	629	50,28	633	11,18	632	14,12	100	101	2
5,61	4,66	0,36	4,36	0,94	1862	19,90	1970	62,01	1916	131,35	0,11	1,67	5,60	4,67	0,36	4,36	0,93	1859	30,22	1970	74,48	1916	41,07	103	106	2
6,78	2,13	0,38	1,68	0,79	2087	15,33	2077	24,93	2081	25,33	0,13	1,32	6,77	2,13	0,38	1,68	0,79	2086	23,14	2077	29,93	2081	19,06	100	100	1
7,86	3,04	0,42	2,05	0,68	2185	26,21	2248	32,51	2213	40,52	0,14	2,37	7,82	3,14	0,42	2,05	0,65	2178	41,34	2247	39,02	2211	28,65	102	103	2
1,03	6,18	0,11	2,95	0,48	831	77,37	683	15,95	718	50,96	0,07	6,08	1,01	6,76	0,11	2,95	0,44	804	127,40	682	19,12	711	35,17	96	85	3
0,48	4,94	0,06	4,05	0,82	394	46,79	401	13,16	400	44,91	0,05	2,97	0,48	5,03	0,06	4,05	0,81	378	66,92	401	15,78	398	16,67	101	106	4
8,36	2,19	0,42	1,75	0,80	2262	39,29	2280	27,99	2269	27,57	0,14	1,36	8,34	2,21	0,42	1,75	0,79	2260	23,42	2280	33,60	2269	20,25	100	101	1
3,66	2,56	0,27	2,10	0,82	1585	40,54	1546	24,06	1561	32,63	0,10	1,48	3,65	2,57	0,27	2,10	0,82	1583	27,67	1546	28,88	1561	20,67	99	98	2
0,88	4,34	0,10	2,17	0,50	653	54,76	638	10,97	641	27,76	0,06	4,03	0,87	4,58	0,10	2,17	0,47	634	86,84	637	13,16	636	21,88	100	100	2
0,96	4,18	0,11	2,14	0,51	708	51,72	678	11,46	684	28,06	0,06	3,76	0,96	4,33	0,11	2,14	0,49	696	80,15	677	13,75	681	21,70	99	97	2
1,79	4,09	0,18	2,11	0,51	1038	47,95	1046	16,98	1043	35,94	0,07	3,67	1,78	4,23	0,18	2,11	0,50	1027	74,25	1046	20,37	1040	27,92	101	102	2
1,49	3,19	0,16	1,88	0,59	899	35,77	940	13,75	927	25,73	0,07	2,81	1,48	3,38	0,16	1,88	0,56	877	58,20	939	16,49	921	20,70	102	107	2
14,35	2,09	0,54	1,69	0,81	2758	41,96	2793	32,08	2771	27,05	0,19	1,25	14,33	2,10	0,54	1,69	0,81	2757	20,48	2793	38,52	2772	20,17	101	101	1
1,19	2,54	0,13	1,69	0,67	764	26,91	809	10,73	796	18,12	0,06	1,94	1,19	2,58	0,13	1,69	0,66	758	41,01	808	12,87	795	14,31	102	107	2
0,90	8,84	0,11	3,12	0,35	654	63,03	654	16,19	653	60,91	0,06	9,67	0,88	10,16	0,11	3,12	0,31	612	208,97	653	19,40	643	49,62	101	107	3
8,15	2,46	0,42	1,73	0,70	2242	40,53	2255	27,52	2246	29,76	0,14	1,78	8,14	2,48	0,42	1,73	0,70	2240	30,70	2254	33,03	2247	22,68	100	101	1
7,29	2,61	0,41	1,93	0,74	2098	20,75	2201	30,12	2146	34,19	0,13	1,79	7,28	2,63	0,41	1,93	0,73	2096	31,39	2201	36,15	2147	23,78	103	105	1
20,23	2,50	0,63	1,91	0,77	3079	17,19	3139	39,73	3100	35,52	0,23	1,61	20,23	2,50	0,63	1,91	0,77	3079	25,71	3139	47,70	3102	24,48	101	102	1
8,84	3,01	0,44	2,05	0,68	2315	52,72	2329	33,44	2319	40,75	0,15	2,28	8,81	3,06	0,43	2,05	0,67	2311	39,08	2328	40,15	2319	28,32	100	101	2
10,43	5,59	0,47	4,31	0,77	2450	169,77	2502	74,93	2471	152,34	0,16	3,95	10,36	5,85	0,47	4,31	0,74	2441	66,93	2500	89,96	2467	55,65	101	102	3
1,59	3,89	0,16	2,14	0,55	976	44,80	961	15,95	965	33,85	0,07	3,44	1,58	4,05	0,16	2,14	0,53	963	70,19	961	19,13	961	25,47	100	100	2
3,25	2,23	0,26	1,65	0,74	1424	19,16	1499	18,42	1467	22,64	0,09	1,52	3,24	2,24	0,26	1,65	0,74	1421	28,97	1499	22,10	1467	17,53	102	105	2
1,39	3,24	0,15	1,91	0,59	887	36,54	885	13,19	885	25,63	0,07	2,71	1,39	3,32	0,15	1,91	0,58	879	56,11	885	15,83	883	19,76	100	101	2
7,55	2,58	0,41	1,79	0,69	2154	21,87	2205	27,89	2177	31,53	0,13	1,89	7,54	2,60	0,41	1,79	0,69	2153	32,96	2205	33,48	2178	23,59	101	102	2
2,90	4,73	0,24	4,27	0,90	1412	119,92	1362	43,84	1381	111,62	0,09	2,06	2,90	4,74	0,24	4,27	0,90	1410	39,36	1362	52,63	1381	36,41	99	97	3
12,60	2,05	0,52	1,66	0,81	2617	13,44	2695	30,51	2648	25,82	0,18	1,21	12,60	2,05	0,52	1,66	0,81	2616	20,16	2695	36,63	2650	19,50	102	103	1
7,42	2,52	0,41	1,78	0,71	2112	21,02	2218	27,85	2161	30,70	0,13	1,79	7,41	2,53	0,41	1,78	0,70	2111	31,47	2218	33,43	2163	22,85	103	105	1
7,41	2,23	0,41	1,71	0,77	2111	16,85	2217	26,84	2161	27,11	0,13	1,45	7,40	2,25	0,41	1,71	0,76	2109	25,48	2217	32,21	2161	20,29	103	105	1
1,51	29,12	0,15	2,48	0,09	1000	452,46	908	17,55	934	155,61	0,07	30,17	1,50	30,27	0,15	2,48	0,08	991	613,58	907	21,06	932	203,73	97	92	2
5,06	3,82	0,33	2,45	0,64	1845	35,76	1817	32,39	1829	53,17	0,11	2,99	5,05	3,87	0,33	2,45	0,63	1842	54,17	1817	38,88	1828	33,31	99	99	3
0,93	4,71	0,10	2,34	0,50	800	58,19	629	11,71	667	32,48	0,06	4,63	0,91	5,19	0,10	2,34	0,45	770	97,40	628	14,04	660	25,47	95	82	2
1,21	2,80	0,13	1,73	0,62	804	30,95	803	10,91	803	19,86	0,07	2,24	1,20	2,83	0,13	1,73	0,61	798	47,01	803	13,09	801	15,83	100	101	2
2,64	3,62	0,23	2,05	0,56	1312	39,18	1311	20,26	1310	36,71	0,08	3,18	2,62	3,78	0,23	2,05	0,54	1300	61,81	1311	24,31	1306	28,18	100	101	5
10,83	2,44	0,49	1,83	0,75	2467	18,32	2561	32,36	2506	32,18	0,16	1,66	10,81	2,47	0,49	1,83	0,74	2464	28,01	2560	38,84	2507	23,23	102	104	1
0,92	3,13	0,11	1,84	0,59	657	36,56	663	9,66	661	19,78	0,06	2,59	0,92	3,18	0,11	1,84	0,58	649	55,71	663	11,59	660	15,55	100	102	2
0,97	4,47	0,11	3,53	0,79	668	39,62	692	19,33	686	53,65	0,06	2,85	0,96	4,54	0,11	3,53	0,78	657	61,22	691	23,19	683	22,83	101	105	3
0,93	3,62	0,11	2,14	0,59	706	41,90	655	11,12	666	25,34	0,06	3,16	0,92	3,82	0,11	2,14	0,56	684	67,56	654	13,33	661	18,73	99	96	2
0,92	3,29	0,11	1,83	0,56	706	39,22	651	9,46	663	20,40	0,06	2,91	0,91	3,44	0,11	1,83	0,53	689	62,15	651	11,34	659	16,82	99	94	2
0,86	4,53	0,10	2,29	0,51	662	56,89	621	11,31	629	29,74	0,06	4,33	0,85	4,90	0,10	2,29	0,47	634	93,32	620	13,56	623	23,09	100	98	2
0,88	3,37	0,11	1,98	0,59	619	39,72	650	10,18	642	21,77	0,06	2,83	0,88	3,45	0,11	1,98	0,57	608	61,18	649	12,21	640	16,52	101	107	2
1,24	4,51	0,14	2,41	0,54	823	53,88	818	15,47	819	37,66	0,07	3,83	1,24	4,53	0,14	2,41	0,53	821	80,05	818	18,57	819	25,78	100	100	2
5,23	2,13	0,33	1,52	0,72	1861	30,37	1855	20,50	1856	22,41	0,11	1,52	5,22	2,15	0,33	1,52	0,71	1858	27,45	1855	24,60	1856	18,50	100	100	1
1,21	2,71	0,13	1,59	0,59	786	31,04	811	10,11	804	18,04	0,07	2,23	1,20	2,74	0,13	1,59	0,58	782	46,93	811	12,13	803	15,33	101	104	1
1,40	3,44	0,15	1,98	0,58	881	39,25	892	13,76	888	27,57	0,07	2,99	1,39	3,59	0,15	1,98	0,55	865	62,08	892	16,51	884	21,41	101	103	2
5,74	2,57	0,36	2,08	0,81	1906	18,09	1967	29,45	1935	35,20	0,12	1,51	5,73	2,57	0,36	2,08	0,81	1905	27,18	1967	35,35	1936	22,48	102	103	1
0,90	3,14	0,11	1,77	0,56	683	37,46	646	9,05	653	18,97	0,06	2,64	0,90	3,18	0,11	1,77	0,56	678	56,50	645	10,86	653	15,42	99	95	2
1,69	4,03	0,17	3,46	0,86	1038	68,91	989	26,48	1004	63,62	0,07	2,09	1,69	4,04	0,17	3,46	0,86	1035	42,29	989	31,78	1003	26,09	99	96	3
0,86	2,87	0,10	1,94	0,67	644	30,61	625	9,61	628	18,97	0,06	2,17	0,85	2,91	0,10	1,94	0,67	636	46,69	625	11,53	627	13,69	100	98	2
7,62	2,61	0,42	1,84	0,71	2135	21,71	2243	29,17	2185	32,73	0,13	1,86	7,61	2,62	0,42	1,84	0,70	2135	32,55	2243	35,01	2187	23,78	103	105	2
1,25	3,59	0,14	1,98	0,55	818	42,27	824	12,78	822	26,94	0,07	3,17	1,24	3,74	0,14	1,98	0,53	804	66,41	823	15,33	818	21,22	101	102	2
1,09	5,39	0,12	1,91	0,35	793	72,10	731	11,01	746	31,59	0,07	5,23	1,08	5,57	0,12	1,91	0,34	783	109,85	731	13,20	744	29,78	98	93	2
5,09	2,26	0,33	1,79	0,79	1833	16,74	1836	23,92	1833	27,09	0,11	1,40	5,08	2,27	0,33	1,79	0,79	1831	25,31	1835	28,71	1833	19,47	100	100	1
1,61	3,82	0,16	2,09	0,55	1002	43,95	963	15,57	974	32,80	0,07	3,19	1,61	3,81	0,16	2,09	0,55	1004	64,65	963	18,69	975	24,15	99	96	2
1,79	3,17	0,17	2,22	0,70	1048	30,72	1037	17,74	1039	32,58	0,07	2,27	1,78	3,17	0,17	2,22	0,70	1047	45,69	1037	21,29	1040	20,86	100	99	2
12,42	2,99	0,51	2,13	0,71	2631	23,48	2644	38,56	2634	43,58	0,18	2,17	12,39	3,04	0,51	2,13	0,70	2628	36,16	2643	46,29	2634	28,99	100	101	1
6,44	2,39	0,37	1,91	0,80	2046	16,96	2028	27,81	2035	31,19	0,13	1,45	6,43	2,40	0,37	1,91	0,80	2045	25,67	2028	33,38	2036	21,33	100	99	1
1,26	2,21	0,14	1,59	0,72	829	18,92	827	10,30	827	15,86	0,07	1,57	1,25	2,24	0,14	1,59	0,71	823	32,80	827	12,36	826	12,72	100	100	1
6,76	2,16	0,39	1,73	0,80	2041	15,40	2121	26,10	2079	26,35	0,13	1,31	6,75	2,17	0,39	1,73	0,80	2040	23,21	2121	31,33	2080	19,39	102	104	1
1,77	3,64	0,17	2,00	0,55	1117	40,94	996	15,40	1034	31,61	0,08	3,23	1,76	3,80	0,17	2,00	0,53	1104	64,54	996	18,47	1030	24,88	97	90	2
1,77	3,63	0,18	1,95	0,54	1008	42,03	1045	15,67	1032	30,75	0,07	3,25	1,75	3,79	0,18	1,95	0,51	995	66,04	1045	18,80	1028	24,79	102	105	2
1,72	3,07	0,17	1,89	0,62	1000	33,07	1025	14,96	1016	26,65	0,07	2,51	1,71	3,15	0,17	1,89	0,60	991	51,13	1025	17,95	1014	20,38	101	103	2
0,79	7,81	0,09	2,70	0,35	747	106,72	551	11,90	590	45,53	0,06	8,95	0,77	9,35	0,09	2,70	0,29	698	190,62	550	14,25	580	42,14	95	79	3
2,16	3,41	0,20	1,96	0,57	1168	37,34	1167	17,46	1166	31,91	0,08	2,89	2,15	3,49	0,20	1,96	0,56	1160	57,32	1166	20,96	1164	24,49	100	101	2
7,09	3,02	0,40	1,98	0,66	2078	26,97	2169	30,42	2121	38,35	0,13	2,33	7,07	3,05	0,40	1,98	0,65	2076	40,99	2168	36,51	2121	27,54	102	104	2
0,99	3,31	0,11	2,41	0,73	877	31,58	646	12,37	699	28,45	0,07	2,32	0,99	3,35	0,11	2,41	0,72	872	48,00	646	14,84	698	17,03	92	74	2
0,82	7,10	0,09	4,88	0,69	783	74,02	561	21,88	606	95,53	0,06	5,45	0,81	7,32	0,09	4,88	0,67	769	114,87	561	26,26	604	33,85	93	73	5
1,48	3,81	0,15	2,09	0,55	934	44,18	917	14,89	921	31,69	0,07	3,50	1,46	4,07	0,15	2,09	0,51	912	71,98	916	17,86	915	24,86	100	100	2
6,49	3,71	0,37	2,73	0,73	2055	29,98	2035	39,77	2043	62,03	0,13	2,58	6,48	3,75	0,37	2,73	0,73	2052	45,51	2034	47,75	2043	33,55	100	99	2
8,05	2,48	0,42	1,84	0,74	2235	42,91	2239	29,00	2235	31,63	0,14	1,72	8,03	2,52	0,42	1,84	0,73	2231	29,84	2238	34,81	2234	23,00	100	100	1
4,85	2,58	0,33	1,78	0,69	1744	22,92	1835	23,79	1791	29,45	0,11	1,88	4,84	2,59	0,33	1,78	0,69	1743	34,44	1835	28,56	1792	22,04	102	105	2
0,72	3,67	0,09	2,90	0,79	629	32,64	535	12,42	553	31,77	0,06	2,30	0,72	3,70	0,09	2,90	0,78	623	49,59	535	14,90	552	15,88	97	86	3
0,85	3,37	0,10	1,89	0,56	666	40,33	614	9,23	625	20,45	0,06	2,78	0,85	3,36	0,10	1,89	0,56	667	59,53	614	11,07	625	15,82	98	92	2
7,55	3,69	0,41	2,34	0,64	2140	33,56	2221	36,77	2177	52,43	0,13	2,99	7,52	3,80	0,41	2,34	0,62	2134	52,34	2220	44,13	2175	34,63	102	104	2
0,98	3,04	0,11	1,94	0,64	706	33,62	691	10,60	694	21,22	0,06	2,41	0,98	3,09	0,11	1,94	0,63	699	51,30	690	12,72	692	15,64	100	99	2
5,45	2,34	0,34	1,56	0,67	1884	21,11	1900	21,37	1891	24,68	0,12	1,76	5,44	2,35	0,34	1,56	0,66	1883	31,65	1900	25,65	1892	20,33	100	101	2
1,31	3,06	0,14	1,79	0,58	837	34,86	857	11,98	850	22,59	0,07	2,50	1,31	3,08	0,14	1,79	0,58	835	52,13	856	14,37	850	17,87	101	103	2
6,13	2,41	0,36	1,78	0,74	1994	19,45	1996	25,51	1993	29,08	0,12	1,64	6,13	2,42	0,36	1,78	0,74	1993	29,16	1996	30,62	1994	21,35	100	100	1
1,32	4,78	0,14	2,81	0,59	861	54,42	852	18,71	854	47,59	0,07	4,20	1,31	5,05	0,14	2,81	0,56	840	87,49	851	22,44	848	29,48	100	101	3
3,55	3,37	0,27	2,82	0,84	1545	23,30	1534	32,18	1537	54,95	0,10	1,87	3,55	3,38	0,27	2,82	0,83	1543	35,10	1534	38,63	1537	27,15	100	99	2
0,91	5,14	0,10	3,55	0,69	726	53,46	637	17,98	657	55,81	0,06	3,97	0,90	5,33	0,10	3,55	0,67	709	84,42	637	21,57	653	25,97	98	90	3
0,60	17,82	0,08	4,67	0,26	473	108,00	478	17,94	476	106,50	0,06	18,14	0,59	18,73	0,08	4,67	0,25	456	402,42	477	21,52	474	73,48	101	105	5
7,11	2,33	0,39	1,72	0,74	2119	18,47	2131	26,04	2123	27,94	0,13	1,58	7,10	2,33	0,39	1,72	0,74	2118	27,67	2131	31,26	2124	20,99	100	101	1
0,69	2,65	0,08	1,72	0,65	753	28,61	484	6,67	533	14,15	0,06	2,09	0,69	2,70	0,08	1,72	0,63	744	44,18	484	8,00	532	11,25	91	65	2
1,98	5,84	0,18	2,86	0,49	1230	68,13	1048	23,12	1108	63,16	0,08	5,23	1,97	5,96	0,18	2,86	0,48	1225	102,65	1048	27,74	1107	40,98	95	86	3
6,73	3,00	0,39	2,09	0,70	2044	25,44	2110	31,49	2075	40,31	0,13	2,22	6,71	3,05	0,39	2,09	0,69	2040	39,17	2109	37,79	2074	27,31	102	103	2
1,61	5,67	0,16	2,98	0,52	967	67,13	976	22,52	973	60,40	0,07	6,19	1,56	6,87	0,16	2,98	0,43	914	127,41	974	26,98	956	43,45	102	107	3
8,51	2,60	0,43	1,96	0,75	2270	47,46	2306	31,79	2285	35,24	0,14	1,72	8,50	2,61	0,43	1,96	0,75	2269	29,68	2306	38,17	2286	24,00	101	102	1
1,51	4,47	0,15	3,99	0,89	1043	27,10	891	27,76	935	78,81	0,07	2,06	1,51	4,49	0,15	3,99	0,89	1037	41,54	891	33,32	934	27,81	95	86	4
1,10	7,80	0,12	2,48	0,32	852	105,88	719	14,08	751	50,05	0,07	7,83	1,09	8,22	0,12	2,48	0,30	838	163,12	719	16,89	748	44,44	96	86	2
7,65	3,46	0,41	2,28	0,66	2174	60,64	2210	35,62	2189	49,07	0,14	2,63	7,64	3,48	0,41	2,28	0,65	2172	45,89	2210	42,76	2190	31,76	101	102	2
0,36	6,84	0,05	6,35	0,93	309	84,15	310	16,06	310	82,60	0,05	2,62	0,36	6,87	0,05	6,35	0,92	296	59,88	310	19,27	309	18,45	101	105	6
0,38	3,64	0,05	2,64	0,72	323	19,67	328	7,04	327	18,37	0,05	2,61	0,38	3,71	0,05	2,64	0,71	309	59,48	328	8,44	326	10,39	101	106	3
5,77	3,62	0,31	3,30	0,91	2142	17,30	1759	42,51	1940	76,84	0,13	1,49	5,76	3,62	0,31	3,30	0,91	2141	26,09	1759	51,04	1941	31,85	91	82	1

BPN-10A (Fm. Ponta Grossa)

SPOT	Grain Length	Grain Width	Length / width	Shape*	Roundness**	Zoning***	# of growth phases	f206c	^{207}Pb	^{206}Pb	U (µg g^{-1}) [a]	Th/U	$^{206}Pb/^{204}Pb$	$^{207}Pb/^{206}Pb$	2s (%)
1.sSMPABC005.TXT	145	55	2,64	elongated	rounded	irregular	2	0,02	33154,88	222625,98	136,52	0,27	775,03	0,15	1,24
1.sSMPABC006.TXT	141	57	2,47	elongated	sa-sr	oscillatory	2	0,07	3107,28	45466,67	73,59	0,26	231,44	0,07	2,41
1.sSMPABC008.TXT	77	46	1,67	oval	sa-sr	oscillatory	2	0,06	4446,00	69346,11	163,83	0,49	286,99	0,06	2,34
1.sSMPABC009.TXT	119	63	1,89	elongated	rounded	irregular	2	0,02	42132,87	246310,25	139,25	0,44	746,51	0,16	1,25
1.sSMPABC010.TXT	154	60	2,57	elongated	rounded	irregular	2	0,01	30643,26	174352,12	84,05	0,30	1052,10	0,17	2,77
1.sSMPABC011.TXT	134	45	2,98	elongated	rounded	irregular	2	0,05	9957,19	126722,78	356,54	0,08	348,58	0,06	2,53
1.sSMPABC012.TXT	115	58	1,98	elongated	rounded	oscillatory	2	0,02	26684,30	152629,26	77,73	0,10	762,80	0,17	2,15
1.sSMPABC014.TXT	115	56	2,05	elongated	rounded	oscillatory	1	0,04	8285,72	64479,84	43,37	0,75	364,56	0,13	2,29
1.sSMPABC015.TXT	101	56	1,80	oval	rounded	oscillatory	1	0,01	26047,57	171152,19	97,45	0,34	1128,11	0,15	1,41
1.sSMPABC017.TXT	91	46	1,98	elongated	sa-sr	homogeneous	1	0,05	34407,69	249644,14	448,16	0,37	350,32	0,07	4,16
1.sSMPABC019.TXT	99	55	1,80	oval (broken)	sa-sr	oscillatory	1	0,03	5735,35	73743,80	97,49	0,43	614,20	0,08	1,84
1.sSMPABC020.TXT	135	54	2,50	elongated	rounded	irregular	2	0,01	21896,03	179256,91	120,86	0,61	1326,13	0,12	1,59
1.sSMPABC025.TXT	92	47	1,96	elongated	rounded	irregular	2	0,01	80075,00	475088,51	289,10	0,43	1341,66	0,14	1,23
1.sSMPABC026.TXT	110	62	1,77	oval	rounded	irregular	1	0,03	7370,94	62643,72	50,44	0,65	504,72	0,12	2,94
1.sSMPABC027.TXT	96	64	1,50	oval	rounded	irregular	2	0,02	24004,95	195571,28	133,70	0,45	829,49	0,12	1,64
1.sSMPABC030.TXT	84	45	1,87	elongated	rounded	oscillatory	1	0,04	4813,42	73884,36	167,91	0,52	485,24	0,06	2,17
1.sSMPABC031.TXT	51	50	1,02	round (broken)	rounded	oscillatory	1	0,01	57382,72	346313,34	197,57	0,21	1753,59	0,16	1,21
1.sSMPABC032.TXT	102	57	1,79	oval	rounded	oscillatory	1	0,01	97001,13	558732,17	318,77	0,39	1878,54	0,16	1,46
1.sSMPABC033.TXT	80	54	1,48	oval	sa-sr	irregular	1	0,04	1381,12	22648,69	58,78	0,41	426,84	0,06	4,47
1.sSMPABC034.TXT	123	50	2,46	elongated	rounded	oscillatory	1	0,01	30045,41	268785,38	216,85	1,08	2015,02	0,11	2,47
1.sSMPABC035.TXT	121	63	1,92	elongated	rounded	irregular	2	0,02	23070,63	204800,27	166,37	0,41	863,32	0,11	1,53
1.sSMPABC040.TXT	116	63	1,84	elongated	rounded	irregular	1	0,01	20232,43	165779,43	114,30	0,38	1463,78	0,12	1,30
1.sSMPABC046.TXT	118	34	3,47	elongated	rounded	oscillatory	1	0,03	6537,27	69319,71	165,65	0,36	531,29	0,06	3,87
1.sSMPABC047.TXT	100	57	1,75	oval	sa-sr	irregular	1	0,01	64064,44	350925,06	211,59	1,14	1717,38	0,15	2,33
1.sSMPABC048.TXT	145	52	2,79	elongated	sa-sr	oscillatory	1	0,03	15122,08	177366,71	511,20	0,41	568,93	0,06	3,23
1.sSMPABC050.TXT	80	46	1,74	oval (broken)	euhedral	oscillatory	1	0,02	12450,39	166153,39	247,80	0,61	719,21	0,07	1,47
1.sSMPABC051.TXT	93	74	1,26	round	sa-sr	irregular	1	0,02	61025,44	479781,34	807,07	0,42	779,55	0,07	2,30
1.sSMPABC052.TXT	105	54	1,94	elongated	rounded	oscillatory	1	0,02	40173,45	255892,59	161,09	0,29	839,90	0,16	1,45
1.sSMPABC054.TXT	104	50	2,08	elongated	rounded	irregular	2	0,08	3830,78	48892,73	87,98	0,61	213,32	0,08	3,37
1.sSMPABC056.TXT	99	66	1,50	oval	rounded	irregular	2	0,01	14240,35	198712,57	334,52	0,43	1387,73	0,07	1,45
1.sSMPABC058.TXT	107	62	1,73	oval	rounded	oscillatory	1	0,03	99312,34	517691,87	292,02	0,43	551,35	0,16	5,10
1.sSMPABC059.TXT	92	60	1,53	oval	rounded	irregular	1	0,04	4952,92	60598,00	100,25	0,72	431,78	0,07	2,40
1.sSMPABC060.TXT	110	55	2,00	elongated (broken)	sa-sr	oscillatory	1	0,04	12345,86	101376,56	73,20	0,42	387,33	0,12	3,31
1.sSMPABC066.TXT	87	41	2,12	elongated	rounded	oscillatory	1	0,02	29055,90	229536,29	217,31	1,05	727,82	0,10	1,61
1.sSMPABC067.TXT	107	56	1,91	elongated	rounded	oscillatory, sector	2	0,02	15599,90	208254,32	373,13	0,55	723,36	0,07	1,60
1.sSMPABC070.TXT	137	59	2,32	elongated	rounded	irregular	2	0,08	50432,91	301613,21	583,05	0,48	212,62	0,07	2,90
1.sSMPABC071.TXT	84	56	1,50	oval	rounded	irregular	1	0,06	1997,94	31627,49	74,96	0,69	274,74	0,06	3,06
1.sSMPABC072.TXT	77	55	1,40	oval	sa-sr	irregular	1	0,02	41792,38	313675,97	253,70	0,25	714,83	0,11	3,36
1.sSMPABC074.TXT	94	56	1,68	oval (broken)	rounded	oscillatory	2	0,01	1243,17	15937,04	32,46	0,79	1557,59	0,07	4,65
1.sSMPABC075.TXT	135	49	2,76	elongated	rounded	oscillatory	2	0,14	5041,13	41151,11	153,16	0,25	130,36	0,06	5,06
1.sSMPABC076.TXT	73	56	1,30	oval	sa-sr	irregular	1	0,00	3302,21	46525,60	78,30	0,51	-5167,01	0,07	3,68
1.sSMPABC077.TXT	135	70	1,93	elongated	rounded	oscillatory	1	0,01	45874,90	263290,59	136,50	0,50	1360,26	0,17	1,27
1.sSMPABC078.TXT	96	70	1,37	oval	rounded	irregular	2	0,01	2945,22	42681,07	84,13	0,37	1180,99	0,07	2,51
1.sSMPABC079.TXT	100	51	1,96	elongated	rounded	oscillatory	1	0,02	47214,24	322060,66	305,75	0,32	751,21	0,10	2,18
1.sSMPABC080.TXT	98	48	2,04	elongated	rounded	oscillatory	1	0,06	6584,67	90563,62	235,34	0,49	314,97	0,06	3,23
1.sSMPABC086.TXT	68	50	1,36	oval	sa-sr	oscillatory, sector	1	0,02	1658,97	25293,12	66,34	0,57	819,72	0,06	4,12
1.sSMPABC088.TXT	120	44	2,73	elongated	rounded	irregular	1	0,02	4904,42	79833,48	183,68	0,48	809,39	0,06	1,96
1.sSMPABC089.TXT	145	72	2,01	elongated	sa-sr	irregular	1	0,08	1876,19	15443,15	11,03	1,57	184,05	0,12	4,00
1.sSMPABC091.TXT	136	70	1,94	elongated	rounded	irregular	1	0,03	6618,81	91467,20	158,17	0,86	591,57	0,07	2,11
1.sSMPABC092.TXT	112	67	1,67	oval	rounded	homogeneous	1	0,01	77120,69	628113,46	611,87	0,12	1172,85	0,10	1,43
1.sSMPABC093.TXT	94	56	1,68	oval	rounded	irregular	2	0,09	1205,70	14753,38	34,46	0,42	189,18	0,06	7,39
1.sSMPABC094.TXT	93	46	2,02	elongated	rounded	oscillatory	2	0,01	18058,87	105626,12	61,37	0,45	1133,64	0,16	2,19
1.sSMPABC095.TXT	102	52	1,96	elongated	sa-sr	irregular	1	0,01	115145,07	577046,90	352,48	0,54	2584,72	0,15	1,62
1.sSMPABC096.TXT	93	48	1,94	elongated	sa-sr	irregular	2	0,04	4274,69	55910,74	85,27	0,60	450,24	0,08	5,08
1.sSMPABC099.TXT	86	52	1,65	oval	sa-sr	oscillatory	2	0,03	6720,30	81546,84	148,39	0,55	552,64	0,07	19,21
1.sSMPABC107.TXT	130	63	2,06	elongated	rounded	oscillatory	1	0,00	98912,97	438959,61	210,92	0,60	2804,08	0,23	2,14
1.sSMPABC108.TXT	79	67	1,18	round	rounded	irregular	2	0,01	32414,97	209602,33	127,23	0,49	1628,39	0,16	1,53
1.sSMPABC110.TXT	113	55	2,05	elongated	sa-sr	irregular	1	0,02	8357,89	107084,89	164,95	0,80	698,72	0,08	10,10
1.sSMPABC112.TXT	136	57	2,39	elongated	rounded	oscillatory	1	0,01	9596,38	125014,22	217,41	0,64	1439,04	0,08	1,54
1.sSMPABC113.TXT	90	45	2,00	elongated	sa-sr	oscillatory, sector	2	0,03	1874,31	30080,58	65,92	0,71	541,74	0,06	3,52
1.sSMPABC115.TXT	147	75	1,96	elongated	rounded	irregular	1	0,05	4802,17	69367,63	209,37	0,50	359,45	0,06	2,81
1.sSMPABC116.TXT	116	55	2,11	elongated	rounded	irregular	2	0,07	8035,39	68932,52	138,19	0,47	236,62	0,07	7,22
1.sSMPABC118.TXT	101	69	1,46	oval	rounded	oscillatory	1	0,03	5018,53	81519,24	214,44	0,54	570,08	0,06	1,94
1.sSMPABC120.TXT	82	48	1,71	oval	sa-sr	oscillatory, sector	1	0,01	1392,41	18946,81	51,82	0,66	1341,37	0,06	5,14
1.sSMPABC125.TXT	73	58	1,26	round	sa-sr	oscillatory, sector	1	0,02	8483,96	68624,83	50,67	1,43	711,54	0,13	5,40
1.sSMPABC128.TXT	131	42	3,12	elongated	euhedral	oscillatory	1	0,04	3505,29	54541,13	149,07	0,60	453,17	0,06	2,74
1.sSMPABC129.TXT	118	57	2,07	elongated	sa-sr	irregular	1	0,14	6970,72	53202,98	153,65	0,62	131,78	0,06	9,93
1.sSMPABC131.TXT	57	50	1,14	round	rounded	irregular	2	0,03	55944,64	333672,45	315,67	0,23	509,02	0,10	3,38
1.sSMPABC133.TXT	87	57	1,53	oval	sa-sr	oscillatory	1	0,06	3526,35	40975,28	63,13	0,34	299,18	0,07	4,01
1.sSMPABC134.TXT	108	62	1,74	oval	sa-sr	oscillatory, sector	1	0,02	1641,68	25038,49	71,17	1,28	771,29	0,06	3,79
1.sSMPABC135.TXT	110	62	1,77	oval	sa-sr	irregular	1	0,02	2257,99	35973,97	94,53	0,36	1100,15	0,06	2,77
1.sSMPABC029.TXT	92	57	1,61	oval	rounded	oscillatory	1	0,05	9777,25	83292,55	153,51	0,50	382,58	0,07	3,41
1.sSMPABC117.TXT	67	47	1,43	oval	rounded	oscillatory	1	0,04	3877,15	49923,16	70,33	0,82	398,15	0,08	3,14
1.sSMPABC105.TXT	85	42	2,02	elongated	sa-sr	oscillatory	1	0,15	12760,50	99015,90	541,86	0,51	125,68	0,05	4,86
1.sSMPABC097.TXT	116	58	2,00	elongated	rounded	oscillatory	2	0,02	12067,30	120640,02	118,12	0,78	908,76	0,10	10,83
1.sSMPABC132.TXT	107	52	2,06	elongated	rounded	oscillatory	1	0,22	64983,51	256638,94	1274,58	0,67	82,58	0,05	8,07
1.sSMPABC007.TXT	124	57	2,18	elongated	sa-sr	irregular	2	0,19	23213,12	139747,90	688,44	0,57	96,83	0,05	11,52
1.sSMPABC057.TXT	131	59	2,22	elongated	euhedral	oscillatory	1	0,03	27535,12	224854,02	290,45	0,49	579,68	0,08	3,86
1.sSMPABC068.TXT	116	45	2,58	elongated	sa-sr	oscillatory	1	0,09	4639,37	53687,40	155,69	0,69	199,39	0,06	3,81
1.sSMPABC013.TXT	123	70	1,76	oval	sa-sr	irregular	2	0,09	6708,80	58664,10	310,11	1,08	202,34	0,05	9,51
1.sSMPABC106.TXT	74	42	1,76	oval	rounded	irregular	1	0,07	7979,45	80097,18	194,00	0,53	260,78	0,06	3,76
1.sSMPABC036.TXT	116	61	1,90	elongated	rounded	irregular	1	0,05	4623,36	59686,52	130,23	0,27	358,72	0,06	2,95
1.sSMPABC049.TXT	127	65	1,95	elongated	rounded	oscillatory	1	0,07	12360,38	136745,37	779,51	0,19	248,76	0,09	2,22
1.sSMPABC111.TXT	112	41	2,73	elongated	rounded	oscillatory	1	0,06	55042,78	397637,81	1008,99	0,19	301,95	0,06	2,28
1.sSMPABC085.TXT	63	44	1,43	oval	rounded	irregular	2	0,05	6599,73	84838,72	216,68	0,21	350,03	0,06	2,98
1.sSMPABC018.TXT	87	42	2,07	elongated	rounded	oscillatory	1	0,04	12708,43	139099,89	389,11	0,20	462,20	0,06	3,38
1.sSMPABC065.TXT	57	42	1,36	oval	rounded	oscillatory	2	0,04	17726,45	132005,37	92,49	0,59	393,66	0,13	8,97
1.sSMPABC087.TXT	93	52	1,79	oval	rounded	oscillatory	1	0,03	44295,27	334532,25	573,49	0,26	633,64	0,07	3,01
1.sSMPABC114.TXT	92	59	1,56	oval	sa-sr	irregular	1	0,05	34428,81	221698,66	413,38	0,25	349,86	0,07	4,37
1.sSMPABC037.TXT	102	53	1,92	elongated	rounded	irregular	1	0,11	9927,21	82207,49	182,02	0,54	159,73	0,06	10,92
1.sSMPABC038.TXT	123	70	1,76	oval	sa-sr	oscillatory	1	0,07	3287,53	45619,09	107,07	0,39	258,53	0,06	5,89
1.sSMPABC130.TXT	100	36	2,78	elongated	rounded	irregular	2	0,05	7134,08	86777,15	258,13	1,32	375,08	0,06	3,75
1.sSMPABC126.TXT	116	36	3,22	elongated	rounded	irregular	1	0,07	5369,00	70800,52	179,13	0,73	245,79	0,06	2,89
1.sSMPABC053.TXT	64	45	1,42	oval	sa-sr	irregular	1	0,02	19776,79	196931,05	289,21	0,24	820,95	0,07	2,21
1.sSMPABC127.TXT	73	47	1,55	oval	rounded	irregular	1	0,02	5196,31	73369,88	159,37	0,30	787,64	0,07	6,27
1.sSMPABC098.TXT	71	39	1,82	elongated	rounded	irregular	2	0,03	7491,64	87573,69	185,34	0,78	564,39	0,06	2,96
1.sSMPABC039.TXT	120	44	2,73	elongated	sa-sr	irregular	1	0,07	5417,92	62045,52	174,94	1,25	261,75	0,06	3,95
1.sSMPABC045.TXT	115	48	2,40	elongated	euhedral	oscillatory	1	0,08	3733,42	59841,04	175,87	0,40	232,70	0,06	4,21
1.sSMPABC073.TXT	135	49	2,76	elongated	rounded	irregular	2	0,04	52819,54	312208,60	582,34	0,21	459,50	0,07	2,96
1.sSMPABC055.TXT	97	57	1,70	oval	sa-sr	irregular	1	0,09	22477,52	190997,81	1015,86	0,63	200,78	0,05	4,32
1.sSMPABC016.TXT	93	52	1,79	oval	sa-sr	irregular	1	0,14	39541,11	213877,93	718,79	1,24	132,38	0,06	5,23

Ratios [b]						Dates [c]						Ratios [c]							Dates [d]								
$^{207}Pb/^{235}U$	2s (%)	$^{206}Pb/^{238}U$	2s (%)	Rho	$^{207}Pb/^{206}Pb$	2s abs	$^{206}Pb/^{238}U$	2s abs	$^{207}Pb/^{235}U$	2s abs	$^{207}Pb/^{206}Pb$	2s (%)	$^{207}Pb/^{235}U$	2s (%)	$^{206}Pb/^{238}U$	2s (%)	Rho	$^{207}Pb/^{206}Pb$	2s abs	$^{206}Pb/^{238}U$	2s abs	$^{207}Pb/^{235}U$	2s abs	% conc [e]	% conc [f]	% Error
8,12	5,53	0,40	5,38	0,97	2294	10,74	2191	50,20	2242	73,70	0,15	1,27	8,10	5,53	0,40	5,38	0,97	2292	21,82	2190	100,77	2243	51,28	98	96	1
1,41	4,09	0,15	3,30	0,81	830	25,37	921	14,16	894	23,57	0,07	2,61	1,40	4,20	0,15	3,30	0,78	810	54,55	920	28,32	888	25,19	104	114	3
0,91	3,97	0,11	3,20	0,81	702	25,14	645	9,83	657	18,21	0,06	2,50	0,90	4,06	0,11	3,20	0,79	684	53,30	645	19,66	653	19,74	99	94	3
9,36	4,56	0,43	4,38	0,96	2415	66,61	2326	42,91	2372	50,96	0,16	1,28	9,35	4,56	0,43	4,38	0,96	2414	21,70	2326	86,09	2372	42,73	98	96	1
12,24	6,70	0,52	6,10	0,91	2577	23,37	2683	67,26	2621	105,47	0,17	2,81	12,22	6,71	0,52	6,10	0,91	2576	46,97	2683	135,22	2622	65,06	102	104	2
0,69	3,95	0,09	3,03	0,77	527	16,83	538	7,82	535	14,91	0,06	2,67	0,69	4,04	0,09	3,03	0,75	511	58,66	537	15,63	532	16,86	101	105	3
11,55	5,15	0,49	4,68	0,91	2570	18,13	2566	49,69	2566	63,02	0,17	2,20	11,53	5,17	0,49	4,68	0,91	2569	36,70	2566	99,75	2567	49,45	100	100	1
6,44	4,40	0,37	3,76	0,85	2044	20,37	2033	32,82	2036	41,87	0,13	2,39	6,42	4,45	0,37	3,76	0,84	2039	42,23	2032	65,79	2035	39,87	100	100	2
9,02	3,73	0,44	3,45	0,93	2338	12,11	2342	33,95	2338	34,15	0,15	1,43	9,00	3,73	0,44	3,45	0,92	2336	24,45	2342	68,07	2338	34,69	100	100	1
1,20	6,46	0,13	4,93	0,76	837	49,81	790	18,37	802	46,30	0,07	4,38	1,20	6,60	0,13	4,93	0,75	824	91,44	790	36,78	799	37,16	99	96	5
1,99	3,46	0,19	2,92	0,85	1104	18,55	1117	15,00	1111	20,86	0,08	1,90	1,98	3,48	0,19	2,92	0,84	1098	37,96	1116	30,03	1110	23,80	101	102	3
6,14	3,52	0,37	3,14	0,89	1956	14,27	2034	27,41	1994	28,79	0,12	1,61	6,13	3,52	0,37	3,14	0,89	1955	28,73	2034	54,93	1994	31,24	102	104	1
8,00	6,08	0,40	5,96	0,98	2278	105,13	2182	55,37	2229	89,37	0,14	1,24	7,99	6,09	0,40	5,96	0,98	2276	21,36	2181	111,20	2230	56,46	98	96	1
4,98	5,80	0,31	5,00	0,86	1892	26,68	1750	38,45	1814	67,49	0,12	3,03	4,96	5,85	0,31	5,00	0,86	1888	54,61	1749	77,12	1813	50,69	96	93	3
6,12	4,78	0,37	4,49	0,94	1969	14,70	2017	38,99	1991	52,43	0,12	1,67	6,11	4,79	0,37	4,49	0,94	1966	29,81	2016	78,21	1991	42,69	101	103	2
0,98	5,39	0,11	4,93	0,92	755	23,09	677	15,87	694	36,71	0,06	2,25	0,98	5,42	0,11	4,93	0,91	745	47,64	676	31,76	692	27,59	98	91	5
9,39	3,28	0,44	3,05	0,93	2409	40,50	2339	29,98	2375	27,23	0,16	1,22	9,38	3,29	0,44	3,05	0,93	2409	20,78	2339	60,09	2376	30,60	98	97	1
9,32	3,52	0,43	3,20	0,91	2410	43,84	2324	31,33	2368	30,66	0,16	1,47	9,31	3,53	0,43	3,20	0,91	2409	25,00	2323	62,81	2369	32,86	98	96	1
0,81	5,66	0,10	3,47	0,61	615	49,06	598	9,92	601	24,08	0,06	4,67	0,80	5,82	0,10	3,47	0,60	603	101,02	598	19,84	599	26,65	100	99	3
4,75	5,72	0,31	5,16	0,90	1805	22,61	1752	39,70	1775	68,36	0,11	2,49	4,75	5,73	0,31	5,16	0,90	1804	45,23	1752	79,64	1776	49,21	99	97	3
4,76	3,49	0,31	3,13	0,90	1820	13,97	1743	23,97	1776	27,37	0,11	1,56	4,75	3,50	0,31	3,13	0,90	1817	28,33	1742	48,02	1776	29,80	98	96	2
6,10	2,98	0,37	2,68	0,90	1967	11,65	2014	23,21	1989	21,54	0,12	1,32	6,10	2,98	0,37	2,68	0,90	1966	23,46	2014	46,50	1990	26,37	101	102	1
0,87	6,84	0,10	5,64	0,82	651	50,81	633	17,03	636	47,87	0,06	4,00	0,87	6,92	0,10	5,64	0,82	641	86,05	632	34,09	634	33,16	100	99	5
8,21	5,30	0,41	4,76	0,90	2309	77,79	2196	44,49	2253	63,82	0,15	2,35	8,21	5,31	0,41	4,76	0,90	2308	40,31	2196	89,28	2254	49,25	97	95	2
0,69	6,13	0,09	5,21	0,85	542	37,89	532	13,32	534	35,47	0,06	3,34	0,69	6,19	0,09	5,21	0,84	532	73,09	532	26,66	532	25,95	100	100	5
1,75	2,96	0,17	2,57	0,87	1053	14,90	1015	12,09	1026	15,56	0,07	1,51	1,74	2,98	0,17	2,57	0,86	1048	30,41	1014	24,20	1025	19,43	99	97	2
1,38	6,04	0,14	5,59	0,92	917	58,56	864	22,62	878	54,01	0,07	2,35	1,37	6,06	0,14	5,59	0,92	911	48,42	864	45,32	877	36,24	98	95	5
8,69	3,10	0,40	2,74	0,88	2412	12,35	2189	25,48	2304	23,96	0,16	1,47	8,68	3,11	0,40	2,74	0,88	2410	25,05	2188	51,06	2305	28,74	95	91	1
1,53	5,58	0,14	4,45	0,80	1150	33,86	854	17,81	940	41,46	0,08	3,67	1,51	5,77	0,14	4,45	0,77	1133	73,09	853	35,64	935	35,85	91	75	4
1,49	5,00	0,15	4,78	0,96	967	14,91	909	20,30	926	39,85	0,07	1,47	1,49	5,00	0,15	4,78	0,96	964	30,07	909	40,66	925	30,83	98	94	4
9,61	7,49	0,44	5,49	0,73	2448	111,09	2340	54,04	2396	97,06	0,16	5,24	9,59	7,58	0,44	5,49	0,72	2446	88,61	2339	108,53	2396	72,24	98	96	4
1,48	4,70	0,15	4,04	0,86	937	36,79	917	17,28	922	32,48	0,07	2,50	1,47	4,75	0,15	4,04	0,85	928	51,35	917	34,60	920	29,15	100	99	4
5,92	6,83	0,35	5,97	0,87	1976	29,79	1954	50,52	1962	96,15	0,12	3,45	5,90	6,89	0,35	5,97	0,87	1970	61,43	1953	101,41	1961	61,70	100	99	3
3,52	4,72	0,26	4,44	0,94	1569	55,07	1506	29,87	1531	46,27	0,10	1,64	3,52	4,73	0,26	4,44	0,94	1565	30,79	1506	59,87	1531	38,10	98	96	2
1,48	2,99	0,14	2,53	0,84	1063	16,19	863	10,21	920	14,61	0,07	1,64	1,47	3,01	0,14	2,53	0,84	1057	33,03	863	20,44	919	18,38	94	82	2
1,11	4,41	0,12	3,32	0,75	817	25,44	736	11,56	756	22,66	0,07	3,16	1,09	4,58	0,12	3,32	0,72	795	66,17	736	23,13	750	24,59	98	92	3
0,95	4,43	0,11	3,20	0,72	719	32,86	664	10,10	676	20,38	0,06	3,27	0,94	4,58	0,11	3,20	0,70	701	69,70	664	20,20	672	22,75	99	95	3
4,74	6,71	0,31	5,81	0,87	1807	99,09	1746	44,58	1772	88,50	0,11	3,43	4,73	6,75	0,31	5,81	0,86	1804	62,41	1745	89,45	1772	58,19	99	97	3
1,12	6,03	0,13	3,84	0,64	781	35,56	759	13,77	764	32,79	0,07	4,70	1,12	6,07	0,12	3,84	0,63	778	98,81	759	27,56	764	33,11	99	98	4
0,50	6,05	0,07	3,32	0,55	441	19,19	407	6,55	412	18,04	0,05	5,88	0,49	6,75	0,07	3,32	0,49	395	131,77	407	13,09	405	22,79	100	103	3
1,51	5,46	0,15	4,03	0,74	969	38,04	920	17,28	934	36,61	0,07	3,67	1,51	5,45	0,15	4,03	0,74	970	74,90	920	34,60	934	33,83	98	95	4
11,98	3,24	0,50	2,98	0,92	2602	10,59	2604	31,97	2600	27,04	0,17	1,28	11,97	3,24	0,50	2,98	0,92	2601	21,32	2604	64,10	2602	30,83	100	100	1
1,25	4,29	0,13	3,47	0,81	911	26,09	794	12,99	825	24,40	0,07	2,55	1,25	4,31	0,13	3,47	0,81	907	52,55	794	26,00	824	24,61	96	88	3
3,48	5,27	0,26	4,79	0,91	1574	63,89	1486	31,89	1521	55,37	0,10	2,23	3,47	5,29	0,26	4,79	0,91	1571	41,79	1485	63,92	1520	42,56	98	95	3
0,82	5,53	0,10	4,49	0,81	625	33,54	605	12,98	609	30,93	0,06	3,42	0,81	5,65	0,10	4,49	0,80	608	74,04	605	25,97	605	26,08	100	99	4
0,82	5,53	0,10	3,69	0,67	625	27,49	605	10,67	609	25,33	0,06	4,22	0,82	5,60	0,10	3,69	0,66	618	90,99	605	21,34	608	25,94	100	98	4
0,96	4,57	0,11	4,13	0,90	668	21,10	690	13,52	684	26,44	0,06	2,00	0,96	4,59	0,11	4,13	0,90	661	42,90	689	27,07	683	23,08	101	104	4
6,16	6,99	0,36	5,73	0,82	1991	36,00	2005	49,53	1996	93,18	0,12	4,36	6,11	7,20	0,36	5,73	0,80	1981	77,60	2003	99,39	1992	64,83	101	101	4
1,51	4,63	0,15	4,12	0,89	1010	21,57	904	17,38	934	32,84	0,07	2,18	1,51	4,66	0,15	4,12	0,88	1004	44,17	903	34,79	933	28,82	97	90	4
3,44	3,07	0,26	2,71	0,88	1547	27,13	1490	18,04	1512	20,26	0,10	1,45	3,43	3,07	0,26	2,71	0,88	1545	27,33	1490	36,14	1512	24,47	99	96	2
0,95	9,29	0,11	5,64	0,61	702	61,88	670	17,98	677	59,21	0,06	8,15	0,94	9,91	0,11	5,64	0,57	676	174,14	670	35,97	671	49,84	100	99	5
9,47	8,02	0,44	7,71	0,96	2411	175,70	2354	76,48	2382	158,18	0,16	2,22	9,45	8,03	0,44	7,71	0,96	2409	37,76	2353	153,85	2383	76,50	99	98	2
8,17	7,74	0,40	7,57	0,98	2313	162,94	2183	70,45	2248	146,92	0,15	1,63	8,17	7,74	0,40	7,57	0,98	2312	28,01	2183	141,68	2250	72,57	97	94	1
1,82	7,44	0,17	5,43	0,73	1127	51,45	1018	25,63	1052	67,15	0,08	5,28	1,81	7,58	0,17	5,43	0,72	1119	105,31	1017	51,34	1050	50,82	97	91	5
1,34	19,58	0,14	3,78	0,19	887	81,06	854	15,15	862	79,63	0,07	19,83	1,33	20,19	0,14	3,78	0,19	879	410,30	854	30,33	861	124,47	99	97	4
17,18	5,40	0,55	4,96	0,92	3039	17,24	2809	56,71	2942	71,67	0,23	2,15	17,17	5,40	0,55	4,96	0,92	3039	34,44	2809	113,91	2944	53,23	95	92	1
9,35	3,35	0,43	2,98	0,89	2420	13,01	2318	29,07	2370	27,72	0,16	1,54	9,34	3,35	0,43	2,98	0,89	2419	26,14	2317	58,28	2372	31,25	98	96	1
1,86	10,61	0,17	3,26	0,31	1176	103,26	1016	15,33	1067	52,15	0,08	10,35	1,86	10,85	0,17	3,26	0,30	1171	204,88	1016	30,68	1066	74,26	95	87	3
1,63	4,37	0,15	4,09	0,94	1149	15,36	909	17,37	981	31,65	0,08	1,56	1,63	4,38	0,15	4,09	0,93	1146	30,94	909	34,78	980	27,91	93	79	4
1,06	6,51	0,12	5,48	0,84	732	37,72	732	18,99	731	49,49	0,06	3,64	1,05	6,58	0,12	5,48	0,83	723	77,16	732	38,02	729	34,81	100	101	5
0,70	5,56	0,09	4,79	0,86	570	32,84	535	12,31	541	30,45	0,06	2,96	0,70	5,63	0,09	4,79	0,85	555	64,58	534	24,64	538	23,82	99	96	5
1,15	8,24	0,13	3,98	0,48	824	44,30	762	14,31	778	41,92	0,07	7,80	1,14	8,75	0,13	3,98	0,45	805	163,20	762	28,64	773	48,48	99	95	4
0,87	3,34	0,10	2,72	0,81	695	20,81	617	8,01	633	13,38	0,06	2,00	0,86	3,38	0,10	2,72	0,81	686	42,74	617	16,03	632	16,02	98	90	3
0,80	6,45	0,10	3,90	0,60	627	31,09	588	10,96	595	29,10	0,06	5,21	0,80	6,51	0,10	3,90	0,60	623	112,45	588	21,93	595	29,73	99	94	4
6,24	7,46	0,36	5,14	0,69	2043	48,51	1979	43,96	2008	84,87	0,13	5,52	6,23	7,54	0,36	5,14	0,68	2040	97,56	1978	88,21	2008	68,23	99	97	5
0,81	6,28	0,10	5,65	0,90	633	46,31	595	16,09	603	43,42	0,06	2,86	0,81	6,33	0,10	5,65	0,89	622	61,61	595	32,20	601	29,11	99	96	5
0,71	10,76	0,09	4,15	0,39	603	41,34	533	10,63	546	39,95	0,06	11,48	0,70	12,21	0,09	4,15	0,34	563	250,19	532	21,26	538	52,32	99	94	4
3,59	6,58	0,26	5,64	0,86	1614	88,22	1501	37,90	1547	79,66	0,10	3,49	3,58	6,64	0,26	5,64	0,85	1609	65,09	1501	76,00	1546	54,10	97	93	4
1,76	5,13	0,17	3,19	0,62	1056	33,38	1016	15,00	1028	29,82	0,07	4,26	1,74	5,32	0,17	3,19	0,60	1043	85,87	1016	30,03	1024	34,90	99	97	3
0,78	5,02	0,09	3,29	0,66	617	22,47	574	9,04	583	20,58	0,06	3,88	0,77	5,09	0,09	3,29	0,65	610	83,88	574	18,08	581	22,76	99	94	3
0,91	4,25	0,10	3,23	0,76	766	29,45	623	9,59	654	19,42	0,06	2,81	0,90	4,28	0,10	3,23	0,75	761	59,35	623	19,20	654	20,85	95	82	3
1,20	26,53	0,13	26,31	0,99	1266	179,20	789	98,50	798	149,70	0,07	3,57	1,19	26,55	0,13	26,31	0,99	#¡NUM!	74,65	789	198,46	795	158,09	99	#¡NUM!	25
2,05	19,28	0,19	19,02	0,99	1178	31,32	1108	97,53	1131	977,54	0,08	3,27	2,04	19,30	0,19	19,02	0,99	1170	64,84	1107	196,49	1128	140,80	98	95	18
0,33	13,95	0,04	13,07	0,94	328	121,02	282	18,08	287	119,66	0,05	5,69	0,32	14,26	0,04	13,07	0,92	277	130,33	282	36,15	281	35,64	100	102	13
3,71	11,56	0,27	4,02	0,35	1643	104,05	1523	27,32	1573	78,53	0,10	11,03	3,71	11,74	0,27	4,02	0,34	1640	204,75	1523	54,76	1573	98,50	97	93	12
0,33	14,86	0,04	12,49	0,84	380	116,22	280	17,13	291	114,95	0,05	10,36	0,32	16,23	0,04	12,49	0,77	304	236,17	279	34,23	282	40,75	99	92	12
0,33	16,78	0,05	12,20	0,73	282	114,48	287	17,14	286	113,19	0,05	14,20	0,32	18,72	0,05	12,20	0,65	214	328,95	286	34,27	279	46,66	103	134	12
2,07	11,62	0,19	10,96	0,94	1179	252,93	1120	56,60	1139	246,51	0,08	3,97	2,07	11,66	0,19	10,96	0,94	1173	78,62	1120	113,68	1137	83,09	98	95	10
0,70	10,94	0,09	10,26	0,94	554	127,80	534	26,34	537	125,06	0,06	4,19	0,69	11,08	0,09	10,26	0,93	527	91,80	534	52,74	532	46,95	100	101	10
0,32	13,63	0,04	9,76	0,72	264	73,53	282	13,46	279	72,29	0,05	10,46	0,31	14,30	0,04	9,76	0,68	232	241,44	281	26,92	276	35,16	102	121	10
0,90	10,65	0,10	9,96	0,94	688	140,42	642	30,48	651	137,07	0,06	4,04	0,89	10,75	0,10	9,96	0,93	668	86,41	641	61,07	647	52,77	99	96	10
0,99	10,39	0,11	9,96	0,96	703	145,82	697	32,98	698	142,04	0,06	3,11	0,98	10,43	0,11	9,96	0,95	690	66,28	697	66,10	695	53,90	100	101	9
0,55	9,85	0,04	9,60	0,97	1421	21,39	281	13,21	446	91,03	0,09	2,40	0,55	9,89	0,04	9,60	0,97	1409	45,93	281	26,44	444	36,18	63	20	9
0,82	9,97	0,10	9,70	0,97	663	122,75	594	27,59	608	119,61	0,06	2,42	0,81	10,00	0,10	9,70	0,97	646	52,02	594	55,28	605	46,60	98	92	9
0,84	9,33	0,10	8,84	0,95	639	105,69	614	25,95	619	102,46	0,06	3,14	0,83	9,38	0,10	8,84	0,94	624	67,76	614	51,98	616	44,28	100	98	8
0,70	9,42	0,09	8,79	0,93	535	94,29	537	22,68	536	91,53	0,06	3,52	0,69	9,47	0,09	8,79	0,93	523	77,17	536	45,42	534	40,10	101	103	8
6,76	12,94	0,37	9,32	0,72	2151	80,53	2010	80,94	2078	262,65	0,13	9,33	6,74	13,19	0,37	9,32	0,71	2146	163,06	2009	162,86	2077	123,85	97	94	8
1,38	8,57	0,14	8,02	0,94	927	113,81	860	32,39	878	109,10	0,07	3,10	1,37	8,60	0,14	8,02	0,93	920	63,71	860	64,93	877	51,81	98	93	8
1,23	8,88	0,13	7,73	0,87	878	104,56	789	28,76	812	100,53	0,07	4,60	1,22	9,00	0,13	7,73	0,86	865	95,34	788	57,63	808	51,42	98	91	7
0,93	13,32	0,11	7,64	0,57	694	106,04	662	24,08	669	103,27	0,06	12,27	0,92	14,46	0,11	7,64	0,53	663	262,98	662	48,21	662	72,84	100	100	7
0,90	9,39	0,11	7,32	0,78	656	85,00	653	22,77	653	81,89	0,06	6,32	0,89	9,67	0,11	7,32	0,76	636	136,02	653	45,60	649	47,46	101	103	7
0,72	8,11	0,09	7,19	0,89	589	67,47	541	18,68	550	64,84	0,06	3,94	0,71	8,20	0,09	7,19	0,88	575	85,62	541	37,39	547	35,27	99	94	7
0,89	7,69	0,10	7,12	0,93	676	72,93	635	21,57	643	69,67	0,06	3,11	0,88	7,77	0,10	7,12	0,92	656	66,76	634	43,18	639	37,54	99	97	7
1,73	7,58	0,17	7,25	0,96	1044	101,87	1008	33,94	1019	96,05	0,07	2,26	1,72	7,60	0,17	7,25	0,95	1039	45,58	1008	68,04	1018	50,03	99	97	7
1,09	9,24	0,12	6,79	0,73	775	84,02	739	23,73	747	80,60	0,06	6,42	1,08	9,34	0,12	6,79	0,73	769	135,13	738	47,53	746	50,59	99	96	6
1,08	7,25	0,12	6,62	0,91	771	71,66	736	23,08	744	67,84	0,06	3,05	1,08	7,29	0,12	6,62	0,91	763	64,29	736	46,24	743	39,15	99	97	6
0,70	7,52	0,09	6,41	0,85	547	55,18	540	16,62	541	52,62	0,06	4,24	0,70	7,68	0,09	6,41	0,83	526	92,86	540	33,26	537	32,54	101	103	6
0,74	7,51	0,09	6,22	0,83	671	45,70	534	15,95	560	52,01	0,06	4,56	0,73	7,71	0,09	6,22	0,81	650	97,93	533	31,92	556	33,56	96	82	6
1,16	6,88	0,13	6,21	0,90	847	66,37	762	22,33	783	62,50	0,07	3,08	1,16	6,93	0,13	6,21	0,90	837	64,09	761	44,72	781	38,45	98	91	6
0,33	7,30	0,05	5,89	0,81	296	28,57	285	8,22	286	27,36	0,05	4,75	0,32	7,56	0,05	5,89	0,78	264	108,98	285	16,44	283	18,83	101	108	6
0,51	7,90	0,07	5,92	0,75	440	41,30	412	11,82	416	39,57	0,05	6,06	0,50	8,47	0,07	5,92	0,70	395	135,95	411	23,64	409	28,92	101	104	6

BPN-11A (Fm. São Domingos)

SPOT	Grain Length	Grain Width	Length / width	Shape*	Roundness**	Zoning***	# of growth phases	f206c	^{207}Pb	^{206}Pb	U (µg g^{-1}) #	Th/U	$^{206}Pb/^{204}Pb$	$^{207}Pb/^{206}Pb$	2s (%)
1.sSMPABC133.TXT	56	48	1,17	round	sa-sr	irregular	1	0,01	29627,37	238290,06	235,32	0,26	1211,24	0,09	2,08
1.sSMPABC134.TXT	83	72	1,15	round	rounded	irregular	1	0,04	5566,83	79144,47	159,43	0,27	472,26	0,07	3,75
1.sSMPABC135.TXT	124	48	2,58	elongated	rounded	oscillatory	1	0,07	3619,81	52577,10	175,91	0,41	266,41	0,05	8,20
1.sSMPABC136.TXT	193	58	3,33	elongated	rounded	oscillatory	1	0,03	30230,35	205159,98	111,43	0,29	573,40	0,14	1,34
1.sSMPABC138.TXT	119	72	1,65	oval	rounded	irregular	2	0,04	3824,62	52975,95	101,69	0,55	409,71	0,06	5,02
1.sSMPABC139.TXT	190	92	2,07	elongated	rounded	oscillatory	1	0,06	4161,40	56911,09	85,53	0,51	264,60	0,07	3,33
1.sSMPABC140.TXT	184	72	2,56	elongated	rounded	irregular	2	0,01	73965,68	490335,42	265,82	0,27	2658,37	0,15	1,19
1.sSMPABC145.TXT	130	59	2,20	elongated	rounded	irregular	2	0,01	43591,35	328173,18	389,53	0,20	2242,50	0,08	2,37
1.sSMPABC146.TXT	77	60	1,28	round	sa-sr	oscillatory	2	0,02	16243,13	175957,60	335,54	0,12	1047,55	0,06	4,60
1.sSMPABC148.TXT	204	60	3,40	elongated	rounded	irregular	1	0,05	2332,23	37285,60	81,84	0,35	367,94	0,06	3,56
1.sSMPABC149.TXT	176	59	2,98	elongated	rounded	irregular	1	0,01	69326,80	413558,52	346,96	0,25	2039,23	0,10	2,05
1.sSMPABC150.TXT	154	82	1,88	elongated	rounded	oscillatory	2	0,01	30080,89	206790,32	177,72	0,38	1546,90	0,09	2,49
1.sSMPABC151.TXT	164	72	2,28	elongated	rounded	irregular	2	0,01	69994,20	440090,69	300,18	0,23	1886,07	0,11	2,23
1.sSMPABC152.TXT	115	64	1,80	oval	euhedral	irregular	2	0,03	6888,58	111458,85	259,06	0,60	703,83	0,06	2,37
1.sSMPABC153.TXT	162	58	2,79	elongated	rounded	irregular	1	0,04	1615,61	26703,48	65,49	0,45	475,72	0,06	4,48
1.sSMPABC154.TXT	144	58	2,48	elongated	rounded	irregular	1	0,07	3062,63	50320,83	116,76	0,20	250,60	0,06	2,68
1.sSMPABC155.TXT	159	67	2,37	elongated	rounded	oscillatory	2	0,01	25273,82	192681,97	132,36	0,46	1776,34	0,13	1,36
1.sSMPABC156.TXT	148	66	2,24	elongated	sa-sr	oscillatory	1	0,01	42465,67	325255,04	215,64	0,32	1629,46	0,13	1,23
1.sSMPABC157.TXT	122	76	1,61	oval	sa-sr	irregular	1	0,01	52247,04	339994,58	293,15	0,40	1749,93	0,09	2,09
1.sSMPABC158.TXT	152	83	1,83	elongated	sa-sr	oscillatory	1	0,01	14856,61	106614,72	57,13	0,38	2187,91	0,15	1,37
1.sSMPABC159.TXT	134	61	2,20	elongated	rounded	irregular	1	0,01	26595,20	200545,18	114,52	0,23	1246,70	0,14	1,14
1.sSMPABC160.TXT	163	69	2,36	elongated	sa-sr	irregular	1	0,01	22438,97	145706,83	80,23	0,49	1433,39	0,15	1,42
1.sSMPABC165.TXT	122	71	1,72	oval	sa-sr	irregular	1	0,01	24265,88	152033,03	76,32	0,94	1016,02	0,16	1,35
1.sSMPABC166.TXT	140	62	2,26	elongated	rounded	oscillatory	2	0,01	70736,59	441815,82	223,14	0,41	2067,58	0,16	1,24
1.sSMPABC167.TXT	165	62	2,66	elongated	rounded	irregular	1	0,04	9452,72	145034,36	503,32	0,18	476,67	0,05	2,81
1.sSMPABC169.TXT	193	54	3,57	elongated	rounded	oscillatory	1	0,05	6843,83	102541,12	364,95	0,65	393,00	0,05	2,43
1.sSMPABC171.TXT	131	63	2,08	elongated	rounded	irregular	2	0,02	41104,33	232967,26	117,09	0,33	886,64	0,17	1,78
1.sSMPABC172.TXT	182	66	2,76	elongated	sa-sr	irregular	1	0,15	1077,30	16668,77	33,11	0,38	118,90	0,06	5,86
1.sSMPABC173.TXT	128	74	1,73	oval	rounded	oscillatory	2	0,04	5183,07	85653,72	211,98	0,11	473,85	0,06	2,62
1.sSMPABC174.TXT	132	57	2,32	elongated	rounded	oscillatory	1	0,01	40465,30	255969,06	151,44	0,34	1523,17	0,16	1,72
1.sSMPABC175.TXT	122	58	2,10	elongated	rounded	oscillatory	1	0,01	61169,00	264517,20	109,64	0,30	1855,16	0,21	1,44
1.sSMPABC176.TXT	161	67	2,40	elongated	sa-sr	homogeneous	2	0,06	1097,98	18341,35	39,48	0,37	303,14	0,06	7,40
1.sSMPABC177.TXT	113	68	1,66	oval	rounded	oscillatory, sector	1	0,01	14509,61	109913,14	61,56	0,60	1028,04	0,14	1,55
1.sSMPABC178.TXT	107	80	1,34	oval	sa-sr	irregular	1	0,01	8812,27	50478,22	22,39	0,32	933,99	0,19	1,88
1.sSMPABC179.TXT	123	75	1,64	oval	rounded	oscillatory	1	0,02	28850,56	163512,18	86,73	0,29	903,53	0,18	1,30
1.sSMPABC180.TXT	155	70	2,21	elongated	sa-sr	oscillatory	2	0,05	28971,05	201869,71	206,15	0,53	362,18	0,08	3,19
1.sSMPABC185.TXT	98	70	1,40	oval	rounded	homogeneous	1	0,16	428,48	4960,98	10,16	0,05	110,53	0,06	15,85
1.sSMPABC186.TXT	127	55	2,31	elongated	euhedral	oscillatory	1	0,05	2895,18	53618,10	167,46	0,55	379,20	0,06	4,39
1.sSMPABC187.TXT	129	62	2,08	elongated	rounded	irregular	2	0,02	9044,59	71321,68	43,79	0,25	993,91	0,13	2,44
1.sSMPABC188.TXT	119	68	1,75	oval	rounded	irregular	1	0,02	36969,99	240586,76	250,56	0,30	954,94	0,08	2,47
1.sSMPABC189.TXT	128	72	1,78	oval	rounded	oscillatory	1	0,01	41305,39	330926,59	302,78	0,21	1766,97	0,09	1,96
1.sSMPABC190.TXT	97	44	2,20	elongated	rounded	oscillatory	2	0,01	47798,21	370235,71	467,82	0,25	1562,99	0,08	2,01
1.sSMPABC191.TXT	119	65	1,83	elongated	sa-sr	irregular	2	0,03	6117,70	90708,80	191,39	0,19	610,69	0,07	2,42
1.sSMPABC192.TXT	173	52	3,33	elongated	rounded	oscillatory	1	0,02	1902,83	47459,47	113,79	0,50	911,30	0,06	3,13
1.sSMPABC193.TXT	110	50	2,20	elongated	rounded	oscillatory	2	0,01	4799,58	67435,71	133,93	0,34	1221,05	0,07	2,38
1.sSMPABC194.TXT	157	75	2,09	elongated	rounded	oscillatory	1	0,06	1727,50	26417,93	67,94	0,73	309,29	0,07	4,08
1.sSMPABC195.TXT	68	61	1,11	round	rounded	oscillatory	1	0,04	5179,97	77878,03	257,50	0,47	419,02	0,06	5,95
1.sSMPABC196.TXT	109	73	1,49	oval	rounded	oscillatory	2	0,01	39378,10	228941,14	104,68	0,47	2224,36	0,18	1,38
1.sSMPABC197.TXT	225	60	3,75	elongated	rounded	oscillatory	2	0,01	18271,03	158590,56	175,54	0,20	1950,04	0,08	2,15
1.sSMPABC198.TXT	147	68	2,16	elongated	sa-sr	oscillatory, sector	1	0,00	21394,46	158758,94	91,17	0,21	3301,67	0,13	1,26
1.sSMPABC199.TXT	156	79	1,97	elongated	rounded	homogeneous	1	0,02	6995,25	102287,04	140,67	0,57	1054,73	0,07	2,04
1.sSMPABC200.TXT	120	58	2,07	elongated	rounded	irregular	1	0,02	43638,77	352662,88	546,59	0,33	1128,22	0,07	3,04
1.sSMPABC205.TXT	119	66	1,80	oval	rounded	irregular	1	0,05	5270,27	74123,75	123,80	0,42	364,90	0,07	3,35
1.sSMPABC207.TXT	160	53	3,02	elongated	rounded	irregular	1	0,15	1334,26	21595,37	49,12	0,84	120,61	0,06	6,04
1.sSMPABC208.TXT	184	82	2,24	elongated	sa-sr	oscillatory	2	0,03	14121,39	107088,65	69,40	0,63	558,53	0,13	1,76
1.sSMPABC209.TXT	114	72	1,58	oval	rounded	oscillatory	2	0,01	15651,56	126435,73	90,48	0,62	1355,99	0,12	3,21
1.sSMPABC212.TXT	90	69	1,30	oval	rounded	oscillatory	2	0,04	5433,47	82787,08	140,52	0,31	470,32	0,07	2,49
1.sSMPABC213.TXT	99	69	1,43	oval	rounded	oscillatory	2	0,01	49159,21	278013,98	121,90	0,40	1483,68	0,19	1,15
1.sSMPABC214.TXT	135	75	1,80	oval	rounded	oscillatory	1	0,00	3965,63	36864,33	25,99	1,10	-3711,00	0,11	2,71
1.sSMPABC215.TXT	127	62	2,05	elongated	rounded	irregular	2	0,04	3229,34	52380,36	106,54	0,19	428,26	0,06	2,74
1.sSMPABC216.TXT	120	63	1,90	elongated	sa-sr	irregular	1	0,01	35932,37	265521,88	149,45	0,61	1862,62	0,14	1,26
1.sSMPABC217.TXT	83	56	1,48	oval	rounded	oscillatory	1	0,04	3451,89	57161,00	136,41	0,39	434,19	0,06	2,55
1.sSMPABC219.TXT	133	76	1,75	oval	rounded	oscillatory	2	0,02	24024,02	182122,76	104,15	0,64	901,97	0,14	1,22
1.sSMPABC220.TXT	135	61	2,21	elongated	rounded	irregular	1	0,05	5878,07	69540,06	75,29	0,44	344,23	0,08	2,12
1.sSMPABC225.TXT	124	55	2,25	elongated	rounded	irregular	2	0,01	5519,54	55340,75	69,25	0,12	1856,36	0,08	3,67
1.sSMPABC226.TXT	134	75	1,79	oval	rounded	oscillatory	1	0,04	4494,86	66768,94	117,77	1,02	462,96	0,07	2,40
1.sSMPABC228.TXT	122	66	1,85	elongated	rounded	oscillatory	1	0,01	18328,81	134462,02	146,90	0,53	1326,22	0,08	2,81
1.sSMPABC229.TXT	132	65	2,03	elongated	sa-sr	oscillatory, sector	2	0,03	11728,38	81300,75	41,78	0,39	566,00	0,16	1,57
1.sSMPABC230.TXT	126	66	1,91	elongated	rounded	oscillatory	2	0,07	2619,90	40842,28	152,30	0,62	265,30	0,05	3,72
1.sSMPABC231.TXT	145	83	1,75	oval	rounded	oscillatory	1	0,06	2605,70	40398,55	95,02	2,36	303,15	0,06	4,23
1.sSMPABC233.TXT	108	90	1,20	round	rounded	irregular	1	0,04	2401,97	38304,06	83,83	0,75	487,00	0,06	3,65
1.sSMPABC234.TXT	146	65	2,25	elongated	rounded	oscillatory	2	0,02	20245,61	162894,65	105,73	0,28	908,60	0,12	1,65
1.sSMPABC235.TXT	147	79	1,86	elongated	rounded	oscillatory	1	0,02	13273,86	100106,69	56,07	0,53	706,29	0,14	6,72
1.sSMPABC236.TXT	167	63	2,65	elongated	rounded	oscillatory	1	0,02	9230,31	111882,66	120,93	0,38	687,72	0,08	1,88
1.sSMPABC238.TXT	160	73	2,19	elongated	rounded	oscillatory	1	0,00	22470,40	167975,58	147,91	0,45	6399,21	0,09	2,42
1.sSMPABC239.TXT	110	54	2,04	elongated	rounded	oscillatory	1	0,00	2557,89	40364,91	85,18	0,47	14711,47	0,06	2,72
1.sSMPABC240.TXT	123	78	1,58	oval	rounded	oscillatory	1	0,03	15166,22	123155,90	88,14	0,61	494,78	0,12	2,47
1.sSMPABC245.TXT	151	74	2,04	elongated	sa-sr	oscillatory	1	0,01	11226,02	83848,44	46,81	0,34	2020,76	0,13	1,54
1.sSMPABC246.TXT	106	61	1,74	oval	sa-sr	oscillatory	1	0,01	6783,23	101639,82	236,35	0,31	3055,98	0,06	2,23
1.sSMPABC247.TXT	124	70	1,77	oval	rounded	oscillatory	2	0,01	24621,73	190360,64	127,16	0,47	2677,67	0,13	1,41
1.sSMPABC248.TXT	117	58	2,02	elongated	rounded	irregular	1	0,03	40908,82	231895,53	252,24	0,61	493,23	0,08	3,12
1.sSMPABC249.TXT	166	60	2,77	elongated	rounded	oscillatory	2	0,03	3191,24	46617,18	76,45	0,88	645,77	0,07	2,68
1.sSMPABC250.TXT	118	75	1,57	oval	rounded	oscillatory, sector	2	0,06	1682,29	23831,94	54,60	0,50	277,21	0,06	6,31
1.sSMPABC251.TXT	145	80	1,81	elongated	rounded	oscillatory	1	0,01	14779,88	191550,01	253,64	0,12	1923,19	0,07	1,53
1.sSMPABC252.TXT	160	77	2,08	elongated	rounded	oscillatory	2	0,02	5943,14	82578,62	123,24	0,37	1012,48	0,07	2,23
1.sSMPABC253.TXT	98	63	1,56	oval	rounded	oscillatory	2	0,00	29974,38	248114,26	157,22	0,60	50299,60	0,12	1,26
1.sSMPABC254.TXT	217	61	3,56	elongated	rounded	oscillatory	2	0,01	16140,11	118032,12	64,35	0,41	1103,79	0,14	1,39
1.sSMPABC255.TXT	152	68	2,24	elongated	sa-sr	irregular	1	0,01	42856,93	318763,94	193,33	0,37	1585,92	0,13	1,68
1.sSMPABC258.TXT	137	56	2,45	elongated	rounded	oscillatory	2	0,04	5611,18	93712,86	248,49	0,08	456,52	0,06	2,20
1.sSMPABC259.TXT	152	56	2,71	elongated	rounded	oscillatory	2	0,02	7946,48	125024,30	320,09	0,65	849,49	0,06	1,74
1.sSMPABC260.TXT	134	72	1,86	elongated	rounded	oscillatory	2	0,03	4382,57	63389,71	100,74	0,23	540,75	0,07	2,31
1.sSMPABC265.TXT	212	66	3,21	elongated	rounded	oscillatory	1	0,06	2450,35	39319,93	102,74	1,17	312,82	0,06	3,07
1.sSMPABC266.TXT	133	69	1,93	elongated	sa-sr	oscillatory	1	0,02	17098,48	251992,85	686,93	0,34	1043,67	0,06	2,23
1.sSMPABC227.TXT	110	68	1,62	oval	rounded	irregular	1	0,02	29146,14	208619,29	385,93	0,18	732,80	0,06	3,65
1.sSMPABC237.TXT	130	69	1,88	elongated	rounded	irregular	1	0,05	6443,41	98397,20	287,81	0,22	384,26	0,07	2,36
1.sSMPABC206.TXT	116	69	1,68	oval	rounded	oscillatory	1	0,04	16046,84	120402,55	299,35	0,60	440,60	0,06	4,22
1.sSMPABC147.TXT	192	77	2,49	elongated	rounded	irregular	1	0,13	344,00	5895,73	16,69	0,96	140,79	0,06	30,43
1.sSMPABC170.TXT	124	62	2,00	elongated	rounded	irregular	1	0,03	31177,06	200467,70	391,11	0,61	676,76	0,06	5,55
1.sSMPABC137.TXT	151	92	1,64	oval	rounded	irregular	1	0,04	7934,43	116329,50	556,82	0,53	445,12	0,05	3,08
1.sSMPABC257.TXT	99	70	1,41	oval	rounded	irregular	2	0,01	107276,34	851825,71	1353,00	0,46	2616,68	0,07	1,88
1.sSMPABC211.TXT	124	89	1,39	oval	rounded	homogeneous	1	-0,01	905,56	11838,53	10,27	0,73	-1160,61	0,10	5,42
1.sSMPABC168.TXT	79	50	1,58	oval	rounded	irregular	1	0,04	11250,45	142218,53	739,50	0,45	465,82	0,05	2,94
1.sSMPABC232.TXT	125	71	1,76	oval	sa-sr	oscillatory	2	0,01	6293,10	56174,13	49,68	0,59	1243,11	0,11	2,47
1.sSMPABC256.TXT	140	67	2,09	elongated	rounded	irregular	2	0,01	31322,04	245397,37	185,25	0,47	1348,92	0,13	1,18

Ratios [b]					Dates [c]						Ratios [c]							Dates [d]								
$^{207}Pb/^{235}U$	2s (%)	$^{206}Pb/^{238}U$	2s (%)	Rho	$^{207}Pb/^{206}Pb$	2s abs	$^{206}Pb/^{238}U$	2s abs	$^{207}Pb/^{235}U$	2s abs	$^{207}Pb/^{206}Pb$	2s (%)	$^{207}Pb/^{235}U$	2s (%)	$^{206}Pb/^{238}U$	2s (%)	Rho	$^{207}Pb/^{206}Pb$	2s abs	$^{206}Pb/^{238}U$	2s abs	$^{207}Pb/^{235}U$	2s abs	% conc[e]	% conc[f]	% Error
2,76	3,83	0,23	3,22	0,84	1325	73,64	1357	32,87	1343	65,89	0,09	2,11	2,75	3,85	0,23	3,22	0,84	1322	40,92	1357	39,46	1343	29,07	101	103	3
1,13	5,13	0,12	3,51	0,68	889	52,47	724	20,07	765	61,20	0,07	3,89	1,12	5,24	0,12	3,51	0,67	880	80,51	724	24,08	763	28,51	95	82	3
0,53	8,64	0,07	2,71	0,31	384	39,10	441	9,64	431	37,90	0,05	8,80	0,52	9,21	0,07	2,71	0,29	361	198,50	440	11,57	428	32,67	103	122	3
8,72	2,09	0,44	1,61	0,77	2271	36,22	2353	26,46	2308	24,74	0,14	1,37	8,70	2,11	0,44	1,61	0,76	2269	23,64	2353	31,76	2308	19,43	102	104	1
1,07	5,85	0,12	2,99	0,51	696	54,40	752	17,73	737	51,43	0,06	5,25	1,06	6,04	0,12	2,99	0,50	684	112,07	752	21,27	735	32,09	102	110	3
1,57	3,85	0,16	1,93	0,50	974	45,92	952	14,28	958	30,31	0,07	3,56	1,56	4,05	0,16	1,93	0,48	959	72,75	951	17,13	953	25,36	100	99	2
8,98	2,35	0,44	2,02	0,86	2320	13,71	2355	33,37	2334	33,80	0,15	1,20	8,98	2,35	0,44	2,02	0,86	2320	20,58	2355	40,06	2336	21,73	101	102	1
2,03	4,40	0,19	3,71	0,84	1124	84,93	1127	32,04	1125	78,66	0,08	2,39	2,03	4,41	0,19	3,71	0,84	1122	47,67	1127	38,47	1125	30,46	100	100	3
1,06	5,61	0,12	3,22	0,57	708	58,07	742	18,81	733	54,94	0,06	4,68	1,06	5,67	0,12	3,22	0,57	704	99,51	742	22,58	732	30,05	101	105	3
0,92	4,14	0,11	2,11	0,51	656	51,77	665	11,12	663	26,93	0,06	3,74	0,91	4,29	0,11	2,11	0,49	643	80,43	665	13,34	660	21,05	101	103	2
3,53	4,28	0,27	3,76	0,88	1555	101,78	1517	42,49	1532	92,48	0,10	2,06	3,52	4,29	0,27	3,76	0,88	1554	38,71	1517	51,02	1532	34,50	99	98	2
3,45	3,58	0,26	2,57	0,72	1522	58,01	1512	28,90	1515	50,29	0,09	2,52	3,45	3,60	0,26	2,57	0,71	1521	47,46	1512	34,70	1515	28,70	100	99	3
5,29	5,31	0,33	4,82	0,91	1874	175,26	1861	65,26	1865	162,66	0,11	2,24	5,28	5,32	0,33	4,82	0,91	1872	40,48	1861	78,39	1866	46,44	100	99	2
0,86	3,12	0,10	2,03	0,65	634	34,38	629	10,13	630	21,01	0,06	2,43	0,86	3,16	0,10	2,03	0,64	627	52,40	629	12,16	628	14,94	100	100	2
0,80	4,95	0,10	2,11	0,43	589	66,10	598	10,04	595	27,73	0,06	4,65	0,79	5,11	0,10	2,11	0,41	578	101,07	598	12,05	593	23,21	101	103	2
0,84	3,19	0,10	1,73	0,54	588	20,08	630	8,67	620	18,12	0,06	2,88	0,83	3,36	0,10	1,73	0,52	566	62,70	630	10,40	616	15,64	102	111	2
6,18	2,87	0,35	2,53	0,88	2088	15,97	1919	35,12	2000	47,88	0,13	1,37	6,18	2,88	0,35	2,53	0,88	2087	24,04	1919	42,17	2001	25,46	96	92	1
6,38	2,50	0,36	2,17	0,87	2081	14,54	1979	30,95	2027	36,66	0,13	1,24	6,37	2,51	0,36	2,17	0,87	2080	21,91	1979	37,16	2028	22,23	98	95	1
3,41	5,86	0,26	5,47	0,93	1523	200,65	1495	61,16	1505	191,10	0,09	2,11	3,40	5,87	0,26	5,47	0,93	1521	39,71	1495	73,46	1505	47,11	99	98	3
9,11	2,06	0,45	1,54	0,75	2314	34,89	2390	25,64	2347	23,66	0,15	1,38	9,10	2,07	0,45	1,54	0,74	2313	23,74	2390	30,78	2348	19,10	102	103	1
7,94	1,88	0,42	1,49	0,79	2192	31,61	2259	23,68	2222	20,94	0,14	1,16	7,93	1,89	0,42	1,49	0,79	2191	20,11	2259	28,42	2223	17,14	102	103	1
9,06	2,16	0,43	1,62	0,75	2369	16,29	2316	26,30	2342	25,63	0,15	1,44	9,05	2,17	0,43	1,62	0,75	2368	24,56	2316	31,57	2343	20,00	99	98	1
10,31	2,00	0,47	1,47	0,74	2432	15,31	2501	25,48	2461	22,48	0,16	1,37	10,30	2,01	0,47	1,47	0,73	2431	23,17	2500	30,58	2462	18,77	102	103	1
10,28	2,95	0,47	2,68	0,91	2438	14,05	2488	46,29	2458	55,28	0,16	1,25	10,27	2,96	0,47	2,68	0,91	2437	21,12	2488	55,58	2460	27,74	101	102	1
0,51	6,21	0,07	5,54	0,89	397	84,99	424	18,95	419	82,85	0,05	2,92	0,51	6,26	0,07	5,54	0,88	384	65,61	424	22,74	417	21,65	101	110	5
0,50	3,08	0,07	1,89	0,61	388	15,29	413	6,31	409	13,92	0,05	2,55	0,49	3,17	0,07	1,89	0,60	372	57,36	413	7,57	406	10,69	102	111	2
11,39	3,69	0,47	3,24	0,88	2603	19,94	2497	56,06	2554	82,13	0,17	1,81	11,38	3,71	0,47	3,24	0,87	2602	30,18	2496	67,33	2555	35,21	98	96	1
1,06	6,66	0,12	3,16	0,48	742	84,85	729	18,18	731	58,18	0,06	6,87	1,03	7,57	0,12	3,16	0,42	701	146,35	728	21,80	721	39,83	101	104	3
0,79	5,99	0,10	5,39	0,90	602	38,20	591	25,41	593	103,43	0,06	2,72	0,79	6,03	0,10	5,39	0,89	591	58,93	591	30,50	591	27,39	100	100	5
8,68	3,25	0,40	2,76	0,85	2420	19,60	2177	42,57	2302	60,17	0,16	1,74	8,67	3,26	0,40	2,76	0,85	2419	29,49	2177	51,12	2304	30,10	94	90	1
15,84	2,90	0,56	2,51	0,87	2872	71,34	2860	48,52	2864	52,30	0,21	1,46	15,82	2,90	0,56	2,51	0,87	2872	23,66	2860	58,26	2866	28,10	100	100	1
0,93	7,84	0,11	2,60	0,33	647	50,15	676	13,90	669	48,19	0,06	7,85	0,92	8,27	0,11	2,60	0,31	630	169,21	676	16,67	665	41,18	102	107	2
8,32	2,38	0,43	1,80	0,76	2237	41,97	2299	29,11	2264	30,23	0,14	1,57	8,30	2,39	0,43	1,80	0,75	2235	27,22	2299	34,94	2265	21,91	102	103	1
14,04	2,70	0,54	1,93	0,72	2718	52,10	2799	36,63	2750	37,05	0,19	1,91	14,03	2,71	0,54	1,93	0,71	2717	31,47	2799	43,98	2751	26,06	102	103	1
10,81	2,19	0,45	1,77	0,80	2606	14,53	2386	29,41	2504	28,56	0,17	1,32	10,79	2,21	0,45	1,77	0,80	2605	22,03	2385	35,31	2505	20,71	95	92	1
2,58	5,52	0,22	4,51	0,82	1315	133,56	1282	43,81	1293	126,18	0,08	3,34	2,56	5,61	0,22	4,51	0,80	1306	64,88	1281	52,58	1290	41,83	99	98	5
0,97	16,32	0,11	3,90	0,24	683	113,63	693	21,38	690	111,60	0,06	18,85	0,95	19,25	0,11	3,90	0,20	637	405,64	692	25,63	679	100,12	102	109	4
0,59	6,42	0,08	4,67	0,73	451	72,56	473	17,80	469	70,34	0,06	4,61	0,58	6,57	0,08	4,67	0,71	435	102,72	473	21,35	466	24,86	101	109	5
6,71	3,61	0,39	2,66	0,74	2042	29,05	2107	39,96	2073	59,46	0,13	2,48	6,70	3,64	0,39	2,66	0,73	2040	43,81	2107	47,98	2073	32,64	102	103	2
2,47	10,23	0,21	9,93	0,97	1294	706,95	1246	94,39	1263	700,62	0,08	2,51	2,47	10,24	0,21	9,93	0,97	1291	48,89	1246	113,42	1262	76,79	99	97	4
3,17	2,85	0,25	2,07	0,73	1456	40,46	1445	22,43	1449	33,68	0,09	1,98	3,17	2,87	0,25	2,07	0,72	1455	37,61	1445	26,92	1449	22,36	100	99	3
1,86	3,35	0,18	2,68	0,80	1083	47,89	1060	21,85	1066	42,61	0,08	2,03	1,86	3,36	0,18	2,68	0,80	1081	40,81	1060	26,23	1066	22,45	99	98	2
1,04	2,96	0,11	1,71	0,58	838	33,98	687	9,28	723	18,99	0,07	2,49	1,03	3,02	0,11	1,71	0,57	831	51,98	687	11,13	721	15,73	95	83	2
0,83	3,54	0,10	1,66	0,47	587	20,28	618	8,18	611	18,56	0,06	3,19	0,82	3,59	0,10	1,66	0,46	582	69,22	618	9,81	610	16,63	101	106	2
1,17	2,90	0,12	1,66	0,57	950	32,82	728	9,52	784	19,29	0,07	2,42	1,16	2,93	0,12	1,66	0,57	947	49,45	727	11,42	783	16,12	93	77	2
0,83	4,71	0,09	2,37	0,50	775	58,24	569	10,75	611	30,81	0,06	4,33	0,82	4,93	0,09	2,37	0,48	759	91,23	569	12,90	608	22,81	93	75	2
0,54	7,02	0,07	3,72	0,53	428	51,42	443	13,28	440	49,67	0,06	6,22	0,54	7,25	0,07	3,72	0,51	414	139,00	442	15,93	438	26,10	101	107	4
13,03	2,45	0,52	2,03	0,83	2656	52,12	2716	37,52	2679	36,17	0,18	1,39	13,02	2,46	0,52	2,03	0,82	2655	23,08	2716	45,05	2681	23,44	101	102	1
2,32	2,81	0,21	1,81	0,64	1226	31,47	1216	16,74	1219	26,65	0,08	2,17	2,32	2,83	0,21	1,81	0,64	1224	42,63	1216	20,09	1219	20,25	100	99	3
7,63	1,91	0,41	1,44	0,75	2151	14,76	2229	22,57	2187	20,58	0,13	1,27	7,63	1,91	0,41	1,44	0,75	2151	22,12	2228	27,10	2188	17,33	102	104	1
1,73	2,65	0,17	1,69	0,64	1003	25,63	1030	13,45	1020	21,81	0,07	2,07	1,73	2,68	0,17	1,69	0,63	999	42,12	1029	16,14	1019	17,38	101	103	2
1,38	5,62	0,15	4,73	0,84	896	113,69	876	32,35	881	108,99	0,07	3,09	1,38	5,65	0,15	4,73	0,84	892	63,80	875	38,83	880	33,80	99	98	4
1,38	4,23	0,14	2,58	0,61	950	46,34	855	17,26	882	41,22	0,07	3,51	1,38	4,36	0,14	2,58	0,59	939	72,03	855	20,70	878	25,96	97	91	2
0,88	6,60	0,10	2,67	0,40	656	88,80	639	13,52	642	43,54	0,06	7,08	0,86	7,56	0,10	2,67	0,35	614	152,92	638	16,21	632	36,25	101	104	3
6,62	2,48	0,37	1,75	0,70	2115	20,75	2009	25,20	2060	29,49	0,13	1,81	6,60	2,52	0,37	1,75	0,69	2111	31,77	2008	30,24	2059	22,45	98	95	2
5,62	4,31	0,33	2,87	0,67	2003	38,53	1843	38,41	1918	69,94	0,12	3,25	5,62	4,33	0,33	2,87	0,66	2002	57,71	1843	46,12	1919	38,05	96	92	3
1,26	3,31	0,14	2,18	0,66	785	35,29	842	14,35	826	28,42	0,07	2,59	1,25	3,38	0,14	2,18	0,64	775	54,44	842	17,22	823	19,27	102	109	2
14,45	2,11	0,55	1,77	0,84	2751	43,99	2820	33,73	2777	28,25	0,19	1,16	14,44	2,11	0,55	1,77	0,84	2750	19,09	2820	40,49	2779	20,28	101	103	1
5,24	3,49	0,34	2,19	0,63	1840	53,68	1875	29,73	1857	44,70	0,11	2,70	5,24	3,48	0,34	2,19	0,63	1841	48,93	1875	35,70	1859	30,09	101	102	3
1,00	3,31	0,12	1,87	0,56	693	24,24	710	10,49	706	21,85	0,06	2,85	1,00	3,41	0,12	1,87	0,55	681	60,96	710	12,58	703	17,46	101	104	2
8,20	1,99	0,42	1,54	0,77	2234	33,59	2274	24,69	2251	22,78	0,14	1,27	8,19	2,00	0,42	1,54	0,77	2234	21,95	2274	29,63	2253	18,24	101	102	1
0,82	3,05	0,10	1,66	0,55	608	37,26	610	8,06	609	16,71	0,06	2,66	0,82	3,14	0,10	1,66	0,53	596	57,70	609	9,67	606	14,43	100	102	2
7,94	1,76	0,42	1,26	0,72	2205	26,46	2245	19,92	2222	17,41	0,14	1,24	7,93	1,77	0,42	1,26	0,71	2203	21,59	2245	23,91	2223	16,08	101	102	1
2,54	3,13	0,22	2,30	0,74	1296	27,70	1274	22,18	1281	37,66	0,08	2,23	2,52	3,20	0,22	2,30	0,72	1287	43,32	1273	26,62	1278	23,53	100	99	3
1,94	5,47	0,18	4,05	0,74	1097	103,04	1093	34,06	1094	97,25	0,08	3,70	1,94	5,49	0,18	4,05	0,74	1095	74,06	1093	40,90	1094	37,43	100	100	4
1,21	3,10	0,13	1,97	0,63	795	27,13	810	12,48	805	24,09	0,07	2,49	1,20	3,18	0,13	1,97	0,62	785	52,39	809	14,97	803	17,77	101	103	2
2,32	3,30	0,21	1,74	0,53	1243	32,72	1204	15,95	1217	28,57	0,08	2,84	2,32	3,33	0,21	1,74	0,52	1241	55,70	1204	19,14	1217	23,91	99	97	4
10,02	2,38	0,47	1,79	0,75	2413	43,21	2465	30,56	2434	30,56	0,16	1,61	10,00	2,41	0,47	1,79	0,74	2411	27,40	2464	36,68	2434	22,46	101	102	1
0,47	4,73	0,06	2,91	0,62	383	29,02	393	9,25	391	27,51	0,05	4,00	0,46	4,94	0,06	2,91	0,59	360	90,20	392	11,09	388	16,06	101	109	3
0,89	4,77	0,10	2,21	0,46	749	60,74	617	10,85	645	30,12	0,06	4,49	0,88	5,01	0,10	2,21	0,44	733	95,17	616	13,01	642	24,11	96	84	2
0,93	4,22	0,11	2,12	0,50	689	52,72	660	11,09	666	27,46	0,06	3,78	0,92	4,34	0,11	2,12	0,49	679	80,83	660	13,30	664	21,36	99	97	2
6,20	2,64	0,36	2,07	0,78	2011	19,63	1999	29,66	2003	36,13	0,12	1,68	6,19	2,66	0,36	2,07	0,78	2009	29,75	1999	35,61	2003	23,53	100	100	1
8,29	9,31	0,43	6,45	0,69	2244	373,49	2285	104,24	2261	358,65	0,14	6,86	8,27	9,42	0,43	6,45	0,69	2242	118,60	2284	125,27	2261	89,09	101	102	5
2,48	4,18	0,22	3,73	0,89	1256	89,71	1273	36,00	1265	82,17	0,08	1,93	2,47	4,20	0,22	3,73	0,89	1251	37,80	1273	43,22	1264	30,83	101	102	3
3,35	3,86	0,26	3,01	0,78	1512	71,88	1478	33,24	1491	63,73	0,09	2,42	3,34	3,87	0,26	3,01	0,78	1511	45,77	1478	39,90	1492	30,68	99	98	3
0,95	3,18	0,11	1,63	0,51	669	20,31	682	8,81	678	18,30	0,06	2,73	0,95	3,18	0,11	1,63	0,51	669	58,39	682	10,57	679	15,86	100	102	2
5,57	3,02	0,33	1,74	0,58	1995	29,57	1835	23,16	1909	32,71	0,12	2,55	5,55	3,09	0,33	1,74	0,56	1991	45,35	1835	27,80	1909	26,90	96	92	2
7,75	2,33	0,42	1,75	0,75	2142	18,00	2268	27,88	2200	28,61	0,13	1,55	7,74	2,33	0,42	1,75	0,75	2141	27,04	2268	33,47	2201	21,19	103	106	1
0,83	6,07	0,10	5,65	0,93	609	118,68	618	27,80	616	115,38	0,06	2,24	0,83	6,07	0,10	5,65	0,93	607	48,41	618	33,38	616	28,44	100	102	5
6,25	3,24	0,35	2,91	0,90	2081	16,68	1945	40,90	2010	61,63	0,13	1,42	6,25	3,24	0,35	2,91	0,90	2080	25,03	1945	49,11	2011	28,78	97	94	1
2,23	5,76	0,20	4,84	0,84	1248	143,94	1161	42,99	1191	137,37	0,08	3,23	2,22	5,82	0,20	4,84	0,83	1241	63,26	1161	51,60	1189	41,58	98	94	5
1,33	3,26	0,14	1,85	0,57	851	27,46	863	12,48	859	24,46	0,07	2,76	1,33	3,32	0,14	1,85	0,56	844	57,38	863	14,98	857	19,42	101	102	2
0,85	6,74	0,10	2,37	0,35	617	40,14	625	11,75	622	38,38	0,06	6,74	0,84	7,14	0,10	2,37	0,33	598	145,92	624	14,10	618	33,63	101	104	2
1,81	2,79	0,18	2,33	0,84	1040	36,95	1051	18,86	1046	31,78	0,07	1,55	1,80	2,80	0,18	2,33	0,83	1038	31,22	1051	22,63	1046	18,43	100	101	2
1,56	3,93	0,16	3,24	0,82	975	30,54	943	23,73	952	55,71	0,07	2,26	1,55	3,95	0,16	3,24	0,82	971	46,18	943	28,49	951	24,71	99	97	3
6,15	3,33	0,37	3,08	0,93	1960	15,10	2033	44,98	1995	67,18	0,12	1,26	6,14	3,33	0,37	3,08	0,93	1960	22,54	2033	54,02	1997	29,53	102	104	1
8,08	2,00	0,43	1,43	0,72	2178	16,25	2310	23,19	2238	21,44	0,14	1,41	8,07	2,01	0,43	1,43	0,71	2176	24,56	2309	27,83	2239	18,32	103	106	1
7,14	4,42	0,39	4,09	0,93	2148	19,68	2110	61,60	2127	120,09	0,13	1,69	7,13	4,43	0,39	4,09	0,92	2147	29,61	2110	73,98	2128	40,20	99	98	1
0,71	3,01	0,09	2,05	0,68	535	20,68	546	8,96	543	18,64	0,06	2,29	0,70	3,07	0,09	2,05	0,67	523	50,24	546	10,74	541	12,98	101	104	2
0,80	4,15	0,09	3,77	0,91	716	24,84	565	17,02	596	50,94	0,06	1,78	0,80	4,17	0,09	3,77	0,90	711	37,80	565	20,42	595	18,93	95	80	4
1,40	2,88	0,15	1,72	0,60	892	32,08	887	11,92	888	21,54	0,07	2,38	1,39	2,94	0,15	1,72	0,59	884	49,25	887	14,31	886	17,53	100	100	2
0,77	3,51	0,09	1,70	0,48	674	44,44	553	7,53	577	18,04	0,06	3,26	0,76	3,68	0,09	1,70	0,46	658	69,90	553	9,03	574	16,25	96	84	2
0,68	4,82	0,09	4,27	0,89	520	62,37	527	18,02	525	59,71	0,06	2,27	0,68	4,84	0,09	4,27	0,88	514	49,89	527	21,63	524	20,00	100	102	4
1,06	17,82	0,12	17,44	0,98	759	122,21	726	100,61	734	69,39	0,06	3,74	1,06	17,84	0,12	17,44	0,98	753	78,98	726	120,89	732	97,63	99	96	17
0,72	13,57	0,08	13,36	0,98	781	33,40	500	53,79	553	380,52	0,06	2,47	0,72	13,59	0,08	13,36	0,98	769	52,10	500	64,57	551	59,48	91	65	13
0,73	13,30	0,09	12,61	0,95	570	463,75	550	55,69	554	460,39	0,06	4,40	0,72	13,36	0,09	12,61	0,94	557	95,87	550	66,87	551	58,48	100	99	12
0,67	32,10	0,08	10,22	0,32	504	522,39	522	42,84	518	470,96	0,06	34,86	0,65	36,33	0,08	10,22	0,28	464	772,43	521	51,39	511	157,34	102	112	10
0,97	11,31	0,11	9,86	0,87	709	441,79	684	53,53	689	438,53	0,06	5,70	0,97	11,39	0,11	9,86	0,87	702	121,29	684	64,27	688	58,54	99	97	9
0,35	9,81	0,05	9,32	0,95	257	180,11	310	23,57	304	178,56	0,05	3,21	0,35	9,86	0,05	9,32	0,95	242	74,05	310	28,28	302	26,10	103	128	9
1,32	8,02	0,14	7,80	0,97	876	293,09	845	51,72	853	288,49	0,07	1,89	1,32	8,03	0,14	7,80	0,97	874	39,10	845	62,12	853	47,42	99	97	7
3,65	7,03	0,28	4,47	0,64	1531	158,95	1581	52,49	1559	150,03	0,10	5,35	3,65	6,97	0,28	4,47	0,64	1534	100,71	1581	63,05	1561	57,17	101	103	7
0,32	5,80	0,04	5,00	0,86	260	49,55	282	11,49	279	48,20	0,05	3,06	0,31	5,86	0,04	5,00	0,85	246	70,59	282	13,78	278	14,34	101	115	5
4,11	3,90	0,27	3,02	0,77	1825	30,22	1525	34,25	1654	67,21	0,11	2,51	4,10	3,92	0,27	3,02	0,77	1823	45,47	1525	41,11	1654	32,53	92	84	2
5,45	2,60	0,31	2,32	0,89	2057	13,98	1746	29,64	1890	39,58	0,13	1,20	5,44	2,61	0,31	2,32	0,89	2056	21,12	1745	35,58	1891	22,65	92	85	1

*Grains with length / width ratios of 1.3-1.8 are considered oval. Grains with higher and lower ratios are considered elongated and round, respectively.

**sa-sr = subangular to subrounded

***Zircon crystals with oscillatory or sector zoning are considered igneous. Homogenous and irregularly zoned grains are interpreted to be metamorphic.

a concentration uncertainty ca. 20%

b ratio not corrected for common-Pb

c date not corrected for common-Pb

d date corrected for common-Pb

e Concordance calculated as (206Pb-238U age/207Pb-205Pb age) *100

f Concordance calculated as (206Pb-238U age/207Pb-206Pb age) *100